Siderophile and chalcophile elements in the Archean mantle-crust system

Chunhui LI

Dissertation submitted to obtain

the academic degree

Doktor der Naturwissenschaften

(Dr. rer. nat.)

Fachbereich Geowissenschaften

Freie Universität Berlin

Disputated at 8th. November. 2016

Freie Universität Berlin

Berlin, July 2016

Referees:

1. First Referee: Prof. Dr. Harry Becker
   Institut für Geologische Wissenschaften,
   Freie Universität Berlin
   Malteserstrasse 74-100, Haus B
   12249 Berlin, Germany

2. Second Referee: Prof. Dr. Gerhard Franz
   Fachgebiet Mineralogie
   Technische Universität Berlin
   Sekr. ACK 9
   Ackerstr. 76
   13355 Berlin, Germany

Selbständigkeitserklärung

Hiermit versichere ich, die vorliegende Dissertation eigenständig und ausschließlich unter Verwendung der angegebenen Hilfsmittel, angefertigt zu haben. Alle Aussagen innerhalb der vorliegenden Arbeit, welche dem Wortlaut oder dem Sinne nach aus anderen Quellen entnommen wurden, einschließlich solcher aus elektronischer Medien, sind im Text kenntlich gemacht und befinden sich in einem vollständigen Verzeichnis.

Die vorliegende Arbeit ist in dieser oder anderer Form zuvor nicht als Prüfungsarbeit zur Begutachtung vorgelegt worden.

Datum, Ort: Unterschrift

Table of Contents

Summary

Late additions of meteoritic components to the Earth brought volatile species essential for a habitable world. The segregation of a metallic core was probably the sole effective process that scavenged iron-loving and sulfide-loving elements, known as siderophile and chalcophile elements, from the bulk silicate Earth (BSE) by different mechanisms. Highly siderophile elements (Os, Re, Ru, Rh, Pt, Pd, Au and Re; HSE) and strongly chalcophile elements (S, Se and Te; SCE) entirely partitioned into the core, which made the BSE be depleted in these elements. However, the abundances of HSE and SCE in the BSE defined by modern peridotites are at least enriched by a factor of 200 relative to the predications from metal-silicate partitioning experiments. Furthermore, relative abundances of HSE and SCE are near chondritic, requiring a chondritic late veneer shortly after the end of core formation. Another meteoritic addition which may have modified the early Earth, besides the late veneer, is the late heavy bombardment which impacted the lunar surface at 4.2-3.75 Ga.

However, here are two issues concerning the late veneer and late heavy bombardment. The budgets of HSE and SCE in the BSE constrained by post-Archean mantle peridotites were recently suggested to be a mixture of depleted mantle peridotites and infiltrating melts. Such a mixture may not be representative of the composition in the BSE. Unfortunately, signatures of the late heavy bombardment, such as impact structures, have not been found in early Archean rocks on the Earth. However, the Acasta Gneiss Complex from northern Canada (Chapter 2) and mantle-derived komatiites (Chapter 3-5) are perfect for addressing the two problems. The Acasta Gneiss Complex represents the Hadean-Neoarchean continental crust, whereas komatiites, products of high-degrees of partial melting, should be representative of the chemical composition in the Archean mantle.

The ages of the Acasta Gneiss Complex expands from 4.2 Ga to 3.6 Ga, which coincides with the late heavy bombardment on the Moon. The Acasta samples investigated in this study include an ultramafic cumulate, medium-grained metagabbros, layered metagabbros, one type of garnet amphibolite, a hornblendite and metatonalite–trondhjemite–granodiorites (TTG). Abundances of HSE and SCE in the Acasta samples are comparable to those in their post-Archean equivalents, and enrichments of HSE or fractionations of SCE caused by meteoritic impacts are not found in these samples. Such similarities of signatures of HSE and SCE in the Acasta gneisses and their post-Archean counterparts indicate that magmatic characteristics of these elements are not significantly lost during multi-stage metamorphisms.

Especially, the T_{MA} Re-Os model age in metadioritic layer AMS 031A of 4.3 ± 0.2 Ga is consistent with the errorchron age of Sm-Nd systematics within uncertainties, illustrating the excellent preservation of magmatic characteristics in AMS 031A. Our data support that the accomplishment of the late veneer mixed in the mantle source of the Acasta predecessors should not be later than 4.2 Ga. Signatures of the late heavy bombardment are absent in the Acasta gneisses.

Archean komatiites and komatiitic basalts investigated in this study can be divided into two groups, the post-2.9 Ga komatiites and pre-2.9 Ga komatiites. The post-2.9 Ga komatiites comprise the 2.4 Ga Victoria's lava lake of the Vetreny Belt, the 2.7 Ga Tony's lava flow of the Belingwe Greenstone Belt and the 2.7 Ga Pyke Hill lava flows of the Abitibi Greenstone Belt. The pre-2.9 Ga komatiites include the ~3.3 Ga Weltevreden Formation and ~3.5 Ga Komati Formation of the Barberton Greenstone Belt and the ~3.5 Ga Carl's flow of the Schapenburg Greenstone Remnant. In this study we determined abundances of a group of trace elements, including S, Se, Te, Cu, Ag, Mo, Tl, In, Cd, Sm and Ba, by employing the isotope dilution inductively coupled plasma mass spectrometry (ID-ICP-MS) method.

Magmatic signatures of the majority of the elements of interest are well preserved in the 2.7 Ga Tony's lava flow of the Belingwe Greenstone Belt. Ratios of incompatible chalcophile elements, such as Se/Te, Cu/Ag and Se/Cu in the Belingwe komatiites are comparable to those of the BSE defined by post-Archean fertile mantle peridotites. The chemical composition of the mantle source of the Tony's lava flow constrained by variations of element-MgO plots are indistinguishable from those of the BSE within uncertainties. Our data are in well agreement with the chalcophile element composition in the BSE defined by post-Archean mantle peridotites. Near-chondritic ratios of S, Se and Te in the Belingwe mantle source require a late veneer of volatile-rich materials. Near-BSE Cu/Ag and Cd/In ratios are in favor of nonchondritic materials which may have built the volatile element inventory in the Earth.

Significant amounts of S, Se and Te in the 2.4 Ga Victoria's lava lake of the Vetreny Belt were lost by magmatic degassing, and Cu and Ag in the 2.7 Ga Pyke Hill lava flows of the Abitibi Greenstone Belt were disturbed remarkably. Magmatic characteristics of volatile chalcophile elements, including S, Se, Te, Cu and Ag are not preserved in the ~3.3 Ga Weltevreden Formation of the Barberton Greenstone Belt and ~3.5 Ga Carl's flow of the Schapenburg Greenstone Remnant. Ratios of S, Se and Te in the Abitibi komatiites and samples from the Komati Formation are comparable to that of the Belingwe komatiites and

BSE. Ratios of Cu and Ag in samples from Victoria's lava lake and the Komati Formation also resemble those of the Belingwe komatiites and BSE. Ratios including Cu/Se and Ag/Se of the Komati Formation, however, are much higher than those of the Belingwe komatiites and BSE. The decoupling of both groups of elements, *i.e.* S, Se and Te versus Cu and Ag, supports the hypothesis that S, Se and Te were delivered by late veneer and may not have been fully homogenized in the mantle source of the Komati Formation. This interpretation is consistent with the progressive mixing model [Maier, W.D., Barnes, S.J., Campbell, I.H., Fiorentini, M.L., Peltonen, P., Barnes, S.-J. and Smithies, R.H., 2009. Progressive mixing of meteoritic veneer into the early Earth's deep mantle. Nature 460, 620-623.]. Our fractional melting model for S and Cu shows that the mantle source of the Weltevreden Formation may have undergone substantial early melt extractions, up to 20%, whereas early melt extractions were likely limited in the Belingwe mantle source.

Magmatic characteristics of Tl and Ba are rarely preserved in the investigated komatiites and komatiitic basalts. With the exception of Mo and Cd in the Belingwe komatiites and Victoria's lava lake, igneous signatures of Mo and Cd are not retained in these samples. In contrast, indium in the investigated samples was not modified by late-stage alteration. Ratios of In and Yb in Al-depleted Barberton-type komatiites from the Komati Formation are slightly lower than those in Al-enriched komatiites of the Weltevreden Formation and Al-depleted Barberton-type komatiites of the Schapenburg Greenstone Belt. High In/Yb ratios indicate the participation of garnet in the formation of these komatiites. BSE-normalized Ce/Sm ratios of pre-2.9 Ga Al-depleted Barberton-type komatiites are higher than post-2.9 Ga Al-undepleted Munro-type komatiites, whereas BSE-normalized Ba/Sm ratios of pre-2.9 Ga Al-depleted Barberton-type komatiites are lower than post-2.9 Ga Al-undepleted komatiites. Besides, abundances of light rare earth elements in Al-depleted Barberton-type komatiites are higher than those of Al-undepleted Munro-type komatiites. These signatures indicate the mantle sources of pre-2.9 Ga Al-depleted Barberton-type komatiites could have been enriched by delamination of reworked mafic crust.

Zusammenfassung

Der späte Eintrag von meteoritischem Material auf die Erde brachte volatile Elemente, die essenziell für eine bewohnbare Erde sind. Die Segregation eines metallischen Kerns vom Mantel war wahrscheinlich der einzige Prozess, der eisen- und sulfidliebende Elemente, die auch als siderophile und chalcophile Elemente bekannt sind, der silikatischen Gesamterdzusammensetzung entzogen hat. Hochsiderophile Elemente (Os, Re, Ru, Rh, Pt, Pd und Re; HSE) und stark chalkophile Elemente (S, Se, Te; SCE) partitionierten komplett in den Erdkern, was dazu führte, dass die HSE und SCE Gehalte in der Silikaterde gegen Null gingen. Wenn jedoch die HSE und SCE Gehalte der Gesamtsilikaterde mit Hilfe von rezenten Mantelperidotiten bestimmt werden, sind diese um den Faktor 200 angereichert im Vergleich zu Vorhersagen aus Metall-Silikat Verteilungsexperimenten. Zudem sind die relativen Häufigkeiten der HSE und SCE nahe am chondritischen Wert, was einen späten Eintrag von chondritischem Material („late Veneer“) kurz nach der Kernbildung bedingt. Ein weiterer meteorischer Eintrag auf der Erde neben dem „Late Veneer“ war wahrscheinlich das „Letzte starke Bombardement“ („late heavy bombartment“), das die Mondoberfläche zwischen 4.2 und 3.75 Milliarden Jahren getroffen hatte.

Es gibt jedoch zwei Probleme mit dem „late Veneer“ und dem „late heavy bombartment“. Die aus post-Archaischen Mantelperidotiten abgeleiteten Gehalte an HSE und SCE für die Gesamtsilikaterde repräsentieren möglicherweise Mischungen aus verarmten Mantelperidotiten und infiltrierenden Schmelzen. Somit sind diese Mischungen möglicherweise nicht repräsentativ für die silikatische Gesamterde. Unglücklicherweise wurden bisher keine Hinweise auf das „Late heavy bombartment“, wie z. Bsp. Impaktstrukturen, in Früharchaischen Gesteinen der Erde gefunden. Jedoch sind der Acasta Gneiss Complex im nördlichen Kanada (Kapitel 2) und aus dem Erdmantel stammende Komatiite (Kapitel 3-5) perfekt für die Bearbeitung dieser beiden Probleme. Der Acasta Gneiss Complex repräsentiert Hadaeische bis Neoarchaische kontinentale Kruste, die Komatiite sind hingegen Produkte von höheren Aufschmelzgraden des Archaischen Mantels und somit sollten sie in ihrer chemischen Zusammensetzung repräsentativ für diesen sein.

Der Zeitraum, den die Bildung der Acasta Gneise abdeckt, zieht sich von 4.2 Mrd. bis 3.6 Mrd. Jahre, überlappend mit dem „Late heavy bombardment“. Die bearbeiteten Acasta Proben beinhalten ein ultramafisches Kumulat, mittelkörnige Metagabbros, lagige Metagabbros, einen Granatamphibolit, einen Hornblendit und Metatonalit-Trondhjemit-Granodiorite (TTG). Die gemessenen HSE und SCE Gehalte in den Acasta Proben sind vergleichbar mit denen von äquivalenten post-Archaischen Gesteinen. Anreicherungen der HSE oder Fraktionierungen der SCE, hervorgerufen durch Impakt-induziierte Entgasung, wurden nicht gefunden. Solche Ähnlichkeiten in den HSE und SCE Signaturen in den Acasta Gneisen und deren post-Archaischen Äquivalenten zeigen, dass die magmatischen Charakteristika dieser Elemente während multiplen metamorphen Ereignissen nicht signifikant verloren gingen. Dies gilt im speziellen für die T_{Ma} Re-Os Modellalter in der lagigen Metadioritprobe AMS031A, deren Alter 4.3 ± 0.2 Mrd. Jahre beträgt und innerhalb der Unsicherheit im Einklang mit dem Sm-Nd Alter steht. Dies zeigt die exzellente Erhaltung von magmatischen Charakteristika in Probe AMS 031A. Unsere Daten unterstützen, dass der „late Veneer“ gegen 4.2 Mrd. Jahre in die Mantelquellen der Gesteine eingemischt wurde aus denen die Acasta Gneise hervorgegangen sind. Signaturen des „late heavy bombartment“ fehlen in den Acasta Gesteinen.

Archaische Komatiite und komatiitische Basalte, die in dieser Arbeit analysiert wurden, können in zwei Gruppen unterteilt werden: Die post-2.9 Mrd. Jahre alten Komatiite und die prä-2.9 Mrd. Jahre alten Komatiite. Die post-2.9 Mrd. Jahre alten Komatiite beinhalten den 2.4 Mrd. Jahre alten Victoria’s lava lake des Veltreny Grünsteingürtels, den 2.7 Mrd. Jahre alten Tony’s lava flow des Belingwe Grünsteingürtels und den 2.7 Mrd. Jahre alten Pyke Hill lava flow des Abitibi Grünsteingürtels. Die prä-2.9 Ga Komatiite beinhalten die ca. 3.3 Mrd. Jahre alte Weltevreden Formation und die ca. 3.5 Mrd. Jahre alte Komatii Formation des Barberton Grünsteingürtels sowie den 3.5 Mrd. Jahre alten Carl’s flow des Schapenburg Grünsteingürtelüberrests. In dieser Arbeit wurden die Häufigkeiten einer Gruppe von Spurenelementen, bestehend aus S, Se, Te, Cu, Ag, Mo, Tl, In, Cd, Sm und Ba, mit Hilfe der Isotopenverdünnungsmethode und induktiv-gekoppelter Massenspektrometrie (ID-ICP-MS) gemessen.

Magmatische Signaturen einer Vielzahl von Elementen sind im Tony’s flow des Beligwe Grünsteingürtels gut erhalten. Verhältnisse von inkompatiblen chalkophilen Elementen wie Se/Te, Cu/Ag, Se/Cu in den Belingwe Komatiiten sind vergleichbar mit denen der silikatischen Gesamterde, deren Zusammensetzung durch fertile Mantelperidotite definiert

wurde. Die chemische Zusammensetzung der Mantelquelle des Tony´s lava flow, belegt durch verschiedene graphische Element-MgO Darstellungen, ist innerhalb des Fehlers ununterscheidbar von jener der BSE. Unsere Daten stimmen gut mit der Zusammensetzung der chalkophilen Elemente in der durch post-Archaische Mantelperidotite definierten BSE überein. Nahezu chondritische Verhältnisse von S, Se und Te in der Mantelquelle der Belingwe Komatiite benötigen eine Zugabe von volatil-reichem Material in Form des „late Veneers“. BSE-ähnliche Cu/Ag und Cd/In Verhältnisse sprechen für nicht-chondritisches Material, dass den Bestand an volatilen Elementen auf der Erde gebildet haben könnte.

Signifikante Mengen an S, Se und Te in dem 2.4 Mrd. Jahre alten Victoria´s lake des Vetreny Grünsteingürtels sind durch magmatische Ausgasung verloren gegangen, und Cu und Ag in dem 2.7 Mrd. Jahre alten Pyke Hill lava folw des Abitibi Grünsteingürtels sind erheblich gestört. Magmatische Charakteristiken von volatilen chalkophilen Elementen wie S, Se, Te, Cu und Ag sind nicht erhalten in der ~3.3 Mrd. Jahre alten Weltevreden Formation des Barberton Grünsteingürtels oder in dem ~3.5 Mrd. Jahre alten Carl´s flow des Schapenburg Grünsteingürtelüberrests. Elementverhältnisse von S, Se und Te in den Abitibi Komatiiten und Proben aus der Komati Formation sind vergleichbar mit den Belingwe Komatiiten und der silikatischen Gesamterde. Elementverhältnisse von Cu und Ag in Proben des Viktoria´s lake und der Komati Formation ähneln ebenfalls denen der Belingwe Komatiite sowie der silikatischen Gesamterde. Kupfer/Se und Ag/Se Verhältnisse der Komati Formation sind jedoch viel höher als die der Belingwe Komatiite und der silikatischen Gesamterde. Die Entkopplung beider Gruppen von Elementen, das sind, S, Se und Te auf der einen Seite, und Cu und Ag auf der anderen Seite, unterstützt die Hypothese, dass S, Se und Te durch den „late Veneer“ eingetragen wurden und dass die Mantelquelle der Komati Formation möglicherweise noch nicht vollständig homogenisiert war. Diese Interpretation stimmt mit dem progressiven Mischungsmodell von Maier et al. (2009) überein [Maier, W.D., Barnes, S.J., Campbell, I.H., Fiorentini, M.L., Peltonen, P., Barnes, S.-J. and Smithies, R.H., 2009. Progressive mixing of meteoritic veneer into the early Earth's deep mantle. Nature 460, 620-623.]. Unser Schmelzfraktionierungsmodel für S und Cu zeigt, dass die Mantelquelle der Weltevreden Formation einen erheblichen frühen Schmelzentzug bis zu 20% erfahren hatte, wohingegen nur geringfügiger früher Schmelzentzug in der Mantelquelle der Belingwe Komatiite eine Rolle spielte.

Hauptsächlich lithophile Elemente wie Mo, Cd, In, Sm, Ba und Tl könnten ebenfalls Aufschluss über die Petrogenese der Komatiite liefern. Magmatische Charakteristiken von Tl

und Ba sind selten erhalten in den bearbeiteten Komatiiten und komatiitischen Basalten. Mit der Ausnahme von Mo und Cd in den Belingwe Komatiiten und im Victoria´s lake, sind magmatische Signaturen von Mo und Cd in den meisten Proben nicht erhalten. Im Gegensatz dazu wurde Indium nicht durch spätere Alteration in den untersuchten Proben verändert. Verhältnisse von den Granat-sensitiven Elementen In und Yb in Al-verarmten Komatiiten des Barberton-Typs der Komati Formation sind leicht niedriger als jene in den Al-angereicherten Komatiiten der Weltvreden Formation sowie als jene der Al-verarmten Komatiiten des Barberton-Typs in dem Schapenburg Grünsteingürtel. Hohe In/Yb Verhältnisse in den Proben der Weltevreden Formation und des Schapenburg Grünsteingürtels deuten auf die Beteiligung von Granat bei der Bildung dieser Komatiite hin. Auf die silikatische Gesamterde normierte Ce/Sm Verhältnisse von prä-2.9 Mrd. Jahre alten Al-verarmten Barberton-Typ Komatiiten sind höher als die der post-2.9 Mrd. Jahre alten Al-unverarmten Munro-Typ Komatiiten. Dahingegen sind die auf die silikatische Gesamterde normierten Ba/Sm Verhältnisse der prä-2.9 Mrd. Jahre alten Al-verarmten Barberton-Type Komatiite niedriger als die der post-2.9 Mrd. Jahre alten Al-unverarmten Komatiite. Außerdem zeigen die leichten seltenen Erdelemente in Al-verarmten Barberton-Typ Komatiiten eine höhere Häufigkeit als in den Al-unverarmten Munro-Typ Komatiiten. Diese Signaturen deuten darauf hin, dass die Mantelquellen der prä-2.9 Mrd. Jahre alten Al-verarmten Barberton-Typ Komatiite durch Delamination von umgelagerter mafischer Kruste angereichert worden sein könnten.

摘要

晚期增积过程中，落到地球上的陨石物质带来了亲气元素或者组分，这些元素或组分是地球能够孕育生命的重要物质基础。金属地核形成过程中发生的不同事件可能将地球中原有的亲铁、亲硫元素不同程度地吸纳到了地核。强亲铁元素（Os、Re、Ru、Rh、Pt、Pd、Au 和 Re；缩写为 HSE）和强亲硫元素（S、Se 和 Te;缩写为 SCE）可能全部进入了金属地核，留下一个亏损这些元素的硅酸盐部分，称之为硅酸盐地球（BSE）。但是，由富集橄榄岩代表的 BSE 中 HSE 和 SCE 的含量比金属-硅酸盐分配实验的预测值要高出两百多倍。而且，HSE 和 SCE 的元素含量之间的比值接近于球粒陨石。这两项证据合在一起，极有可能指示在金属地核形成以后，在一次晚期增积事件（late veneer）中，有大量球粒陨石物质加入到了地幔里面，而没有进入地核。除这次晚期增积事件（44 亿年左右）之外，还有一期陨石撞击事件可能影响到了地球，那就是发生在月球上的晚期陨石大撞击事件（late heavy bombardment；42 亿年-37.5 亿年之间）。考虑到地月之间距离较近，而且地球有更大的引力面，如果月球受到了晚期陨石大撞击的影响，那么地球也极有可能在所难免。

然而，两期后期增生事件仍有两个疑点需要解答。BSE 中 HSE 和 SCE 的含量主要是通过富集橄榄岩测定的，但是最近有研究认为富集橄榄岩并不能真正代表 BSE。这是因为富集橄榄岩（比如二辉橄榄岩）可能是亏损橄榄岩（比如方辉橄榄岩）受后期地幔熔体叠加形成，是一种混合物，故而不能代表 BSE。此为第一个疑点。第二个疑点就是发生在月球上的晚期陨石大撞击究竟有没有影响到地球，这是因为在地球上太古代岩石里面并没有发现与撞击有关的撞击构造。位于加拿大北部的 Acasta 片麻岩杂岩体（主要涉及第二章）和太古代科马提岩（主要涉及第三章至第五章）非常适合被用来研究上述两个疑点。Acasta 片麻岩杂岩体可以

代表冥石代-太古代的大陆地壳，而太古代科马提岩作为地幔高度熔融的产物，当能代表太古代地幔的成分。

Acasta 片麻岩杂岩体的年龄在 42 亿年到 36 亿年之间，恰与发生在月球上的晚期陨石大撞击事件吻合。本次研究中收集的样品包括超基性堆晶岩、中粒变辉绿岩、层状变辉绿岩、石榴石角闪岩、角闪岩和变英云闪长岩-变奥长花岗岩-变花岗闪长岩（所写为 TTG）。此处的“变”指的是变质作用。这些古老样品中的 HSE 和 SCE 的含量和太古代之后的地壳样品中的含量几乎相当，既没有发现由于陨石加入而带来的元素富集，也没有发现因陨石撞击而造成的 SCE 之间的分馏。Acasta 片麻岩杂岩体中 HSE 和 SCE 的含量特征也表明这些元素基本上保留了他们在岩浆母岩中的特征，受后来多期变质作用的影响并不大。需要特别指出的是，变闪长岩 AMS 031A 的 Re-Os 模式年龄为 43 ± 2 亿年，和由 Sm-Nd 得出的年龄数据一致，证明 AMS 031A 中的 HSE 和 SCE 没有受到变质作用的影响。本次研究获得的数据证明后期增积事件（late veneer）带来的陨石物质在 42 亿年之前就已经均匀地混合到了地幔里面，同时也证明发生在月球上的后期陨石大撞击事件（late heavy bombardment）至少没有影响 Acasta 地区。

本次研究中涉及的科马提岩依据其年龄可以分为两组，老于 29 亿年的为一组，晚于 29 年的为另一组。晚于 29 亿年的科马提岩包括采自 Vetreny 岩带中 24 亿年的 Victoria’s lava lake 样品、Belingwe 绿岩带中 27 亿年的 Tony 岩浆流样品和 Abitibi 绿岩带中 27 亿年的 Pyke Hill 岩浆流（包括岩浆流 1 和岩浆流 2）。早于 29 亿年的科马提岩包括 35 亿年的 Komati Formaiton，33 亿年的 Weltevreden Formation 和 Schapenburg 绿岩带残留体中的 Carl 岩浆流样本。在本次研究中，我们用同位素稀释法准确测定了这些科马提岩中 S、Se、Te、Cu、Ag、Mo、Tl、In、Cd、Sm 和 Ba 的含量。

Belingwe 绿岩带中 27 亿年的 Tony 岩浆流样品很好地保留了这些元素的原始岩浆特征。中度不相容亲硫元素含量之间的比值，比如 Se/Te、Cu/Ag 和 Se/Cu，和 BSE 中的一致。通过这些元素与 MgO 含量之间的线性负相关关系，可以计算产生 Tony 岩浆流的地幔源区的元

素含量。计算结果表明，Tony 岩浆流地幔源区中本文所涉及的元素含量与 BSE 在误差范围内一致。Tony 岩浆流地幔源区的 S、Se 和 Te 的比值与球粒陨石一致，证明这些元素极有可能是晚期增积事件（late veneer）带来的。Tony 岩浆流地幔源区的 Cu/Ag 和 Cd/In 比值与 BSE 一致，与陨石值不一致，证明 Tony 岩浆流地幔源区中 Cu、Ag、Cd 和 In 的含量受其它机制控制，比如地核形成或者这些元素本来就不是由我们现在知道的陨石带来的。

Victoria's lava lake 样品中 S、Se 和 Te 受到了岩浆去气作用的影响，而其中 Cu 和 Ag 的岩浆特征并没有受到后期事件的影响。Pyke Hill 样品中的 Cu 和 Ag 受到了后期改造作用的影响，而其中的 S、Se 和 Te 大致保存了岩浆特征。在老于 29 亿年的 Schapenburg 和 Weltevreden 样品中 S、Se、Te、Cu 和 Ag 的岩浆特征都被后期事件破坏了，而在 Komati Formation 中这些元素似乎没有受到明显的后期改造。Victoria's lava lake 和 Komati Formation 中 Cu/Ag 比值与 Belingwe 样本和 BSE 一致。Pyke Hill 和 Komati Formation 中的 S、Se 和 Te 元素含量之间的比值也和 Belingwe 中的一致（故而也与球粒陨石一致）。然而，有趣的是，Komati Formation 中 Cu/Se 和 Ag/Se（也包括 Cu-Ag 与 S-Te-Pd 之间的相互比值）高于 BSE 值。也就是说 S-Se-Te-Pd 和 Cu-Ag 在 Komati Formation 中发生了解耦。经本文研究，这一解耦现象或许并非是由岩浆去气（因为 S、Se 和 Te 受排气作用控制，而 Pd 不受排气作用影响）造成的，而有可能反映了 Komati Formation 地幔源区的特征。若真如此，那么就为 Maier 等人于 2009 年基于科马提岩中 Pd 的元素含量而提出的地幔渐进演化模型提供了独立证据。与此同时，本文提供的分异部分熔融模型表明，Weltevreden Formation 的地幔源区可能有过较大程度的先期岩浆抽离事件，而 Belingwe 的地幔源区受早期岩浆抽离事件的影响并不是特别明显。

本次研究中所涉及的主要展现亲石特性的元素（Sm、Ba、In、Cd、Mo 和 Tl）或能为科马提岩成因提供新的视角。在本次研究的科马提岩样本中，Tl 和 Ba 几乎无一例外的或多或少地受到了后期作用的改造，其岩浆特征大多已经丧失。Mo 和 Cd 的岩浆特征也仅保留与 Belingwe 样本和 Victoria's lava lake 样本中。有趣的是，In 的岩浆特征非常完好地保留在了所

有本次研究的科马提岩中。以 Komati Formation 为代表的铝亏损型科马提岩中 In/Yb（这两个元素不相容性相近）低于同为铝亏损型科马提岩的 Schapenburg 样本和铝富集型科马提岩的 Weltevreden Formation 样本。这一特征表明 In/Yb 高的科马提岩形成过程中有石榴石参与，而 In/Yb 较低的科马提岩形成过程中石榴石参与不多。另一需要特别指出的特征是铝亏损型科马提岩（Komati Formation 和 Schapenburg 样本）中轻稀土元素的含量高于铝不亏损型科马提岩（Victoria's lava lake、Belingwe 和 Pyke Hill）和铝富集型科马提岩 Weltevreden Formation 样本。而且，铝亏损型科马提岩的 Ce/Sm 也高于铝不亏损型科马提岩。这两个特征可能暗示铝亏损型科马提岩地幔源区中的稀土元素含量受到了某种拆沉作用的影响。

Chapter 1

Introduction

1.1 The formation of the Earth-Moon system

Our solar system evolved from a hot disk of dust and gas which circulated around the infantile sun at 4.567 Ga (Amelin et al., 2002). During the following several million years, chondrites formed through a series of element condensation (Palme et al., 2014), growth and sticking of dust grains (~0.1 mm - <1 m; Testi et al., 2014; Torsten et al., 2000), and turbulent concentration of larger bodies (meter to hundred meter-sized; Jeffrey et al., 2001). Subsequently, terrestrial planets started to accrete via gravitational focusing and runaway growth of planetsimals (kilometer-sized; Chambers, 2014), oligarchic growth of planetary embryos (Kokubo and Ida, 1998; Philip et al., 2015), and orderly growth (Kokubo and Ida, 2000) and giant impacts after ~50% of the total solid mass condensation reached (Agnor et al., 1999). During the planetary accretion a metallic core segregated from a silicate mantle. The assumption is that the planetary differentiation was a continuous process with already entirely or partially differentiated embryos and differentiation of molten accreting objects present. For the proto-Earth, its violent closing stage was marked by the Moon-forming giant impact, late veneer and late heavy bombardment (Fig.1.1). These three events, dramatically modified the physicochemical environment of the Earth-Moon system by introducing angular momentums into the Earth and the Moon (Canup, 2012; Canup and Asphaug, 2001; Ćuk and Stewart, 2012), delivering volatiles to the Earth which were essential to the origin of life (Wang and Becker, 2013), and creating a thermal layer that may have hosted all beginning life on Earth (Abramov and Mojzsis, 2009).

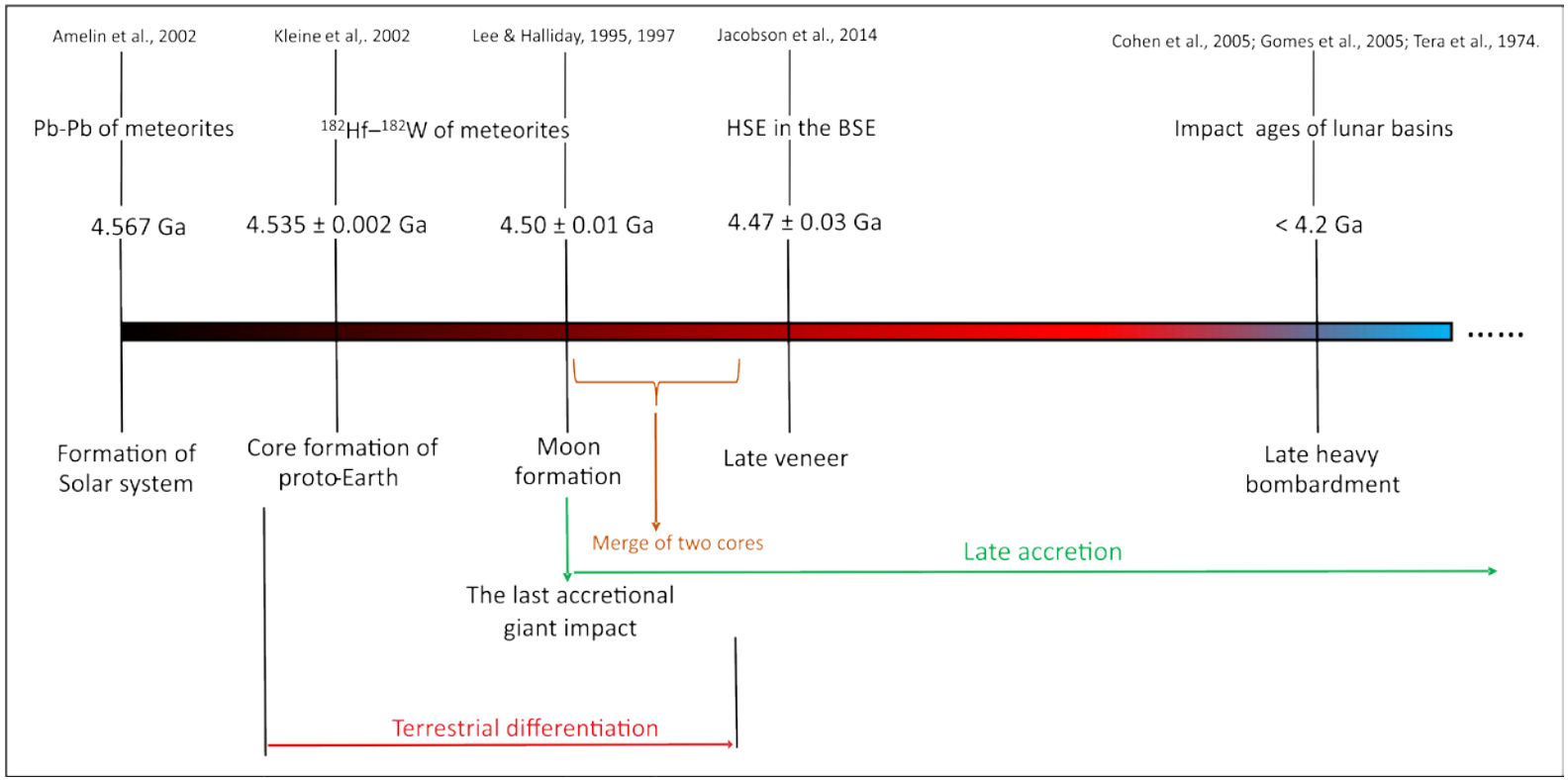

Figure 1.1 The timescale of the Solar system. Formation age of the Solar system was constrained by the Pb-Pb age of chondrules and calcium-aluminum-rich inclusions of chondrites (Amelin et al., 2002; Bouvier and Wadhwa, 2010). The timing of terrestrial core formation and Moon formation were constrained by the short-lived Hf-W systematic (Kleine et al., 2002; Lee and Halliday, 1995; Lee et al., 1997). The timing of late veneer was estimated from time-integrated addition of HSE to an Earth-like planet (Jacobson et al., 2014). The age of late heavy bombardment is based on impact ages of lunar basins (Cohen et al., 2005; Gomes et al., 2005; Tera et al., 1974).

1.1.1 Late accretion

Several terms are in use by various scientific societies to portray the different states of the Earth-Moon system. These terms are *late heavy bombardment*, *late veneer*, and *late accretion*. The original intention of introducing these terminologies is to address how the Earth acquired the last portion of its mass compositionally and dynamically. However, confusions arose over differences in the definitions of these terms. Therefore, it is necessary to retrospect the arguments and evidence which were used to define those terms.

The Late Heavy Bombardment was initially termed as "the lunar cataclysm" based on the narrow ages of 4.0-3.8 Ga, determined by U-Th-Pb, K-Ar and Rb-Sr methods, defined in impact-melt lunar rocks returned by the Apollo 17 mission (Tera et al., 1974). The late heavy bombardment was defined as the spike of intense meteoritic impact on the lunar surface between 4.0 Ga and 3.8 Ga. Before and after this time interval the magnitudes of meteoritic impacts defined by the ages of lunar impact-melt rocks might be far less significant. Since then this term has evolved from its initial connotation and has been interpreted in various ways. This extraordinary impact may have reset isotopic clocks of older rocks (Hartmann, 1975). Ryder, (1990) suggested that the age spike indicated that the intensity of meteoritic impacts before and after 4.0-3.8 Ga was not as prominent as the late heavy bombardment. However, this late heavy bombardment hypothesis was challenged by evidence for a declining impact influx that may have any remarkable spikes (G. Neukum and Ivanov, 1994; Hartmann et al., 2007; Morbidelli et al., 2012). Given its massive body and large gravitational cross-section, the Earth was speculated to be hit more intensively during the late heavy bombardment (Abramov et al., 2013; Cohen et al., 2005; Schoenberg et al., 2002). The coincidence of the late heavy bombardment and the earliest sign of life at around 3.85 Ga from Greenland sediments (Mojzsis et al., 1996) may suggest the evidence for the impact-induced habitability of the Earth.

The Late Veneer was proposed to explain the abundances of highly siderophile elements (iron-loving elements; Os, Ir, Ru, Rh, Pt, Pd, Re and Au; HSE) in the BSE. The coexistence of strong HSE depletion in the BSE relative to CI chondrites and their *near-chondritic ratios* were initially interpreted as results of chondritic influx during late heavy bombardment (Chou, 1978; Chou et al., 1983). Subsequent experiments on metal-silicate partition coefficients of HSE showed that the budgets of HSE are two orders of magnitude higher than expected in the equilibrium terrestrial differentiation model (Holzheid et al., 2000;

Mann et al., 2012). Although it was found that Ru/Ir and Pd/Ir in the BSE are superchondritic (Becker et al., 2006) and the partitioning behavior of Pd dependents on temperature, pressure, and oxygen fugacity (Righter et al., 2008), the combined effects of P-T-fO_2 did not yield partition coefficients of HSE nearly identical to each other (Morbidelli and Wood, 2014). In fact, the hypothesis of late veneer has been very much disputed (Kruijer et al., 2015; Maier et al., 2009; Touboul et al., 2015; Wang and Becker, 2013) until today. Recently, it was proposed that a significant amount of water on the Earth may also be delivered by late veneer (Wang and Becker, 2013), implying a link between the late veneer and the origins of volatile elements in the terrestrial mantle.

The Late Accretion, mainly defined by accretion models, does not refer to a particular event but take meteoritic impacts after the Moon-forming giant impact as a whole notion. Because no evidence for impacts within the first billion years is available on the Earth after extensive geological activities, the knowledge about late accretion was mainly acquired from studies on ancient crater records on extraterrestrial bodies, including the Moon and other planets in the inner solar system. The total mass that the Moon accreted can be calculated from the number and sizes of impact basins. Then, the total mass accreted by the Earth can be calculated by scaling the total accreted mass by the Moon to the accreted mass by the Earth by multiplying the Earth-Moon ratio of the gravitational cross-section. The conservative estimate for the accreted mass by the Earth can be calculated by assuming that the largest meteorite that bombarded the Earth is of the same size as Ceres with a diameter of ~900 km (Marchi et al., 2014).

Altogether, the term “late heavy bombardment” emphasizes the impact influx surge between 4.2-3.8 Ga on the Moon, “late veneer” refers to the relative chondritic ratios of HSE in the BSE, whereas the term “late accretion” describes the particular size-frequency distribution of projectiles that bombarded inner solar system bodies. This means that “late heavy bombardment” considers a specific time interval (4.2-3.8 Ga), the definition of “late veneer” requires a specific spectrum of composition (chondrites), and “late accretion” neither explicitly considers time nor composition but emphasizes the total masses accreted by the Earth and Moon after the Moon-forming giant impact.

1.1.2 Terrestrial differentiation

Terrestrial differentiation refers to the segregation of a metallic core from a silicate mantle. This process was thought to be the most significant event in the Earth's history, considering the core formed from a homogeneous body of the size of the present Earth (Li and Agee, 1996). However, it is more likely that the core segregated concomitantly with accretion (Wood et al., 2006). The information of core formation is mainly recorded by siderophile and chalcophile (sulfur-loving) element abundances in mantle peridotites that define the BSE (Becker et al., 2006; Chou, 1978; Fischer-Gödde et al., 2011; Meisel et al., 1996; Newsom and Palme, 1984; Wang and Becker, 2013, 2015a). The variable depletions of these elements in the BSE were either attributed to the core segregation as in the case of W, Mo, Cu and Ag, or to the late veneer as in the case of HSE and S, Se, and Te.

In equilibrium models, the terrestrial core segregation from the proto-Earth should have scavenged HSE and S, Se and Te completely from the overlying silicate mantle. Assuming crystallization of a shallow magma ocean on the eary Earth, other siderophile and chalcophile elements should have been depleted variably according to their metal-silicate or sulfide-silicate partition coefficients (Ertel et al., 1999). Metal-silicate partition coefficients obtained under low-pressure-temperature experiments advocate that HSE budgets of the BSE were accreted late after the core formation ceased. In the case of a deep magma ocean metal-silicate partition coefficients of siderophile elements would be variably lower than those of a shallow magma ocean (Brenan and McDonough, 2009; Mann et al., 2012). Then, the HSE abundances in the BSE might be a result of the mixing of residues of core formation and late veneer. In models of disequilibrium planetary accretion, a minor portion of the core of the Moon-forming impactor may have not been merged with the core of proto-Earth (Jacobson et al., 2014). This might have significantly elevated HSE, S, Se and Te abundances of the silicate mantle without requiring extra late veneer.

Early crust formation would further complicate the interpretation of HSE and S, Se and Te abundances of the BSE. Abundances of Pt and Pd in Archean komatiites were found to increase with time from 3.5 Ga to 2.9 Ga to estimate values for the BSE that are based on the HSE abundances in komatiite magmas (Maier et al., 2009). The increase of Pt and Pd in Archean komatiites was used to argue for a progressive homogenizztion of the late-accreted materials within the mantle. The progressive mixing model was challenged by more detailed studies on HSE in Archean komatiites (*e.g.* Puchtel et al., 2014) which did not show the

secular growth of HSE abundances of respective mantle sources. Positive ^{182}W anomalies in the Isua Greenstone Belt and Acasta Gneiss Complex (AGC) were interpreted to represent the pre-late veneer mantle which was isolated from mantle convection (Willbold et al., 2011; Willbold et al., 2015). However, this could only be true if the mantle sources of the Isua Greenstone Belt and Acasta gneisses are poor in HSE and S, Se and Te.

Thus, the attempt to trace the terrestrial differentiation by studying mantle peridotites can be supplemented by constraining HSE and S, Se and Te abundances of Archean mantle-derived and crustal rocks.

1.2 Magmatism of the Archean mantle-crust system

1.2.1 Representative rocks of the earliest crust

Archean crustal rocks are exposed in the stable cratons which are distributed on present-day continents. The well-documented cratons include the Slave craton and the Superior craton in North America, the Kaapvaal craton in South Africa, the Yilgarn craton and the Pilbara craton in Australia, as well as the North China craton in China. The oldest crustal rocks that ever have been identified were found in the Acasta Gneiss Complex (AGC) of the Slave craton from northwestern Canada. The AGC is used as the threshold between the Hadean and the Archean era (Guitreau et al., 2014). The crystallization ages of the AGC are 4030~3940 Ma as obtained from zircon U-Pb dating (Bowring et al., 1989b; Stern and Bleeker, 1998) which overlap with the timing of the late heavy bombardment (Mojzsis et al., 2014). The core of a zircon xenocryst yields a U-Pb age of 4203 ± 58 Ma, indicating that parental magmas of orthogneisses assimilated even older crustal materials (Iizuka et al., 2006b; Iizuka et al., 2009). The coupled Nd-Hf isotopic systematics of the AGC indicated that the older Hadean crust was not destructed after it formed at 4310 Ma years ago (Roth et al., 2014). Recent work on W isotopes of the AGC suggested that 3960 Ma rocks could have sampled an isolated pre-late veneer mantle (Willbold et al., 2015). Considering the iron enrichment, oxygen isotopes, negative Eu anomalies and unfractionated rare earth element patterns, Reimink et al., (2014) suggested that the tectonic setting of the AGC is similar to that of modern Iceland where the interaction of a mid-ocean ridge and a mantle plume cause the volcanic activities. From several points of view, the AGC is the key locality which could provide insights into processes that took place in the first billion years of the Earth. If the late heavy bombardment had impacted the Acasta area, not only HSE, and S, Se and Te

abundances would be significantly elevated (Sharp et al., 2014) but also chondritic ratios of these elements should be expected. On the other hand, if the parental magma of the AGC had

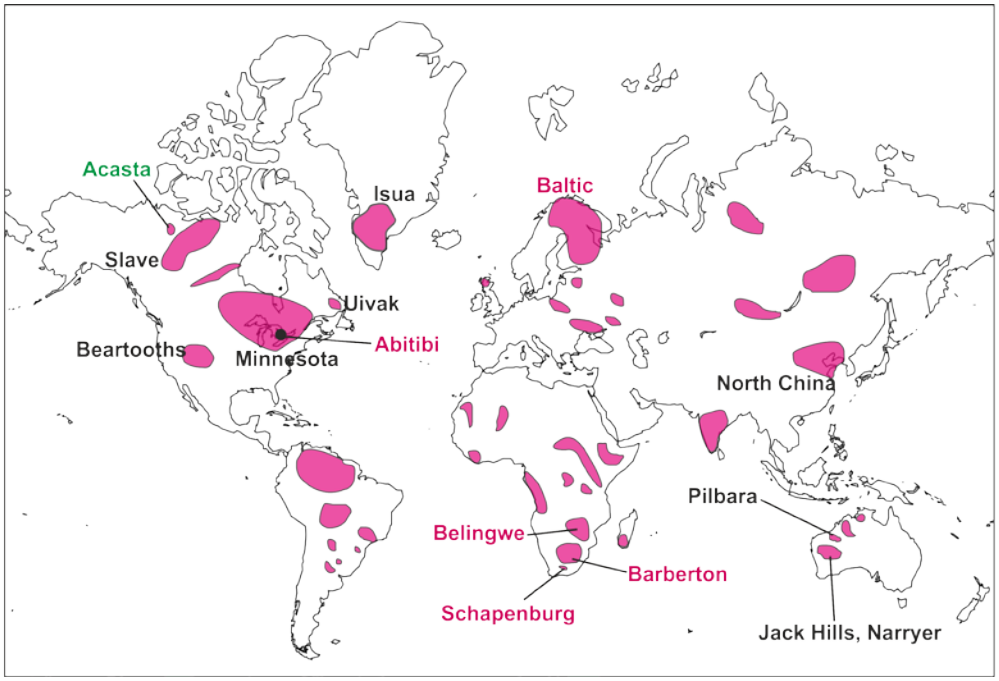

Figure. 1.2 Known Archean cratons and locations of the samples investigated in this dissertation. This map was modified on the basis of Bleeker (2003) and Tang et al. (2013).

tapped the pre-late veneer mantle, HSE and S, Se and Te abundances of AGC would be approximately 20 times lower than found in the BSE (Walker et al., 2004).

1.2.2 Representative rocks of the Archean mantle

Tholeiites and komatiites exposed in Archean greenstone belts sandwiched between felsic plutonic bodies are thought to be derived from the Archean mantle. Compared to Archean tholeiites, contemporary komatiites were produced by much higher degrees of partial melting (30-50%; Arndt et al., 2008) which should have exhausted mantle sulfides (Peach et al., 1990). The complete exhaustion of mantle sulfides makes komatiites suitable for constraining abundances of siderophile and chalcophile elements in the Archean mantle because incompatible chalcophile elements of comparable incompatibility should not be fractionated during magma transport and lava differentiation of a non-crustally contaminated komatiite magma. The pioneering work on HSE in Archean komatiites (Maier et al., 2009) showed a temporal increase of Pd and Pt abundances of Archean mantles, which was interpreted to reflect the slow mixing of late veneer into the terrestrial mantle. However, this

interpretation is challenged by subsequent studies on HSE abundances and Re-Os isotopic compositions of Archean komatiites (*e.g.* Puchtel et al., 2014). Highly siderophile element abundances of komatiites cannot just be related to eruption ages of komatiites. The 2.8 Ga Kostomuksha (Russia) komatiites have positive $\mu^{182}W$ values (deviation of $^{182}W/^{184}W$ in sample relative to that in the BSE; Touboul et al., 2012) but ~80% HSE abundances relative to the BSE (Puchtel et al., 2005). This is in contrast to the Barberton komatiites (South Africa) which have no W isotopic anomalies (Touboul et al., 2012) but 50% HSE abundances relative to the BSE (Puchtel et al., 2014). These conflictions promoted the critique whether abundance of HSE in Archean komatiites are a valid indicator for late veneer. Another group of chalcophile elements which could be used to be diagnostic for a late veneer signature in Archean komatiites is S, Se, and Te. Near-chondritic ratios of S, Se, and Te in modern peridotites were interpreted to result from a volatile-rich late veneer (Wang and Becker, 2013).

1.2.3 Fractionation of lithophile elements during partial melting

The approach of using canonical trace element abundance ratios of oceanic basalts, mainly mid-ocean ridge basalts (MORB), to map the trace element composition of mantle magma sources and further the BSE is generally accepted as a reliable approach (Arevalo Jr and McDonough, 2010; Gale et al., 2013; Hémond et al., 2006; Workman and Hart, 2005), although some canonical pairs, for instance, Pb/Ce, of oceanic basalts were found significantly variable (Sims and DePaolo, 1997). However, it is yet not known whether these canonical trace element abundance ratios of MORB can be also observed in mantle-derived rocks produced by high-degree of partial melting, such as komatiites.

Oceanic basalts are the products of moderate degree (<12%) partial melting during which clinopyroxene (cpx) controls the melt-silicate partitioning of trace elements (Baker and Stolper, 1994; Hirschmann et al., 1998). Therefore canonical trace element abundance ratios of oceanic basalts may not necessarily reflect the chemical composition of the mantle sources from which oceanic basalts were derived (Shorttle, 2015). The reason behind the convention of using canonical trace element abundance ratios to constrain the chemical compositions of the mantle is that partition coefficients of these elements are similar to mantle phases. If an element is hosted by several phases in certain proportions, ostensibly it may still keep constant ratios with other elements during the petrogenesis of MORB. However, it will be inaccurate to use these constant ratios to estimate the chemical composition of the mantle.

During the formation of komatiites, mantle phases may have been melted to the same extent as they are in the mantle (Arndt et al., 2008). This particular characteristic implies that the chemical composition of the mantle may be better deduced from Archean komatiites. Another specialty of komatiites is that different types of komatiites mainly reflect the retention of residual garnet. Garnet does not enter the melt during the formation of Al-depleted Barberton-type komatiites, whereas it is consumed in the petrogenesis of Al-undepleted Munro-type komatiites. Therefore, the role of garnet in the partitioning of trace elements can be investigated through different types of komatiites. For instance, experiments on silicate-melt partition coefficients showed that garnet is the main reservoir of In compared to other mantle phases (Adam and Green, 2006). Thus it is reasonable to expect that the relative abundance of In to other trace elements is higher in Al-undepleted Munro-type komatiites than in Al-depleted Barberton-type komatiites. However, to our knowledge, this issue has not been addressed *in extenso*.

1.3 Objectives of this dissertation

In this dissertation, a variety of rocks from the Acasta Gneiss Complex of northwestern Canada were measured for abundances of HSE and chalcophile elements and Os isotopes, with the aim of investigating the history of late meteoritic bombardments on the early Earth and terrestrial differentiation. Archean komatiites from localities across the world were analyzed for abundances of chalcophile and lithophile elements, with the objective to verify the chalcophile element composition of mantle based on mantle peridotites and magmatic fractionations of lithophile elements that are controlled by mantle heterogeneity and partial melting. The goal of this dissertation is to provide a coherent understanding of HSE, chalcophile and lithophile elements in the early mantle-crust system, which shall provide a more detailed knowledge about the meteoritic bombardment environment on the early Earth and time-intergrated evolution of late-accreted materials within the terrestrial mantle.

The present project is in general based on the China Scholarship Council (CSC) proposal designed by Harry Becker and drafted by Chunhui Li, with additional financial supports from Freie Universität Berlin and Trangregio TRR 170 (DFG). The work on the Acasta Gneiss Complex is in collaboration with Eric Scherer (Universität Münster) and Peter Sprung (Universität zu Köln). The studies on Archean komatiites are in collaboration with Igor Puchtel (University of Maryland).

1.3.1 Chapter 2: Highly siderophile elements, chalcophile elements and osmium isotopic compositions in Hadean-Eoarchean rocks of the Acasta region, northwestern Canada

Harry Becker designed the project and obtained the required sample powders from Eric Scherer and Peter Sprung. Chunhui Li carried out the sample digestion, column separation and performed the data analysis on the inductively coupled plasma-mass spectrometry (ICP-MS) and thermal ionization mass spectrometry (TIMS) as well as the data reduction and interpretation. All the work was done in Freie Universität Berlin.

Chapter 2 concerns the possibility of the late heavy bombardment of the oldest terrestrial rocks and the speculative pre-late veneer mantle reservoir. We analyzed the abundances of HSE and chalcophile elements (S, Se and Te) and Os isotopes in 21 samples from the Acasta Gneiss Complex. The samples comprise a felsic group of metadiorites, foliated gneisses, metatonalites and foliated metagranodiorites, and an ultramafic-mafic group of ultramafic cumulate, medium-grained metagabbros, layered metagabbros, amphibolites and hornblendites. Here we discuss the origin of these elements in Acasta samples and its implications for late meteoritic bombardments.

1.3.2 Chapter 3: Abundances of trace elements in the 2.7 Ga komatiites from Belingwe Greenstone Belt, Zimbabwe

Harry Becker designed the project and obtained the required sample powders from Igor Puchtel. Chunhui Li carried out the sample digestion, column separation and performed the data analysis on ICP-MS as well as the data reduction and interpretation. All the work was done in Freie Universität Berlin.

In Chapter 3 we discuss the fractionation of trace elements (S, Se, Te, Cu, Ag, Tl, In, Cd, Mo, Sm and Ba) in the well-preserved 2.7 Ga komatiites from the Belingwe Greenstone Belt (Zimbabwe). The data shed significant insight on the fractionation of these elements during partial melting and lava differentiation. The data show that ratios of these elements in Belingwe komatiites are comparable to those obtained from mantle peridotites. This chapter lays the foundation for understanding the behavior of chalcophile elements in other komatiites with a more complex history.

1.3.3 Chapter 4: Abundances of S, Se, Te, Cu, and Ag in Archean komatiites and komatiitic basalts: implication for the origins of chalcophile volatile elements in the terrestrial mantle

Harry Becker designed the project and obtained the required sample powders from Igor Puchtel. Chunhui Li carried out the sample digestion, column separation and performed the data analysis on ICP-MS as well as the data reduction and interpretation. All the work was done in Freie Universität Berlin.

In chapter 4, we deal with chalcophile element fractionation (S, Se, Te, Cu and Ag) in komatiites of more complex histories. We analyzed the abundances of chalcophile elements in komatiites and komatiitic basalts from the Abitibi Greenstone Belt (Canada), the Barberton Greenstone Belt (South Africa), the Schapenburg Greenstone Remnant (South Africa) and the Victoria's lava lake in the Vetreny Belt from the southeast Baltic Shield. The results reveal that secondary alteration and magmatic degassing (in the case of komatiitic basalts) significantly modified the chalcophile element composition and inevitably bring difficulties in interpreting the information they carried from the mantle.

1.3.4 Chapter 5: Abundances of In, Cd, Tl, Mo, Sm and Ba in komatiites and komatiitic basalts: implication for komatiite petrogenesis and mantle evolution

This study was designed by Harry Becker, and the required sample powders were obtained from Igor Puchtel. Chunhui Li carried out the sample digestion, column separation and performed the data analysis on ICP-MS as well as the data reduction and interpretation. All the work was done in Freie Universität Berlin.

Chapter 5 focuses on the question of lithophile element fractionation during the high degree partial melting. We examine the abundances of trace elements, including In, Cd, Tl, Mo, Sm and Ba, in Archean komatiites as studied in Chapter 4. The results show that igneous volatile loss has little influence on the interested elements, whereas secondary alteration can cause considerable modifications to these elements. The source heterogeneity is a dominant factor which leads to variable trace element abundance ratios.

Chapter 2

Highly siderophile element and chalcophile element abundances and osmium isotopic composition of Hadean-Eoarchean rocks of the Acasta region, north-western Canada

2.1 Abstract

Concentrations of highly siderophile elements (HSE) and strongly chalcophile elements (S, Se and Te), coupled with osmium isotopic compositions in the Acasta Gneiss Complex (AGC) from northwestern Canada, were utilized to constrain the effects of the Hadean meteoritic bombardment on these rocks and the mixing history of late accreted material in the Earth's mantle. The abundances of HSE, S, Se and Te in ultramafic cumulate, layered and isotropic metagabbros and various metamorphosed evolved crustal rocks are comparable to those in their Phanerozoic equivalents. Rhenium, Au, S and Pd display depletions in some rocks that are most likely related to partial mobilization of these elements into fluids, presumably at amphibolite-grade metamorphic conditions. Re-Os isotopic systematics were disturbed in most samples, most likely also due to fluid infiltrations in the postmagmatic metamorphism. Some samples display apparently undisturbed Re-S-Se-Te systematics. The T_{MA} Re-Os model age of metadioritic layer (AMS 031A) of 4.3 ± 0.2 Ga is consistent with the Sm-Nd age obtained on the same sample. The agreement of ages constrained by different isotopic systematics suggests that the metadioritic layer retained the chemical characteristics of the magmatic protolith. The similarity of the HSE and S-Se-Te abundances and ratios with Phanerozoic rocks of similar composition indicates that late veneer must have been homogenized in the mantle source of the Acasta gneisses substantially before 4.0-3.7 Ga. The Acasta gneisses also lack any impact-inducing abundance excesses of HSE and S, Se and Te, indicating that the crust in this area was not affected by a late heavy bombardment with chondritic material.

2.2 Introduction

The early Earth is characterized by multi-stage late additions of extraterrestrial components. After the Moon-forming giant impact, the Earth-Moon system may have been bombarded disproportionally by the late veneer and late heavy bombardment (LHB), which were speculated to have modified the physical and chemical states of the Earth dramatically. The largest body-size of late terrestrial impactors may be over 2500 kilometers in diameter (Bottke et al., 2010), which is massive enough for impactors to penetrate the upper continental crust and reach the middle or lower ones. Reservoirs formed by core-mantle segregation or early mantle differentiation may have survived these impact events, including the Moon-forming giant impact which could lead to a late terrestrial magma ocean. Since the half-life of ^{182}Hf-^{182}W systematic is ~8.9 Ma (Vockenhuber et al., 2004), excesses of ^{182}W in terrestrial rocks can be used to constrain processes of terrestrial differentiation. Recent studies on ^{182}W in terrestrial rocks revealed the existence of long-survived isolated reservoirs which may not have been influenced by late impact events (Rizo et al., 2016; Touboul et al., 2014; Touboul et al., 2012; Willbold et al., 2015). Though the mantle sources of 3.8-3.3 Ga ultramafic rocks of the Isua greenstone belt and 2.8 Ga Kostomuksha komatiites do not show strong depletions in highly siderophile (iron-loving) elements (HSE) compared to Phanerzoic mantle peridotites, positive anomalies of μ^{182}W (~15 ppm) were found in the these samples (Rizo et al., 2016; Touboul et al., 2012). Comparable positive μ^{182}W anomalies (15 ± 2 ppm) were also found in the 3.96 Ga Acasta gneisses of Northwest Territories, which were interpreted to represent a pre-late veneer (Willbold et al., 2015).

Highly siderophile elements (Re, Os, Ir, Ru, Rh, Pt, Pd and Au) and strongly chalcophile (sulfide-loving) elements (S, Se and Te) are excellent indicators of intense meteoritic bombardment. The highly siderophile and strongly chalcophile elements in the Earth should have substantially partitioned into the metallic core (Mann et al., 2012; Rose-Weston et al., 2009), leaving behind an extremely HSE- and strong chalcophile element-depleted silicate mantle. The early crust extracted from such a HSE-poor mantle should be similarly or even more depleted in these elements and be characterized by significant fractionation between compatible IPGE (Os, Ir and Ru) and less compatible PPGE (Rh, Pt and Pd) and chalcophile elements. This is mainly because these elements are compatible to moderately incompatible during terrestrial magmatism (Harvey and Day, 2016). Any subsequent meteoritic addition to such a crust would elevate the abundances of highly siderophile and chalcophile elements remarkably, and even be able to reset the relative

element abundances of PGE to be near-chondritic if the added material had a chondritic composition. Some of the elements of interest, including Os, Re, S, Se and Te, are also volatile during terrestrial magmatism (Greenland and Aruscavage, 1986; Handler et al., 1999; Lassiter, 2002; Norman et al., 2004), and phases containing these elements could be vaporized by the heat of intense meteoritic impacts. Therefore, volatile losses of Os, Re, S, Se and Te, coupled with enrichments of non-volatile Ir, Ru, Pt and Pd, could be inferred to reflect the involvement of meteoritic materials.

Besides of timing melt extraction events, ^{187}Re-^{188}Os isotopic systematic in early crustal rocks can also provide constraints on impact events. In contrast to the compatible Os which is retained in the mantle source, incompatible Re is extracted into mantle-derived melts during partial melting. Therefore, time-integrated growth of isotopic ratios of ^{187}Os and ^{188}Os in mantle-derived rocks would be interrupted and reset by sudden additions of extraterrestrial components, yielding Re-Os model ages older than the Earth. Two end members mixing trends of Os isotopes may be observed if the HSE- and chalcophile element-depleted crust was bombarded by materials of chondritic composition, as shown in some lunar rocks (Fischer-Gödde and Becker, 2012).

Through the investigation of HSE abundances in the Earth's early crust, we can better understand the mixing history of late-accreted meteoritic components within the terrestrial mantle. Based on a secular increase of PPGE abundances of the mantle sources of Archean komatiites, Maier et al., 2009 suggested that the late-accreted meteoritic material may have not been homogenized in the mantle until 2.9 Ga. The progressive mixing model, however, was challenged by subsequent more detailed studies of HSE abundances of Archean komatiites (Puchtel et al., 2014). These studies showed that the abundances of HSE in mantle sources of Archean komatiites of different ages did not simply increase from older to younger komatiite lavas. These authors advocated that the variable HSE abundances of Archean komatiite sources probably reflected a slush mixing of meteoritic components within a hypothesized magma ocean in the early history of the Earth (*e.g.* Puchtel et al., 2014). At least in some segments of the Earth's early crust, abundances of HSE should be lower than those of the modern continental crustal rocks if the late-accreted meteoritic materials were not entirely homogenized within the mantle before 3 Ga.

The Acasta Gneiss Complex (AGC) of northwestern Canada bears the oldest known crustal rock fragments. Ion microprobe U-Pb analyses of zircons suggested that the AGC was the oldest gneisses on the Earth (Bowring et al., 1989b). The oldest age obtained by the

authors was 3.96 Ga. Ten years later they reported an older zircon of 4.03 Ga by using SHRIMP zircon U-Th-Pb dating (Bowring and Williams, 1999), and then an zircon of 4.2 Ga was discovered to be magmatic (Iizuka et al., 2006b). Another younger cluster of zircon of ~3.6 Ga was reported as well (Iizuka et al., 2009). The age distribution of the AGC, 4.2 Ga to 3.6 Ga, overlaps with the proposed timing frame of the late heavy bombardment (LHB; Fernandes et al., 2013; Tera et al., 1974), making the AGC the best site for studying the influence of the LHB on the Earth. Although the signal of the LHB, as displayed as HSE, S, Se and Te abundances of the AGC, may be affected by multi-stage crustal reworking, abundances and fractionation of HSE, S, Se and Te in the AGC may have been inherited from their precursor lithology. Tungsten isotope composition of rocks from the AGC showed that the 3.96 Ga AGC components may have sampled a pre-late veneer reservoir (Willbold et al., 2015). Because HSE, S, Se and Te in the modern silicate Earth bear the signature of late accretion, rocks older than 3.96 Ga may be significantly depleted in HSE, S, Se and Te.

Here we report the first dataset of HSE, S, Se and Te abundances and osmium isotopic compositions of rocks from the AGC by applying the isotope dilution technique. Because abundances of these elements are low in continental crustal rocks, especially HSE, data quality is an important issue. The influence of mantle composition, impacts and the subsequent polymetamorphic history on these elements will be discussed.

2.3 Geological background and sample descriptions

The AGC, located on the western border of the Archean Slave Craton, is exposed along the Acasta River, north of Yellowknife (Northwest Territories, Canada; Bleeker, 2003; Bowring and Williams, 1999; Iizuka et al., 2007b). The AGC has two tectonomagmatic units. The western unit comprises a layered gneiss series which are interlayered with foliated metagranites that preserve igneous textures, whereas a felsic gneiss series with interlayered medium-grained metagabbros constitute the eastern unit. In the lake between the two units, an island was blasted with explosives and fresh specimens of several potential precursors to the AGC were exposed. Northwest-southeast striking mafic dikes crosscut the two units dispersedly, and various enclaves and inclusions sharply contact with their hosts. A detailed

geological map of the Acasta area were provided by previous publications (Bowring and

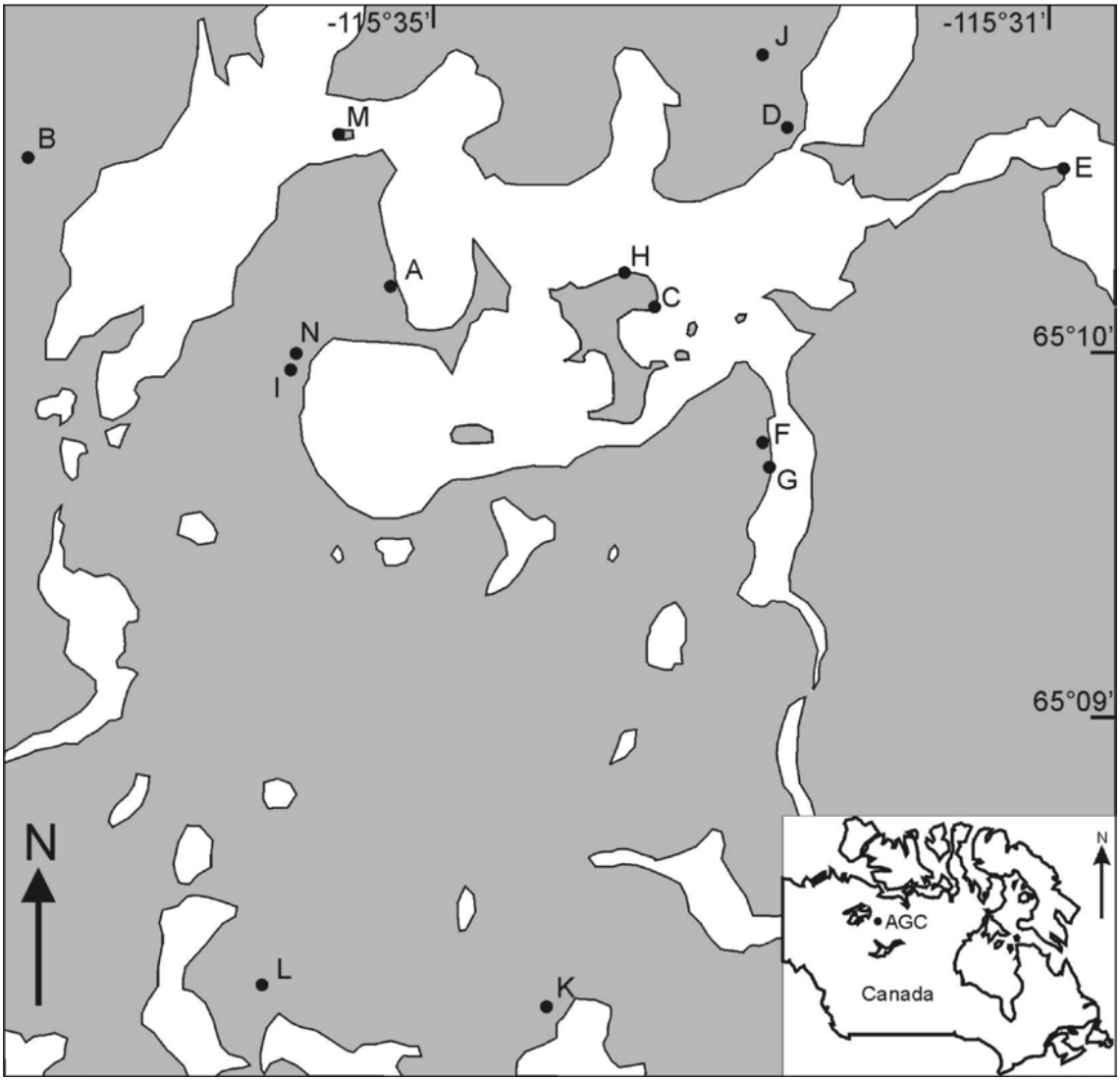

Fig. 2.1 Simplified geological map of the Acasta Gneiss Complex, Slave Province, northwestern Canada (Sprung, 2010). The locations of the analyzed samples are indicated.

Williams, 1999; Guitreau et al., 2014; Iizuka et al., 2007a; Mojzsis et al., 2014). In Fig. 2.1 the locations of the interested samples are indicated. The interested samples comprise an ultramafic-mafic series of ultramafic cumulate, garnet amphibolite, hornblendite, medium-grained metagabbros and layered metagabbros, and a felsic series of metatonalite-trondhjemite-granodiorite (TTG), metadioritic layers and metagranites.

Ultramafic rocks

AMS 024 was sampled from a dyke-like ultramafic body to the east of the AGC (not indicated in Fig. 2.1). The field investigation suggested that AMS 024 (Fig. 2.2A) may relates to the younger 2.7 Ga greenstone belts. AMS 043A is a garnet amphibolite band sampled from a layered to finely layered gneiss at location G. Amphibole are rotated around garnet and quartz and plagioclase appear to fill in the shadows of garnet (Fig. 2.2B). AMS 004 is a hornblendite lens collected from location C at the central island of the Acasta River. Hornblendite lenses exposed at the boundary between mafic and felsic gneisses are commonly associated with metagranite veins or gabbroic gneiss.

Mafic rocks

A strongly deformed layered metagabbro (AMS 054; Fig. 2.2C) was sampled at location B. AMS 054 was split into two hornblende-, plagioclase-, and biotite-bearing layers (AMS 054A, C) and one biotite-free layer (AMS 054B) that shows recrystallization of plagioclase in thin section. Another layered metagabbro (AMS 038) intruded by a light metatonalite (AMS 040) was collected at location F.

Medium-grained metagabbros (AMS 007B, AMS 048B and AMS 049) were collected from a ~170 × 70 m enclave of medium-grained metagabbro at location D in Fig 2.1. Although being veined to various degrees by secondary quartz, medium-grained metagabbros preserve an igneous gabbroic texture (Fig 2.2D). These samples were collected within 10 m of each other.

A gabbroic gneiss collected at location C of the central island can be divided into two parts, once at direct contact with coarse K- feldspar-bearing metagranodiorite and another in a domain (AMS 003) virtually free of veins.

Continental crustal evolved rocks

Locality A (AMS 030A-B and AMS 031A)

This outcrop is approximately 200 m north of SAB94-134 (Bowring and Williams, 1999) and BNB99-15B (Mojzsis et al., 2014), consisting of heterogeneous layered gneisses with layering at mm to dm scale. The geological meaning of U-Pb zircon ages of samples from this outcrop was interpreted differently. Bowring and Williams 1999 suggested that zircon ages of 4031 ± 3 Ma should represent the igneous event that formed the protolith of the gneiss (Bowring and Williams, 1999), whereas Mojzsis et al., 2014 argued that pre-4000 Ma

zircons of the AGC were inherited from pre-existing older crustal rocks and the main body of the AGC formed around 3920 Ma (Mojzsis et al., 2014).

Sample AMS 030 was cut along the foliation into five separate layers. Of these, AMS 030A-B can be compared to lithology 1 from BNB99-15B**,** which yielded a U-Pb zircon age of 4004 ± 13 Ma (Mojzsis et al., 2014). It differs from the other layers in containing significantly more biotite and plagioclase but less quartz. Sample AMS 031 (Fig. 2.2.E), sampled approximately 0.5 -1 m from AMS 030, was separated into a more mafic layer (AMS 031A) dominated by plagioclase, biotite and hornblende, and another crosscutting granitic vein.

Locality C (AMS 001, AMS 003 and AMS 009)

This outcrop on the northeastern end of the central island was blasted with explosives and thus provides access to fresh specimens. All samples collected here were sampled from boulders that correspond to rock types identified in the outcrop. Granitic veins and a metagranite dike (AMS009) intruded all other rock types. Besides trace zircon and minor mica veins, AMS 009 consists almost entirely of quartz and reddened K- feldspar (Fig. 2.2.F). A dark, hornblende-, plagioclase- and biotite-rich gabbroic gneiss was sampled twice: once at direct contact with coarse K- feldspar-bearing metagranodiorite and in a domain (AMS 003) virtually free of veins. Two metatonalite samples differ from each other in that one samples contains garnet (AMS 001) and the other lacking no garnet. Hornblendite lenses are commonly associated with metagranite veins or gabbroic gneisses and exposed at the boundary between mafic and felsic gneisses (Iizuka et al., 2007b).

Localities H (AMS 013)

At locality H, foliated metagranodiorite (AMS 013), containing abundant partly reddened K- feldspar, and small amounts of preserved muscovite, was sampled. Previous in-situ U-Pb zircon dating of a sample from the same outcrop yielded a 3370±7 Ma age of zircon domains with igneous zoning and inherited zircon cores having ages up to 3824 Ma (Bleeker and Stern, unpublished).

Locality F (AMS 040, AMS 041, and AMS 043A)

There are five lithotypes that exhibit partially preserved crosscutting relationships: A layered metagabbro (AMS 038) was intruded by a light metatonalite (AMS 040). A dike of

metadiorite (AMS 041) intruded into a darker metatonalite (AMS039). Metagranite veins scaling from mm to a few cm widths cut across all other rock types in the outcrop. In-situ U-Pb dating of zircon yielded crystallization ages of ~3600 Ma for the metagranite and the light metatonalite and ~3750 Ma for the metadiorite.

Locality G (AMS 050) and K (AMS 053)

Locality G and K are within the southern part to the geological map of the Acasta region (Iizuka et al., 2006a; Iizuka et al., 2007b). AMS 050 is a garnet-bearing metatonalite, and AMS 053 is a weakly foliated tonalitic gneiss.

Rocks from Massiccio dei Laghi

Besides rocks from the AGC, four magmatic rocks of the Massiccio dei Laghi, Southern Alps (Northwest Italy) were analyzed in comparison with the investigated rocks of the AGC. The intrusion age of these rocks, constrained by Rb-Sr whole-rock, is around 275 Ma (Pinarelli et al., 1988). These late Permian intrusive rocks are considered to be representatives of post-Archean continental crustal rocks.

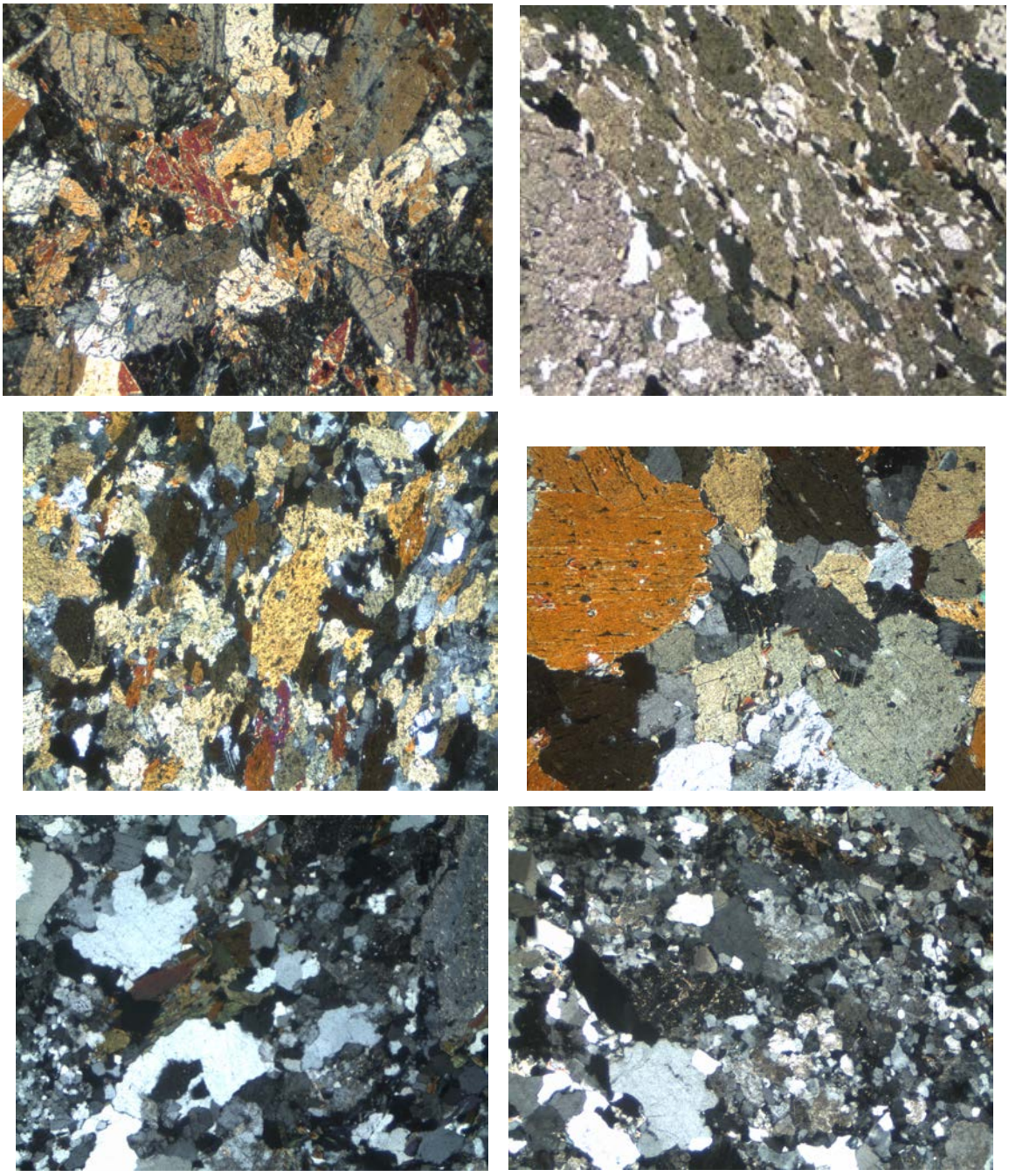

Fig. 2.2 Thin section photographs of ultramafic cumulate AMS 024A (A), garnet amphibolite AMS 043A (B), layered metagabbros AMS 054A (C), medium-grained metagabbro AMS 007 (D), metadioritic layer AMS031A (E) and metagranite AMS 009 (F). Amphibole, amp; biotite, bi; pyroxene, pry; K-feldspar, kfs; garnet, grt; plagioclase, pl; quartz, qrt.

A

B

2.4 Analytical methods

2.4.1 Sample digestion

Concentrated reverse aqua regia combined with high-pressure asher (HPAS, Anton Paar^{TM}) was employed to digest the samples. Detailed analytical protocols were published previously (Fischer-Gödde et al., 2011; Gleißner et al., 2012; Wang et al., 2013). Around 2.5 g sample powder with ^{185}Re, ^{190}Os, ^{191}Ir-^{99}Ru-^{194}Pt-^{105}Pd, ^{77}Se-^{125}Te and ^{34}S spike solutions were mixed with 2.5 ml 9 mol l^{-1} HCl and 5 ml 14 mol l^{-1} HNO_3 into 90 ml HPAS vessels. The acids used for digestion were two times quartz and two times Teflon distilled (sub-boiling; 2QD2TD). Immediately the vessels sealed by Teflon-tape were heated in a HPAS for 16 hours at 320 ℃ under 100 bar. Subsequently the vessels were taken out of the HPAS, the digested acid solutions were transferred into 50 ml Teflon-tubes which were placed in ice water to prevent Os evaporation.

2.4.2 Chemical separation

Liquid parts of digestion solutions were immediately transferred into 50 ml Teflon tubes with 3 ml $CHCl_3$. After the tubes were vertically vibrated (by hand) and centrifuged for several minutes, $CHCl_3$ with Os was extracted into 15 ml Teflon beakers with 4 ml HBr. Following another 3 ml and 2 ml $CHCl_3$ were added into the digestion solutions and the homogenization and extraction processes were repeated. Teflon beakers with 4 ml HBr and 8 ml $CHCl_3$ with Os were capped and heated for several hours at 80-85 ℃ to ensure the complete back-extraction of Os from $CHCl_3$ into HBr. After cooled down to room temperature, immiscible $CHCl_3$ was drawn out, leaving behind HBr for further evaporation. Around 40 µl HBr with Os was left and transferred to the cap of a 5 ml conical bottom beaker for further complete evaporation. 15 µl HBr was placed into the conical bottom of Teflon vial. Around 30-60 µl H_2SO_4-dichromote solution was added onto the cap where the Os-HBr solution was dried down. The cap was screwed to the vessel. Subsequently the Teflon vessel warped by Al foil was place inverted on the hotplate at 80-85 ℃ for several hours. The purified Os was concentrated into 15 µl HBr which was ready for Os isotope measurements.

The chemical separation method of HSE aliquots in this study mainly followed the previous studies (Becker et al., 2006; Fischer-Gödde et al., 2011). Column calibrations of 10 ml cation resin (100-200 mesh) were carried out to check the elution curve of the HSE in

Permian diorite (GL 21) and appinite (GL 14) from northwest Italy. Based on the previous method (Fischer-Gödde et al., 2011), 0.5 mol l^{-1} HCl-40% (v/v) acetone (60% 0.83 mol l^{-1} HCl + 40% distilled acetone) was applied to equilibrate the pre-cleaned cation exchange column and collect the elution. 20 ml HCl-acetone solution were used for column equilibrations prior to the sample loading. 10 ml sample dissolved in the same HCl-acetone solution was loaded on the column by three cuts of 4 ml, 3 ml and 3 ml, and the elution was collected respectively. 17 ml HCl-acetone solution was added to the column by another five cuts of 3 ml, 3 ml, 2 ml, 6 ml and 3 ml, and the elution was also collected respectively. Intensities obtained by using a single pass Scott-type spray chamber showed that intensities of Rb and Cd were very high. Tough Aridus, which could yield very low oxidation rates (CeO/Ce = 0.5-1%), was used to reduce the interference of Rb-O on Ru, samples of low Ru abundances Rb still may be influenced. Cadmium can be removed by a clean-up procedure using 2 ml pre-clean cation resin of 100-200 mesh (Fischer-Gödde et al., 2011). Intensities of Zr reached a spike at the second cut in appinite GL 14, but no Zr spike was observed in diorite GL 21. Therefore, the Zr spike observed in GL 14 might indicate the over-abundance of accessory zircon, which was not the case in GL 21. Because the Acasta samples likely have variable Zr contents, during the analysis of Pd in the Acasta samples intensities of Zr were also monitored.

On the basis of a two-step ion exchange chromatography chemical separation procedure (Fehr et al., 2004; Wang and Becker, 2014; Wang et al., 2013), the separation of Te was facilitated by an extra 9 mol l^{-1} HCl step after samples were loaded to separate Pd, Ag and Cd. Finally, Te was collected in 6 ml 0.4 mol l^{-1} HCl. Recoveries of S and Se in this method were satisfying (Wang and Becker, 2014), but the recovery of Te depends on matrix compositions. Ferric iron compounds may form during HPAS digestion and absorb some Te, resulting low Te intensities (see 2.4.5).

2.4.3 Mass spectrometry

In this study, we principally utilized the Os isotopic measurement methods (Birck et al., 1997; Creaser et al., 1991; Völkening et al., 1991) with several improvements. 2.8 ampere electric current was used for baking platinum filaments, and 0.5 ampere for evaporating Os-containing HBr and 0.6 ampere for drying down activator-$Ba(OH)_2$. The 35 µg/g UMD Os standard in HBr was diluted to 10 ng/g by HBr to be comparable to the Os abundance of samples. Pipette tips were precleaned in hot <1 mol l^{-1} HCl for more than 24 hours. The total

procedural Os blank was lower when using cooked tips, indicating that the amount of Os contributed by tips should be taken into consideration when investigating Os-poor samples. Osmium isotope ratios were determined by negative thermal ionization mass-spectrometry (TIMS; Thermal-Finnigan^{TM}, Freie Universität Berlin) in the peak hopping mode using a static multiple collector. In-run precisions of all samples were normally better than 0.2% double relative standard error (2 RSE) at > 80000 counts per second for intensities of ^{190}Os. During this study, ^{187}Os/^{188}Os of 10 ng/g aliquots of the UMD Os standard was 0.114 ± 0.008 (1 STD, n = 15) which is in the range of reported values. Details of mass spectrometric methods on the ICP-MS can be found in publications (Fischer-Gödde and Becker, 2012; Fischer-Gödde et al., 2011; Gleißner et al., 2012; Wang and Becker, 2014; Wang et al., 2013). As mentioned before, ^{85}Ru, ^{87}Sr, ^{89}Y and ^{94}Zr were also monitored in order to better understand the influence of isobaric interferences.

2.4.4 Analytical blanks

Total procedural Os blanks were 0.1-0.5 pg with ^{187}Os/^{188}Os of 0.3-6.2. The average Os blank is 0.2 ± 0.1 pg (1 STD, n = 5) with ^{187}Os/^{188}Os of 2 ± 2 (n = 5). Other HSE procedural blanks during this study were 1.3 ± 0.7 pg for Re, 1.0 ± 0.5 pg for Ir, 1 ± 1 pg for Ru, 50 ±10 pg for Pt, 50 ± 10 pg for Pd and 3 ± 2 pg for Au. The S procedural blanks vary from 1.5 μg to 9.4 μg with a mean of 6 ± 3 μg. The cation resin represents the main contributor to S blanks. Because of the instability of the background during hydride generation, total procedural blanks of Se varied from 0.1 to 2.5 ng with a mean of 1.3 ± 0.9 ng; total procedural blanks of Te vary from 3 to 25 pg with a mean of 12 ± 8 pg. Due to the lithogic diversity, blank contributions of different elements vary from sample to sample, for instance blank contributions of S vary from ~ 1% in the majority of samples to 69% in AMS 004. The limit of detection (LOD), which is the lowest concentration can be reliably detected, was defined as the total procedural blank plus its 3 × standard deviation.

2.4.5 Data quality

The low abundances of HSE in most crustal samples from this study lead to relatively large uncertainties. In addition the potential influence of isobaric and molecular interferences in specific samples must be evaluated carefully. Intensities of Ru isotopes in garnet amphibolite (AMS 043A) and garnet-bearing metatonalite gneiss (AMS 050) were comparable to that of background intensities of 0.28 mol l^{-1} HNO_3. Oxides of Rb and Sr and

Zn argides may interfere with Ru measurements in these samples. Owning to the very low intensities of ^{101}Ru and interferences from Zn argides, $^{102}Ru/^{101}Ru$ and $^{104}Ru/^{101}Ru$ of medium-grained metagabbros (AMS 007, AMS 048 and AMS 049) and garnet-bearing amphibolite (AMS 043A) were lower than the natural ratios. Though intensities of Zn in samples were not monitored, results of column calibration showed high intensities of Zn in appinite GL 21 and diorite GL 14, indicating the potential of Zn argides. Similarly, intensities of Pt in metatonalite (AMS 001), metagranite (AMS 009) and medium-grained metagabbro (AMS 048B) were comparable to that of background intensities of 1 mol l^{-1} HCl. Consequently, these data cannot be used.

The application of hydride generation ICP-MS to determinations of Te in mafic rocks was problematic. This was attributed to some transition elements hindering the HG reaction and conversion of Te^{+4} to Te^{-2} (Yu et al., 1983). Recent work showed that sample matrix affected Te yields and intensities of Te in peridotites, gabbros and komatiites which had significant amount of precipitates and potential undigested material after HPAS digestion (Wang et al., 2013). Their observations were confirmed by this study, especially by comparison of intensities of Te in garnet amphibolite AMS 043A and its HPAS residue (details of the residue are in the next passage). Though the residue of AMS 043A has 0.99 ng/g Te, intensities of ^{125}Te were over 1 million counts per second. In contrast, intensities of ^{125}Te in AMS 043A were seldom higher than 10 000 counts per second. Furthermore, intensities of the spike isotope ^{125}Te in AMS 043A were lower or comparable to ^{126}Te. This demonstrates that HG reaction of Te were inhibited by some cations of transition elements, whereas these elements did not perform significant role in case of matrix-free or little matrix HPAS digestions. The sample-acid contrast of intensities of ^{125}Te in metagabbros, garnet amphibolite and hornblendite were also lower than expected. Therefore, these Te data obtained by HG cannot be used.

Due to a large amount of rock powders (~2.5 g) digested in this study, about 1.5 g of precipitates and potential undigested material remained after HPAS digestion. The precipitates and undigested material of garnet amphibolite AMS 043A and metadioritic layer AMS 030A-B were rinsed 5 times in nanopure water and centrifuged each for 15 minutes to remove the spikes added during the HPAS digestion. The rinsed water was quickly analyzed by ICP-MS to check whether spikes were still left in the residues. After being rinsed 5 times spikes were removed out of the solid residues completely. The cleaned residues of AMS 043A and AMS 030A-B were dried, weighted and mixed with ^{185}Re, ^{191}Ir-^{99}Ru-^{194}Pt-^{105}Pd, ^{77}Se-

^{125}Te and ^{34}S spike solutions with 5 ml ultrapure 24 mol l^{-1} HF (47-51%, J.T. Baker®) and 10 ml 14 mol l^{-1} HNO_3 in 60 ml Teflon beakers. The beakers were heated on the hotplate at 150 ℃ for 72 hours. No solid particles were spotted after HF-HNO_3 digestion visually. The chemical separation procedure and mass spectrometric methods for the residues of AMS 043A and AMS 030A-B were the same as that used for samples. The abundances of Au in the residue of AMS 030A-B is 0.050 ng/g (see 2.8). This is unlikely true because more than 90% of all the other elements were released by the reverse aqua regia-HPAS digestion method. The high Au abundance of the residue of AMS 030A-B likely reflects analytical problems. Abundances of S, Se and Te in the residue of AMS 043A account for 12-18% of the total element abundances, implying the existence of undigested trace sulfides included in silicates. Overall, with a few exceptions, the reverse aqua regia-HPAS digestion method applied to these rocks released all the HSE budgets. Details about the analysis of the residues can be found in 2.8.

The total uncertainty on element abundance consists of contributions from the uncertainty of spikes, the uncertainty of instrumental analysis and the uncertainty propagated from blank to sample. For instance, the relative standard deviation (2 RSD) of ^{34}S spike solution was 0.6%, the instrumental uncertainty (2 RSD) was typically 1%, and the uncertainty (2 RSD) contributed from intensities of ^{34}S in blanks to ^{34}S in samples is 0.8%. The total uncertainty (2 RSD) was defined as the sum of the three independent uncertainties. In the case cited above, the total uncertainty would be 2.4 %, which is the relative standard deviation of the S abundance. For instance, if the abundance of S in a specific sample is 250 µg/g, then the standard deviation (2 SD) is 250 µg/g × 2.4% = 6 µg/g. In Table 2.1, the abundance of S in this example would be expressed as 250(6) µg/g.

2.5 Results

2.5.1 HSE, S, Se and Te abundances

The whole rock HSE, S, Se and Te abundances of rocks from the AGC are given in Table 2.1 and their BSE-normalized patterns are presented in Fig. 2.3-2.5. The sequence of the elements in the BSE-normalized diagrams are in the order of increasing incompatibility during partial melting of the mantle (Harvey and Day, 2016; Wang et al., 2013). Abundances of ^{192}Os are utilized instead of Os abundances in the BSE-normalized patterns to avoid distorting effects from the contribution of radiogenic ^{187}Os from the *in situ* decay of ^{187}Re.

As displayed in the BSE-normalized diagram (Fig. 2.3), the ultramafic cumulate AMS 024 is characterized by a slightly fractionated HSE, S, Se and Te pattern. The Pd/Ir is four times higher than that of the BSE (Becker et al., 2006). The S/Se is ~6 times higher than that of the BSE, whereas the Se/Te of AMS 024 is considerably lower than that of the BSE (Wang and Becker, 2014). The $Re/^{192}Os$ (2.8-4) of AMS 024 is *c.a.* 6 times higher than that of the BSE (Becker et al., 2006).

The most fractionated BSE-normalized patterns (Fig. 2.3) are shown by garnet amphibolite (AMS 043A) and hornblendite (AMS 004). The IPGE and Pt abundances of AMS 043A are close to the LOD, whereas abundances of Pd, Au and Re in AMS 043A are relatively high for normal crustal rocks. The Re abundance of AMS 043A is the highest among the investigated samples, leading to $Re/^{192}Os$ of 28 000. The hornblendite pod AMS 004 displays depletions of Au and Se relative to their neighboring elements. The abundance of S in AMS 004 was lower than the LOD.

The layered metagabbros investigated in this study show BSE-normalized patterns different from each other (Fig. 2.4). The layered metagabbro AMS038 is characterized by strong fractionation between PPGE and IPGE and Au depletion. Abundances of IPGE in the layered metagabbro AMS 054A are significantly higher than those in AMS 038, and Au is enriched in AMS 054A.

Element abundances of the analyzed medium-grained metagabbros are comparable to each other (Table 2.1), though Ir, Ru, Pt and Pd abundances are in the range of the LOD. The BSE-normalized patterns of Se, Re and S in these samples are similar and relatively flat, with depletions of Re in two of the samples (Fig. 2.4).

Evolved continental rocks from the AGC are characterized by fractionated BSE-normalized patterns, which are not systematically different from each other (Fig. 2.5). Palladium abundances of metadioritic layers AMS 030A-B and AMS 031A are depleted compared to neighbor elements and are lower than the LOD. Abundances of Re vary between undepleted and depleted relative to Se and S, similar as in medium-grained metagabbros (Fig. 2.4). Metagranite and metagranodiorite tend to have the lowest abundances of HSE and chalcophile elements.

Except the enrichment of Au in the Permian intermediate to felsic rocks of the Massiccio dei Laghi (Fig. 2.5), abundances of the other elements are comparable to the rocks

of the AGC. Metagranite BB 6 differs from the other Permian rocks in high Re abundance (0.252 ng/g) and low Au abundance (0.382 ng/g).

Table 2.1 Highly siderophile element and strongly chalcophile element abundances, and osmium isotopic compositions of samples from the Acasta Gneiss Complex. Data on rocks from Massiccio dei Laghi, South Alps (Northwest Italy) are shown for comparison.

Locality	Sample	Rock type	Re	Os	^{192}Os	Ir	Ru	Pt	Pd	Au	S	Se	Te	^{187}Re/^{188}Os	^{187}Os/^{188}Os	$T_{(MA)PM}$
	Ultramafic		ng/g	ng/g	ng/g	ng/g	ng/g	ng/g	ng/g	ng/g	µg/g	ng/g	ng/g			Ga
	AMS 024[4]	ultramafic rock	1.27(1)	1.117	0.456	1.35(1)	6.73(1)	6.43(3)	11.9(1)	1.45	617(22)	105(4)	23(3)	1.699(3)	0.13765(8)	-
	duplicate[19]		1.89(2)	1.165	0.430	1.32(1)	7.38(1)	7.62(5)	11.2(1)	1.76	628(12)	89(10)	27(8)	7.828(4)	0.13725(8)	-
C	AMS 004	hornblendite pod	0.284(4)	0.0023	0.0007	0.53(2)	1.70(2)	5.6(9)	10.7(5)	0.054	7.4(1)	12(2)	-	793(193)	2.5(6)	0.18(6)
F	AMS 043A[13]	garnet amphibolite	13.8(5)	-	-	0.0045(1)	0.011(1)	0.170(3)	100(18)	-	1419(74)	129(4)	-	-	-	-
F	*duplicate*[16]		14.0(8)	0.5550	0.0006	0.0030(3)	0.001(2)	0.140(3)	66(25)	4.91	1437(127)	145(6)	-	-	-	*4(5)*
F	*duplicate*[31]		12(2)	0.5043	0.0012	0.0005(1)	0.001(1)	0.151(2)	-	5.66	1459(30)	96(4)	-	79099(42725)	4929(2668)	*4(3)*
F	*duplicate*[46]		16(2)	0.5897	0.0007	0.0031(1)	0.015(1)	0.016(2)	42(28)	4.04	-	-	-	57412(17595)	3268(1004)	*3(1)*
	Mafic															
B	AMS 054A	layered metagabbro	0.220(3)	0.365	0.146	0.339(4)	0.587(4)	6.8(6)	12.4(5)	5.61	157(7)	53(2)	-	2.98(1)	0.3180(1)	4.29(2)
F	AMS 038	layered metagabbro	0.104(3)	-	-	0.0020(1)	0.020(1)	-	4.32(7)	0.061	244(17)	40(4)	-	-	-	-
D	AMS 007B	medium-grained metagabbro	0.124(6)	0.0159	0.0007	0.0044(2)	0.006(1)	0.052(2)	9.7(2)	0.152	84(4)	33(2)	-	25.4(6)	5.58(9)	-
D	ANS 048B[2]	medium-grained metagabbro	0.078(4)	0.0064	0.0013	0.0037(2)	0.005(1)	-	-	0.161	330(16)	90(4)	-	45.7(3)	11.7(6)	-
D	*duplicate*[17]		0.094(3)	0.0065	0.0008	0.0021(1)	0.002(1)	0.032(1)	0.107(1)	0.255	316(13)	90(4)	-	286(26)	24(2)	4.8(6)
D	*duplicate*[32]		0.093(3)	0.0050	0.0006	0.0010(1)	-	0.028(1)	0.085(1)	0.216	313(6)	83(2)	-	2837(7758)	238(644)	-
D	*duplicate*[47]		0.105(3)	0.0073	0.0009	0.0029(1)	0.009(1)	0.023(1)	-	0.275	-	-	-	254(53)	20(4)	5(1)
D	AMS 049[3]	medium-grained metagabbro	0.044(3)	0.0056	0.0009	0.0067(2)	-	0.042(1)	-	0.200	328(14)	90(2)	-	38(3)	14(1)	-
D	*duplicate*[18]		0.083(3)	0.0062	0.0010	0.0016(1)	0.005(1)	0.037(1)	0.129(2)	0.279	321(12)	87(4)	-	173(10)	12.9(8)	4.3(4)
D	*duplicate*[33]		0.085(3)	0.0053	0.0018	0.0023(1)	0.004(1)	-	0.124(2)	0.212	325(6)	70(2)	-	291(86)	21(6)	*4(2)*
D	*duplicate*[48]		0.102(3)	0.0066	0.0012	0.0024(1)	0.003(1)	0.042(1)	-	0.255	-	-	-	183(29)	11(2)	3.5(8)
C	AMS 003	dark gabbroic gneiss	0.407(9)	0.0190	0.0015	0.0050(1)	0.011(1)	0.122(2)	0.223(1)	0.231	569(12)	60(2)	-	564(68)	34(4)	3.5(6)

Locality	Sample	Rock type	Re	Os	^{192}Os	Ir	Ru	Pt	Pd	Au	S	Se	Te	^{187}Re/^{188}Os	^{187}Os/^{188}Os	$T_{(MA)PM}$
	Felsic															
A	AMS 030A-B	dioritic layer	0.057(3)	0.0122	0.0044	0.0117(2)	0.042(1)	0.209(3)	0.003(1)	0.067	227(9)	51(2)	7(1)	25(1)	1.27(1)	2.7(1)
A	AMS 031A	dioritic layer	0.092(3)	0.0126	0.0034	0.0087(1)	0.036(1)	0.189(3)	-	0.041	352(9)	68(2)	5(1)	53(3)	4.05(7)	4.3(2)
SW of A	AMS 037	garnet -bearing layered gneiss	0.048(3)	0.0065	0.0021	0.0101(3)	0.012(1)	0.57(2)	0.355(3)	0.142	285(9)	49(2)	4.9(5)	47(2)	2.35(7)	2.8(1)
SW of A	AMS 015B3	strongly foliated garnet-bearing gneiss	0.275(3)	0.0142	0.0030	0.0043(1)	0.020(1)	0.172(3)	0.250(3)	0.363	998(70)	100(6)	3.9(5)	186(4)	7.7(2)	2.40(8)
G	AMS 050[23]	garnet-bearing metatonalite gneiss	0.513(3)	0.0329	0.0004	-	0.003(1)	-	-	1.19	554(13)	-	12(2)	4202(1021)	418(102)	*6(2)*
G	*duplicate*[34]		0.519(6)	0.0327	0.0004	0.0005(1)	0.002(1)	0.010(1)	0.95(2)	0.721	486(12)	77(4)	13(1)	3544(2126)	347(209)	*6(5)*
South of A	AMS 035	layered gneiss	0.102(3)	0.0177	0.0054	0.0495(5)	0.097(2)	2.24(9)	1.3(2)	0.080	426(15)	120(2)	7(1)	37(1)	2.86(3)	4.3(1)
C	AMS 001	metatonalite	0.115(3)	0.0051	0.0005	0.0017(1)	0.003(1)	0.046(1)	0.374(3)	0.834	2572(136)	48(2)	15(1)	522(206)	29(11)	3(2)
C	AMS 009	metagranite	0.012(3)	0.0015	0.0005	0.0012(1)	0.010(1)	0.024(1)	-	0.139	32(2)	8(2)	0.5(1)	53(19)	2.2(3)	2.3(9)
H	AMS 013	foliated metagranodiorite	0.008(3)	0.0029	0.0011	0.0058(1)	0.009(1)	0.073(2)	0.208(3)	0.055	55(2)	6.8(6)	1.8(4)	15(3)	0.6(1)	1.9(6)
F	AMS 039	metatonalite	0.144(3)	0.0154	0.0040	0.0096(2)	0.021(1)	0.155(3)	1.32(2)	0.103	294(6)	49(2)	1.8(6)	72(1)	4.7(7)	3.7(8)
F	AMS 041	metadiorite	0.59(1)	0.0309	0.0030	0.0068(1)	0.019(1)	0.165(3)	0.370(2)	0.198	1440(47)	252(6)	11(1)	405(24)	26(2)	3.7(3)
G	AMS 053	weakly foliated metatonalite gneiss	0.009(3)	0.0018	0.0007	0.0021(1)	0.013(1)	0.065(1)	0.311(5)	0.084	192(5)	30(2)	-	31(4)	1.01(9)	1.7(3)
Massiccio dei Laghi, South Alps (Northwest Italy)	GL 14	appinite	0.020(6)	0.0065	0.0023	0.006(1)	0.027(2)	0.458(8)	0.757(6)	6.83	732(24)	76(4)	-	216(13)	1.3(2)	0.33(6)
	GL 17	diorite	0.056(6)	0.0083	0.0033	0.0014(3)	-	0.205(3)	0.925(5)	3.18	272(19)	22(2)	-	35(2)	0.36(4)	0.40(7)
	GL 21	diorite	0.039(6)	0.0022	0.0008	0.0040(3)	0.002(2)	0.102(2)	0.646(3)	3.34	57(5)	18(2)	11(2)	101(19)	1.2(4)	0.6(3)
	BB 6	metagranite	0.252(7)	0.0024	0.0009	0.0014(3)	-	0.154(2)	0.749(4)	0.382	60(8)	1.6(8)	-	540(85)	0.5(1)	0.04(1)

Note: Separate digestions are marked by digestion numbers, *e.g.* AMS 024[4], indicating that another aliquot of the rock powder was digested. Duplicate analyses of the same digestion are given as *duplicate*. [3]T_{MA} in italic are values with large uncertainties. [4]Elemental abundances below the limit of detection and measurement problems due to high backgrounds are indicated with symbol -. Number in parentheses represent the analytical uncertainty (2σ) of the last digit. The analytical uncertainty was propagated from the uncertainty of spike, the instrumental uncertainty and the uncertainty contributed by blank to sample.

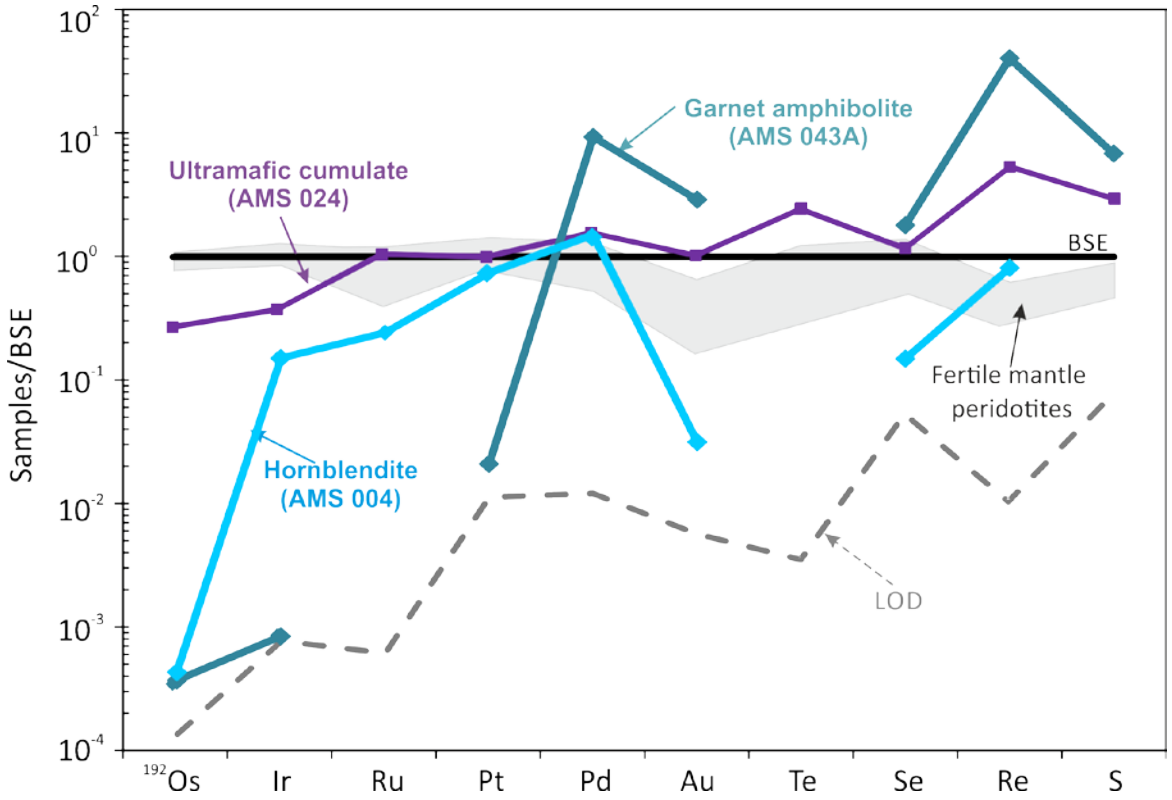

Fig. 2.3 Highly siderophile element and strongly chalcophile element abundances in the ultramafic cumulate, garnet amphibolite and hornblendite pod from the AGC normalized to the BSE (Becker et al., 2006; Fischer-Gödde et al., 2011; Wang et al., 2013). The grey shaded band represents fertile mantle peridotites (Fischer-Gödde et al., 2011; Wang et al., 2013). The dash dark gray line represents the limit of detection (LOD).

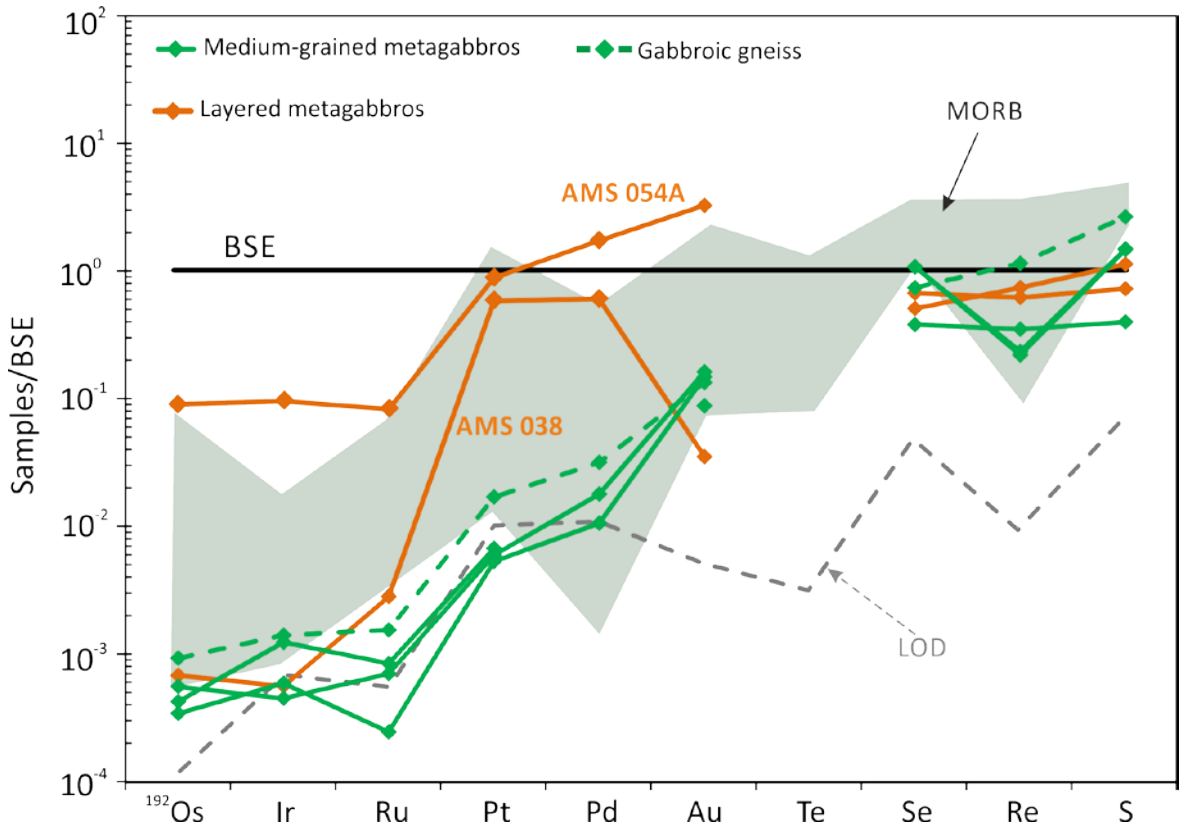

Fig. 2.4 Highly siderophile element and chalcophile element abundances in medium-grained metagabbros and layered metagabbros from the AGC normalized to the BSE (Becker et al., 2006; Fischer-Gödde et al., 2011; Wang et al., 2013). The transparent brown band represents the MORB (Jenner and O'Neill, 2012; Lissner et al., 2014). The dash dark gray line represents the limit of detection (LOD).

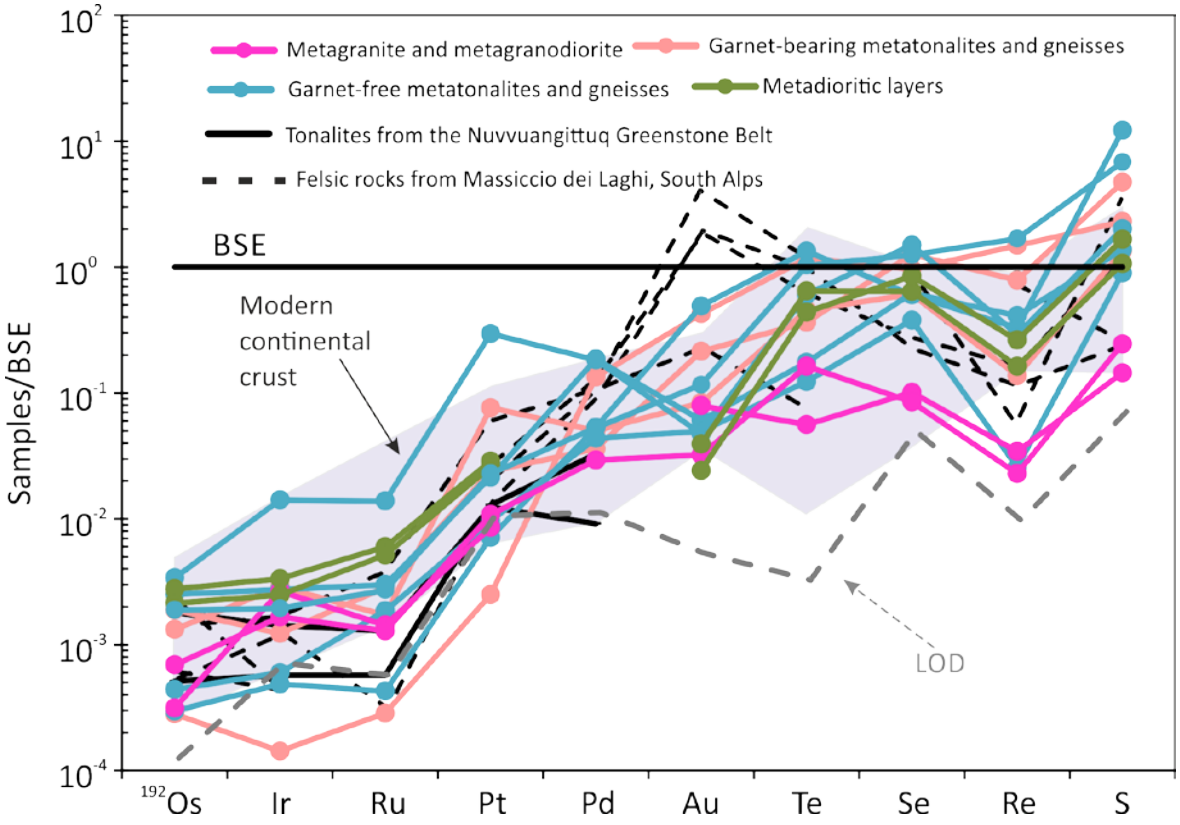

Fig. 2.5 Highly siderophile element and chalcophile element abundances in evolved crustal rocks from the AGC normalized to the BSE (Becker et al., 2006; Fischer-Gödde et al., 2011; Wang et al., 2013). Metatonalites from the Nuvvuangittuq Greenstone Belt are plotted for comparison (Touboul et al., 2014a). The gray shaded band represents the range of modern rocks representing the evolved continental crust (Plessen and Erzinger, 1998; Wang and Becker, 2014a). The dash dark gray line represents the limit of detection (LOD).

2.5.2 Re-Os isotopic systematics

The Acasta rocks exhibit a wide range in osmium isotopic compositions (Table 2.1). $^{187}Os/^{188}Os$ and $^{187}Re/^{188}Os$ of ultramafic cumulate AMS 024 are 0.13725 and 7.828, respectively. $^{187}Os/^{188}Os$ and $^{187}Re/^{188}Os$ of garnet amphibolite AMS 043A are the highest among the investigated samples, but have large uncertainties. We note that the Os isotopic composition of AMS 043A were poorly reproduced among three replicates. $^{187}Os/^{188}Os$ and $^{187}Re/^{188}Os$ of hornblendite AMS 004 are 2.5 and 793, respectively. $^{187}Os/^{188}Os$ and $^{187}Re/^{188}Os$ of layered metagabbro AMS 054A are 0.3180 and 2.98, respectively. $^{187}Os/^{188}Os$ and $^{187}Re/^{188}Os$ of the medium-grained metagabbros vary from 5.58 to 12.9 and from 25.4 to 173, respectively. $^{187}Os/^{188}Os$ and $^{187}Re/^{188}Os$ of evolved continental crustal rocks of the AGC vary considerably. $^{187}Os/^{188}Os$ and $^{187}Re/^{188}Os$ of garnet-bearing metatonalite AMS 050 are 347 and 3544, respectively; $^{187}Os/^{188}Os$ and $^{187}Re/^{188}Os$ of garnet-free samples range from 0.6 to 34 and from 15 to 563, respectively. The Permian rocks of the Massiccio dei Laghi are characterized by variable $^{187}Os/^{188}Os$ and $^{187}Re/^{188}Os$. $^{187}Os/^{188}Os$ varies from 0.36 to 1.3, and $^{187}Re/^{188}Os$ varies from 35 to 540.

2.6 Discussion

Abundances of the HSE and strongly chalcophile elements in the rocks of interest from the AGC are comparable to those of Phanerozoic equivalents (Fig 2.3-2.5). The ultramafic cumulate AMS 024, compared to Phanerozoic fertile mantle peridotites, is depleted in compatible IPGE and enriched in less compatible Te, Re and S. Garnet amphibolite AMS 043A is remarkably enriched in Pd, Re and S and depleted in IPGE. With the exception of depletions of Os and S, abundances of IPGE in hornblendite AMS 004 appear depleted relative to fertile mantle peridotites, though abundances of PPGE are comparable to fertile mantle peridotites.

The BSE-normalized patterns of medium-grained metagabbros of interest are similar to those of MORB and oceanic gabbros. Element abundances of layered metagabbros AMS 038 are comparable to Phanerozoic oceanic mafic rocks, though Au is strongly depleted compared to Pd. In contrast, layered metagabbros AMS 054A is characterized by BSE-like ratios IPGE and Se, Re and S.

Abundances of HSE and strongly chalcophile elements in the continental crustal rocks of the AGC are comparable to their Phanerozoic equivalents, though Permian rocks from Massiccio dei Laghi display Au enrichments. The metadioritic layers differ from the other

samples in Pd depletion. Anomalies of Re relative to Se and S vary from strongly to weakly negative, which is not evident in the few available Phanerozoic continental rocks.

2.6.1 Influence of metamorphism, melting and associated metasomatism

Polymetamorphism, crustal melting and associated open-system behavior undergone by some rock associations in the AGC may have modified the distribution of the interested elements. Although PGE in Archean komatiites undergoing greenschist facies were immobile (Puchtel et al., 2009b; Puchtel et al., 2014), whereas in rocks of amphibolite facies, where complex hydrothermal fluid are commonly involved (Sassani and Shock, 1990; Simon and Pettke, 2009), effects of late-stage alterations on HSE and strongly chalcophile elements may be more aggressive. For instance, the formation of gold deposits in Archean greenstone belts requires the involvement of hydrothermal fluids (Cameron and Hattori, 1987; Ridley et al., 1996; Yardley and Cleverley, 2013). The AGC underwent epidote to amphibolite metamorphism (Iizuka et al., 2007a), mobilization of HSE, S, Se and Te may have happened. Preferred mobilization of specific elements may be deduced from negative anomalies in normalized element concentration diagrams (Fig. 2.3-2.5). The elements of interest in BSE-normalized diagrams are arranged from the left to right with increasing incompatibility during partial melting of the mantle. Therefore, if an element was mobilized, it would be enriched or depleted relative to its neighboring elements in BSE-normalized diagrams.

Ultramafic rocks investigated in this study show variable secondary modification of AMS 024 these elements. The slight depletion of Au relative to its neighboring elements Pd and Te apparently indicates that Au was mobilized (Fig. 2.3). The depletion of S and Se relative to neighbor elements in AMS 024 may be caused by xenolith-host rock interaction. The hornblendite pod AMS 004 is characterized by depletion of Os, S, Au and Se relative to their neighbor elements (Fig. 2.3). As in the case of ultramafic cumulate AMS 024, depletions of these elements in AMS 004 may have resulted from losses into a fluid phase during amphibolite-grade metamorphism.

Garnet amphibolite AMS 043A is characterized by high abundances of Pd, Au, Re and S in contrast to low abundances of Os, Ru, Pt and Se (Fig. 2.3). Garnet amphibolite is probably representative of residues of TTG melts, of which the low S capacity indicates that the majority of sulfur would be locked in residual sulfides. The relatively high Pd abundance of AMS 043A seems to be consistent with the experimental result (Prouteau and Scaillet,

2013). It could also be that the relatively high abundances of Pd, Au, Re and S in AMS 043A may be introduced by sulfides during migmatization as revealed by enrichments of light rare earth elements relative to heavy rare earth elements. However, considering the abundances of HSE, S, Se and Te in evolved continental rocks (Fig 2.5), it is unlikely that enrichments of Pd, Au, Re and S in AMS 043A could be supplied by these evolved rocks.

Layered metagabbro AMS 054A is characterized by enrichments of Pd and Au relative to the other HSE and the more incompatible Se and S (Fig. 2.4). The latter elements and Os, Ir, and Ru display BSE-like ratios, suggesting that the variations are mostly inherited from the mantle source. The layered metagabbro AMS 038 displays a more fractionated element pattern and the strong depletion of Au compared to Pd and Au, indicating the mobilization of Au after the formation of AMS 038 by amphibolite-grade metamorphism. Remarkably, Pt, Pd, Se, Re and S in AMS 038 are little fractionated compared to BSE values, suggesting that these elements were rather immobile during post-intrusive processes. The nearly unfractionated behavior of Re and the other chalcophile elements suggests that these samples may have preserved their primary Re inventory. As displayed in the BSE-normalized diagram (Fig. 2.4), variations of the interested elements are limited, indicating that the mobilization of Pt, Pd, Se, Re and S in the medium-grained metagabbros are negligible.

As indicated in Fig. 2.5, BSE-normalized patterns of the element abundances in the evolved crustal rocks are more uniform than mefic rocks and similar to modern continental crust, with the exception of Pd depletion in metadioritic layers AMS 030A-B and AMS 031. Systematic element anomalies are minor, providing strong evidence that these elements in the evolved rocks were not significantly mobilized during high- and low-temperature metamorphic processes. The processes which depleted Pd in metadioritic layers are not known. Palladium is considered to be less mobile than Au in hydrothermal fluids. Specific mobilization of Pd is also indicated by the variation of Pd anomalies which vary from negative in metadioritic layer to positive in garnet-free metatonalites and gneisses. Stronger variations of Au anomalies are also evident in the evolved continental crustal rocks, especially in garnet-free metatonalites and gneisses, ranging from negative anomalies to no anomaly. It indicates that Au was mobilized in these samples during late-stage alterations, whereas in other samples the impacts of late-stage alterations on Au are less significant. The variations of Te anomalies in evolved continental rocks of the AGC range from slightly negative to slightly positive, but such variations of Se were not observed. Either the variations of Te anomalies indicate a specific redistribution of Te during metamorphic processes, or such features are

inherited from igneous protoliths. The extents of negative Re anomalies relative to its neighboring elements S and Se decrease from metagranite and metagranodiorite to gabbroic gneiss and garnet-bearing metatonalites and gneisses (Fig. 2.5). The Re depletions in highly evolved rocks may reflect the retention of Re in residual sulfide and perhaps garnet during the extraction of granitic and TTG melts from parental basaltic rocks in the middle- and lower-crust. Sample AMS 043A may represent a complementary residual rock.

Influences of metamorphism, melting and associated metasomatism on the AGC rocks are not significant and most of the magmatic signatures are preserved by the HSE, S, Se and Te. This is slightly different from the HSE behavior during subduction and arc magmatism, during which strong fluid flux were found to have mobilized Pt, Pd and Re (Dale et al., 2007; Dale et al., 2012). Such a difference of HSE between the AGC rocks and modern subduction-arc magmatic rocks implies that the moderate temperature of metamorphism undergone by the AGC.

2.6.2 Interpretation of Re-Os T_{MA} model ages

Some of the Re-Os T_{MA} model ages of ultramafic to mafic rocks from the AGC seem to have preserved their magmatic signature. The ultramafic cumulate AMS 024 which underwent amphibolite facies metamorphism has near-chondritic $^{187}Os/^{188}Os$, preventing the calculation of Re-Os model age. T_{MA} Re-Os model ages obtained from different aliquots of garnet amphibolite AMS 043A, though with considerable uncertainties, are around 4 Ga, possibly recording a melt extraction event. This in turn is consistent with that the enrichment of Re in AMS 043A is probably a pristine characteristic. The T_{MA} Re-Os model age of hornblendite AMS 004 is ~0.18 Ga which unlikely reflects magmatic events. This can be confirmed from the variable BSE-normalized abundance pattern of Te, Se, Re and presumably S (Fig. 2.3). Considering the unfractionated Os-Ir-Ru and Se-Re-S pattern (Fig. 2.4), the Re-Os T_{MA} model age (4.29 ± 0.02 Ga) of layered metagabbros AMS 054A likely records the timing of the melt extraction event. Re-Os model ages of medium-grained metagabbros, thought variable, are around 4 Ga, possibly timing the melt extraction event which led to intrusions of gabbros. Gabbroic gneiss AMS 003 has a Re-Os model age of 3.5 Ga, which likely records the magmatic event of its precursor.

Re-Os T_{MA} model ages of evolved continental rocks of the AGC can be separated into three groups, ~4 Ga, 2.7-3.5 Ga and <2.7 Ga. Metadioritic layer AMS 031A and layered

gneiss AMS 035 have similar Re-Os T_{MA} model ages of ~4.3 Ga. Both rocks do not show evidence for element mobilization (Fig 2.5) and were collected not far from each other. Remarkably, the Re-Os model age of AMS 031A (4.3 ± 0.2 Ga) is comparable to the Sm-Nd errorchron age (Scherer et al., 2010; Sprung, 2010), suggesting that the Re-Os isotopic systematic in AMS 031 was not disturbed by late-stage events. Metatonalite AMS 039 and metadiorite AMS 041 have Re-Os model ages of 3.7 Ga. As mentioned in 2.3, AMS 041 intruded AMS 039. The Re-Os isotopic systematic of these two rocks may have been equilibrated and the Re-Os model ages records the intrusive event of AMS 041. Garnet-bearing rocks and rocks displaying clear evidence for foliation generally have Re-Os model ages younger than 3.0 Ga. We note that Re-Os model ages of AMS 030A-B, AMS 037 and AMS 015B3 from the western unit cluster at 2.4-2.8 Ga, while metagranite AMS 009 and foliated metagranodiorite AMS 013 collected from the central island and weakly foliated tonalitic gneiss AMS 053 from the eastern unit have Re-Os model ages 1.7-2.3 Ga. The Re-Os model ages of 2.4-2.8 Ga coincide with the age (2.6 Ga) of metagranite intrusion (Iizuka et al., 2007a), whereas the Re-Os model ages of 1.7-2.3 Ga may reflect an overprint of metamorphism related to Wopmay orogeny which occurred at around 1.9-1.8 Ga (Hildebrand et al., 2010; Sano et al., 1999).

2.6.3 Petrogenesis of rocks of the present study

The petrogenesis of different lithologic units of the AGC was mainly discussed on the basis of constrains from zircon (Bowring and Housh, 1995; Bowring and Williams, 1999; Bowring et al., 1989b; Iizuka et al., 2006a; Iizuka et al., 2009; Iizuka et al., 2007b; Mojzsis et al., 2014; Roth et al., 2014; Willbold et al., 2015) and whole rock Sm-Nd isotope system (Bowring et al., 1989a; Maltese et al., 2015; Moorbath et al., 1997; Roth et al., 2014; Scherer et al., 2010; Sprung, 2010). Current understanding about the AGC is that the earliest magmatism event occurred at 3.96 Ga and the older zircons were inherited from a felsic crustal precursor. Though many outcrops of ultramafic and mafic rocks were identified in the AGC, few of them have been considered from the view of petrogenesis. With the exception of Re incorporated in silicates, HSE and strongly chalcophile elements are generally controlled by sulfides, a relatively simple system compared to lithophile elements during magmatic evolution. This makes it possible for investigating the geochemical characteristics of the precursor to the AGC by using HSE and strongly chalcophile elements.

2.6.3.1 Ultramafic and mafic rocks

AMS 024 likely was accumulated from melt produced by high-degree of partial melting. AMS 024 is distinguished from mafic rocks from oceanic crust by high Os, Ir, and Ru abundances (Dale et al., 2007; Dale et al., 2012). In comparison to refertilized mantle peridotites (Becker et al., 2006; Fischer-Gödde et al., 2011; Wang et al., 2013), AMS 024 is characterized by stronger fractionation of Os, Ir and Ru (Fig. 2.3). AMS 043A is also different from mantle harzburgites which are depleted in Pt, Pd, Te, Se and S (Fischer-Gödde et al., 2011; König et al., 2015a; Wang et al., 2013). The normalized HSE pattern of ultramafic cumulate AMS 024 is similar pattern of to the boninite cumulates from the Isua supracrustal belt in western Greenland (Szilas et al., 2015), suggesting that AMS 024 is probably a magmatic cumulate segregated from relative high-degree partial melts. Such an interpretation is supported by the Pd/Pt ratios in Fig. 2.7 which shows the Se/Pt ratio of AMS 024 is plotted along the trend defined by Phanerozoic mantle peridotites. This suggests that AMS 024 must be accumulated from a sulfide-undersaturation magma which is derived from a mantle source indistinguishable from the BSE.

The T_{MA} Re-Os model ages yielded by different sample aliquots of AMS 043A seem to indicate that the latest melt extraction happened roughly around 4 Ga, which is comparable to the oldest age of the evolved crustal rocks of the AGC (Mojzsis et al., 2014). However, enrichments of incompatible trace lithophile elements and high LREE/HREE ratios (Sprung, 2010) suggest the role of migmatization. The enrichment of Re in garnet amphibolite, considering the enrichment of Pd and Au, likely reflects the role of sulfides. Experimental data suggested that Re is incompatible with garnet in the condition of QFM-0.7 to QFM+1.6 (Mallmann and O'Neill, 2007). Another phase may be a potential host of Re is amphibole which could host Re^{4+} as it hosts Ti^{4+}. However, considering the low abundance of Re in hornblendite lens AMS 004, the role of amphibole is doubtful in partitioning Re. For the origin of sulfides in AMS 043A, considering the Re-Os model ages, it is possible that sulfides are residual otherwise the secondary introduction of Re would lead to young Re-Os model ages. Therefore the HSE and incompatible lithophile elements are decoupled in AMS 043A, which indicates the garnet amphibolite AMS 043A cannot simply excluded as residual after melt extractions. The section photography of AMS 043A illustrated the existence of quartz in garnet shadows (Fig 2.2), implying that felsic melts may have been extracted from AMS 043A.

Radiogenic Re-Os isotopic composition and the very recent T_{MA} Re-Os model age (0.18 Ga) of AMS 004 indicate that the Re-Os system was disturbed late in the history of this rock. The hornblendite may be residual but mainly records the information of its magmatic source and emplacement as indicated by the normalized Ir-Ru-Pt-Pd pattern. The high abundances of Ir, Ru, Pt and Pd imply that the hornblendite was originally a cumulate from high-degree partial melts. Late recrystallization occurred at fluid-present conditions during amphibolite-grade metamorphism may have resulted in the losses of Os, Se and S in AMS 004.

The two layered metagabbros investigated in this study are of distinct petrogenesis. AMS 054A appears to have formed by accumulation of silicates from sulfide-undersaturated magmas, whereas AMS 038 may be derived from alloy-saturated magmas. This is shown by the abundances of IPGE and fractionation between IPGE and PPGE in these rocks. Abundances of Os, Ir and Ru in AMS 038 were close to or lower than the LOD, whereas Pt, Pd, Se, Re and S display BSE-like ratios, which can only be explained if this rock was formed from Os-Ir-Ru alloy-saturated magmas (Mungall and Brenan, 2014). The depletion of Os, Ir and Ru in AMS 038 is unlikely caused by sulfide segregation during magma transport (in contrast to MORB, Fig. 2.4), otherwise Pt, Pd and other chalcophile elements should also have been depleted and fractionated. The HSE signatures of AMS 038 probably is inherited from its mantle source. The T_{MA} Re-Os model age (~4 Ga) of AMS 054A is similar to the errorchron age of Sm-Nd but older than errorchron age of Lu-Hf, which are around 3.7 Ga, indicating that the Lu-Hf isotope systematics may have been reset by metamorphism, but likely not the Re-Os system as indicated by the BSE-like ratios of Re with other HSE (Fig. 2.4). Surprisingly, AMS 054A has a Se/Pt ratio plotted along the trend of Phanerozoic mantle peridotites (Fig. 2.7) and a Pd/Pt ratio indistinguishable from ultramafic cumulate AMS 024 (Fig. 2.6). This clearly demonstrates that layered metagabbro AMS 054A is crystallized from sulfide-undersaturated magma.

The medium-grained metagabbros investigated in this study are characterized by PGE abundances which were close to or lower than the LOD. Abundances of Au, Te, Se, Re and S are much more enriched compared to PGE and the latter elements appear to be strongly fractionated. These patterns are much more similar to modern MORB than layered metagabbro AMS 054A, indicating that the medium-grained metagabbros formed predominately from low-degree partial melts. Similar to layered metagabbro AMS 038, the medium-grained metagabbros were collected from mafic lenses in felsic gneiss series of the

eastern unit. The Re-Os model ages of the medium-grained metagabbros are marginally older than Sm-Nd and Lu-Hf errorchron dates, which are around 3.7 Ga, however, within uncertainties the dates yielded by different radiogenic isotope systems overlap. This suggests that the Re depletion of these rocks occurred within a few hundred million years of the formation of the igneous protoliths.

2.6.3.2 Evolved crustal rocks

Evolved crustal rocks of the AGC were thought to be mixture of reworked older continental crustal materials and juvenile magmas (Iizuka et al., 2009; Mojzsis et al., 2014). Previous studies on lithologic field relationships of the AGC showed that the felsic gneiss series of the eastern unit may represent multiple generations of the protolith, including emplacements of intermediate-felsic magmas (Iizuka et al., 2007a). The gneissic structure of the igneous protoliths was developed lately by multiple stages of metamorphism and deformation. Similar tectonomagmatic events were also identified in the layered gneiss series of the western unit, including emplacements of mafic-intermediate protoliths and metamorphism and deformation of all lithotypes (Iizuka et al., 2007a). Studies on Lu-Hf systematics showed that metagranitoids and metatonalites of 3.97-3.9 Ga were characterized by negative $\varepsilon Hf_{(T)}$, suggesting some of the rocks in the AGC contained contributions of older metagranitoids (Iizuka et al., 2009; Mojzsis et al., 2014). The results of ^{146}Sm-^{142}Nd systematics suggested that two compositional end-members for the AGC, a felsic component with $^{142}Nd/^{144}Nd$ indistinguishable to the modern Earth and a mafic component with negative $^{142}Nd/^{144}Nd$ (Roth et al., 2014).

As discussed in 2.6.3.1, the enrichments of Re and Pd in garnet amphibolite probably indicate the effect of residual sulfides. In contrast, Re and Pd are depleted in metadioritic layers AMS 030A-B and AMS 031A. Remarkably, T_{MA} Re-Os model ages (~4 Ga) of garnet amphibolite and metadioritic layer AMS 031A are identical within uncertainties, implying the genetic link between the two lithologic units. Garnet amphibolite AMS 043A possibly represents the residue after the extraction of metadioritic magma. This interpretation indicates that reworking of mafic crust may also be an important process for the generation of intermediate-felsic rocks in the AGC.

We note that the sole Re depletion in Archean TTGs is probably not a criteria for reworking of mafic crust. Permian appinite GL 14 of Massiccio dei Laghi is also characterized by strong Re depletion, but this rock is probably not related to rework of mafic precursors but assimilation-fractionation-contamination (Pinarelli et al., 1988). Similarly, Re

depletions relative to Se and S in metagranite AMS 009, metagranodiorite AMS 013 and foliated metatonalite gneiss AMS 053 do not necessarily indicate that they are genetically related to mafic precursors.

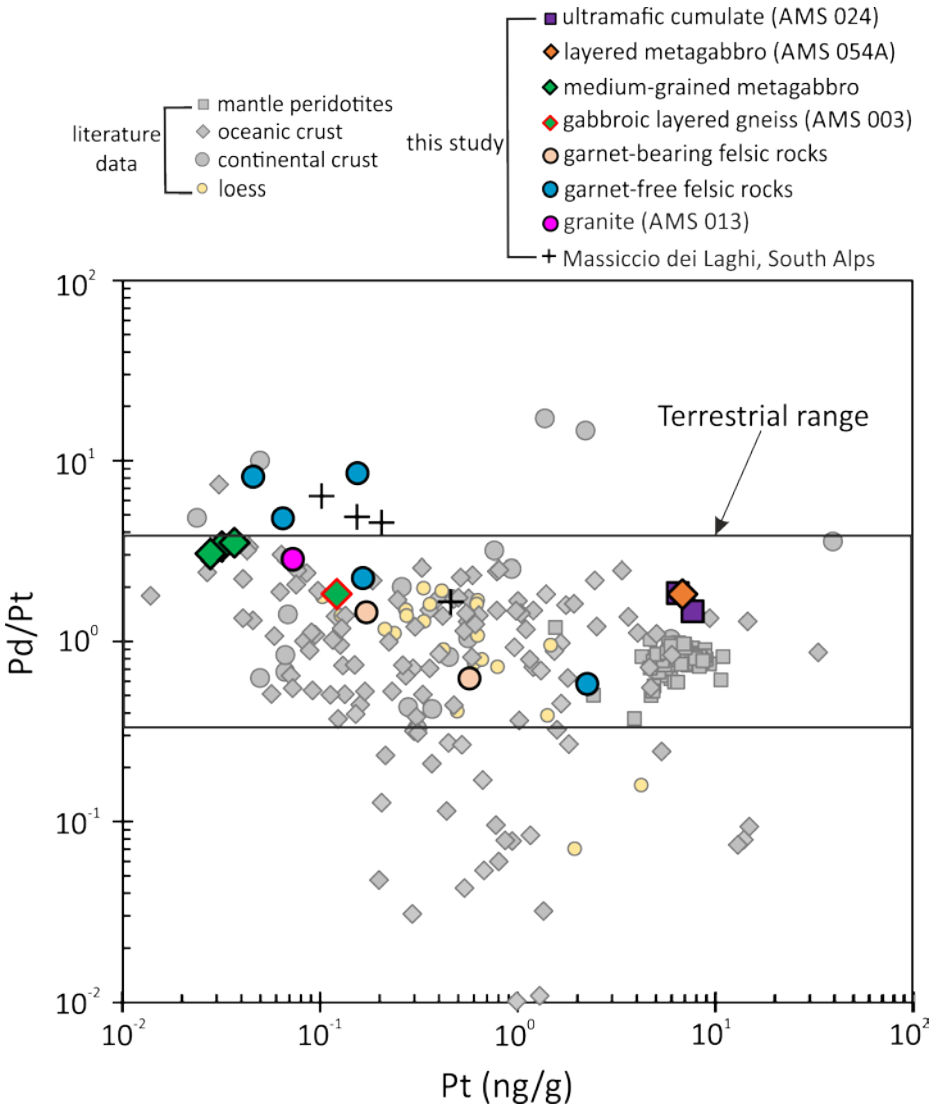

Fig. 2.6 Variations of Pd/Pt with Pt abundances in terrestrial samples. Literature data sources: Phanerozoic mantle fertile peridotites (Becker et al., 2006; Fischer-Gödde et al., 2011; Wang et al., 2013), oceanic crust (Dale et al., 2009; Dale et al., 2008; Peucker-Ehrenbrink et al., 2003; Peucker-Ehrenbrink et al., 2012), loess (Park et al., 2012; Peucker-Ehrenbrink et al., 2003), continental crustal rocks (Wang and Becker, 2014a). Pd/Pt ratios and Pt abundances of the Acasta samples are indistinguishable from their post-Archean equivalents. Pd/Pt in terrestrial rocks are variable in limited range.

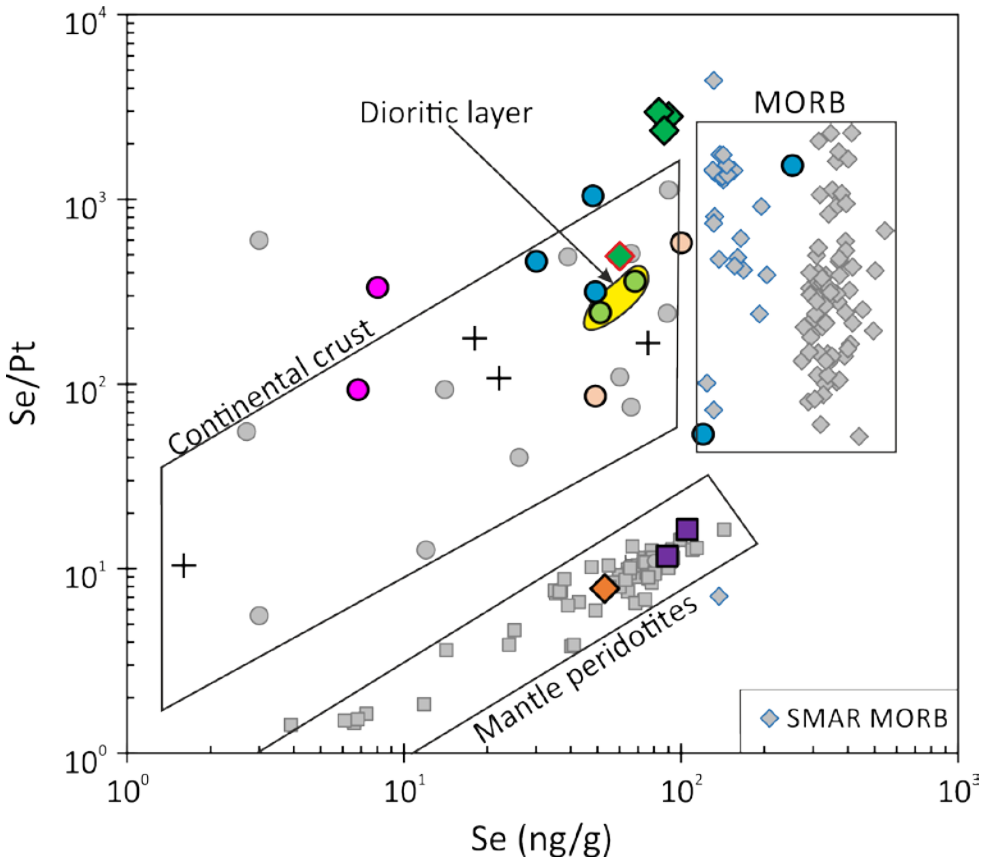

Fig. 2.7 Variations of Se/Pt with Se abundances in terrestrial samples. Legends are given in Fig. 2.6. Literature data sources: Phanerozoic mantle fertile peridotites (Wang and Becker, 2013; Wang et al., 2013), oceanic crust (global MORB) (Jenner and O'Neill, 2012), SMAR (South Mid-Atlantic Ridge) MORB (Lissner et al., 2014), continental crust (Wang and Becker, 2014b). The increase of Se/Pt with Se abundances in mantle peridotites indicates that Se is more incompatible than Pt during melt infiltration or extraction or both. The invariability of Se abundances and significant variations of Se/Pt in MORBs suggest the magmatic sulfide segregation of Pt or preferential retention of Pt in mantle sources or both. Se/Pt and Se abundances in the Acasta samples, including metadioritic layer of Re-Os T_{MA} age of 4.3 Ga, are indistinguishable from their post-Archean equivalents.

2.6.4 Constrains on late accretion processes during the Hadean

2.6.4.1 The late heavy bombardment

Recent studies showed that the size of bolides accreted during the LHB may be comparable to planetsimals or planetary embryos (Bottke et al., 2010). Large planetsimals are capable of penetrating the terrestrial crust (Bottke et al., 2010), whereas the accretion of small embryo-sized objects would disturb larger portion of the silicate Earth. Therefore the oldest rocks of the AGC and their precursors should have recorded such large-scale and intense bombardment with bodies of approximately chondritic bulk composition. The portion affected by the LHB are expected to have elevated abundances of HSE and strongly chalcophile elements S, Se and Te. Though such elevations could be diluted by progressive reworking of the crust, none of the investigated samples shows remarkable enrichments of HSE, S, Se and Te compared to modern continental rocks. And the element ratios of Pd, Pt and Se in Acasta gneisses are in the range of post-Archean samples, as shown in Fig 2.6-2.7. Though Pd/Pt ratios in Acasta samples appear to decrease with increasing Pt abundances, these ratios are in the range of terrestrial rocks sampled post-Archean mantle sources. Fig. 2.7 shows that Se/Pt ratios in Acasta rocks fall into the range of their Phanerozoic equivalent. Ultramafic cumulate AMS 024 and layered metagabbros AMS 054A, displaying no depletion of Se or Pt, are plotted along the trend of Phanerozoic mantle peridotites. Metadioritic layer AMS 031A, whose Re-Os model age is older than 4.0 Ga, has a Se/Pt in the range of post-Archean continental rocks (Fig. 2.7), providing no evidence for impact-induced loss of Se. These data support that the mantle source of ultramafic and mafic rocks from the AGC is not different from the post-Archean mantle in terms of the HSE, S, Se and Te. These data also prove that the felsic rocks from the AGC do not record any geochemical trace which might be attributed to meteoritic impacts. Re-Os systematics of the studied samples do not show evidence for being interrupted or reset by additions of meteoritic components either. This is clear in contrast to the speculations from simulations which indicated that the Acasta crust may be affected by the LHB (Mojzsis et al., 2014).

Several possibilities could explain the absence of the LHB in the AGC. (1) The LHB during 4.2 Ga to 3.75 Ga did not affect the Acasta area. Recent numerical simulations showed that less than 10% of the Earth's surface would be covered by melt sheets produced by the LHB (Abramov et al., 2013). The oldest rocks of the AGC and their precursors could be possibly beyond the influence of the LHB. (2) Impactors bombarded the Acasta area were not

massive enough to reach the precursors to the AGC in the middle-lower crustal level. It was found that the inner solar system may have been bombarded by two groups of objects, one group comprising of bodies of similar sizes as the present asteroid belt and the other one containing bodies of less than 0.02-100 kilometers (Robert et al., 2015). Therefore, the precursors to the AGC in the middle-lower crust may have not been directly impacted by the bodies reached the surface of Acasta area. (3) The impact influx on the Earth may be smoother because no prominent impact spikes at 4.1 Ga or 3.9 Ga were yielded by U-Pb dating (Grange et al., 2013). The impact influx spike at 3.9 Ga was not consistent with the lunar crater densities (Neukum and Ivanov, 1994), which suggested that impact influx declined exponentially since 4.1 Ga (Morbidelli et al., 2012; Neukum and Ivanov, 1994). These explanations do not possess evident advantages over the other, but the absence of the LHB in the AGC suggests that search for signals of the LHB many consider other areas than Acasta.

2.6.4.2 The late veneer

A recent study showed the presence of positive $\varepsilon^{182}W$ anomalies in samples of the AGC. These anomalies were interpreted to reflect the existence of a pre-late veneer early differentiated mantle reservoir (Willbold et al., 2015). This pre-late veneer mantle reservoir was speculated to have escaped homogenization with late-accreted components before being tapped by late Hadean-Eoarchean magmatism. This interpretation should be consistent with independent constrains from HSE abundances and ratios. Abundances of HSE in rocks from pre-late veneer reservoir should be depleted compared to those derived from mantle source with late accreted materials. Though abundances of HSE, S, Se and Te were not determined on the same rocks constrained by W isotopes, the samples in the present study cover diverse lithologies and some of the rocks are collected from the same outcrop as these which have W isotope data. Therefore, representativeness of the samples in this study is reasonable. As shown in Fig. 2.5, abundances of HSE and strongly chalcophile elements in the studied samples are not distinctly depleted relative to post-Archean continental crustal rocks, suggesting that the igneous protoliths of the AGC rocks likely are derived from post-late veneer mantle source. The contradiction between HSE and W isotopes deserves explanations.

It is necessary to evaluate the enrichment of W caused by secondary addition. Because the incompatibility of W is between Th and Nd, in mantle-derived magmas the enrichment factor of W, α, can be calculated.

$$\alpha = 2 \times C^{W}_{Sample} / [\ (\frac{C^{Th}_{Sample}}{C^{Nb}_{Sample}}) / (\frac{C^{Th}_{BSE}}{C^{Nb}_{BSE}})\ ]$$

The BSE values of Th and Nb in the calculation are 62.6 ng/g and 460 ng/g (Lyubetskaya and Korenaga, 2007). The α value of the samples investigated by (Willbold et al., 2015) varies from α = 0.03 for AG09-015, α = 0.05 for AG09-016, α = 0.9 for AG09-017N and α = 2.4 for AG09-020. Magmatic signatures of W likely were not well-preserved in some of these samples. Additionally, ε^{182}W values increase with α values. Enrichments of W were also observed in mafic and ultramafic rocks from the Isua supracrustal belt (Rizo et al., 2016). Though the relations between the mobilization of W and distribution of ^{182}W anomalies are still enigmatic, the possibility of positive ^{182}W anomalies redistributed by secondary processes cannot be ignored. Because HSE seem to be immobile in the AGC, at least in the evolved continental crustal rocks, W isotope systematics and HSE may be decoupled by late-stage processes.

If positive ε^{182}W values can be attributed to the precursors to the AGC, the pre-late veneer mantle with 0.2 wt.% core materials should be characterized by μ^{182}W = +15 and ~ 75% of HSE in the BSE (Willbold et al., 2015). Such an interpretation is problematic when considering that chondritic materials of ~0.5 wt.% Earth mass delivered by late veneer, required to reduce the μ^{182}W = +15 to μ^{182}W = 0, would elevate abundances of HSE and strongly chalcophile elements in the mantle source of the precursors to the AGC by a factor of 1.75. Such elevations of element abundances of the AGC are not observed in the studied samples.

The decoupling of W isotope systematics and HSE were also found in the 2.8 Ga Kostomuksha komatiites (Touboul et al., 2012) and rocks of the Isua supracrustal belt (Rizo et al., 2016), which were interpreted to reflect an isolated reservoir formed by core-mantle segregation or large-scale mantle differentiation between 60 Ma and 100 Ma after the formation of the solar system, which would be contemporaneous with or slightly later than the Moon-forming giant impact. A mantle portion characterized by positive μ^{182}W anomalies requires another reservoir of negative μ^{182}W anomalies. Early differentiated hidden reservoirs were used to explain the positive ε^{142}Nd anomalies in terrestrial rocks (Caro, 2011). Mantle reservoirs of negative μ^{182}W and ε^{142}Nd anomalies must be deeply isolated somewhere without being involved in mantle convection and terrestrial magmatism, because no negative μ^{182}W and ε^{142}Nd anomalies in terrestrial rocks have been identified yet.

2.7 Conclusions

We report the first dataset of highly siderophile element and chalcophile element abundances and osmium isotopic compositions on 21 samples from the Hadean to Eoarchean Acasta Gneiss Complex in northwestern Canada.

The main observation of this study is that the abundances of HSE, S, Se and Te in the Acasta rocks are comparable to their post-Archean equivalents. Although some of these rocks display evidence for the mobilization of specific elements during late-stage processes, the magmatic characteristics of their protoliths (evolved continental intrusive rocks, residual crustal rocks, gabbros and cumulates) are largely preserved. This demonstrates that neither the Acasta rocks nor preexisting crust in which the protoliths of these rocks intruded were contaminated with HSE-rich meteoritic materials which were assumed to be delivered by the late heavy bombardment between 3.8 Ga and 4.2 Ga.

The conclusion implies that if the HSE, S, Se and Te were delivered to the silicate Earth by late-accreted materials, it must have been homogenized within the mantle domain from which the precursors for the Acasta rocks were derived. This is in contrast to results from ^{182}W isotopic data, which showed that the 3.96 Ga Acasta rocks may have been derived from a pre-late veneer mantle source (Willbold et al., 2015). However, it remains unclear how W isotopic systematics may have been decoupled from the HSE, S, Se and Te systematics. We suggest that W isotopic systematics were subjected to late-stage alteration, but confirming this interpretation abundances of HSE in the samples characterized by μ^{182}W anomalies are needed.

2.8 Appendix Chapter 2

Treatment of the HPAS residues

Residues and precipitates of the garnet amphibolite (AMS 043A) and metadioritic layer (AMS 030) after HPAS digestion were re-digested to evaluate the reliability of the aqua regia-HPAS digestion method. The residues were rinsed five times with 15 ml Nanopure and were centrifuged for at least 15 minutes at the highest speed. The first and fifth aliquots were collected to check whether all the pre-added spikes were rinsed away. The residues were transported to 15 ml Teflon beakers and dried at 80 ℃. Subsequently, the powders of the dried residues were weighted into 60 ml Teflon beakers and ^{185}Re, ^{191}Ir-^{99}Ru-^{194}Pt-^{105}Pd, ^{77}Se-^{125}Te and ^{34}S spike solutions were added with 5 ml 24 mol l^{-1} HF (47-51%, J. T. Baker®) and

10 ml 14 mol l^{-1} HNO_3. After the residues were heated on the hotplate at 150℃ for 72 hours. Subsequently, the transparent HF-HCl solutions were dried down and 20 ml 14 mol l^{-1} HNO_3 was added and dried down. 1 ml 6 mol l^{-1} HCl was used for chloride conversion. The chloride conversion step was repeated once. Finally the materials of the residues were dissolved in 6 ml 1 mol l^{-1} HCl.

The method of chemical separation and mass spectromic procedures were the same as the aqua regia-HPAS digestion. The first and fifth aliquots of rinsed solution were measured directly without any chemical separation or purification. The results of the two residues are given in the Table S2.1. The aqua regia-HPAS digestion method is reliable concerning the HSE, S, Se and Te, although 12-18% of S, Se and Te were retained in the residue of garnet amphibolite AMS 043A. This may be due to sulfide inclusions incorporated in undigested silicates during the aqua regia-HPAS digestion. Insoluble residual phases, including spinel presumably, during the HF digestion stages, were dissolved completely. We did not observe any black particles after HF-HNO_3 digestion.

The results showed that 100% of Ir, Ru, Pt and Pd were released by using aqua regia-HPAS method. In metadiorite AMS 030A-B more than 90% of Re, S, Se and Te were released. The high Au abundance of the residue of AMS 030A-B likely reflects an analytical issue.

Table S2.1 Comparison of element abundances of garnet amphibolite AMS 043A and metadioritic layer AMS 030A-B

Sample	Ir	Ru	Pt	Pd	Au	Re	Te	Se	S
	ng/g	ng/g	ng/g	ng/g	ng/g	ng/g	ng/g	ng/g	µg/g
AMS 043A	0.0035	0.007	0.154	69	4.87	14	8.7	123	1436
Residue	< 0	< 0	< 0	< 0	0.176	0.298	0.866	10.31	90
Δ	100%	100%	100%	100%	93%	96%	**82%**	**85%**	**88%**
AMS 030A-B	0.0117	0.042	0.209	< 0	***0.067***	0.057	7.1	51.3	225
Residue	< 0	< 0	< 0	< 0	***0.050***	< 0	0.358	1.67	11
Δ	100%	100%	100%	100%	***15%***	100%	90%	94%	91%

Chapter 3

Abundances of rare chalcophile and lithophile elements in the 2.7 Ga komatiites from the Belingwe Greenstone Belt, Zimbabwe

3.1 Abstract

Archean komatiites, produced by high-degrees partial melting of probably the deep mantle, can provide constraints on the secular evolution of the chemical composition of incompatible chalcophile elements in the mantle. Data on Archean komatiites can also verify the composition of these elements in the bulk silicate Earth (BSE) defined by mantle peridotites and mantle-derived magmatic rocks. In this study we analyzed the abundances of 11 trace elements, including six chalcophile elements, in well-preserved Archean komatiites from the 2.7 Ga Tony's flow (TN) of the Belingwe Greenstone Belt by using the isotope dilution ICP-MS to obtain constrains on mantle source compositions in comparison to data obtained from mantle peridotites. Except for the fluid-mobile element Ba and S, Ag and Tl in the chilled margin subzone (A_1), which were modified by late-stage alterations, abundances of these elements in Belingwe komatiites preserve their magmatic compositions. Ratios of incompatible chalcophile elements in the studied komatiites, including Se/Te, Cu/Ag and Se/Cu, were little fractionated during partial melting or lava differentiation. Calculated element abundances of S, Se, Te, Cu, Ag, In, Cd and Mo Belingwe mantle source are comparable to the BSE obtained from data on fertile post-Archean mantle peridotites and mantle-derived ultramafic rocks within uncertainties. The carbonaceous chondrite-like S/Se and Se/Te of the Belingwe mantle source requires late accretion of volatile-rich materials. The BSE-like Cu/Ag of the Belingwe mantle source either reflects high temperature and pressure core formation or a nonchondritic Cu/Ag of Earth's building materials or both. The depletion of Cd relative to In in the BSE may reflect nonchondritic building materials for the volatile element inventory in the Earth.

3.2 Introduction

Recently it was proposed that the chalcophile elements S, Se and Te in the bulk silicate Earth (BSE) were mostly delivered by volatile-rich late-accreted material with a chemical composition similar to CM-type carbonaceous chondrites (Wang and Becker, 2013). However, on the ground of new metal-silicate partitioning data and a new estimate of the $\delta^{34}S$ value of the BSE it has been argued that a large fraction of the S inventory of the BSE (210-250 µg/g) may be inherited from core formation (Boujibar et al., 2014; Labidi et al., 2013). Other workers believe that mantle lherzolites cannot be used to constrain the chalcophile element composition of the BSE because they are commonly modified by melt infiltration (König et al., 2015a; König et al., 2014; König et al., 2015b; Lorand et al., 2010; Wang and Becker, 2015b). Most terrestrial basic magma types likely formed and evolved at sulfide saturated conditions (Brenan, 2015; Jugo, 2009; Li and Ripley, 2005; Mavrogenes and O'Neill, 1999). Thus, fractionation of chalcophile elements during segregation of magmatic sulfides prevents the use of basic magma compositions for a reliable determination of the abundances of chalcophile elements in the BSE (Hertogen et al., 1980; Lissner et al., 2014; Peach et al., 1990). An alternative approach for the determination of the abundances of moderately incompatible elements in the BSE is the study of komatiites.

As komatiites and related ultramafic igneous rocks formed via high-degrees of partial melting (30-50%), these rocks have been proved to be useful probes into the evolution of terrestrial mantle. Several groups of komatiites have been identified, Al-depleted (Barberton-type) komatiites, Al-undepleted (Munro-type) komatiites, and Al-enriched komatiites from Gorgona Island (Arndt et al., 2008). The Al_2O_3/TiO_2 ratio was adopted as a classification indicator which reflects differences in mantle source compositions and petrogenesis. Experimental results showed that Al_2O_3 depletion relative to TiO_2 in the Barberton-type komatiite occurred because of the retention of garnet during partial melting, whereas garnet was completely consumed during the formation of Munro-type komatiite (Robin-Popieul et al., 2012). In contrast to the mantle sources of the Barberton-type and Munro-type komatiites, mantle sources of Al-enriched komatiites experienced larger degrees of melting prior to the extraction of Al-enriched komatiite melt (Arndt et al., 2008; Robin-Popieul et al., 2012).

Sulfides in the mantle would be exhausted after 20-25% partial melting (Brenan, 2015; Peach et al., 1990), and therefore komatiite magma produced by 30-50% partial melting would stay S-undersaturated en route to the surface of the Earth, if no assimilation of S-rich

crustal rocks occurred. Unlike S-saturated mafic magmas, such as MORB, sulfide segregation in the S-undersaturated komatiite magma is not expected; therefore ratios of chalcophile elements should not be fractionated during komatiite magma transport. Systematic work on highly siderophile element abundances (HSE; Re, Os, Ir, Ru, Pt, Rh and Pd) of Archean komatiites found that the PGE were essentially immobile after emplacement and, therefore the HSE abundances of mantle sources can be calculated (Puchtel et al., 2009b). The relative abundances of HSE that behave incompatibly in the source of Archean komatiites (Connolly et al., 2011) seem to be indistinguishable from those of the BSE obtained from post-Archean peridotite massifs and xenoliths (Becker et al., 2006). Thus, in principle it is feasible to use the less chalcophile but more incompatible elements such as S, Se, Te, Cu, Ag, In, Cd, Tl and Mo in Archean komatiites to investigate the composition and origins of these elements in the mantle source of Archean komatiites and potentially in the BSE, if these elements were not mobilized during post-emplacement alteration.

In this study we report the abundances of S, Se, Te, Cu, Ag, In, Cd, Tl, Mo, Ba and Sm in Al-undepleted komatiites from the 2.7 Ga Tony's lava flow (TN) from the Belingwe Greenstone Belt in Zimbabwe. These komatiites are little affected by aqueous alteration processes such as serpentinization (Puchtel et al., 2009b). After evaluating the effects of post-emplacement alteration and volatility-controlled losses by magmatic degassing, we discuss the fractionation of chalcophile elements during partial melting and lava differentiation, as well as the composition and origin of these elements in the mantle source of Belingwe komatiites.

3.3 Geological background, sample description and previous studies

The Belingwe Greenstone Belt comprises two volcano-sedimentary sequences, the 2.90-2.83 Ga Mtshingwe Group and the 2.7 Ga Ngezi Group, which overlie 3.5 Ga old tonalitic gneisses. The Mtshingwe Group consists of mafic-intermediate volcanic and volcanoclastic rocks as well as siliciclastic sedimentary rocks. The Ngezi Group consists of four formations from bottom to top, the Manjeri Formation of a sedimentary sequence, the Reliance Formation and Zeederbergs Formation of ultramafic and mafic volcanic rocks, and the Cheshire Formation of a sedimentary unit. The Ngezi Group is better preserved and less metamorphosed than the Mtshingwe Group. The Belingwe komatiites mainly occur in the Reliance Formation.

As revealed by the SASKMAR drilling project (Nisbet et al., 1987), TN flow is the best preserved among the six lava flows from the Reliance Formation. Subzones of the TN flow are entirely exposed to the surface and contain unaltered silicate minerals and even pristine glass hosted in olivine crystals (Puchtel et al., 2009b). TN flow (Fig. 3.1) is approximately 14 meters thick and differentiated into a chilled margin top (A_1), an upper spinifex zone (A_{2-3}), a lower cumulate zone (B_{1-2}) and a chilled bottom. The spinifex zone can be further divided into two subzones, an upper random spinifex subzone (A_2) and a lower plate subzone (A_3). The cumulate zone has two subzones, an upper subzone of foliated skeletal olivine (B_1) and a lower subzone of cumulate olivine (B_2). Nine samples were analyzed in this study, including one from A_1, two from A_2, one from A_3, and five from B_2. One sample from A_3 (ZV-14) and two samples from B_2 (ZV-10 and ZV-77) were collected from the outcrop of TN flow, and the other samples were from the drill core. A schematic section through TN flow and location of samples were presented in an earlier publication (Fig. 3.1; Puchtel et al., 2009b).

Field investigations, petrographic studies, and studies of the lithophile element and isotopic systematics were reported previously (Arndt et al., 1988; Blichert-Toft et al., 2004; Nisbet et al., 1987; Renner et al., 1994; Shimizu et al., 2005). A Pb-Pb isochron age of 2692 $\pm$ 9 Ma was reported for the komatiitic sequence in the Reliance Formation (Chauvel et al., 1993). More recently, studies have focused on the HSE systematics of the komatiite lava flows in the Reliance Formation (Puchtel et al., 2009b; Walker and Nisbet, 2002; Zhou, 1994).

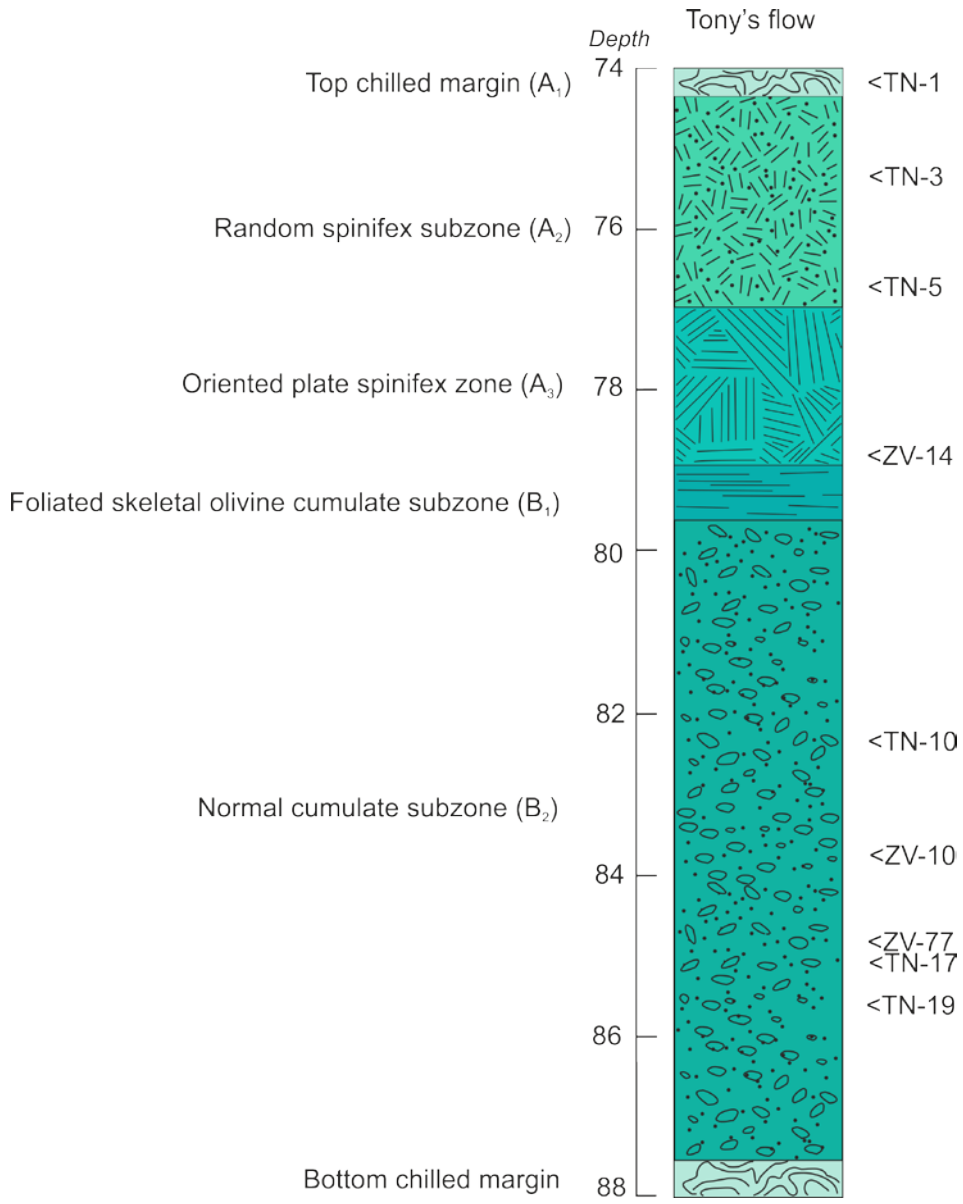

Fig. 3.1 Schematic section through the TN flow of the Belingwe Greenstone Belt and location of the analyzed samples. It was modified after Puchtel et al., 2009b.

Table 3.1 Bulk rock abundances of the elements of interest in geological reference materials

Reference material	Bobms	S (ppm)	2σ	Se (ppb)	2σ	Te (ppb)	2σ	Cu (ppm)	2σ	Ag (ppb)	2σ	In (ng/g)	2σ	Cd (ng/g)	2σ	Tl (ng/g)	2σ	Mo (ng/g)	2σ	Sm (ng/g)	2σ	Ba (µg/g)	2σ
OKUM 4218/1164 (komatiite)	a	230	5	146	2	24.6	0.4	46.5	0.6	3.54	0.08	31.2	0.2	49.3	0.7	15.4	0.3	-	-	-	-	5.38	0.08
	b	239	4	143	2	24.2	0.6	43.8	0.3	6.80	0.06	32.7	0.2	-	-	-	-	228	2	745	9	5.63	0.07
	c	232	4	142	2	23.5	0.5	46.2	0.3	5.34	0.07	33.3	0.3	49.6	0.6	15.4	0.2	223	2	755	9	5.62	0.07
	d	234	4	143	2	26	3	45.1	0.3	5.69	0.06	32.1	0.5	49.4	0.6	15.4	0.2	233	3	719	9	5.47	0.07
	Mean	**234**	4	**144**	2	**25**	2	**45**	1	**5.3**	1.4	**32**	1	**49.4**	0.2	**15.4**	0.1	**228**	5	**740**	19	**5.5**	0.1
OKUM 4210/1114 (komatiite)	a	234	5	144	2	24.3	0.4	46.5	0.6	3.97	0.08	30.4	0.2	49.4	0.7	15.1	0.3	276	3	-	-	5.33	0.08
	b	233	4	144	3	25.1	0.4	48.6	0.3	4.21	0.06	32.9	0.3	50.7	0.6	15.4	0.3	185	2	765	15	5.69	0.09
	c	232	4	141	3	23.9	0.3	42.7	0.3	3.59	0.07	32.9	0.2	49.0	0.6	16.2	0.2	230	3	748	9	5.91	0.07
	d	229	4	140	2	25.3	0.7	45.0	0.3	4.19	0.07	32.4	0.3	48.8	0.6	15.6	0.2	194	2	732	9	5.58	0.07
	e	232	4	143	2	24.1	0.7	44.7	0.3	5.07	0.09	32.9	0.4	48.8	0.9	15.5	0.3	256	5	729	10	5.58	0.07
	f	231	4	143	2	24.6	0.6	46.7	0.3	3.5	0.2	32.6	0.5	49.0	0.8	15.4	0.2	201	3	745	9	5.54	0.07
	g	234	4	144	3	28.4	0.7	43.5	0.3	3.63	0.07	31.2	0.3	49.4	0.7	17.8	0.3	180	2	744	9	5.6	0.07
	Mean	**232**	2	**143**	2	**25**	2	**45**	2	**4.1**	0.5	**32**	1	**49**	1	**15.9**	0.9	**217**	37	**744**	13	**5.6**	0.2
MUH-1 (harzburgite)	a	140	2	78	1	16.9	0.3	19.1	0.1	10.81	0.08	6.44	0.07	17.8	0.2	3.82	0.06	383	7	64	1	4.62	0.06
	b	140	2	78	1	16.4	0.3	19.0	0.1	8.92	0.07	6.54	0.07	18.0	0.2	3.79	0.06	398	7	64	1	4.62	0.06
	c	-	-	-	-	12.1	0.2	18.3	0.1	9.57	0.08	6.55	0.07	17.4	0.2	3.64	0.06	301	4	62.6	0.9	4.87	0.06
	d	151	3	78	1	12.3	0.1	19	0.1	9.52	0.08	5.97	0.08	17.7	0.3	-	-	380	5	65	1	4.75	0.06
	e	138	3	76	1	11.2	0.2	19.8	0.1	13.6	0.1	6.52	0.09	18.7	0.3	2.91	0.07	328	5	66.5	0.9	4.59	0.06
	Mean	**142**	**6**	**78**	1	**14**	3	**19.0**	0.5	**10.5**	1.9	**6.4**	**0.3**	**18.1**	0.5	**3.5**	0.4	**358**	41	**64**	2	**4.7**	0.1
PK 3	a	158	3	54	1	13.1	0.1	14.63	0.08	5.2	0.2	13.6	0.1	23.5	0.5	_	_	37	1	253	3	1178	16
	b	156	3	54	1	12.9	0.1	14.37	0.08	4.77	0.07	13.9	0.1	23.5	0.3	9.1	0.1	43	1	255	3	1192	16

3.4 Analytical methods and data quality

3.4.1 Analytical methods

Abundances of the studied trace elements were determined by isotope dilution ICP-MS in the same sample aliquots using HF-HNO_3 digestion in PFA beakers enclosed in pressure bombs. The details of this technique are referred in the recent publication (Wang et al., 2015) and an overview is given here.

Samples, spike solutions (^{34}S, ^{97}Mo, ^{77}Se-^{125}Te, ^{137}Ba, ^{65}Cu-^{109}Ag-^{113}In-^{110}Cd-^{149}Sm and ^{203}Tl), and HF-HNO_3 (4 ml: 1 ml) were weighted into 15 ml PFA beakers. Two Teflon beakers were then placed into one Teflon liner and sealed in a pressure bomb. The whole digestion process went on in an oven for three days at 190 ℃. After digestion, the transparent solutions were converted into chloride form, parts of which were then loaded on pre-cleaned anion resin columns. The Ba-Sm-S-Se cut was collected in 3.5 ml 4.5 mol l^{-1} HCl with matrix elements, and the Cu-In-Te-Mo cut was subsequently collected in 8 ml 0.4 mol l^{-1} HCl. The Ag-Cd-Tl fraction was collected at last by 28 ml 0.7 mol l^{-1} +1 ml H_2O_2. The Ag solution was dried and then dissolved in 4 ml 0.28 mol l-1 HNO_3. Intensities of $^{107, 109}$Ag, $^{110, 111, 112, 114}$Cd and $^{203, 205}$Tl were measured by Aridus-ICP-MS.

The Ba-Sm-S-Se fraction was separated into two aliquots, one for Ba-Sm and the other one for S-Se. The Ba-Sm fraction was dried and re-dissolved in HNO_3 Intensities of $^{135, 136, 137, 138}$Ba and $^{147, 149, 152, 154}$Sm were determined by spray chamber ICP-MS.The S-Se cut was dried and re-dissolved in 1 ml 0.28 mol l^{-1} HNO_3. The re-dissolved solution was further purified on cation resin, and S and Se were collected in 3 ml 0.1 mol l^{-1} HNO_3. Intensities of $^{77, 78, 82}$Se were obtained by hydride-generation method using a double pass Scott-type spray glass chamber and intensities of $^{32, 33, 34}$S in the same fraction was measured in medium-precision model of ICP-MS using a single pass Scott-type spray chamber.

The Cu-In-Te-Mo fraction with ascorbic acid was further purified on anion resin chromatography. The elements of interest were collected in 4.5 ml 0.4 mol l^{-1} HCl and ~0.1 ml H_2O_2 was added remove the ascorbic acid. The solution was dried and then dissolved in 4 ml 0.28 mol l^{-1} HNO_3. Intensities of $^{63, 65}$Cu, $^{113, 115}$In, $^{125, 126, 128}$Te and $^{98, 100}$Mo were determined by using Aridus-ICP-MS.

3.4.2 Data quality

The total procedural blanks (± 1 SD) of the interested elements during the long term measurement were 1.1 ± 0.4 μg (n = 17) for S, 0.10 ± 0.01 ng (n = 15) for Se, 0.01 ± 0.01 ng for Te (n = 10), 0.02 ± 0.02 μg for Cu (n = 10), 0.04 ± 0.03 ng for Ag (n = 10), 0.02 ± 0.03 ng for In (n = 10), 0.014 ± 0.009 ng for Cd (n = 17), 0.03 ± 0.02 ng for Tl (n = 11), 0.9 ± 0.4 ng for Mo (n = 11), 0.02 ± 0.03 ng for Sm (n = 14) and 0.6 ± 0.3 ng for Ba (n = 11). These values are comparable to data in (Wang et al., 2015).

Three geological reference materials were analyzed during the duration of this study, including two komatiites (OKUM 4218/1164 and 4210/1114) and a harzburgite (MUH-1). The results of the interested element abundances in the reference materials are given in Table 3.1. Mass fractions of S, Se, Te, Sm, and Ba in OKUM 4218/1164 and 4210/1114 agree very well with the published data by using various analytical methods (IAG, 2015a, b; Wang et al., 2015). The new S, Se, and Te data display better reproducibility than previously published data (Wang et al., 2015). To our knowledge, no Ag, Cu, In, Cd, Mo and Tl mass fraction data are available for these geological reference materials, and thus, we provide the first dataset of Ag, Cu, In, Cd, Mo, and Tl mass fractions in these reference materials. As shown in Table 3.1, the reproducibility of Ag between different digestion aliquots is, in general, less satisfactory (about 20-25%, 2 SD), possibly implying heterogeneity of Ag-hosted trace phases in the powder of the reference materials at the relatively small sample weights (~0.4 g). For Te, similar effects are observed with reproducibility of mass fractions between different digestion aliquots of about 10% (2 SD). The latter may stem from trace telluride phases, which are known to occur in mantle rocks (König et al., 2015a; König et al., 2012).

3.5 Results

Abundances of these trace elements in Belingwe komatiites are given in Table 3.2. With the exception of S, Ag, Tl and Ba, abundances of Se, Te, Cu, In, Cd, Mo and Sm in the chilled margin TN-01 (A_1) are higher than those in the cumulate subzone (B_{2-3}) but lower than those in the spinifex subzone (A_{2-3}). The S abundance of the chilled margin TN-01 is 718 μg/g, whereas S abundances vary from 466 μg/g to 611 μg/g in the spinifex subzone (A_{2-3}) and from 329 μg/g to 420 μg/g in the cumulate subzone (B_{2-3}). The distribution of Ag and Tl in the komatiite subzones are similar to that of S, being enriched in the chilled margin relative to the other subzones. Another feature is that the spinifex sample ZV-14 collected at the outcrop tends to have higher element abundances than the other samples. For example, Ba abundance

in ZV-14 is 23.7 μg/g, higher than 6.04-17.7 μg/g in the other samples; Ce abundance in ZV-14 is 2.68 μg/g, also higher than 2.51-2.48 μg/g in the other samples.

With the exception of Ba in the investigated samples, and S, Ag and Tl abundances in the chilled margin TN-01 (A_1), abundances of these elements in other subzones of the TN flow display a negative linear correlation with MgO contents (Fig. 3.2). For S, Se, Te and Cd, intersections of the correlations with the MgO axis are at higher MgO (Fig. 3.2A-C, 3.3B) than the average MgO content (50 wt.%) of cores of olivine from the cumulate subzone (Puchtel et al., 2009b). The intersections of correlations for Cu and Mo with the MgO axis, however, are near the average MgO content of cores of olivine from the cumulate subzone (Fig. 3.2D, 3.3C). The intersections of linear correlations for Ag, Tl, Sm and Ba with the MgO axis are lower than the average MgO content of cores of olivine from the cumulate subzone (Fig. 3.2E-F, 3.3D-E).

Table 3.2 Bulk rock abundances of the lements of interest in TN komatiites from the Belingwe Greenstone Belt*[1]

Sample number	Lithology*[2]	S (µg/g)	2σ	Se (ng/g)	2σ	Te (ng/g)	2σ	Cu (µg/g)	2σ	Ag (ng/g)	2σ	Tl (ng/g)	2σ	In (ng/g)	2σ	Cd (ng/g)	2σ	Mo (ng/g)	2σ	Sm (ng/g)	2σ	Ba (µg/g)	2σ
TN01	A_1	718	12	143	2	18	2	59.7	0.7	26.4	0.4	32.1	0.9	28.5	0.3	56	1	44.3	0.2	626	6	17.7	0.2
duplicate		712	13	143	3	20.7	0.6	56	1	26.1	0.5	32	1	29.1	0.2	56	1	44.6	0.2	653	8	18.2	0.2
TN3	A_{2-3}	466	8	149	4	19.4	0.2	67.2	0.6	16.8	0.2	13.7	0.4	70.6	0.8	71	2	55.3	0.2	814	10	16.9	0.2
TN5	A_{2-3}	611	11	160	3	22.4	0.7	-	-	19.4	0.2	13.8	0.4	49.6	0.2	73	2	49.6	0.2	866	12	13.3	0.2
duplicate		610	10	160	3	21.4	0.6	76.7	0.6	19.4	0.2	13.4	0.4	-	-	73	2	-	-	774	7	12.5	0.2
ZV14	A_{2-3}	481	8	154	2	19.9	0.7	78	1	21	0.4	5.9	0.2	51.6	0.2	84	2	51.6	0.2	966	12	23.8	0.3
ZV77	B_{1-2}	420	7	119	2	14.3	0.8	45.1	0.6	12.5	0.2	6.0	0.1	25.3	0.2	55	1	36.3	0.2	642	8	6.09	0.08
duplicate		406	7	120	2	16.1	0.4	61	1	12.6	0.2	3.8	0.1	25.8	0.4	55	2	39.5	0.2	651	8	6.11	0.07
TN10	B_{1-2}	384	7	109	3	13.1	0.1	47.2	0.6	10.7	0.2	3.9	0.1	21.9	0.1	53	2	32.8	0.1	536	6	9.1	0.1
ZV10	B_{1-2}	392	7	116	3	14.5	0.4	53.1	0.6	14.3	0.2	5.8	0.1	24.7	0.1	58	1	35.5	0.1	633	8	7.46	0.09
TN17	B_{1-2}	328	6	96	2	13.3	0.2	43.4	0.6	11.8	0.3	7.1	0.2	20.0	0.1	48	2	29.8	0.1	419	4	8.2	0.1
duplicate		330	6	-	-	16.7	0.3	44.2	0.6	11.7	0.3	8.7	0.3	19.8	0.2	48	1	30	2	419	5	8.7	0.1
TN19	B_{1-2}	357	6	101	2	12.8	0.6	49.2	0.8	9.7	0.2	3.8	0.1	20.5	0.2	50	1	38.7	0.2	485	6	6.04	0.08

*[1]Samples are arranged according to the depth in drill core (Puchtel et al., 2009b). *[2] A_1, A_{2-3} and B_{1-2} represent chilled margin, spinifex subzone and cumulate subzone, respectively. The data of replicates were obtained from new digestions of the same sample powder.

3.6 Discussion

3.6.1 Secondary alteration and magmatic degassing

In previous studies of komatiites, two techniques were used to investigate element mobility and magmatic degassing in komatiites. One way is to evaluate element concentration data in diagrams vs. MgO contents in which samples undisturbed by secondary alteration processes should follow a linear correlation line (Puchtel et al., 2009b). Another method is to consider relative element abundances in BSE-normalized abundance diagrams (Robin-Popieul et al., 2012).

It has been shown that HSE define tight trends negatively correlated with MgO and intersect at average MgO contents comparable to that of cores of olivine from the cumulate zone ($B_{2\text{-}3}$; Puchtel et al., 2009b), indicating negligible effects of magmatic degassing and secondary mobilization. Sulfur, Ag and Tl abundances in the chilled margin (A_1), which deviate from the linear lines defined by samples from the spinifex and cumulate subzones (Fig. 3.2A, E, F), may have been enriched as a result of late-stage alteration.

Abundances of S, Ag and Tl in the chilled margin are enriched relative to rocks from the spinifex subzone. For instance, variations of Tl in the samples from the cumulate subzone and depletions of Ag compared to its neighboring elements (Fig. 3.3) suggest the mobilization of Tl by fluids. The abundances of Ag and S in the chilled margin are higher than in the other subzones (Fig. 3.2A, E). Furthermore, Tl abundances in the investigated samples seem to have been elevated in comparison to other elements, as displayed by the stronger enrichment of Tl in the BSE-normalized diagram (Fig. 3.4). It is likely that these variations and enrichments of S, Ag and Tl reflect element redistributions by late-stage alterations. Because estimates for Tl in the BSE vary in a limited range (Hertogen et al., 1980; Nielsen et al., 2014; Palme and O'Neill, 2014), it is likely that Tl abundances in Belingwe komatiites were enriched by post- and/or syn-emplacement processes, which is also displayed by the weak Tl-MgO correlation which may have been disrupted. Another possibility for enrichments of Tl in the BSE-normalized diagrams is that the underestimate of the BSE Tl budget (see 3.6.4.1). For the lithophile elements, only the fluid-mobile element Ba shows substantial disturbance (Fig. 3.3E and 3.4).

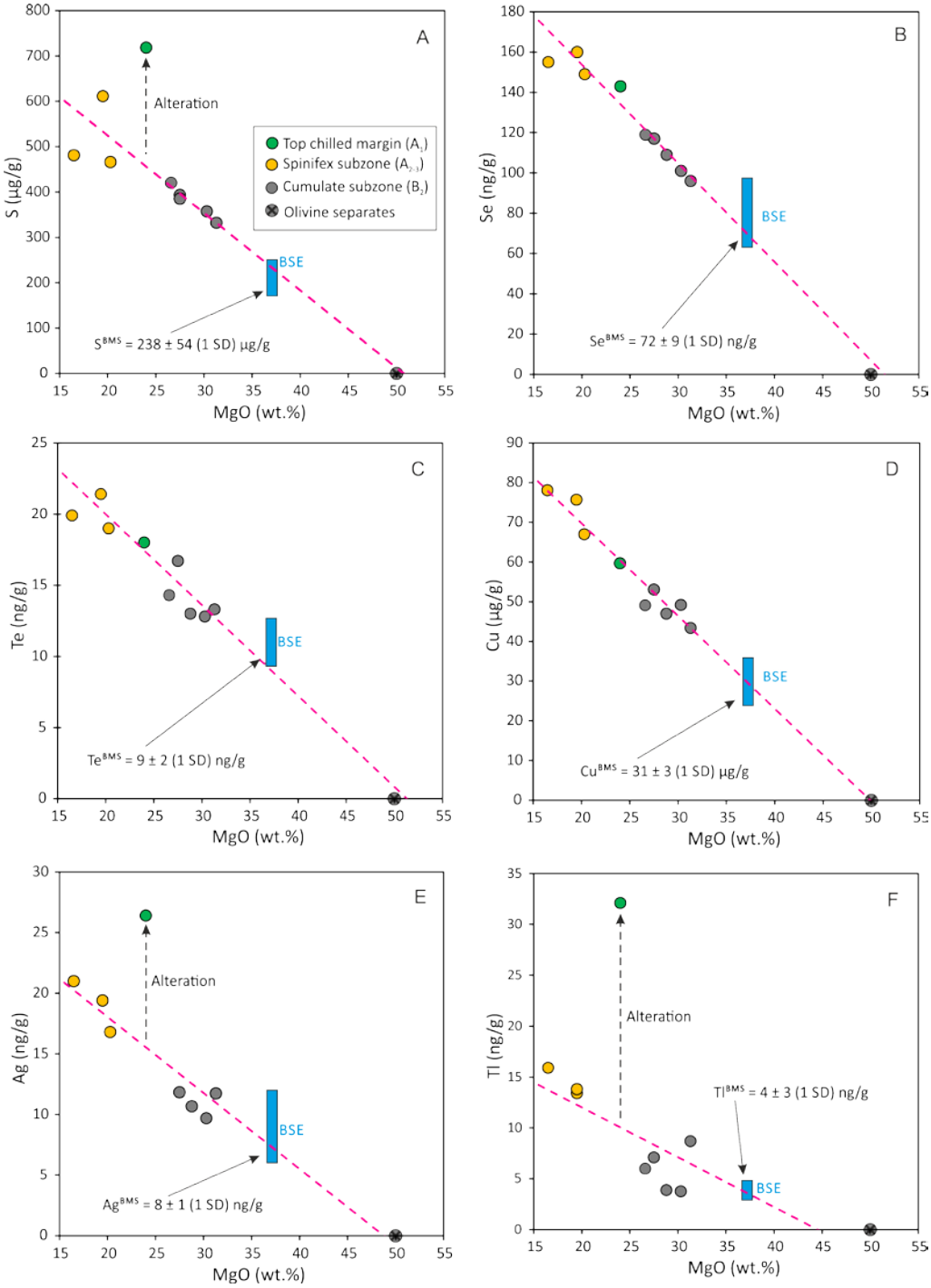

Fig. 3.2 Element variation diagrams of S, Se, Te, Cu, Ag and Tl as well as MgO contents of Belingwe komatiites. Abundances of S, Se, Te, Cu and Ag in the BSE are adopted from (Wang and Becker, 2013, 2015a), and the abundance of Tl in the BSE is adopted from Palme and O'Neill, 2014. Abundances of S, Se, Te, Cu and Ag in Belingwe Mantle Source (BMS) are calculated by projecting to MgO = 36.77 wt.% in the BSE (Palme and O'Neill, 2014). This technique has been applied to the studies of HSE in Archean komatiites (Puchtel et al., 2009b).

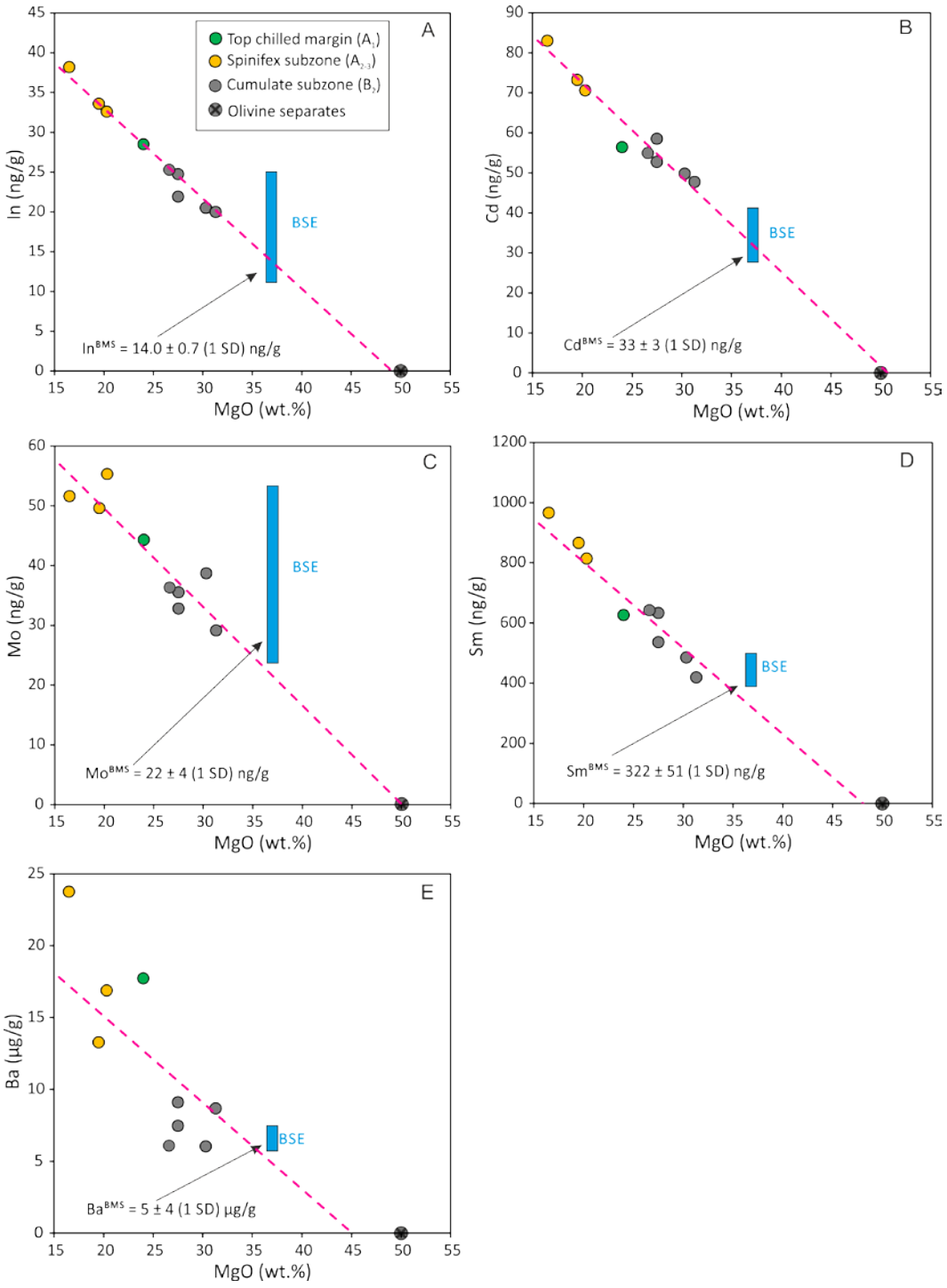

Fig. 3.3 Element variation diagrams of In, Cd, Mo, Sm and Ba with MgO contents of Belingwe komatiites. Abundances of these elements in the BSE are adopted from Palme and O'Neill, 2014. Abundances of In, Cd, Mo, Sm and Ba in Belingwe Mantle Source (BMS) are calculated by projecting to MgO = 36.77 wt.% in the BSE (Palme and O'Neill, 2014).

Volatile losses in Belingwe komatiites were likely negligible, as shown by studies on H_2O contents in fluid inclusions (Danyushevky et al., 2002; Kent et al., 2009). Copper is unlikely volatile in magmatic processes and ratios of Cu to potential volatile elements are useful indicators for the influence of igneous degassing (Handler et al., 1999). As shown in Fig 3.5D, Se/Cu in the Belingwe komatiites are not depleted relative to the BSE value, clearly suggesting the minimal volatile loss of Se. Sulfur abundances are not depleted relative to Se (Fig. 3.4), meaning that magmatic degassing had little effect on S abundances in the Belingwe komatiites. Another piece of evidence is that S abundances in the investigated samples are linearly correlated with MgO contents (Fig. 3.2A), and the intersection of the S-MgO correlation on MgO-axis is approximate to the average MgO content of cores of olivine from the cumulate subzone. If a significant amount of S was systematically lost by magmatic degassing, the intersection should be lower than the average MgO content of cores of olivine from the cumulate subzone. Minimal volatile losses of S and Se are also consistent with that the Belingwe komatiites are S-undersaturated rocks (see 3.6.2.1), in which these elements are dissolved in silicate melts and are unlikely degassed.

Therefore, we conclude that, with the exception indicated, the majority of the interested element abundances in the investigated samples represent the original magmatic composition of the rock units which formed TN flow. Thus, in the discussion of magmatic processes and compositions, S, Ag and Tl abundances in the chilled margin will not be considered.

3.6.2 Element fractionation during magmatic differentiation and partial melting

The Belingwe komatiites are characterized by strong depletions in highly incompatible elements such as light rare earth elements (LREE) and positive $\varepsilon^{143}Nd$ (Puchtel et al., 2009b), both indicating previous melt extractions. Some of these elements we studied are normally more incompatible than or comparable to Ce, such as Tl, Ba and Mo which likely underwent previous extraction events. Elements such as Tl and Ba, as discussed in 3.6.1, likely were affected by later-stage alteration leading to element enrichments or redistributions. Therefore, the sequence of these elements, together with HSE, in the BSE-normalized diagram (Fig. 3.4) is arranged in the order of increasing incompatibility. The order of the PGE, which are more compatible than the other elements, were well established based on the ultramafic-mafic magmatism (Becker and Dale, 2016; Puchtel et al., 2009b). The incompatibility of Cd is comparable to heavy rare earth elements such as Yb (Witt-Eickschen et al., 2009) and Dy (Yi

et al., 2000), whereas In is likely more incompatible than Cd as shown by the increase of In/Cd with In abundances in MORB (Yi et al., 2000) and mantle peridotites (Wang et al., 2016). Therefore, Cd and In are more compatible than Sm, as arranged in Fig. 3.4. The incompatibility of Mo and Tl were reported to be comparable to Ce (Nielsen et al., 2014; Sims et al., 1990). These elements (Cd, In, Sm, Mo, Ba and Tl) are arranged after chalcophile elements (Ag, Cu, Se, S and Re) the order of which are recently reported both on natural samples (König et al., 2014; Wang and Becker, 2015a; Wang et al., 2013) and sulfide-silicate partitioning experiments (Brenan, 2015; Li, 2014; Li and Audétat, 2012).

If magmatic signatures of these element are preserved, degrees of element abundance enrichments relative to the BSE should reflect their incompatibility during partial melting and lave differentiation. For the HSE, the degree of element abundance enrichments increases from Os, Ir, Ru below the BSE line to Pt, Pd and the other elements above the BSE line (Fig. 3.4), indicating that the latter elements are incompatible during the partial melting process that led to the formation of komatiites.

Differences in element abundances among the chilled margin (A_1), the spinifex subzone (A_{2-3}) and the cumulate subzone (B_{1-2}) can be used as an indicator of incompatibility during lava differentiation. The chilled margin (A_1) was interpreted to represent the primary and undifferentiated komatiite magma composition which differentiated into the spinifex subzone (A_{2-3}) and the cumulate subzone (B_{1-2}) (Puchtel and Humayun, 2001). Osmium, Ir and Ru abundances of the cumulate subzone (B_{1-2}) are higher than those of the spinifex subzone (A_{2-3}), whereas abundances of the other elements in spinifex subzone (A_{2-3}) are higher than those in the cumulate subzone (B_{1-2}) (Fig. 3.4).

3.6.2.1 Moderately and strongly Chalcophile elements

In 3.6.2.1, moderately to strongly siderophile elements are discussed, and elements are weakly chalcophile and predominantly lithophile during mafic-ultramafic magmatism will be discussed in 3.6.2.2. Ratios of S, Se, Te, Cu and Ag display little fractionation among the subzones of TN komatiites (Fig. 3.5), indicating that TN magma was not saturated in sulfides which, because of significant differences in sulfide-silicate partition coefficients ($D^{sulfide/silicate}$), would cause variable fractionation of these elements due to sulfide segregation in the mantle source and during magma transport. Platinum and Pd ($D^{sulfide/siulicate} > 10^5$; see review in Mungall and Brenan, 2014) are undepleted relative to S, Se, Te, Cu and Ag (Fig. 3.4; $D^{sulfide/siulicate} < 3000$; Brenan et al., 2016a; Li and Audétat, 2012; Liu and Brenan, 2015),

which clearly indicates that the parent lava flow was not saturated in sulfides. Because $D^{sulfide/siulicate}$ of Os, Ir, Ru, Pt and Pd are high and show limited variation (Mungall and Brenan, 2014), the depletion of Os, Ir and Ru relative to Pt and Pd was not caused sulfide segregation during magma transport or sulfide retention in the Belingwe mantle source. The depletions of Os, Ir and Ru most likely reflect the solubility of alloys of these elements in magma during partial melting (Borisov and Palme, 1995; Brenan and Andrews, 2001; Fonseca et al., 2011; Puchtel et al., 2009b).

The Se/Te ratios of the different subzones of TN flow are similar to the values of the BSE defined by post-Archean mantle peridotites, but much lower than those of MORB (Fig. 3.5B). The fractionated and variable Se/Te in MORB reflect the different $D^{sulfide/silicate}$ of these elements (Brenan, 2015) and retention of sulfide phases in the mantle (Lissner et al., 2014). As shown in Fig 3.5A, the majority of S/Se in MORB are comparable to those of mantle peridotites and Belingwe komatiites.

With the exception of Cu/Ag of TN-19 from the cumulate subzone (B_{1-2}), Cu/Ag ratios of Belingwe komatiites agree well with Cu/Ag of the BSE and the majority of MORB (Fig 3.5C). The slightly higher Cu/Ag of TN-19 from the cumulate subzone may either reflect minor redistribution of Cu or Ag. The komatiite data support previous conclusions from studies of mantle peridotites and MORBs that Cu and Ag are only little fractionated at moderate to high degrees of partial melting of the Earth's mantle (Wang and Becker, 2015a). This observation requires similar sulfide-silicate and bulk partition coefficients during a wide range of partial melting conditions.

Ratios of Se/Cu of Belingwe komatiites (Fig. 3.5D) are comparable to that of the BSE defined by mantle peridotites (Wang and Becker, 2015a) and MORBs from the southern Mid-Atlantic Ridge (Lissner et al., 2014).and some other MORBs (Jenner and O'Neill, 2012). In fact, Se/Cu ratios of global MORB show two trends (Fig. 3.5D). Se/Cu in some MORBs increase with Se abundances, whereas other MORBs do not show an increase with Se abundances and Se/Cu similar or only marginally higher than the value of the BSE. Divergent trends can also be observed by plotting Se/Cu against FeO contents of MORB (see 3.8 Appendix), especially when FeO contents exceed ~11%. The different trends of Se/Cu in MORB seem to be caused by sulfide segregation because $D^{sulfide/silicate}$ of Cu is higher than that of Se when FeO contents over ~11% (see the modelling in 3.8; Brenan, 2015). Previous explanations for the fractionated Se/Te in MORBs from the southern Mid-Atlantic Ridge

require that Se partially partitioned into monosulfide-solid solution (Mss; Lissner et al., 2014). If this was true, Se/Cu in these MORBs should have been fractionated because Cu was not thought to be in Mss (Fleet and Pan, 1994; Liu and Brenan, 2015; Mungall et al., 2005).

3.6.2.2 Predominantly lithophile elements

As shown in Fig. 3.6A, the apparent increase of Cd/In with Cd abundances in mantle peridotites indicates that Cd is more compatible in peridotites undergone low-moderate degrees of partial melting and late-stage melt percolation (Wang et al., 2016; Witt-Eickschen et al., 2009). Variations of Cd/In with In abundances in the Belingwe komatiites (Fig. 3.6B) showed that rocks of the cumulate subzone have low Cd abundances relative to the chilled margin but high Cd/In ratios relative to the spinifex subzone and chilled margin, indicating the partition of Cd into olivine dominating the mineral composition of the cumulate subzone. The three lithologic units of TN lava flow have distinct Cd/In ratios, implying that the Cd/In ratio of the chilled margin unlikely represents the mantle source ratio. The general decrease of Cd/In with In abundances in mantle peridotites, komatiites and MORBs also suggests the retention of Cd in residual mantle phases.

The ratio of Mo and Ce in oceanic basalts and continental rocks were found to be invariable and were used to constrain the Mo abundance in the BSE (Palme and O'Neill, 2014; Sims et al., 1990). However, as shown in Fig. 3.7, variations of Mo/Ce in mantle-derived rocks, including Archean komatiites, komatiitic basalts and oceanic basalts, are in the range of 0.005-0.1, a factor of 20. Furthermore, Mo/Ce in the two Indian MORBs measured by (Sims et al., 1990) are much lower than the other MORBs. Magmatic fractionation between Mo and Ce likely occurred if other processes were not involved in the formation of these rocks (Fig. 3.7). Recent work on Mo isotope compositions of Archean komatiites illustrated variable δ^{98}Mo (‰) of the lower Komati Formation from δ^{98}Mo = 0.08 in chilled margin BV 02 to δ^{98}Mo = 0.37-0.71 in rocks from the cumulate subzones (Greber et al., 2015), which were interpreted to reflect the incorporation of a ^{98}Mo-rich phase in the cumulate subzone. This indicates that Mo/Ce may be fractionated during lava differentiation. Mo/Ce in the lower Komati Formation are significantly lower than the other Archean komatiites (Fig. 3.7), though Mo abundances in the lower Komati Formation are comparable to that in the Weltevreden Formation, the Belingwe Greenstone Belt and Abitibi Greenstone Belt. Mo/Ce in the Victoria's Lava Lake are also lower than komatiites from the Weltevreden Formation, Belingwe, Abitibi and MORBs (Fig. 3.7). Sm-Nd isotopic data showed that Victoria's lava

lake likely was overprinted by continental materials (Puchtel et al., 1997), which may have decoupled Mo from Ce. Though the incompatibility of Mo was recently proposed to be similar to La rather than Ce (Yang et al., 2015), this is unlikely responsible for variations of Mo/Ce in mantle-derived ultramafic-mafic rocks. In contrast to komatiites from the other komatiites, Mo in the Belingwe komatiites display a negative correlation tightly following the

olivine control line (Fig. 3.3C) and limited fractionation between Mo and Ce (Fig. 3.7) in different lithologic units, indicating the preservation of magmatic signatures of Mo in the Belingwe komatiites.

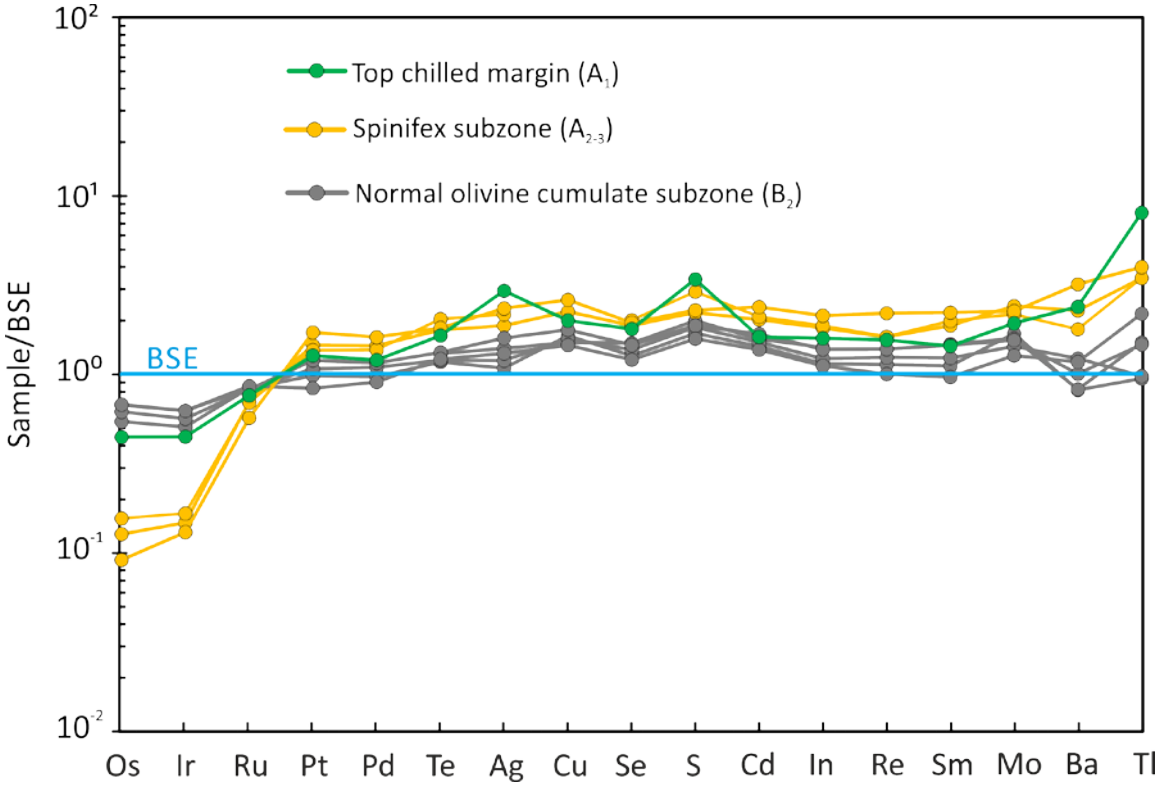

Fig. 3.4 Abundances of the interested elements in TN komatiites normalized to those of the BSE. The order of the interested elements are arranged according to their incompatibility in terrestrial mafic and ultramafic magmatism (see text). Abundances of HSE in the BSE are adopted from (Becker et al., 2006). Abundances of S, Se, Te, Cu and Ag in the BSE are adopted from Wang and Becker 2013, 2015. Abundances of the other elements in the BSE are adopted from Palme and O'Neill, 2014. Abundances of Os, Ir and Ru in samples of the cumulate subzone are higher than those in the spinifex subzone, indicating that these elements are compatible during partial melting and lava differentiation, while the other elements are incompatible. Abundances of S, Ag, Tl and presumably Ba in the chilled margin sample (A_1) are higher than those in the spinifex subzone, indicating that these elements may have been modified by late-stage alterations. For most elements, magmatic characteristics in TN komatiites were well-preserved.

Table 3.3 Comparison between the calculated and the measured element abundances of the emplaced magma (A_1)

	MgO	Os	Ir	Pd+Pt	S	Se	Te	Cu	Ag	Tl	In	Cd	Mo	Sm	Ba
	wt.%	ng/g	ng/g	ng/g	µg/g	ng/g	ng/g	µg/g	ng/g	ng/g	ng/g	ng/g	ng/g	ng/g	µg/g
Calculated	25	1.74	1.45	19.5	410	123	19	59.5	14.3	8.6	26.9	61.1	40	728	11.3
A_1(TN-01)	24	1.72	1.55	18.1	718	143	18	59.7	26.4	32.1	28.5	56.4	44	626	17.7
Δ(%)	-5%	-1%	7%	-7%	75%	16%	-7%	0%	84%	273%	6%	-8%	9%	-14%	56%

$$\Delta(\%) = (A_1\text{-Calculated}) / A_1 \times 100$$

3.6.3 Element abundances of the parent magma and the mantle source

3.6.3.1 Element abundances of the emplaced magma

As for the HSE (Puchtel et al., 2009b), chalcophile element abundances of the primary komatiite magma before emplacement and its putative mantle source may be calculated by extrapolation to the MgO content of the parent magma and the mantle source, respectively. The mass-balance-calculated results of the emplaced magma are presented in Table 3.3. The equation for the mass-balance calculation is given below:

$$C_0^i = \frac{L_{A2}}{L_{A2}+L_{A3}+L_{B1-2}} \times 100 \times \overline{C}_{A2}^i + \frac{L_{A3}}{L_{A2}+L_{A3}+L_{B1-2}} \times 100 \times \overline{C}_{A3}^i + \frac{L_{B1-2}}{L_{A2}+L_{A3}+L_{B1-2}} \times 100 \times \overline{C}_{B1-2}^i$$

Where $\overline{C}$ is the average abundance of element *i* in rocks from a specific lithologic unit; *L* is the mass of respective subzone; *0* represents the undifferentiated parent magma; A_2, A_3, and $B_{1\text{-}2}$ indicate the upper spinifex subzone, lower plate subzone and cumulate subzone, respectively. C_0^i is the abundance of *i* in the emplaced magma.

Calculated abundances of Cu, Te, Pt + Pd, Os, Ir, Mo, In and Cd in the emplaced undifferentiated parent magma are in agreement with abundances of these elements in the chilled margin (A_1) within 10%. The calculated abundances of S, Se, Ag, Sm, Tl and Ba deviate from abundances of these elements in the chilled margin (A_1) from 14% (Sm) up to a factor of 2.7 (Tl). With the exception of Sm, abundances of S, Se, Ag, Tl and Ba in the chilled margin (A_1) are higher than those calculated based on the mass-balance of subzones. The chilled margin underwent stronger aqueous alteration, whereas the other subzones were shielded from such processes by the chilled margin. Despite the deviations of S, Se, Ag, Tl and Ba in the chilled margin from calculated abundances, good agreements between Cu, Te, Pt + Pd, Os, Ir, Mo, In, and Cd abundances of the chilled margin and the calculated parent magma composition suggest that the differentiation of TN lava mainly proceeded in a closed system without tapping earlier lava flows or subsequent replenishment.

3.6.3.2 Element abundances in the mantle source

The method used to calculate element abundances in the komatiite mantle was applied to HSE in previous studies (*e.g.* Puchtel et al., 2009b). This method requires that similar sequences of mineral crystallization during magma differentiation and phases entering melt during partial melting, and mantle sulfides and silicates have the same rate of being extracted into melts. Because Belingwe komatiites are products of high-partial melting (Arndt et al.,

2008) which should have quantitatively consumed certain phases (Arndt et al., 2008) and resulted into S-undersaturated magma (see 3.6.2.1). It is thus possible to use linear correlations between these elements and magmatic proxies, such as MgO, to estimate element abundances in the mantle source by extrapolation to 36.77 wt.% MgO in the BSE (Palme and O'Neill, 2014). Due to significant differences in mineral-melt partition coefficients (Adam and Green, 2006), ratios of the incompatible lithophile elements may be affected by magmatic differentiation.

The calculated chalcophile element abundances (± 1 SD) of the Belingwe mantle source are, 251 ± 45 μg/g for S, 73 ± 8 ng/g for Se, 9 ± 1 ng/g for Te, 27 ± 3 μg/g for Cu and 6 ± 2 ng/g for Ag (Fig. 3.2A-E), assuming 36.77 wt.% MgO in the mantle source (Palme and O'Neill, 2014), very similar to the BSE model composition calculated from post-Archean mantle peridotites. We note that LREE of Belingwe komatiites are slightly depleted relative to the heavy rare earth elements (HREE) (Puchtel et al., 2009b), indicating that the Belingwe mantle source likely was slightly depleted in highly incompatible elements. Therefore, the results obtained from Belingwe komatiites may represent the lower limit of these elements in the BSE.

The calculated abundances (± 1 SD) of In, Cd and Mo in the Belingwe mantle source are, 11.4 ± 0.4 ng/g for In, 32 ± 2 ng/g for Cd and 20 ± 3 ng/g for Mo (Fig. 3.3A, B), assuming 36.77 wt.% MgO in the mantle source (Palme and O'Neill, 2014), which are also in the range of the BSE model composition calculated from post-Archean mantle peridotites. The calculated abundance of Mo in the Belingwe mantle source is 20 ± 3 ng/g for Mo, which is identical to the 23 ± 3 ng/g for Mo calculated from other Archean komatiites used to define the BSE Mo budget (Greber et al., 2015). We note that the calculated Sm abundance of the Belingwe mantle source is much lower than that of the BSE (Fig. 3.3D). Belingwe komatiites were depleted in light rare earth element abundances relative to the heavy rare earth elements (Puchtel et al., 2009b), which may reflect previous melt extraction.

Barium and Tl are more incompatible than the other elements of interest during partial melting of the Earth's mantle and are known to be highly mobile during aqueous alteration. Since Sm was depleted by previous melt extraction (Puchtel et al., 2009b), Ba and Mo should have been depleted more strongly. Therefore, the low values for Ba and Mo abundances in the Belingwe mantle source compared to the BSE (Fig. 3.3C, E) reflect the extraction of previous melt events. The abundance of Tl in the Belingwe mantle source obtained via the Tl-MgO

correlation (Fig. 3.2F) either reflects secondary enrichments of Tl or indicates the underestimate of Tl abundance in the BSE.

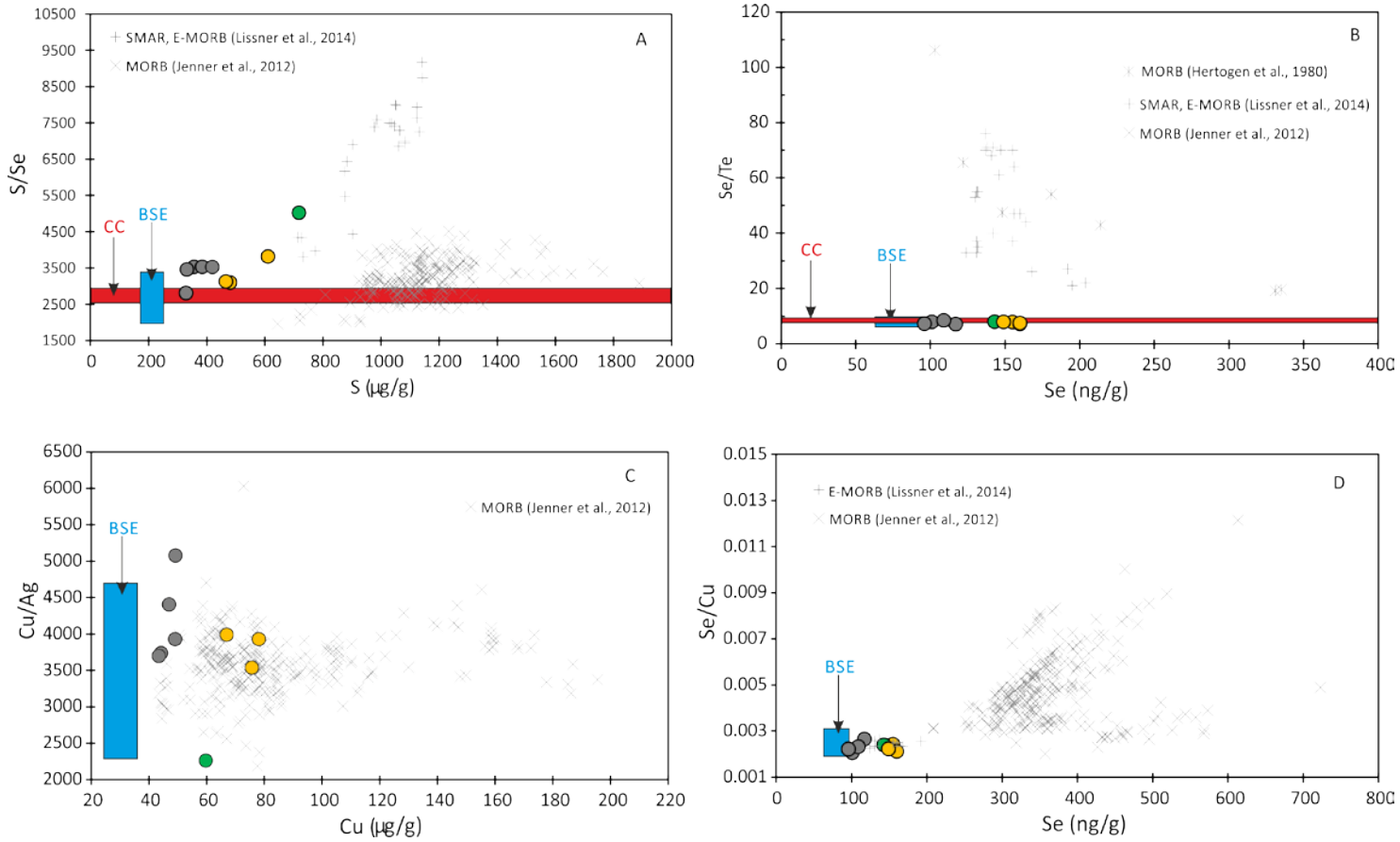

Fig. 3.5 Chalcophile element ratios plotted against element abundances, S/Se-S (A), Se/Te-Se (B), Cu/Ag-Ag (C) and Se/Cu-Se (D). Chalcophile element ratios of the BSE were obtained from mantle peridotites (Wang and Becker, 2013, 2015a). Oceanic basalts data were obtained by different workers using various techniques (Hertogen et al., 1980; Jenner and O'Neill, 2012; Lissner et al., 2014). Chalcophile element ratios of carbonaceous chondrites (CC) are calculated from Wang and Becker, 2013. Although the S/Se of TN komatiites agrees with that of the BSE within uncertainties, it may be higher than that of CC. Se/Te ratios of TN komatiites are identical to those of the BSE and CC within uncertainties. The Cu/Ag and Se/Cu of TN komatiites do not differ from those of the BSE within uncertainties.

3.6.4 Constrains on accretion and core formation

3.6.4.1 Origins of S, Se, Te, Cu and Ag in the BSE

The S/Se (3306 ± 856 1SD) of Belingwe mantle source is comparable to that of the BSE (2670 ± 700) that is in the range CI chondrites (2750 ± 200; Fig. 3.5A), whereas the Se/Te (8.0 ± 2.0) of Belingwe mantle source is comparable to those of the BSE (7.9 ± 1.6) and CI chondrites (8.5 ± 0.7; Fig. 3.5B). The carbonaceous chondrite-like S/Se and Se/Te in the Belingwe mantle source require late accretion of volatile-rich material after the cessation of core formation (Wang and Becker, 2013). Abundances and chondritic ratios of S, Se and Te in the Belingwe mantle source are in agreement with the timing of homogenization of late accreted materials in the terrestrial mantle suggested by Pt and Pd abundances in Archean komatiites (Maier et al., 2009). The constraints from abundances of Se and Te in the BSE are consistent with the observation that stable Se and Te isotopic compositions of terrestrial rocks overlap with data on chondrites within measurement uncertainties (Fehr et al., 2004; Vollstaedt et al., 2015). The S isotope composition of MORBs and metasomatised mantle xenoliths are $\delta^{34/32}S = -1.28 \pm 0.33$ ‰ and $\delta^{34/32}S = -5.4$ to -1.4 ‰, respectively (Giuliani et al., 2016; Labidi et al., 2013). The negative, non-chondritic S isotope composition in these rocks was thought to suggest that the mantle sulfur budget was established by the terrestrial core formation (Labidi et al., 2013). However, as revealed in 2.8, the sulfide segregation in sulfide-saturated MORBs is likely an ubiquitous process potentially leading to S isotope fractionation which was found in magmatic sulfide ore deposits (Ackermn et al., 2015; Fiorentini et al., 2012b; Seal, 2006). Metasomatised mantle xenoliths in kimberlite which is enriched in volatile species could have been affected by rock-fluid interaction (Stefánsson et al., 2015) and magmatic degassing (Handler et al., 1999). Neither lithology is without flaws with respect to constraining the S isotope composition of the BSE. Other lithologies, such as fresh fertile mantle peridotites and unaltered and barren sulfide-undersaturated komatiites, may provide additional constraints on the S isotope composition of the BSE.

Ratios of Cu/Ag in the Belingwe mantle source (3875 ± 613 1SD) are comparable to that of the BSE as defined by mantle peridotites (Wang and Becker, 2015a). Late accretion after terrestrial core formation can be excluded as an influential process controlling the budgets of Cu and Ag in the BSE on the basis of mass balance calculations (Wang and Becker, 2015a). The Cu/Ag of the Belingwe mantle source does not match any chondrites, which was

also observed in work on mantle peridotites (Wang and Becker, 2015a). This may reflect the disproportional segregation of Cu and Ag into the terrestrial core at high pressure-temperature conditions or a nonchondritic Cu/Ag in Earth's building materials or both. In low pressure-temperature core formation scenarios, Ag should be less depleted than Cu in the BSE (Wood et al., 2014). However, Ag is depleted by a factor of 5-6 relative to Cu in the BSE. In high pressure-temperature core formation scenarios involving carbon- and sulfur-bearing metal, Cu can be depleted to its current value in the BSE (Righter, 2011). For Ag, the situation is unclear, because no high pressure-temperature experimental data have been published. Recent work on the Cu isotopic composition of terrestrial rocks and chondrites suggests that segregation of a sulfide matte from enstatite chondrite-like accreted material may explain the difference in Cu isotopic composition between the BSE and enstatite chondrites (Savage et al., 2015). However, if sulfide matte was able to fractionate Cu isotopes during the late stage of core formation, one would expect that Cu isotopes would also fractionate among mantle peridotites, Archean komatiites and MORB, which was not observed (Savage et al., 2015). In fact, the Cu isotopic composition of the BSE (δ^{65}Cu = 0.07 ± 0.1‰, 2SD) is similar to that of CI chondrites within uncertainties (Liu et al., 2015; Savage et al., 2015). Recent studies on the Si isotopic composition of terrestrial rocks and chondrites excluded enstatite chondrite as building materials of the Earth (Dauphas et al., 2015; Fitoussi and Bourdon, 2012). The Cu and Ag isotopic data (Schönbächler et al., 2010) are most consistent with carbonaceous chondrite-like material as the source of the Earth's inventory of these elements. The role of metal or sulfide segregation at high pressure-temperatures in setting the Cu/Ag abundance ratio in the BSE remains to be evaluated.

Because of the high incompatibility of Tl during terrestrial magmatism, its abundance in the BSE was poorly constrained. Based on the Tl/Rb in MORBs (Hertogen et al., 1980), Plame and O'Neil suggested that the BSE Tl budget of 4 ± 1 (1SD) ng/g (Palme and O'Neill, 2014). Tl/Ce in MORBs (Nielsen et al., 2014) likely suggested that the abundance of Tl in the BSE is 1.5 ± 0.4 ng/g. The abundance of Tl in the Belingwe mantle source constrained by the weak correlation between Tl and MgO is 4 ± 3 ng/g, the significant uncertainty of which likely reflects the late-stage disturbance of Tl in the studied rocks. Though abundances of Tl in continental rocks were determined (Heinrichs et al., 1980; Marowsky and Wedepohl, 1971), the relative behavior of Tl to Ce or Rb in continental crust is not well understood. Taking the estimate for the BSE Tl and Ce budgets from Palme and O'Neill 2014, the abundance of Tl in continental crust (Wedepohl, 1995) is enriched by a factor of 130 relative to the BSE value,

whereas the Ce in continental crust (Wedepohl, 1995) is just enriched by a factor of 34. Behaviors of Tl and Ce in the continental crust apparently differ from in the oceanic crust. We note that the enrichment factor of Rb in continental crust is similar to Tl. Tl/Rb in global MORBs (Jenner and O'Neill, 2012) is 0.014 ± 0.008 (1 SD) that yields 8 ± 5 ng/g Tl in the BSE using the BSE Rb budget of 605 ng/g (Palme and O'Neill, 2014). This is distinctive from previous estimates, indicating that the BSE Tl budget may be higher.

3.6.4.1 Origins of In and Cd abundances in the BSE

The abundances of In and Cd in the Belingwe mantle source are comparable to their abundances in the BSE obtained from fertile mantle peridotites (Wang et al., 2016). It was noticed before that the less volatile Cd is far more depleted in the BSE than In (Witt-Eickschen et al., 2009). High-pressure-temperature metal-silicate partition coefficients of Cd and In relevant for terrestrial accretion show that In is more siderophile than Cd (Wang et al., 2016), indicating that the depletion of Cd relative to In in the BSE was not caused by core formation. Recent work proposed that the relative depletion of In, Cd, and Zn in the BSE was not relevant to core formation at various conditions (Wang et al., 2016). According to these authors, the element patterns were caused by non-chondritic materials of the Earth that underwent volatile fractionation at non-solar conditions.

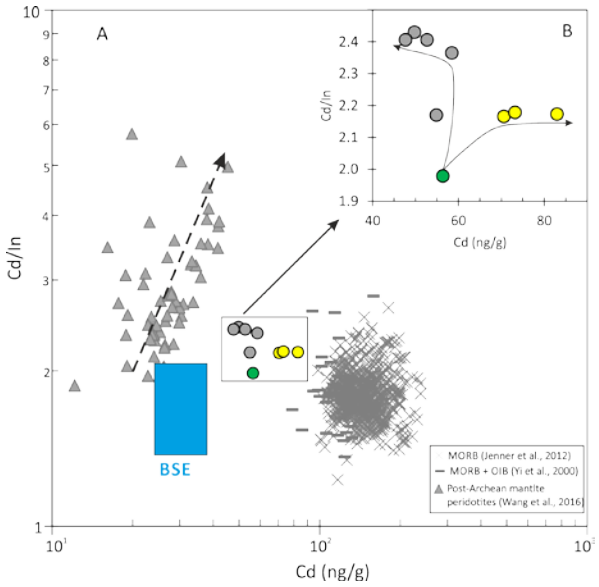

Fig. 3.6 Cd/In plotted against abundances of Cd. Abundances of these elements in the BSE (Palme and O'Neill, 2014). Abundances of In and Cd in MORB and OIB are adopted from Jenner and O'Neill (2012) and Yi et al. (2000). Data on fertile mantle peridotites are adopted from Wang et al. (2016). The variation of Cd/In with Cd abundances likely indicates that Cd is more compatible than In.

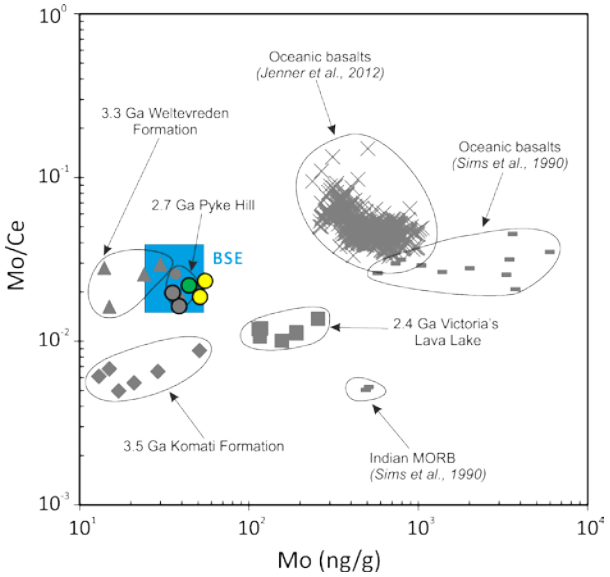

Fig. 3.7 Mo/Ce plotted against Mo abundances. Abundances of these elements in the BSE (Palme and O'Neill, 2014). Abundances of Mo and Ce in MORB and OIB are adopted from Jenner and O'Neill (2012), Newsom et al.(1986) and Sims et al. (1990). Abundances of Mo and Ce in Archean komatiites are from literature (Greber et al., 2015; Puchtel et al., 2013; Puchtel et al., 1997; Puchtel et al., 2004). The variation of Mo/Ce in mantle-derived rocks likely suggests the heterogeneity of mantle sources.

3.7 Summary and conclusion

In this study we report the abundances of chalcophile elements (S, Se, Te, Cu, Ag and Tl), mostly lithophile elements (In, Cd, Sm, Mo and Ba) and siderophile element Mo in the 2.7 Ga Tony's komatiites from the Belingwe Greenstone Belt in Zimbabwe by using the isotope dilution ICP-MS method. The main contribution of this study is that the investigated Belingwe komatiites, produced by high-degree of partial melting, were not saturated in sulfides, leading to little fractionation of incompatible chalcophile and lithophile elements. Because of the limited alteration of these rocks, the samples can be used to constrain abundances and ratios of these elements in the mantle source of the komatiites.

Except for S, Ag and Tl in the chilled margin (A_1), chalcophile elements in Belingwe komatiites preserve their magmatic characteristics. The calculated abundances of S, Se, Te, Cu and Ag in Belingwe mantle source agree with those obtained from fertile mantle peridotites. The approximately CI chondritic Se/Te ratio in the Belingwe mantle source require late accretion of volatile-rich materials. The Cu/Ag ratio is indistinguishable from the BSE value derived from mantle peridotites, which is not chondritic, either reflect core formation at high temperature and pressure conditions, or the composition of nonchondritic building materials of the Earth.

Abundances of In, Cd, and Sm in the Belingwe komatiites were not affected by late-stage alteration. The Belingwe mantle source composition of In and Cd is comparable to that of the BSE defined by mantle peridotites. Although Cd is less volatile than In during condensation in solar gas, it is more depleted than In in the BSE, which implies a non-chondritic origin for In and Cd in the Earth. The abundance of Mo in the Belingwe mantle source is in agreement with recent constrains from Archean komatiites.

3.8 Appendix Chapter 3

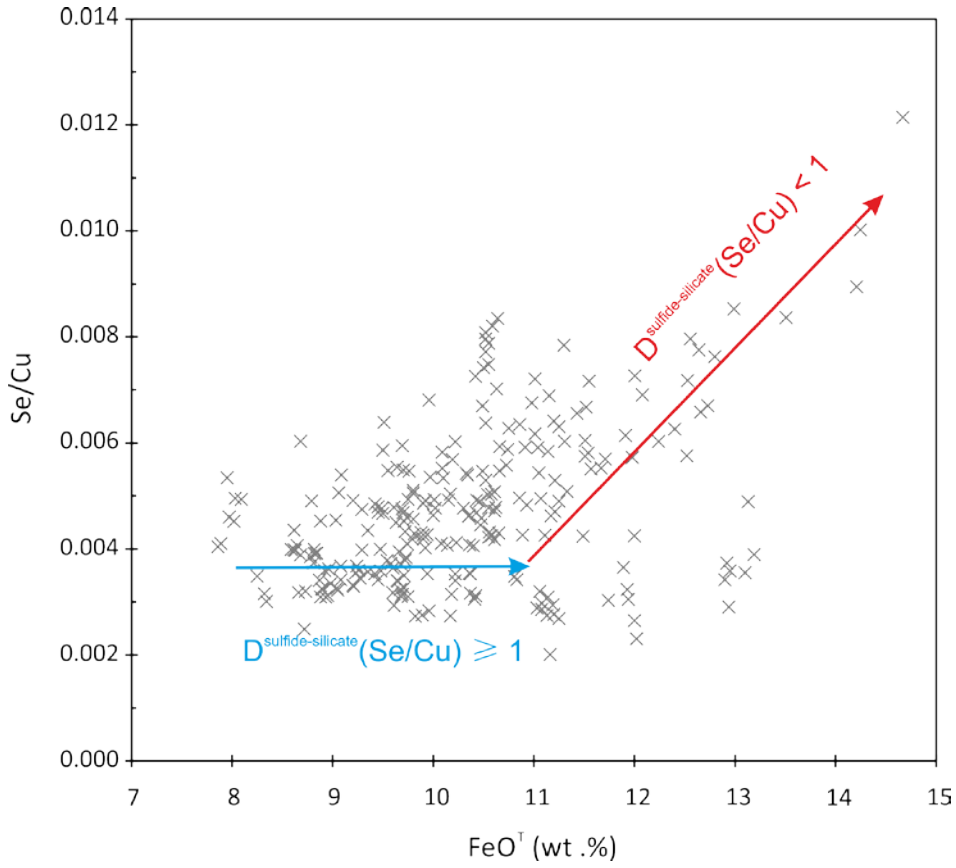

Fig. S3.1 Se/Cu in MORB plotted against FeO^{T}. Data on MORB were reported by Jenner and O'Neill (2012). As discussed in the text, the divergent trends of Se/Cu as a function of FeO contents may reflect the removal of Cu by sulfide segregation, because Cu tends to be more chalcophile than Se in sulfide-saturated MORB when FeO contents exceed 11 wt.% (Brenan, 2015). The increase in Se/Cu was interpreted to indicate a Cu-rich sulfide mineral (Barnes et al., 2009; Brenan, 2015).

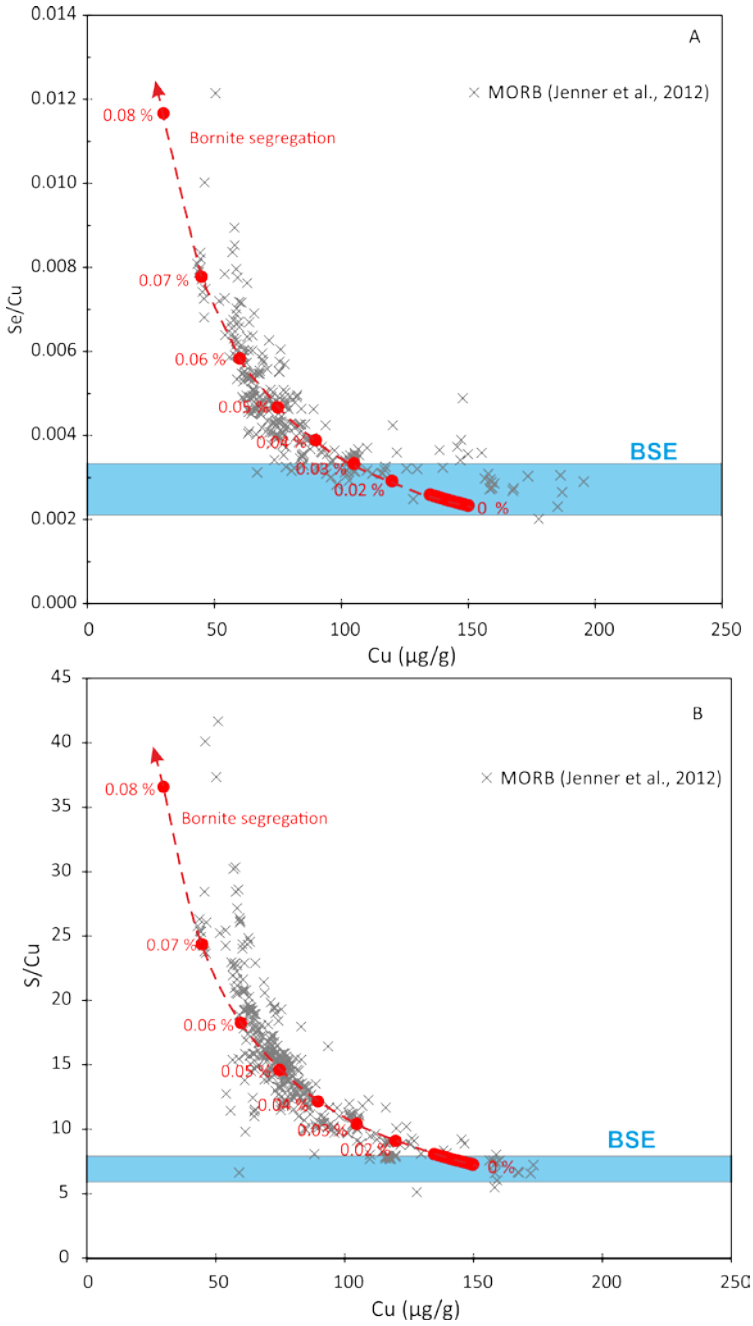

Fig. S3.2 Modelling of bornite segregation in MORB resulting into variations of Se/Cu and S/Cu with Cu abundances. Data on MORB were reported by (Jenner and O'Neill, 2012). Details about this modelling are explained below.

Variations of Se/Cu in MORB were thought to reflect the increasing $D_{Cu}^{sulfide/silicate}$ with FeO^T and decreasing MgO contents caused by magnetite crystallization (Brenan, 2015). Sulfide liquid-silicate melt partitioning experiments showed that $D_{Cu}^{sulfide/silicate}$ / $D_{Se}^{sulfide/silicate}$ evolved to be higher than 1 as FeO^T exceeding 11 wt.%, which may be caused by the segregation of bornite (Cu_5FeS_4) during magma evolution (Brenan, 2015). Here we modelled the effect of bornite segregation on variations of Se/Cu and S/Se with Cu abundances in MORB. Copper and S account for 63 wt.% and 26 wt.% in bornite (Cu_5FeS_4), which means that more Cu will be consumed by bornite segregation. In this simplified model we assume that Se does not partition into bornite and the abundance of Se is 350 ng/g that is corresponding to the mean value of Se in MORB (Jenner and O'Neill, 2012). The initial abundance of Cu was assumed to be 150 μg/g that is obtained by Se/Cu = 0.0027 ± 0.0006 in the BSE (Wang and Becker, 2015a) and the initial S abundance (1100 μg/g) is in the range of the S solubility in mafic melts (Mathez, 1976; O'Neill and Mavrogens, 2002).

The modelling shows that Se/Cu and S/Cu increase with decreasing Cu abundances by segregation of bornite (0% to 0.08%), which agree perfectly with the MORB data. This demonstrate that bornite segregation is responsible for variations of Cu, S and Se in global MORB, especially those are saturated in sulfide. Former studies thought that either Mss-sulfide partitioning or sulfide-silicate partitioning was the fundamental mechanism fractionating chalcophile elements in MORB (Lissner et al., 2014). The modelling here implies that the segregation of certain types of sulfides may result in systematic depletions of chalcophile elements. Sulfide liquid-silicate melt partition coefficients of Cu and Se are approximately 400-1200 and 300-1700, respectively (Brenan, 2015; Kiseeva and Wood; Li, 2014; Li and Audétat, 2012), whereas Mss-silicate partition coefficients of Cu and Se are 300-500 (Brenan, 2015; Li, 2014) and ~1200 (Brenan, 2015; Liu and Brenan, 2015), respectively. Together with these experimental data and the modelling, the fractionation of Cu, Se and S in MORB is predominantly controlled by sulfide liquid-silicate melt partitioning.

The formation of bornite in MORB requires two conditions, sulfide-saturated and FeO^T contents greater than 11 wt.%. However, from the current data it is in question about the relations between bornite and FeO^T in basaltic melts. Work on natural samples and experiments rarely investigated such details.

Chapter 4

Abundances of S, Se, Te, Cu and Ag in Archean komatiites and komatiitic basalts: Implication for the origins of chalcophile volatile elements in the terrestrial mantle

4.1 Abstract

The chalcophile element (S, Se, Te, Cu and Ag) composition of the terrestrial mantle have important implications for the accretion history of Earth. Near-chondritic ratios of S, Se and Te in Phanerozoic fertile mantle peridotites were interpreted to reflect a late addition of volatile-rich materials after core formation. The Cu/Ag in the bulk silicate Earth (BSE) is distinctive from the known groups of chondrites, which may be a combination of the effect of core formation and the composition of the building blocks for the Earth. In this study we attempt to use the chalcophile element composition in 45 well-characterized Archean komatiites, komatiitic basalts and olivine separates from different localities to understand the mechanisms controlling the budgets of these elements in the terrestrial mantle. Ratios of S, Se and Te in Pyke Hill flows (Abitibi Belt, 2.7 Ga) and Tony's flow (Belingwe, 2.7 Ga, Chapter 3) are indistinctive from those of fertile mantle peridotites. Cu/Ag ratios in Victoria's lava lake (Vetreny Belt) and Tony's flow (Belingwe, 2.7 Ga; Chapter 3) are within the estimate for the BSE from fertile mantle peridotites. The rocks from a single differentiated lava flow in the Komati Formation have S/Se, Se/Te and Cu/Ag ratios indistinguishable from the BSE, but Cu/Se, Ag/Se and Cu/Pd in these rocks are higher than the BSE. This discrepancy either reflects a Rayleigh-type degassing of volatile S, Se and Te in the Komati Formation, or indicates the different origins of two groups of elements (S- Se-Te-Pd vs. Cu-Ag) in the mantle source of Komati Formation. The Cu abundance in the primary magma, represented by a chilled margin sample, of the Weltevreden Formation may be resulted from a two-stage model involving early melt extraction events and the magmatism which formed the Al-enriched komatiites.

4.2 Introduction

Generally, chalcophile elements such as S, Se, Te, Cu and Ag are classified as cosmochemically moderate volatile elements and their budgets in the bulk silicate Earth (BSE) are normally constrained by mantle peridotites. Half mass condensation temperatures of these elements vary from ~1000 Kelvin of Cu and Ag to ~600 Kelvin of S, Se, and Te (Lodders, 2003), covering a broad range that is suitable to study volatile depletion of chalcophile elements during terrestrial accretion. The sulfide-silicate melt partitioning coefficients of these elements decrease from 2277 to 4565 of Te to 450-1680 of Cu and Ag and 258-407 of Se (Brenan, 2015; Li, 2014; Li and Audétat, 2012; Liu and Brenan, 2015), so diverse that the sulfide-related segregation in the early terrestrial mantle and magmatism can be evaluated. Recently S, Se and Te in the BSE were proposed to be late-accreted after the cessation of terrestrial core formation (Wang and Becker, 2013), whereas Earth's Cu and Ag seemed to be mainly controlled by core formation (Wang and Becker, 2015a). However, other studies suggested that the dominant fraction of Earth's volatiles could not be delivered by the late veneer (Labidi et al., 2013; Morbidelli and Wood, 2014). Some of the arguments these authors used might be problematic. Infulences of magmatic fractionation on S isotope composition in mid-ocean ridge basalts (MORBs) are not investigated *in extenso* which may weaken the argument that the S isotope composition of MORBs is representative of the BSE. Recent work on Cu and Ag in mantle peridotites showed that Cu and Ag in the BSE likely reflect the core formation or the composition of building blocks for the Earth (Wang and Becker, 2015a). This is consistent with the evidence from Cu and Ag isotope composition of the BSE (Liu et al., 2015; Savage et al., 2015; Schönbächler et al., 2010). However, as mentioned above these chalcophile/siderophile volatile elements differ in volatility and sulfide-silicate or metal-silicate partitioning, treating them as a whole group of similar geochemical behaviors may lead to confusions.

Controversy also exists about the chalcophile element composition in the BSE. Fertile mantle peridotites were not thought to represent the chalcophile element composition of the BSE, but a combination of depleted peridotites and infiltrating melts (König et al., 2014; König et al., 2015b; Lorand and Alard, 2010). The use of mantle-derived mafic rocks for estimating the chalcophile element composition of their mantle sources are impeded by sulfide segregation during the magma transport (König et al., 2014; Lissner et al., 2014). However, ratios of S, Se and Te in fertile mantle peridotites likely were not fractionated without addition or segregation of external magmatic sulfides (Wang and Becker, 2015b),

implying that melt infiltration in mantle leading to refertilization of depleted peridotites does not change the ratios of S, Se and Te. Here we attempt to constrain the behavior of moderately incompatible chalcophile elements in well-characterized Archean komatiites.

Komatiites and related ultramafic igneous rocks formed via high-degrees (30-50%) partial melting of the mantle have been proved to be useful probes into the evolution of terrestrial mantle (Arndt et al., 2008). Several groups of komatiites have been identified, including Al-depleted (Barberton-type) komatiite, Al-undepleted (Munro-type) komatiite, and Al-enriched komatiite from Gorgona Island (Arndt et al., 2008). The Al_2O_3/TiO_2 ratio was adopted as a petrogenesis indicator which reflects the difference in mantle compositions and melt evolution. Experimental results showed that the depletion of Al_2O_3 relative to TiO_2 in Barberton-type komatiites likely was caused by garnet retention during partial melting, and when garnet was melted, in the case of Munro-type komatiites, such a depletion would not occur (Robin-Popieul et al., 2012). In contrast to Barberton-type and Munro-type komatiites, Al-enriched komatiites were derived from a more depleted mantle source characterized by a high portion of garnet (Arndt et al., 2008; Robin-Popieul et al., 2012).

Some of the highly siderophile elements (HSE; Re, Os, Ir, Ru, Pt, Rh, Pd and Au) in Archean komatiites are essentially immobile after lava emplacement and, therefore the HSE composition of Archean mantle sources were constrained (Puchtel et al., 2009b). Though the incompatibility of HSE varies significantly during partial melting, the calculated composition of HSE in Archean komatiite mantle sources (Connolly et al., 2011) seem to be indistinguishable from those in the BSE defined by post-Archean peridotites massifs (Becker et al., 2006). However, a secular increase of Pt and Pd abundances in several Archean komatiite mantle sources was also reported (Maier et al., 2009). Thus, well-preserved Archean komatiites can be used to constrain the lithophile, siderophile and chalcophile element composition of Archean mantle reservoirs. This suggests that the composition of S, Se, Te, Cu and Ag, which are less chalcophile, but more incompatible than Pt and Pd, in Archean mantle reservoirs in principle can be estimated via Archean komatiites.

Sulfides in Earth's mantle should be exhausted when the degree of partial melting approaches 25% (Brenan, 2015; Peach et al., 1990), and, therefore komatiite magmas produced by 30-50% partial melting are likely to be S-undersaturated in their mantle source and en route to the surface of Earth, if no extensive assimilation of S-rich wall-rocks in the crust occurs. In contrast to MORBs, which are often saturated in sulfides, sulfide segregation

unlikely arises in komatiite magmas; therefore, mantle values of chalcophile element ratios should be preserved in Archean komatiites.

In this study, we report the abundances of S, Se, Te, Cu and Ag in well-characterized Archean komatiites and komatiitic basalts from various regions. The magmatic fractionation of chalcophile elements in the investigated rocks is discussed after the evaluation of post-emplacement alteration and potential volatile degassing on these elements. The origin of these chalcophile elements in the Earth will be discussed as well.

4.3 Samples and their preparation

Samples investigated in this study are from the 2.4 Ga Victoria's lava lake of the Vetreny Belt, the 2.7 Ga Pyke Hill flows of the Abitibi Greenstone Belt, the 3.3 Ga Weltevreden Formation and 3.5 Ga Komati Formation in the Barberton Greenstone Belt, and the 3.5 Ga Carl's flow of the Schapenburg Greenstone Remnant. Details about drilling core or cross section profiles of the investigated lava flows and petrology of the samples are referred to early publications (Puchtel and Humayun, 2001; Puchtel et al., 2004; Puchtel et al., 2009a; Puchtel et al., 2009b; Puchtel et al., 2014); here we summarize the information on petrogenesis, aqueous alteration and crustal contamination. Profiles of core drills or outcrops of the studied sequences are given in 4.8.1 Appendix.

Nine samples and two olivine separates analyzed in this study were collected from the surface outcrop of the 2.4 Ga Victoria's lava lake in the Vetreny Belt in Fennoscandia on the Baltic Shield. Most samples are komatiitic basalts with MgO contents lower than 18 wt.%, and a few samples are from the olivine cumulate subzone. Al_2O_3/TiO_2 ratios of the Victoria's lava lake are ~20, in the category of Munro-type komatiites. The Sm-Nd systematics revealed minor contamination (up to 7 mass %) by continental crustal materials during the formation of Victoria's lava lake (Puchtel et al., 1997, 2016b).

Twelve samples from two independent lava flows (Pyke Hill-I, II) of Munro-type komatiites in the drill core of the 2.7 Ga Abitibi Greenstone Belt from Munro Town in Canada were analyzed in the present work. In contrast to the well-preserved komatiites of the Belingwe Greenstone Belt (Chapter 3), the Abitibi komatiites were serpentinized significantly. No evidence for crustal contamination of the komatiite magma was found in the Abitibi komatiites based on Sm-Nd systematics of $\varepsilon^{143}Nd = +2.9 \pm 0.2$ (Puchtel et al., 2009b).

Ten samples from the surface outcrop of the 3.27 Ga Weltevreden Formation of the Barberton Greenstone Belt, South Africa, were selected for this study. They were collected from three independent differentiated lava flows, SA501 (501-3 to 501-10), KBA12 (12-2 to 12-8) and SA564 (564-4 and 564-6) in the Pioneer type locality. Samples investigated in this study are characterized by suprachondritic Al_2O_3/TiO_2 ratios (~30) and are categorized as Al-enriched komatiites. Primary silicate minerals in the Weltevreden Formation are rarely preserved (Kareem, 2005). Sm-Nd and Lu-Hf isotope systematics ($\varepsilon^{143}Nd = +0.50 \pm 0.11$ and $\varepsilon^{176}Hf = +4.7 \pm 0.8$) show that the Weltevreden komatiites were not significantly contaminated by interaction of komatiite magma with older crustal materials (Puchtel et al., 2013).

Six samples from the 3.48 Ga Komati Formation of the Barberton Greenstone Belt, South Africa, were studied, and they were collected from the surface outcrop of the differentiated lava flow 4 at the hillcrest in the Fig. 3 of Viljoen and Viljoen, 1969a; Viljoen and Viljoen, 1969b. The Komati Formation is the typical representative of Al-depleted (Barberton-type) komatiites of subchondritic Al_2O_3/TiO_2 ratios (~10). The Barberton Greenstone Belt underwent amphibolite facies metamorphism, and primary olivine and pyroxene are usually replaced by chlorite, serpentine, magnetite, basite and tremolite (Blichert-Toft et al., 2015; Robin-Popieul et al., 2012). Similar to the Weltevreden Formation from the same greenstone belt, Sm-Nd and Lu-Hf isotope systematics do not show evidence for significant assimilation of older crustal materials by komatiitic parent magma in the Komati Formation (Puchtel et al., 2013).

Six samples from Carl's flow in drill core of the 3.5 Ga Schapenburg Greenstone Remnant, South Africa, were analyzed in this study. The Schapenburg komatiites belong to the Barberton-type. Earlier studies showed that Al_2O_3 and high field strength elements (HFSE) are deviated from the olivine control line, indicating the mobilization of major oxides and some trace elements (Blichert-Toft et al., 2004; Lécuyer et al., 1994). Though samples selected for this study show well-preserved magmatic textures (Puchtel et al., 2009a), secondary metamorphic assemblages, including serpentine, amphibole, chlorite and magnetite, dominate the lava flow (Blichert-Toft et al., 2004). Recently the decoupled Hf and Nd systematics ($\varepsilon^{143}Nd = -2$ and $\varepsilon^{176}Hf = +5$) in clinopyroxene and their host rocks of Komati Formation were interpreted such that they require the presence of oceanic sediments in the mantle source of the Barberton Greenstone Belt (Blichert-Toft et al., 2015).

Abundances of platinum-group-elements (PGEs) in the investigated samples obtained by early studies showed limited secondary mobilization of by aqueous alteration. Platinum and Pd in the selected samples define negative correlations with MgO contents following the olivine control line. On the one hand this indicates that Pt and Pd likely were not altered by late-stage aqueous processes, and on the other hand it suggests that Pt and Pd are moderately incompatible during the evolution of komatiite magmas in contrast to compatible Os, Ir and Ru which do not show such negative correlations with MgO.

Details about sample preparation were given in previous studies (*e.g.* Puchtel et al., 2009b) and they are described briefly here. Due to the fact that samples were collected either from drill cores (Abitibi, Belingwe and Schapenburg) or surface outcrops (Victoria's lava lake, Komati and Weltevreden), they were processed in different protocols. For the samples collected from drill cores, each sample, 400-600 g in weight, was equally divided into four pieces by a diamond saw and one piece was used for the chemical studies. After removal of drill bit and saw marks by SiC sandpaper, the samples were washed in Milli-Q water, dried and crushed in an alumina-faced jaw crusher. Around 100 g of crushed sample was ground in an alumina shatter box and then re-ground in an alumina-faced disk mill. For the hand specimens, slabs of several hundred grams were initially separated for the chemical studies. Any visible weathering or alteration were removed by the diamond saw. The subsequent processing of the hand-specimens were the same to the drill core samples.

4.4 Analytical Techniques and data quality

Abundances of chalcophile elements were determined by isotope dilution ICP-MS in the same digestion aliquots using HF-HNO_3 digestion in PFA beakers in pressure bombs. The details of this technique were reported in (Wang et al., 2015). An abridged summary was given in Chapter 3. Total procedural blanks of chalcophile elements during this study were given in Chapter 3. Abundances of S, Se, Te, Cu and Ag in geological reference materials analyzed in the course of the present work are given in Table 3.1 in Chapter 3.

Table 4.1 Bulk rock abundances of chalcophile elements in Archean komatiites and komatiitic basalts*

Locality	Sample number[1]	Lithology	MgO (wt.%)[2]	LOI[2]	S (µg/g)	2σ[3]	Se (ng/g)	2σ	Te (ng/g)	2σ	Cu (µg/g)	2σ	Ag (ng/g)	2σ
Victoria's lava lake. 2.4 Ga Vetreny belt. Baltic Shield	12110	Scoria	13.7	2.25	512	9	151	3	12.6	0.1	85.5	0.6	41.0	0.6
	12111	upper chilled margin	13.6	1.54	112	2	112	2	31	1	89.5	0.7	30.2	0.3
	12117	pyroxene spinifex	11.2	0.58	234	4	96	2	6.36	0.07	103	1	31.5	0.3
	12101	pyroxene spinifex	10.1	0.74	98	2	144	2	6.5	0.1	98.7	0.7	37.7	0.6
	12124	fine-grained basalt	7.42	0.25	166	3	116	2	7.5	0.1	103.0	0.8	37.9	0.6
	12107	fine-grained basalt	7.77	0.35	148	3	105	2	8.6	0.08	99.4	0.7	35.2	0.6
	12001	olivine cumulate	26.4	2.99	202	3	80	1	3.4	0.1	64.8	0.8	19.9	0.4
	12105	olivine cumulate	26.6	3.21	206	3	80	7	3.4	0.1	65.8	0.8	19.8	0.2
	12106	olivine cumulate	21.5	1.06	138	2	106	1	3.8	0.1	83.4	0.6	24.5	0.4
	12001 Ol	olivine	45.2	0.01	3.5	0.1	2.0	0.2	3.77	0.05	4.34	0.02	0.44	0.07
	12105 Ol	olivine	44.1	0.01	5.0	0.2	2.6	0.2	12.4	0.3	3.84	0.02	2.61	0.09
Pyke Hill flow. 2.7 Ga Kidd-Munro Assemblage. Abitibi greenstone belt. Canada	***PH-I***													
	PH13	olivine spinifex	24.1	6.01	255	4	129	2	23	2	36.9	0.6	11.2	0.2
	PH14	olivine spinifex	23.5	5.67	242	4	131	2	22	2	32.9	0.4	8.4	0.2
	PH18	olivine cumulate	30.3	5.93	326	5	142	3	18.2	0.8	43.5	0.6	9.9	0.2
	PH20	olivine cumulate	32.4	7.15	370	6	112	2	14.9	0.4	5.16	0.06	2.3	0.4
	PH22	olivine cumulate	29.2	6.63	398	6	162	3	19.3	0.6	29.2	0.4	4.9	0.2
	PH23	chilled margin	27.5	6.73	479	7	167	4	27	1	22.5	0.2	5.1	0.2
	PH-II													
	PH25	upper chilled margin	27.8	6.88	419	7	145	3	14.7	0.6	32.6	0.4	5.8	0.2
	PH26	olivine spinifex	27.4	6.98	444	7	180	8	18.5	0.6	35.3	0.4	4.8	0.1
	PH28	olivine spinifex	26.8	6.11	391	6	151	2	14.1	0.6	70.0	0.8	16.9	0.2
	PH32	olivine cumulate	33.1	8.5	305	5	116	3	16.9	0.4	5.60	0.06	8.6	0.1
	PH33	olivine cumulate	31.8	7.64	316	5	119	8	15.7	0.4	8.6	0.1	6.7	0.1
	PH34	lower chilled margin	26.9	6.19	400	6	187	3	26	1	91	1	23.2	0.4
3.3 Ga Weltevreden Formation. Barberton greenstone belt. South Africa	***SA 501***													
	501-3	olivine spinifex	31.0	7.85	239	4	66	1	13.0	0.4	28.4	0.4	3.79	0.09
	501-4	olivine spinifex	-	-	296	5	129	2	6.41	0.12	23.3	0.2	3.78	0.09
	501-8	olivine cumulate	42.3	10.1	51	1	60	1	5.56	0.12	2.56	0.02	2.11	0.08
	501-9	olivine cumulate	42.1	9.79	55	1	41.7	0.8	3.64	0.1	1.06	0.02	1.56	0.08
	501-10	olivine cumulate	41.5	6.85	47	1	37	1	4.2	0.2	3.52	0.04	0.91	0.07
	duplicate				45	1	37	1	3.9	0.1	1.49	0.02	1.6	0.2
	KBA 12													
	12-2	olivine spinifex	28.9	8.08	71	1	75	2	7.0	0.1	27.3	0.2	21.0	0.2
	dupliacte				68	1	75	1	7.0	0.1	26.5	0.2	20.9	0.2
	12-6	olivine cumulate	40.7	9.36	67	1	38.2	0.9	4.6	0.1	4.08	0.04	1.51	0.08
	12-8	olivine cumulate	41.5	11.0	52	1	28	2	1.6	0.1	1.39	0.02	1.07	0.07

Table 4.1 continued

Locality	Sample number	Lithology	MgO (wt.%)[2]	LOI[2]	S (µg/g)	2σ	Se (ng/g)	2σ	Te (ng/g)	2σ	Cu (µg/g)	2σ	Ag (ng/g)	2σ
3.3 Ga Weltevreden Formation	***SA 564***													
	564-6	chilled margin	28.8	7.89	99	2	78	1	9.9	0.1	18.8	0.2	6.2	0.1
	564-4	olivine spinifex	28.8	7.89	29	1	25	1	29.5	1	13.5	0.1	4.8	0.1
Flow 4. 3.48 Ga Komati Formation. Barberton greenstone belt. South Africa	BV06	chilled margin	25.3	4.26	66	1	28	0.7	3.7	0.1	51.8	0.8	23.4	0.4
	BV05	olivine spinifex	28.2	6.23	189	3	58	1	6.1	0.1	45.1	0.6	10.3	0.2
	BV08	olivine spinifex	27.8	6.44	62	1	23.9	0.7	3.4	0.1	23.3	0.2	9.1	0.2
	BV04A	olivine spinifex	29.5	6.96	14.2	0.9	14.7	0.4	8.5	0.1	75	1	2.81	0.09
	BV04B	olivine cumulate	31.3	7.82	54	1	20.2	0.4	3.5	0.1	35.7	0.4	8.5	0.2
	BV03	olivine cumulate	35.3	5.79	66	1	31.0	0.6	9.1	0.2	26.3	0.4	12.6	0.2
Carl's flow. 3.5 Schapenburg greenstone remnant. South Africa	SCH1.1	olivine spinifex	26.5	4.15	473	8	104	2	24.1	0.7	288	5	111	2
	SCH1.5	olivine spinifex	25.9	2.80	317	5	78	2	14.4	0.2	146	1	66	1
	SCH1.9	olivine cumulate	32.3	7.09	24.6	0.7	4.1	0.6	1.0	0.1	0.40	0.04	4.7	0.1
	SCH1.10	olivine cumulate	36.0	8.27	45.9	0.9	13.5	0.8	2.7	0.1	0.50	0.04	4.3	0.1
	SCH1.20	olivine cumulate	32.5	7.11	62	1	11.7	0.7	1.47	0.05	0.57	0.04	2.5	0.2
	SCH1.21	olivine cumulate	30.0	6.19	46	1	14.1	0.5	0.87	0.05	2.79	0.06	3.0	0.2

[1]Samples are arranged according to the depth in drill core. Schematic profiles of the cores were presented by previous studies (Puchtel et al., 2016a; Puchtel et al., 2013; Puchtel et al., 2016b; Puchtel et al., 2009b; Puchtel et al., 2014) and are given in Appendix 4.8 for convenience. [2]Contents of MgO and LOI in these samples have been published previously (Puchtel et al., 2016a; Puchtel et al., 2013; Puchtel et al., 2016b; Puchtel et al., 2009b; Puchtel et al., 2014). [3]2σ represents in run precision defined by 2 standard deviation reflecting the analytical state of the instrument, the uncertainty of the element abundance of spike solutions and the contribution of total procedural blanks.

4.5Results

As shown in Table 4.1 and Fig. 4.1, abundances of S, Se, Te, Ag and Cu in pre-2.9 Ga komatiites (Schapenburg, Komati and Weltevreden) are systematically lower than those of post-2.9 Ga komatiites (Abitibi, Victoria's lava lake and Belingwe in Chapter 3). In contrast, contents of MgO in pre-2.9 Ga komatiites vary from 25.89 wt.% to 42.3 wt.%, which on average is higher than contents of MgO (16.5 wt.%-33.1 wt.%) in post-2.9 Ga komatiites. Abundances of S in pre-2.9 Ga komatiites range from 13.2 μg/g to 453 μg/g, whereas abundances of S in post-2.9 Ga komatiites range from 97 μg/g to 500 μg/g. Abundances of Se in pre-2.9 Ga komatiites and post-2.9 Ga komatiites vary from 3.81 ng/g to 119 ng/g and 95 ng to 175 ng/g, respectively. Abundances of Te in pre-2.9 Ga komatiites vary significantly from 0.82 ng/g to 27.2 ng/g, whereas abundances of Te in post-2.9 Ga komatiites range from 3.3 ng/g to 18.0 ng/g. The variation of Cu abundances of pre-2.9 Ga komatiites are larger than that of post-2.9 Ga komatiites, 0.4-276 μg/g and 5.11-102.7 μg/g, respectively. Abundances of Ag in Schapenburg komatiites vary from 2.3 μg/g to 106 μg/g, whereas in rocks from the Komati Formation and Weltevreden Formation abundances of Ag are less variable (1 μg/g to 22.4 μg/g). Abundances of Ag in post-2.9 Ga komatiites, 2.1-37.8 μg/g, are overall higher than those in rocks from the Komati Formaiton and Weltevreden Formation.

Another observation is that abundances of S, Se, Te, Cu and Ag tend to increase from cumulate subzones to spinifex subzones. For instance, in the PH-II lava flow, abundances of S in the cumulate subzone range from 329 μg/g to 393 μg/g, whereas in the spinifex subzone abundances of S are above 466 μg/g and up to 611 μg/g. Abundances of Cu in the same lava flow display a similar trend, 43.4-53.1 μg/g in cumulate subzone and 75.7-82.9 μg/g in spinifex subzone.

The third notable feature is that variations of S, Se, Te, Cu and Ag abundances of spinifex subzones are larger than abundance variations in the cumulate subzones. For instance, the variation of S abundances of the cumulate subzone of PH-II lava flow is around 13 μg/g, but in the spinifex subzone it is 46 μg/g. The variation of Cu abundances of the cumulate subzone of PH-II is around 8 μg/g, whereas in the spinifex subzone the variation is around 50 μg/g.

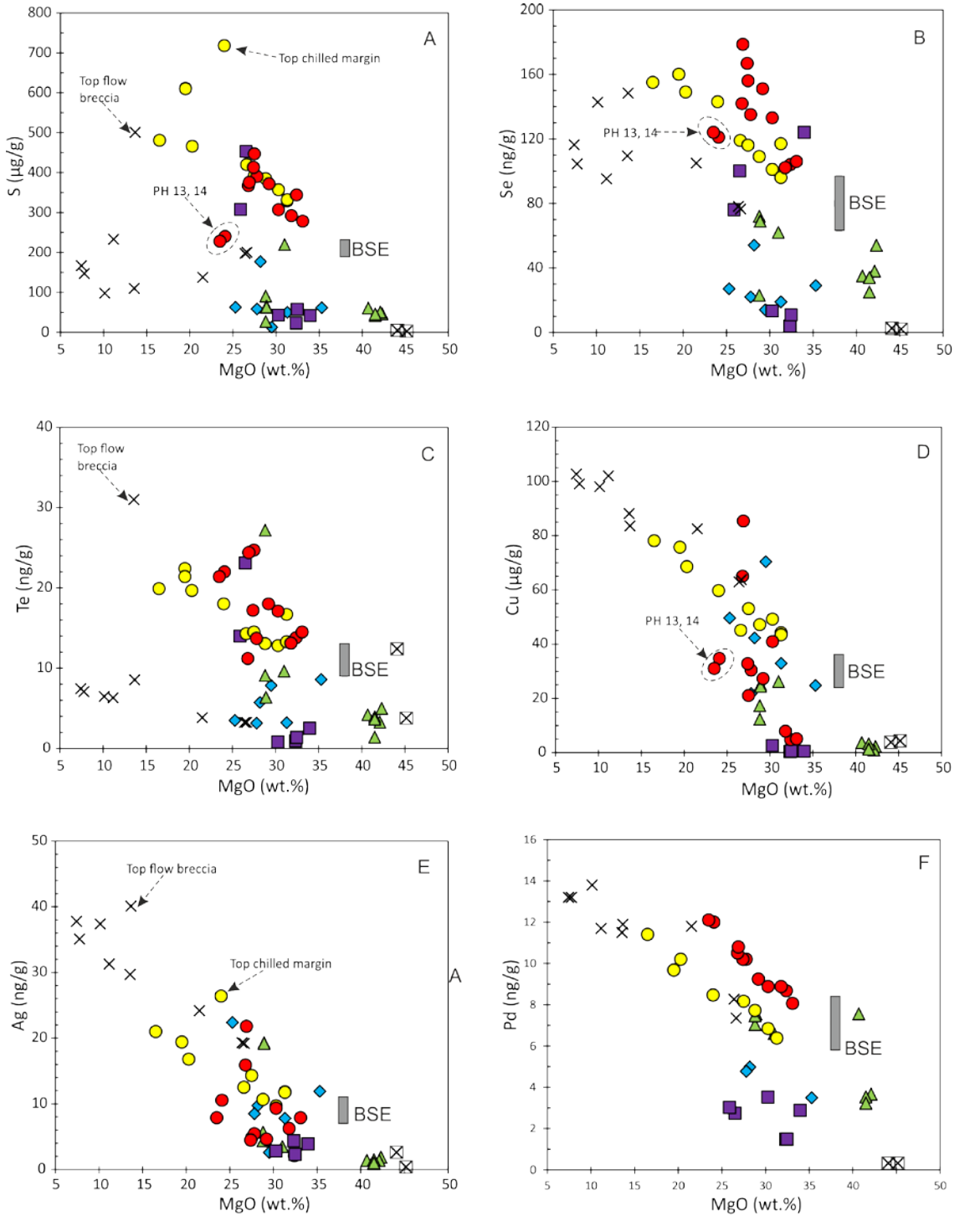

✕ 2.4 Ga Victoria's lava lake, Vetreny Belt
○ 2.7 Ga Tony's flow, Belingwe Greenstone Belt
● 2.7 Ga Pyke Hill flows, Abitibi Greenstone Belt
△ 3.3 Ga Weltevreden Formation, Barberton Greenstone Belt
◆ 3.5 Ga Komati Formation, Barberton Greenstone Belt
■ 3.5 Ga Carl's flow, Schapenburg Greenstone Remnant
⊠ Olivine separates of the olivine cumulate subzone of the 2.4 Ga Victoria's lava lake, Vetreny Belt

Fig. 4.1 Element variation diagrams of S, Se, Te, Cu, Ag and Pd abundances against MgO contents of Archean komatiites and komatiitic basalts. Abundances of S, Se, Te, Cu and Ag in the BSE are adopted from Wang and Becker (2013, 2015a). Abundances of chalcophile elements in the Belingwe Greenstone Belt were given in Chapter 3. Abundances of Pd plotted are referred to the published works (Puchtel and Humayun, 2001; Puchtel et al., 2009a; Puchtel et al., 2009b; Puchtel et al., 2014). Abundances of S, Se and Pd in pre-2.9 Ga komatiites from the Komati Formation, Weltevreden Formation and Schapenburg Greenstone Remnant are lower than those in pre-2.9 Ga komatiites from the Belingwe Greenstone Belt and Abitibi Greenstone Belt. Abundances of S, Se and Pd in the majority of pre-2.9 Ga komatiites are also lower than those in the BSE. Abundances of S, Se and Te in rocks from Victoria's lava lake deviate from the trends defined by Belingwe and Abitibi komatiites, whereas abundances of Pd, Cu and Ag in rocks from Victoria's lava lake define the same trends of Belingwe and Abitibi komatiites. The deviations of S, Se and Te in the Victoria's lava lake indicate the influence of magmatic degassing. Abundances of S, Te and Ag in the other subzones of Victoria's lava lake are much lower than those in the top flow breccia which may be altered by secondary processes. Abundances of S, Se and Cu in PH13 and PH14 from the spinifex subzone of PH-I lava flow slightly deviate from the trends defined by the other komatiites of PH flows.

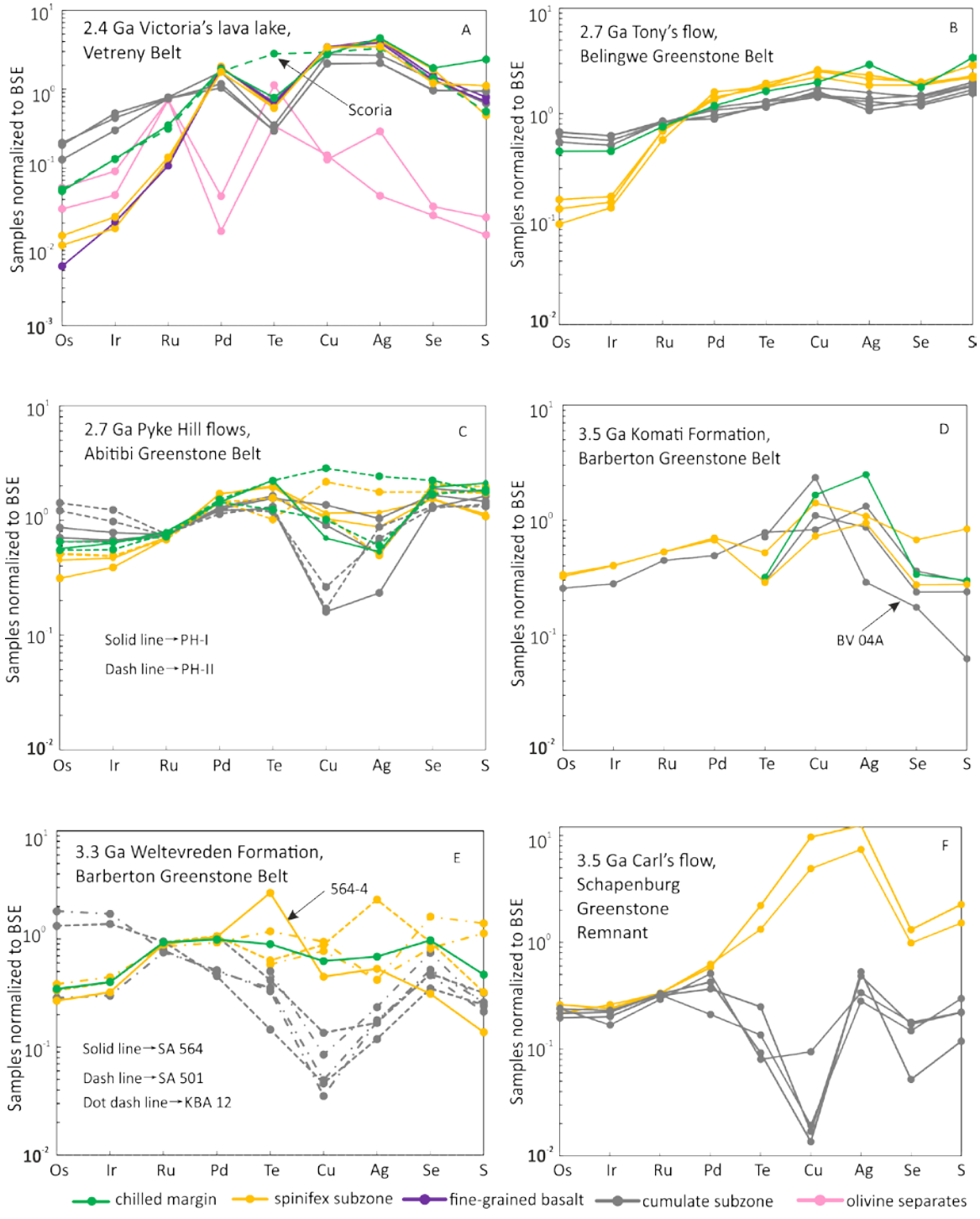
2.4 Ga Victoria's lava lake, Vetreny Belt
A
Scoria
2.7 Ga Tony's flow, Belingwe Greenstone Belt
B
2.7 Ga Pyke Hill flows, Abitibi Greenstone Belt
C
Solid line→PH-I
Dash line→PH-II
3.5 Ga Komati Formation, Barberton Greenstone Belt
D
BV 04A
3.3 Ga Weltevreden Formation, Barberton Greenstone Belt
E
564-4
Solid line→SA 564
Dash line→SA 501
Dot dash line→KBA 12
3.5 Ga Carl's flow, Schapenburg Greenstone Remnant
F
Samples normalized to BSE
Os Ir Ru Pd Te Cu Ag Se S
chilled margin
spinifex subzone
fine-grained basalt
cumulate subzone
olivine separates

Fig. 4.2 Abundances of chalcophile elements in Archean komatiites and komatiitic basalts normalized to those of the BSE. The order of the interested elements are arranged according to their incompatibility in terrestrial magmatism. Abundances of S, Se, Te, Cu and Ag in the BSE are adopted from Wang and Becker (2013, 2015a). Abundances of Os, Ir, Ru and Pd are adopted from Becker et al., 2006. Abundances of chalcophile elements in the Belingwe Greenstone Belt were given in Chapter 3. The depletions of Te, Se and S relative to Pd, Cu and Ag in rocks from Victoria's lava lake (Fig. 4.2A) were resulted from magmatic degassing. Magmatic signatures of PGE, Te, Se and S in PH flows of the Abitibi Greenstone Belt were well-preserved, whereas abundances of Cu and Ag likely were redistributed (Fig. 4.2C). With the exception of BV 04A, abundances of these elements in the Komati Formation were not significantly mobilized by secondary alteration (Fig. 4.2D). Magmatic characteristics of Te, Cu, Ag, Se and S in the Weltevreden Formation (Fig. 4.2E) and Carl's flow of the Schapenburg Greenstone Remnant (Fig. 4.2F) may have not been retained.

4.6 Discussion

4.6.1 Preservation of magmatic signatures of chalcophile elements

From the well-preserved Belingwe komatiites (Chapter 3) several useful pieces of information can be derived for understanding the basics of magmatic fractionation of chalcophile elements in sulfide-undersaturated komatiite magmas. Osmium, Ir and Ru behave compatibly during partial melting and lava differentiation, resulting to depletions of these elements in komatiite magmas relative to the BSE, and relatively higher abundances of these elements in cumulate subzones than spinifex subzones (representative of melt). Platinum, Pd, Cu, Ag Te, Se and S are moderately incompatible elements during komatiite magmatism, meaning that abundances of these elements should be enriched in komatiite magmas relative to the BSE, and should be higher in spinifex subzones than cumulate subzones. Limited fractionations occurred among these incompatible chalcophile elements, evidenced by the differentiated subzones of the Tony's flow are characterized by comparable ratios of these elements which are identical to that of the BSE. These signatures are presented in Fig. 3.4 and Fig. 3.5 in Chapter 3 and also shown in Fig. 4.2B. We here use the Belingwe komatiites as a criterion to get insight into the primary magmatic signature of these chalcophile elements in the other komatiites studied in this work.

The inspection of Fig 4.1 and Fig. 4.2 shows that uniform patterns observed in the Belingwe komatiites are rare in the other komatiites, indicating that other processes, including magmatic degassing and late-stage alteration, may have modified the primary magmatic signature. Reading of magmatic signatures of these elements are complicated by the fact that the elements of interest were disturbed variably in different komatiite suites. For instance, in Victoria's lava lake most elements behave similarly as in the Belingwe komatiites (Fig. 4.2A), indicating the preservation of primary magmatic signatures, but Te, Se and S are remarkably depleted relative to their neighboring elements. These depletions must have been related by other processes than pure magmatic fractionation such as the segregation of magmatic sulfides that would lead to the depletion of Pd in these samples (such a depletion is absent). The BSE-normalized patterns of the chalcophile elements in PH-I from the Abitibi Greenstone Belt resemble PH-II (Fig. 4.2C), indicating that these two lava flows may be derived from a common source. What remarkably different is the distribution of Cu and Ag showing depletions and enrichments (Fig. 4.2C), in contrast to all the other elements in the Abitibi komatiites. Cu/Ag ratios in the Abitibi komatiites vary considerably from 650 to 7400

(Fig. 4.4B), in contrast to the invariable S/Se and Se/Te (Fig 4.3A-B), implying the devastation of primary magmatic signatures of Cu and Ag in these rocks. The rocks from the Komati Formation display enrichments of Cu and Ag relative to the other elements including Pd, Te, Se and S (Fig. 4.2D). Differing from the distribution of Cu and Ag in the Abitibi komatiites which show enrichments and depletions, the Komati Formation show overall enrichments of Cu and Ag, though BV 04A is depleted in Ag, but Cu/Ag values in the range of the BSE (Fig. 4.4A). Interestingly, though S/Se and Se/Te in the Komati Formation are comparable to the Belingwe komatiites (Fig. 4.3A-B), Cu/Se and Ag/Se in the Komati Formation are much higher (Fig. 4.5A-B). These signatures observed in the Komati Formation indicate the operation of processes other than pure magmatic fractionation. The rocks from the Weltevreden Formation and Schapenburg Greenstone Remnant have the most complex BSE-normalized patterns, as shown in Fig 4.2E-F. Copper, Ag and Te in samples from the cumulate subzone of the Schapenburg Greenstone Remnant are generally depleted relative to Pd and Se and are also significantly depleted relative to the spinifex subzones (Fig 4.2F), indicating that the primary magmatic signatures are barely preserved. Ratios of chalcophile elements in the Weltevreden Formation show significant variations (Fig. 4.3C-D, 4.4B), which also indicate the poor preservation of magmatic signatures of these elements. Though Os, Ir, Ru and Pd display uniform patterns in the Schapenburg komatiites, Cu, Ag, Te, Se and S show divergent patterns (Fig. 4.2F) and variable element ratios of chalcophile elements (Fig. 4.3C-D). In rocks from the spinifex subzone Cu and Ag are also relatively enriched compared to Te, Se and S (Fig. 4.2F). The rocks from the cumulate subzone are significantly depleted in Cu relative to the other elements (Fig. 4.2F). We consider such signatures in the Schapenburg komatiites cannot be an indication of primary magmatism.

In conclusion, primary magmatic signatures of Cu and Ag in Victoria's lava lake and S, Se and Te in the Abitibi komatiites are preserved. All the other elements in the investigated komatiites likely were modified to variable degrees by other processes, including magmatic degassing and late-stage alteration which we discuss in the next sections (4.6.2 and 4.6.3).

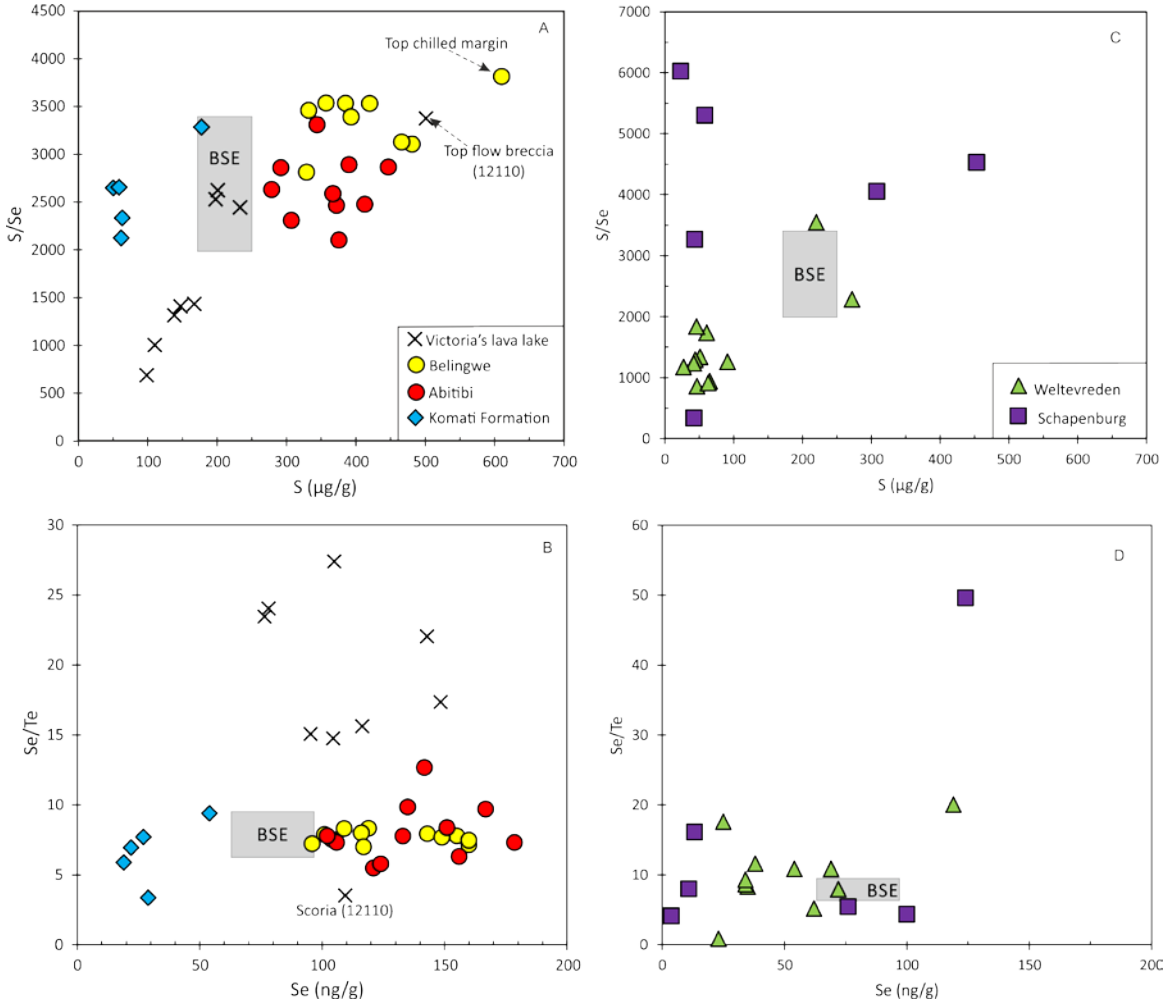

Fig. 4.3 Ratios of S, Se and Te in Archean komatiites and komatiitic basalts. Abundances of S, Se and Te in the BSE are adopted from Wang and Becker (2013). S/Se ratios of komatiites of the Belingwe Greenstone Belt, Abitibi Greenstone Belt and Komati Formation are comparable to that in the BSE, whereas the majority of S/Se ratios of the Victoria's lava lake are lower than that in the BSE (Fig. 4.3A). Low S/Se ratios of the Victoria's lava lake were resulted from the greater effect of magmatic degassing on S than Se. Se/Te ratios of the Belingwe Greenstone Belt, Abitibi Greenstone Belt and Komati Formation are comparable to that in the BSE, whereas the majority of Se/Te ratios of the Victoria's lava lake are higher than that in the BSE (Fig. 4.3B). Combined with Fig. 4.2A, high Se/Te ratios of the Victoria's lava lake seem to be caused by magmatic degassing. Near-chondritic ratios of S, Se and Te in the Belingwe Greenstone Belt, Abitibi Greenstone Belt and Komati Formation require late addition of volatile-rich chondritic components. Ratios of S, Se and Te vary significantly (Fig. 4.3C-D) in Schapenburg and Weltevreden komatiites.

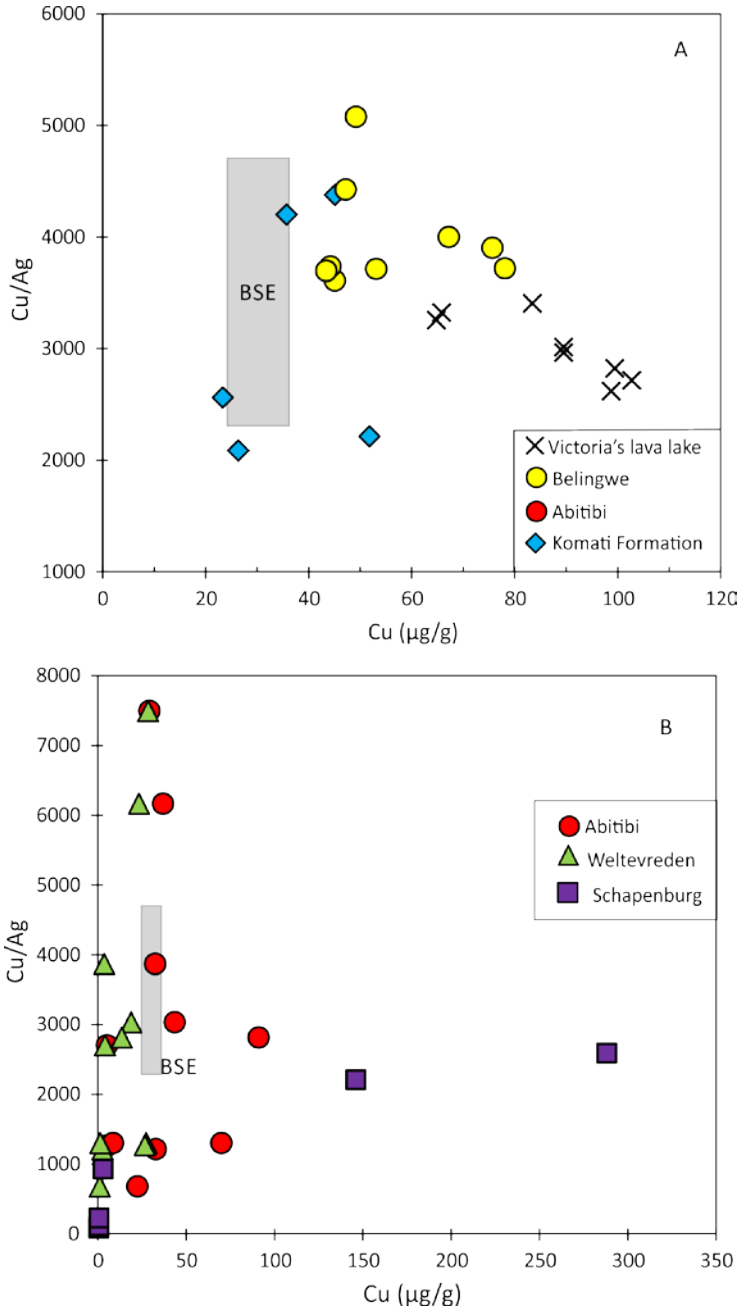

Fig. 4.4 Ratios of Cu and Ag in Archean komatiites and komatiitic basalts. Abundances of Cu and Ag in the BSE are adopted from Wang and Becker (2015a). Though slightly lower than those of the Belingwe komatiites, Cu/Ag ratios of the Victoria's lava lake are comparable to those in the Komati Formation as well as MORB as shown in Fig. 3.5C in Chapter 3. Ratios of Cu and Ag in various mantle-derived rocks are canonical. Cu/Ag in the rocks from Abitibi, Weltevreden and Schapenburg show significant variations.

4.6.2 Effects of magmatic degassing

Several elements investigated in this study, such as S, Re and presumably Se and Te, may be volatile in magmatic processes (Greenland and Aruscavage, 1986; Norman et al., 2004; Sun et al., 2003; Yi et al., 2000) and, therefore, they may be depleted in magmas that erupt at the surface by degassing of vapor phases. Temperatures of Archean ultramafic lava subsequently differentiated into komatiites were suggested to be higher than 1400 ℃ (Fauer et al., 2006; Nisbet et al., 1993; Shore and Fowler, 1999), volatile species, such as H_2O, were degassed (Fiorentini et al., 2012c). One way to study the degassing history of volatile elements in komatiites magmas is via melt inclusions enclosed in primary olivine (Asafov et al., 2015; Danyushevsky et al., 2002; Woodhead et al., 2005). Their results suggested variable losses of volatile S, CO_2, Cl, and H_2O in Abitibi komatiites. For instance, H_2O contents of the inclusions in high-MgO olivine of PH komatiites appear to display positive correlation with the size of these inclusion (Sobolev et al., 2016), interpreted to reflect degassing accompanying crystallization or diffusional losses of hydrogen from host olivine. Another approach might be to investigate the mass-dependent isotopic fractionation of volatile elements. However, $\delta^{34}S_{V\text{-}CDT}$ values of rocks, gas and aerosol in Masaya and Erta Ale indicate little isotope fractionation relevant to degassing (de Moor et al., 2013), though S outputs exceed 5.7×10^8 mols per year and 5.7×10^9 mols per year via gas plumes, respectively. Work on S isotope composition in Archean komatiites focused on Ni-Cu-(PGE) ores (Bekker et al., 2009; Fiorentini et al., 2012a), and no whole-rock data on S isotope composition of komatiites were reported.

Here we adopt a less precise approach of plotting the element abundances against their relative depths in drill cores (Yi et al., 2000). The depth of PH-I ranges from 253.4 m to 256.4 m (Puchtel et al., 2004), whereas the depth of PH-II ranges from 649.2 m to 652.2 m (Puchtel et al., 2004; Puchtel et al., 2009b). If volatile losses were evident in the magmatic system of PH lava flows, the shallower PH-I should be more depleted than the deeper PH-II. Abundances of S in PH-I and PH-II, however, are comparable, varying from 228 μg/g to 447 μg/g and 278 μg/g to 413 μg/g, respectively. Therefore evidence for volatile losses in PH lava flows was not found by applying the depth-element abundance approach. Abundances of S in the single differentiated lava flows from the Komati Formation are not relevant to the depth of samples either, providing no evidence for volatile degassing. Though SA 501 and KBA 12

from the Weltevreden Formation are not capped with chilled margins, abundances of S in 501-8, 501-9 and 501-10 from the cumulate subzone of SA 501 are comparable.

Though element abundances are not impressively correlated with the depth of samples from Victoria's lava lake, abundances of S, Se and Te in the investigated samples were likely depleted by magmatic degassing. The depletions of Te, Se and S relative to Cu and Ag in Victoria's lava lake cannot be caused by other processes than magmatic degassing. The segregation of magmatic sulfides can be excluded because the absence of depletions of Pd and Cu, which are commonly more chalcophile than Se. The depletion of S relative to Se suggests that S is the most volatile among the studied elements. In the case of Victoria's lava lake the volatility of these chalcophile elements during magmatic degassing likely is Pd ≈ Cu ≈ Ag < Te < Se < S. One might ask the question why Victoria's lava lake underwent magmatic degassing, whereas volatile losses of the Belingwe Greenstone Belt, Abitibi Greenstone Belt, and Komati Formation must have been minor or negligible. The difference in lithology of Victoria's lava lake and the other regions is that basalts prevail in Victoria's lava lake and komatiites in the other regions. Solubility of S in mafic magmas compositionally depends on FeO contents (Haughton et al., 1974; Mathez, 1976; O'Neill and Mavrogens, 2002; Wallace and Carmichael, 1992), indicating that S might be strongly bound to Fe in S undersaturated silicate magmas which would limit the efficiency of volatile losses of S.

The effect of magmatic degassing on these elements in Victoria's lava lake can be reproduced in a Rayleigh-type degassing model (Fig. 4.5). As mention in 4.2 and proved in Chapter 3 that typical komatiites likely are not saturated in sulfides and therefore in the Rayleigh-type model the starting element ratios of interest were set to be same to the BSE. In the consideration of the mantle heterogeneity, variable abundances of Se and Te in the starting primary magma were adopted in the model (Fig. 4.5). Details about the equations and parameters used in the model Rayleigh-type degassing are given in 4.8.3. As shown in Fig.4.5, S, Se and Te in Victoria's lava lake underwent significant volatile losses, presumably up to 70 mass %. The data of recent work on Victoria's lava lake showed that $(Re/Pd)_N$ in the investigated rocks varies from 0.5 to 0.9 (Puchtel et al., 2016b) and $(Re/Cu)_N$ from 0.3 to 0.5 (this work), which also indicate the volatile losses of Re in Victoria's lava lake. The model also confirms the conclusion in Chapter 3 that the Belingwe rocks underwent limited magmatic degassing. Interestingly the Rayleigh-type degassing model (Fig.4.5) indicates that the depletions of S, Se and Te in the Komati Formation might be resulted by variable magmatic degassing. However, refractory PGEs, including Pd, are also depleted relative to Cu

and Ag (Fig. 4.2D), indicating that there might be alternative for the depletions of S, Se and Te in the Komati Formation (see 4.6.6).

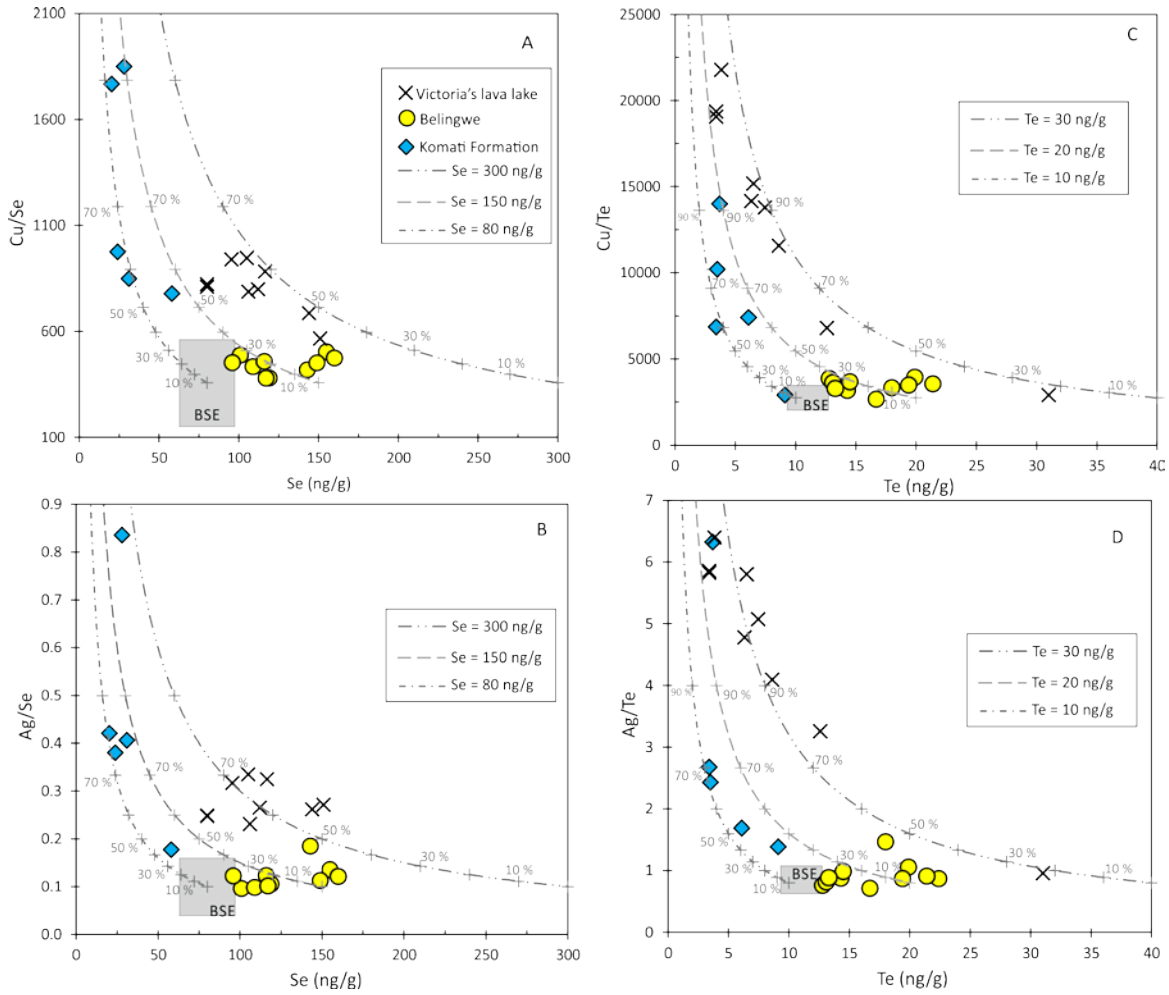

Fig. 4.5 Variation diagrams of chalcophile elements in Archean komatiites and komatiitic basalts. Abundances of Se, Te, Cu and Ag in the BSE were adopted from Wang and Becker (2013, 2015a). The dash curves represent the magmatic degassing on element ratios by Rayleigh-type degassing models. The numbers on the curves donate to the percentage of element lost due to magmatic degassing. The dash curves differ in the initial abundances of elements of interest in the primary magma prior to igneous degassing. The equations used for Rayleigh-type modelling are given in 4.8.

4.6.3 Mobilization of chalcophile elements in syn- to post-magmatic processes

Replacements of primary minerals by secondary phases is ubiqiutous in komatiites and also in the investigated samples. Although primary HSE abundances in the studied komatiites from the Abitibi Greenstone Belt and Victoria's lava lake were not disturbed by late-stage alterations (Puchtel et al., 2009b), both regions underwent significant serpentinization and prehnite-pumpellyite facies metamorphism. Furthermore, komatiitic basalts from Victoria's lava lake were overprinted by up to ~7% crustal assimilation of older continental materials, as implied by Sm-Nd isotope systematics (Puchtel et al., 1997). Because of low-temperature alteration, one would expect modifications of labile chalcophile elements in both regions. In general, greenschist and amphibolite grade metamorphism of pre-2.9 Ga komatiites are stronger than that of post-2.9 Ga ones. The Barberton Greenstone Belt and Schapenburg Greenstone Remnant were subjected to amphibolite facies metamorphism and recrystallization. Olivine in these rocks was commonly replaced by serpentine, amphibole, chlorite and magnetite (Blichert-Toft et al., 2004; Lécuyer et al., 1994). Therefore, it is important to understand the effect of aqueous alteration on these elements in the different suites.

Several techniques can be used to investigate the element mobility in komatiites. Though komatiite subzones differ in the proportion of olivine, abundances of incompatible elements in a single differentiated lava flow should be correlated with magmatic proxies, such as MgO, if the lava flow did not tap other lava flows or was not replenished. Another way is using BSE-normalized diagrams (Robin-Popieul et al., 2012). For a specific element, samples collected from an undisturbed lava flow should be characterized by similar relative depletion or enrichment of Cu, Ag, Se and S, as these elements are all incompatible. If an element was similarly enriched as related elements in a komatiite but depleted in another komatiite from the same lava flow, this element was likely mobilized by degassing or by aqueous alteration. The two methods were successfully applied to lithophile trace elements and HSE (Puchtel et al., 2009a; Robin-Popieul et al., 2012). In the following discussion on late-stage alterations, we applied both approaches to the investigated samples.

Compared to Ag and Cu in the Belingwe komatiites (Fig. 4.2B), Ag and Cu in the Abitibi komatiites were disturbed considerably (Fig. 4.2C). In contrast to the linear correlations of S, Se and Te with MgO contents of the Abitibi rocks intersecting at the average MgO content of cores of olivine separates (Fig. 4.1A-C, 4.6A, B and E), the relations of Cu and Ag abundances with MgO contents in the Abitibi komatiites do not pass the average MgO content of cores of olivine separates (Fig. 4.1D- E, Fig. S4.9 in Appendix Chapter 4.8). Copper and Ag in these samples were at least re-distributed within the lava flow during serpentinization, because overall abundances of Cu and Ag in the Abitibi komatiites are comparable to the Belingwe komatiites. The abundances of S, Se and Te in the Abitibi komatiites showing little evidence for secondary alteration are also comparable to the Belingwe rocks (Fig. 4.1A-C, 4.6A, B and E). It was proposed that in oxidized and neutral hydrothermal fluids (Seo et al., 2012), Cu might be more mobile than Ag which is incline to form relatively insoluble Ag-Cl complex (Stefánsson and Seward, 2003). This difference may explain the less variations of Ag than Cu in the Abitibi komatiites as shown in the BSE-normalized diagram (Fig. 4.2C). In the Cu- and Ag-MgO variation diagrams (Fig. 4.1D, E), abundances of Cu and Ag in samples from Victoria's lava lake are well correlated with MgO and do not deviate from the trend defined by Belingwe and Abitibi komatiites (Fig. 4.6C-D). There is also little variation of Cu and Ag in the BSE-normalized diagram for samples from Victoria's lava lake (Fig. 4.2A). Thus, the primary magmatic compositions of Cu and Ag in samples from Victoria's lava lake are preserved.

Inspection of element variation diagrams of S, Se and Te in the Weltevreden Formation (Fig. 4.1A, B and C) indicates the deviation of these elements from trends defined by Belingwe and Abitibi komatiites. The BSE-normalized diagram of the Weltevreden Formation (Fig. 4.2E) exhibits considerable variations and shows element depletions or enrichments, which indicates poor preservation of magmatic characteristics of S, Se and Te in the Weltevreden Formation. Sample 564-6 of the chilled margin of SA 564 lava flow was depleted in S relative to unfractionated Se and Te, whereas 564-4 of the spinifex subzone displays remarkable fractionation of S, Se and Te (Fig. 4.2E). Samples (12-6 and 12-8) from the cumulate subzone of KBA 12 lava flow display similar S, Se and Te patterns (Fig. 4.2E), which are distinct from that of 12-2 from the spinifex subzone. Variations of depletions of S, Se and Te in the spinifex subzone of SA 501 lava flow are different from those of the cumulate subzone, indicating the modification of these elements in SA 501. As displayed the BSE-normalized diagram (Fig. 4.2E) variations of depletions of Cu and Ag in the spinifex

subzones of the Weltevreden Formation are larger than those of the cumulate subzones. Such a difference indicates that the spinifex subzones of the Weltevreden Formation were more prone to late-stage alteration. Abundances of Cu and Ag in the Weltevreden Formation are mainly in two clusters in the MgO-element variation plots (Fig. 4.1D and E), and there are no true relations between Cu, Ag and MgO. The depletion of Cu relative to Ag in cumulate subzones is similar to that in the Abitibi Greenstone Belt, which may be indicative of the oxidation state of hydrothermal fluids at these sites. Sample 12-2 from the spinifex subzone of KBA 12 was significantly enriched in Ag relative to all the other elements (Fig. 4.2E), indicating late addition of Ag.

Ssmples from the Komati Formation have systematically lower abundances of these elements compared to Abitibi and Belingwe komatiites (Fig. 4.1A-C). With the exception of BV04A, limited variations of S, Se and Te ratios in the other samples of the Komati Formation (Fig. 4.2D, 4.3) show that processes undergone by these samples likely do not fractionate these elements. Because BV 04A was collected near to the boundary of the spinifex subzone and cumulate subzone, sulfides in BV04A may have been subject to stronger modification, presumably by leaching or degassing (see 4.6.2). Abundances of Cu and Ag in the Komati Formation are higher compared to S, Se and Te (Fig. 4.2D) and are characterized by slight variations among different samples. Though no simple correlation between MgO and Cu or Ag can be obtained (BV 04A excluded, Fig. 4.1D and E), they likely were only moderately modified by late-stage alteration.

The Schapenburg komatiites in this study display the largest variations of element abundances, and no simple relations can be obtained from the S-, Se- and Te-MgO diagrams (Fig. 4.1A, B and C). As discussed in 4.6.1, chalcophile elements in samples from the Schapenburg Greenstone Remnant are likely resulted from late-stage alteration. In comparison to komatiites from the other greenstone belts Schapenburg komatiites may have undergone more sever late-stage alteration.

4.6.4 Magmatic fractionation of chalcophile elements in Archean komatiites

4.6.4.1 Element fractionation in single differentiated lava flow

Magmatic fractionations of siderophile and chalcophile elements occurred in Archean komatiites during lava differentiation. As displayed in Fig. 4.2A, B, C and E, cumulate

subzones were enriched in Os and Ir relative to the other elements, which indicates the compatibility of Os and Ir during lava differentiation. Magmatic sulfides are unlikely to be the host of Os and Ir in the investigated samples (Barnes et al., 2016; Puchtel et al., 2009b). Otherwise the other highly siderophile elements, such as Ru, Pt and Pd, should have also been enriched in cumulate subzones. Os-Ir-(Ru) alloys were suspected to form as the crystallization of silicate phases which pack Os-Ir alloys into its crystal lattice. However, Os-Ir-Ru spectra were found to be homogenous across chromite grains from komatiite, tholeiite and boninite (Locmelis et al., 2011; Pagé et al., 2012), providing no evidence for alloys. Experimental data showed that silicate-melt D_{Ir} and D_{Ru} increased with decreasing oxygen fugacity (Brenan et al., 2005; Brenan et al., 2003), which might reflect the direct incorporation of ions of these elements in silicates such as olivine (Brenan et al., 2016b). The order of incompatibility of HSE, on the basis of Archean komatiites, is that $D_{Os} > D_{Ir} > D_{Ru} > D_{Pt} \approx D_{Pd} > D_{chalcophile\ elements}$ (D represent solid-melt partition coefficients). Ruthenium is equally distributed in spinifex subzones and cumulate subzones of Archean komatiites, indicating that the bulk solid-melt partition coefficient of Ru is probably close to 1.

Samples from spinifex subzones, which more closely represent the melt composition, tend to have higher concentrations of chalcophile elements than samples from the cumulate subzones (Fig. 4.2A, B and C), indicating the incompatibility of chalcophile elements during differentiation of komatiite lava flows. Notably, S/Se and Se/Te in Abitibi and Belingwe komatiites (Fig. 4.3A-B, 4.4A) display no variations related to changes of lithologic units, suggesting the limited element fractionation.

4.6.4.2 Relations of chalcophile elements

Ratios of S, Se and Te as well as ratios of Cu and Ag in samples from the Abitibi Greenstone Belt, Belingwe Greenstone Belt and Komati Formation are comparable to those of the BSE (Fig. 4.3A-B, 4.4A). S/Se and Se/Te in Abitibi and Belingwe komatiites do not increase with S and Se abundances, respectively (Fig. 4.3A-B). Though abundances of S, Se and Te in the Komati Formation are lower than those of the Belingwe Greenstone Belt and Abitibi Greenstone Belt, ratios of S, Se and Te in the three regions are comparable to chondritic ratios of these elements in the BSE defined by post-Archean mantle peridotites (Fig. 4.3A-B). This demonstrates that incompatible chalcophile elements are not fractionated during the formation of komatiites. This is consistent with that magmatic Ni-Cu-PGE ore deposits in komatiites require external sulfur (Bekker et al., 2009; Fiorentini et al., 2012a).

Enrichments of Cu and Ag relative to Pd and Te in the Komati Formation were not caused by segregation of magmatic sulfides because Pd and Te are not depleted relative to Se and S (Fig. 4.2D). This is also shown in diagrams of element ratio-element abundance (Fig. 4.3-4.5). Ratios of S, Se and Te in the Komati Formation are comparable to those of Belingwe and Abitibi komatiites (Fig. 4.3), and ratios of Cu and Ag are also similar to those of the Belingwe Greenstone Belt and Victoria's lava lake (Fig. 4.4). Cu/Se and Ag/Se ratios of the Komati Formation, however, are much higher and more variable than those of the Belingwe Greenstone Belt (Fig. 4.5). Though, as discussed in 4.6.1 and 4.6.2, the influence of late-stage alteration and magmatic degassing on S, Se and Te in the Komati Formation cannot be entirely excluded, the high Cu/Se, Ag/Se and Cu/Pd ratios of Komati Formation may have other explanations (see 4.6.6).

Table 4.2 Comparison between the calculated and the measured element abundances of the emplaced magma (A1)

	MgO (wt.%)	Cr (µg/g)	Os (ng/g)	Ir (ng/g)	Pd+Pt (ng/g)	S (µg/g)	Se ng/g)	Te (ng/g)	Cu (µg/g)	Ag (ng/g)
PH I										
Calculated	28.0	2531	2.63	1.97	20.5	326	142	16		
A_1 (PH23)	27.5	2694	2.22	2.21	20.3	447	156	18		
Δ(%)	-2%	6%	**-19%**	11%	-1%	**27%**	9%	9%		
PH II										
Calculated	29.8	2525	3.97	3.16	18.4	339	131	15.7		
A_1 (PH25)	27.8	2759	2.54	2.26	20.8	390	135	13.7		
Δ(%)	-7%	8%	**-56%**	**-40%**	12%	13%	3%	-15%		
Vicotia's lava lake										
Calculated	15.3	1478	0.20	0.45	22.8	136	115	5.9	89.6	29.8
A_1 (12111)	13.9	1374	0.20	0.46	21.6	110	110	31	88.1	29.7
Δ(%)	-10%	-8%	-2%	1%	-5%	**-23%**	-4%	81%	-2%	-0.2%
Koamti Formation										
Calculated	31.7	1933				60	26	24	23.3	10.2
A_1 (BV 06)	25.3	2281				63	27	18	49.6	22.4
Δ(%)	**-25%**	15%				5%	5%	**-31%**	**53%**	**54%**

$\Delta(\%) = (A_1\text{-Calculated}) / A_1 \times 100$

4.6.5 Element abundances in erupted liquids and early melt extraction

4.6.5.1 Concentrations and ratios of S, Se, Te, Cu and Ag in erupted liquids

The chilled margin of komatiite is suggested to form instantaneously after emplacement of the lava, and it does not undergo any differentiation and, therefore, should be representative of the major and trace element composition of the melt from which it formed (*e.g.* Puchtel et al., 1996; Puchtel and Humayun, 2001). Because of element mobility in some samples, mass-balance calculations do not work for every element in each location. The results of mass-balance calculations (mass-balance equation in 3.6.3.1 in Chapter 3) of subzones of a single differentiated lava are provided in Table 4.2. Mass-balance calculations of Cr, Pt, Pd and Ir for the Komati Formation, Abitibi and Victoria's lava lake are also listed. Agreements between the calculated Cr abundances in the erupted liquids of these komatiites and Cr abundances in the top chilled margins of PH lava flows and Victoria's lava lake suggest that squeeze of other differentiated lave flows likely are limited. This also indicates that the differentiation of the komatiite lava flows likely proceeded in a closed systems. Early work on PGEs and Cr abundances in Victoria's lava lake also suggested that the fractionation in the lake progressed without tapping or replenishment (Puchtel and Humayun, 2001). In contrast to PH lava flows and Victoria's lava lake, calculated Cu and Ag abundances for erupted liquid of the Komati Formation (lava flow 4) are 50% higher than those in the chilled margin BV 06. The MgO content and Te abundance in BV 06 are over 25% higher than the mass-balance calculated value. We note that the thickness of Lava Flow 4 of Komati Formation is only ~1.75 m and it is interlayered with Lava Flow 5 and Lava Flow 3 as illustrated in Fig. 1 in Fig. S4.3 and Puchtel et al., 2013. Element influx from other komatiite lava flows may have modified the chemical composition of Lava Flow 4 of the Komati Formation.

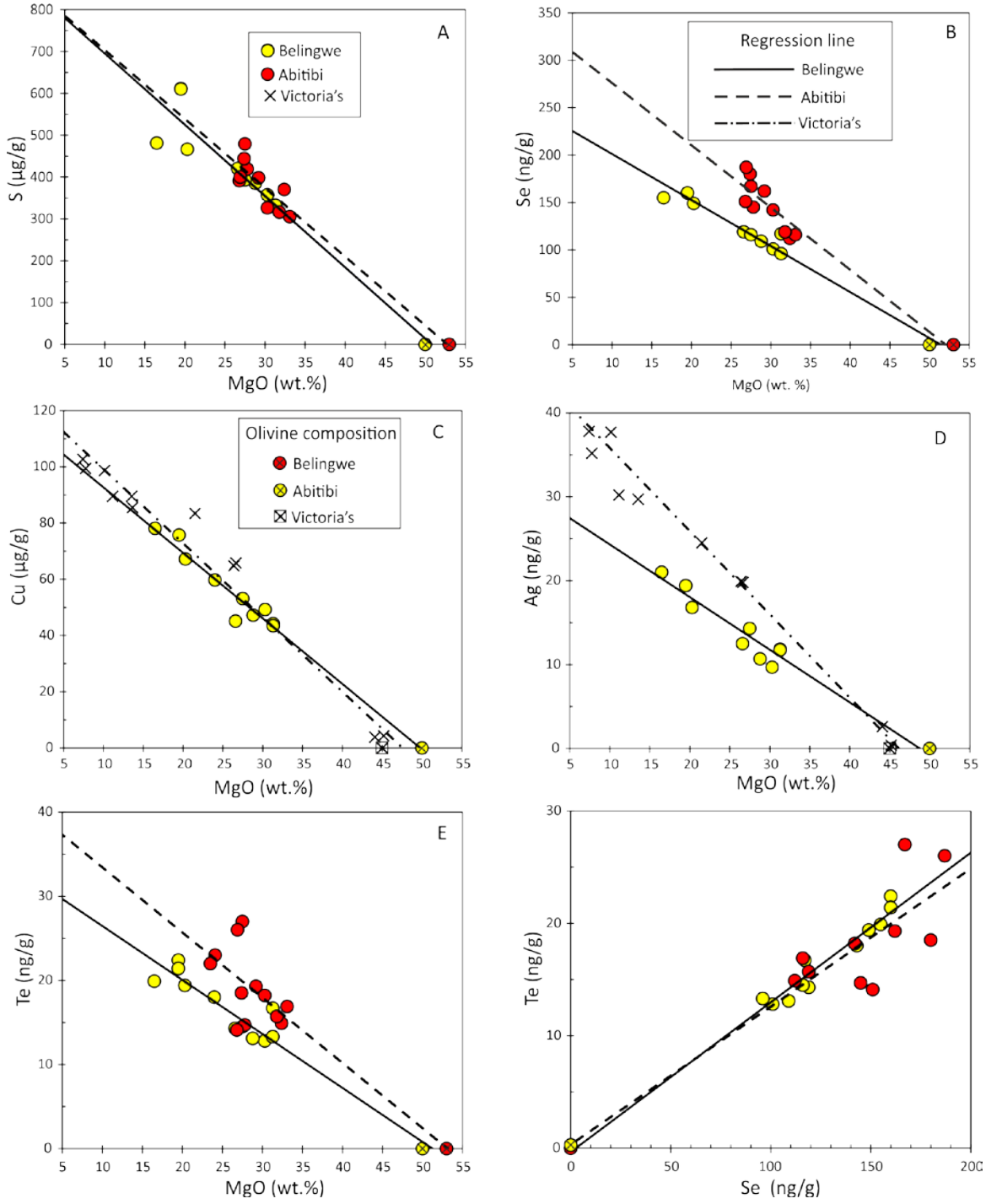

Fig. 4.6 Variation diagrams of element abundances against MgO contents of Archean komatiites and komatiitic basalts. R^2 is the coefficient of determination which represents how well data fir the linear correlation. Abundances of S, Se, Te, Cu and Ag in mantle sources of the Victoria's lava lake of the Vetreny Belt, the TN flow of the Belingwe Greenstone Belt and PH flows of the Abitibi Greenstone Belt by extrapolation to MgO=36.77 wt.% in the BSE (Palme and O'Neill, 2014). Correlations of Se-Te in Belingwe and Abitibi are presented for comparison. The results are given in Table 4.3.

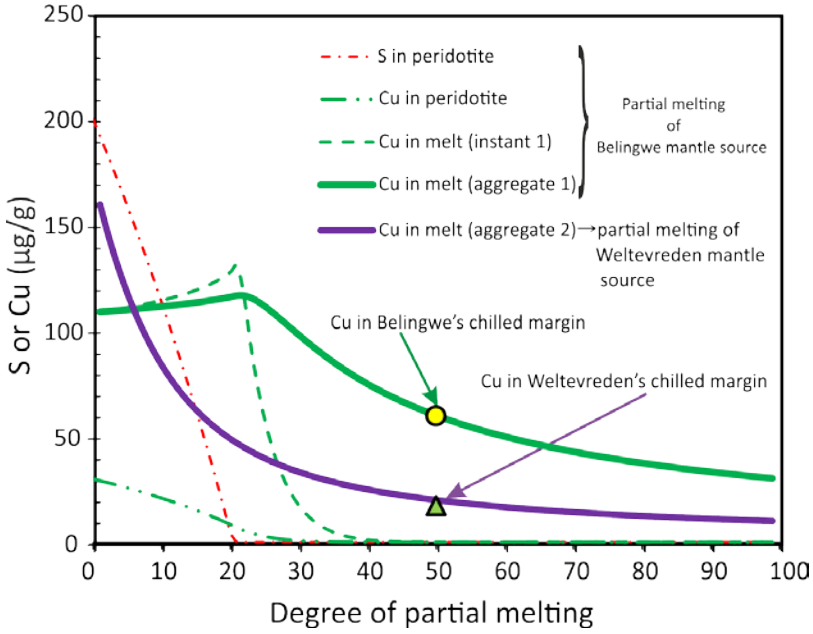

Fig. 4.7 Evolution of Cu or S abundances as degrees of fractional partial melting in single- and two-stage models. The model of fractional melting is modified from Lee et al. (2012) which was based on the peridotites at upper mantle conditions. We assume here that the mantle source of the Belingwe komatiites is represented by lherzolites, and therefore the parameters used for modeling the fractional melting of the BSE-like mantle source are the same as (Lee et al., 2012). The temperature required to generate komatiite magmas is ~ 1600 ℃, which is higher than 1350 ℃ used in that model. Therefore, we adjusted the sulfide-silicate partition coefficient of Cu to be 400 which is in the range of reported values (Kiseeva and Wood, 2015). As shown by Lee et al. (2012), however, partition coefficients of Cu are not sensitive to temperature. For the 20% depleted mantle source, the abundance of S was assumed to be ~ 3 µg/g, which is roughly equal to 0.001% sulfide. The degree of partial melting required to produce Belingwe and Weltevreden komatiite magma was assumed to be 50%. As the degree of partial melting approaches 20%, sulfides in lherzolites become exhausted. In the case of a lherzolite-like mantle source, abundances of Cu in the aggregate melt reach 100 µg/g, which is subsequently diluted as more silicate melt enter the aggregate melt. In the case of melting of a ~20% depleted mantle source, sulfides in peridotites were exhausted at the very beginning and abundances of Cu in aggregate melt continue to be diluted. This model shows that sulfides in the mantle source of Belingwe komatiites may have not been consumed by early melt extraction, whereas sulfides in Weltevreden komatiite mantle source were nearly exhausted by early melt extractions.

4.6.5.2 Influence of early melt extraction on the abundances of S and Cu in erupted liquids

Studies on lithophile elements revealed the presence of early melt extraction in mantle sources of most Archean komatiites. The mantle sources of the komatiites of interest, excluding that of Victoria's lava lake which might have assimilated crustal materials (Puchtel et al., 1997; Puchtel et al., 2016b), are characterized by initial positive $\varepsilon^{143}Nd$ (Blichert-Toft et al., 2015; Puchtel et al., 2016a; Puchtel et al., 2013; Puchtel et al., 2007; Puchtel et al., 2009b), evidencing for early melt extraction. Al-depleted Barberton-type komatiites from the Komati Formation and Schapenburg have $(Ce/Sm)_N$ of 1.0-1.2 (Puchtel et al., 2016a; Puchtel et al., 2013), contrasting to 0.4-0.7 of Al-undepleted Munro-type komatiites of Abitibi and Belingwe and Al-enriched komatiites of Weltevreden Formation (Fan, 1995; Puchtel et al., 2013; Puchtel et al., 2009b). This also indicates that the mantle sources of Belingwe, Abitibi and Weltevreden komatiites might have undergone melt extractions prior to the formation of komatiites. However, influence of early melt extraction on incompatible chalcophile elements of interest have not been given much attention.

With the purpose of understanding such influence, we modelled the variations of Cu and S abundances in partial melts and mantle residues during fractional melting modified from the model of (Lee et al., 2012). This model was based on the assumption that Cu budget of the mantle source of these komatiites prior to any melt extraction is 30 µg/g (Wang and Becker, 2015a). The sulfide-silicate partition coefficient of Cu was adjusted to 400 based on recent results (Kiseeva and Wood, 2015; Li and Audétat, 2012), and the bulk solid-melt partition coefficient of Cu was calculated to be 0.05. The accumulating degree of early partial melting is estimated to be ~15%, which is close to the maximum degree required for producing MORB (Falloon and Green, 1988; Hirschmann et al., 1998). After such degrees of fractional melting, ~10 µg/g Cu would be left in the depleted peridotite residuum. 50% of fractional partial melting of this depleted mantle would produce a primary melt with ~18 µg/g Cu, comparable to the abundance of Cu in the chilled margin of 564-6 from SA 564 lava flow of Weltevreden Formation (Fig. 4.7). The Cu abundanceof partial melt from a mantle source of 30 µg/g Cu matches well with the abundance of Cu in the top chilled margin from TN flow in the Belingwe Greenstone Belt (Fig. 4.7). This suggests that the mantle source of Welterveden Formation likely underwent stronger early melt extraction than the mantle source of Belingwe komatiites.

4.6.6 Concentrations of S, Se, Te, Cu and Ag in the mantle sources of komatiites

Abundances of Pd and Pt of mantle sources of komatiites were obtained by extrapolation to a MgO content of komatiite mantle sources (Puchtel et al., 2016b; Puchtel et al., 2009b). We applied this technique to calculate abundances of S, Se and Te in the Abitibi komatiite source, abundances of Cu and Ag in the mantle source of Victoria's lava lake by using MgO = 36.77 wt.% (Palme and O'Neill, 2014). Eement-MgO correlations are given in Fig. 4.6 and the abundances of these elements in the respective mantle sources are provided in Table 4.3.

As shown in Table 4.3, the element abundances of the Abitibi komatiite mantle source are comparable to those of the mantle source of the Victoria's lava lake within uncertainties. The calculated element abundances of post-2.9 Ga Archean mantle, represented by mantle sources of the Belingwe Greenstone Belt (Chapter 3), Abitibi Greenstone Belt and Victoria's lava lake, are in agreement with those of the BSE which was defined by oceanic basalts, upper mantle peridotites and several Archean komatiites (McDonough and Sun, 1995; Morgan, 1986; Nielsen et al., 2014; Palme and O'Neill, 2007; Wang and Becker, 2013, 2015a). These data support the BSE estimates based on post-Archean mantle lherzolites and suggest large-scale homogeneity of chalcophile element composition of the post-2.9 Ga upper mantle. Because of the variable extent of alteration, and presumably degassing, it is much difficult to constrain the chalcophile element composition of pre-2.9 Ga mantle reservoirs. This impedes us evaluating the progressive mixing theory proposed by Maier et al., 2009 from the perspective of S, Se and Te in mantle sources of pre-2.9 Ga komatiites. However, ratios of chalcophile elements of interest in the rocks of Komati Formation may be used to get an insight into the pre-2.9 komatiites (see 4.6.7).

Table 4.3 Calculated abundances of chalcophile elements in the mantle sources of Abitibi and Victoria's lava lake

Locality	Element variation ($y-x$)	Regression	R^2	Abundances (1 σ_{est})[3] @ MgO = 36.77 wt.%[1]
Abitibi	S-MgO	$y=-16.5x+868$	0.93	S = 261 ± 34 (μg/g)
	Se-MgO	$y=-6.57x+34$	0.92	Se = 99 ± 14 (ng/g)
	Te-MgO	$y=-0.78x+41.2$	0.72	Te = 13 ± 4 (ng/g)
	Se-Te	$y=0.13x+0.32$	0.79	Te = 11 ± 3 (ng/g) @ Se^{BSE} = 80 ± 17 (ng/g)[2]
Victoria's	Cu- MgO	$y=-2.64x+126$	0.97	Cu = 30 ± 8 (μg/g)
	Ag- MgO	$y=-0.99x+46$	0.95	Ag = 10 ± 3 (ng/g)

[1]The MgO content of the BSE was 36.77 wt.% (Palme and O'Neill, 2014). [2]The BSE value of Se was reported by Wang and Becker, 2013. [3]σ_{est} represents the standard error of the calculated element abundances. It reflects the degree of deviation of the samples from the regression line. $\sigma_{est} = \sqrt{1/(n-2)} \times \sqrt{\sum (y-\bar{y})^2 - [(x-\bar{x})(y-\bar{y})]^2 / \sum (x-\bar{x})^2}$. $\bar{x}$, $\bar{y}$ represent the mean value of x, y, respectively; n represents the number of samples. The abundances of Cu and Ag in the Abitibi mantle source are not given because that they were likely affected by late-stage alteration (see 4.6.1.2), and the abundances of S, Se and Te in the mantle source of Victoria's lava lake were not calculated because they underwent magmatic degassing (see 4.6.2).

4.6.7 Origin of the high Cu/Se and Ag/Se in the Komati Formation

As highlighted in 4.6.2, S/Se, Se/Te and Cu/Ag in the 3.5 Ga Komati Formation are essentially comparable to those of post-2.9 Ga komatiites and the BSE (Fig. 4.3A-B, 4.4A; Wang and Becker, 2013, 2015a), but Cu/Se and Ag/Se in the Komati Formation are a factor of 3 to 6 higher (Fig. 4.5). The high Cu/Se and Ag/Se ratios may have been caused by two processes, degassing of S, Se and Te during lava emplacement and depletion of S, Se and Te (but not Cu and Ag) in the mantle source of the Komati Formation. Though the trends of S/Se and Se/Te with S and Se abundances are in a similar fashion as those in Victoria's lava lake (Fig. 4.3A), such variations are mainly dictated by one sample: BV 05.

Notably, Pd/Pt ratios (1.0 ± 0.1, 2SD) in the Komati Formation (Puchtel et al., 2014) are in the range of the BSE (Becker et al., 2006), whereas Cu/Pd and Ag/Pd ratios are marginally higher than those in the BSE (Fig. S4.8). Cu/Pd of BV 03 and BV 05 of the Komati Formation are approximately 7100 and 8500 (Fig. S4.8A), and Ag/Pd of these two samples are 3.41 and 1.96 (Fig. S4.8B). Alternatively, the depletions of S, Se, Te and the PGE (Pd and Pt) relative to Cu and Ag could be inherited from the mantle source of the Komati Formation. The high Cu/Se and Ag/Se ratios in the mantle source of Komati Formation would be consistent with the model proposed by Maier et al., 2009 that progressive mixing and homogenization of late accreted material the in terrestrial mantle may be detectable by means of low concentrations of the HSE in komatiites formed between 3.6 Ga to 2.9 Ga This model was based on the discovery that abundances of Pt in Archean komatiites increased from ~4 ng/g at ~3.5 Ga to 8-12 ng/g at 2.9 Ga. It is thought that komatiites are derived from the tails of mantle plumes originating in the lower mantle and possibly even the core-mantle boundary (Campbell et al., 1989). Maier et al., 2009 interpreted the low abundances of Pt and Pd (and by inference other HSE) in Mesoarchean komatiites as evidence for slow mixing of late accreted material in the lower mantle.

CI chondritic ratios of S, Se and Te in the BSE, as observed in post-Archean lherzolites and in most Archean komatiites (this study and Chapter 3), were proposed to reflect late addition of volatile-rich materials similar to carbonaceous chondrites (Wang and Becker, 2013). If the high Cu/Se, Ag/Se and Cu/Pd ratios in the Komati Formation were indeed inherited from their mantle sources these data would be independent evidence for the progressive mixing model of Maier et al., 2009.

4.7 Conclusions

With the aim of constraining the origins of chalcophile elements in the terrestrial mantle, abundances of S, Se, Te, Cu and Ag in Archean komatiites of various petrogenesis and ages from different regions are reported in this study. Sulfur, Se, and Te in the samples from the 2.7 Ga Pyke Hill komatiites (Abitibi Greenstone Belt) were little mobilized relative to Cu and Ag and can be used to characterize the mantle source of Abitibi komatiites. Abundances of S, probably also Se and Te in the 2.4 Ga Victoria's lava lake of the Vetreny Belt were lost by magmatic degassing. However, Cu/Ag of Victoria's lava lake were not fractionated during magmatic differentiation and therefore could be used to estimate the Cu and Ag contents of the Victoria's source. Abundances of chalcophile elements in pre-2.9 Ga komatiites of the Weltevreden Formation and Schapenburg Greenstone Remnant underwent strong late-stage alterations. The least modified 564-6 from the chilled margin of SA 654 lava flow were used to constrain the degree of early melt extractions. The 3.5 Ga Komati Formation is distinguished from the others by near-BSE S/Se, Se/Te and Cu/Ag ratios but supra-BSE Cu/Se and Ag/Se ratios, which might reflect the progressive mixing of the late accreted material in the mantle.

Near-chondritic S/Se and Se/Te of post-2.9 Ga komatiites confirmed that S, Se and Te contents in the BSE were delivered via late accretion after the cessation of terrestrial core formation. This is consistent with current data on Se and Te isotope compositions of the terrestrial mantle which are indistinguishable from chondrites (Fehr et al., 2004; Vollstaedt et al., 2015), though S isotope compositions of MORBs and mantle xenoliths in kimberlite are deviated from chondrites (Boujibar et al., 2014; Giuliani et al., 2016; Labidi et al., 2013). Ratios of Cu/Ag in post-2.9 Ga komatiites agree with that of the BSE, which do not match Cu/Ag of the known groups of chondrites (Wang and Becker, 2015a). The Ag and Cu isotope composition of mantle-derived rocks seems to indicate a chondritic origin of Ag in the BSE (Liu et al., 2015; Savage et al., 2015; Schönbächler et al., 2010). The nonchondritic Cu/Ag ratio in the BSE could have several implications, including high temperature and pressure core formation or a nonchondritic Cu/Ag of Earth's building materials or both.

4.8 Appendix Chapter 4

4.8.1 Profiles of core drills or outcrops of the studied samples

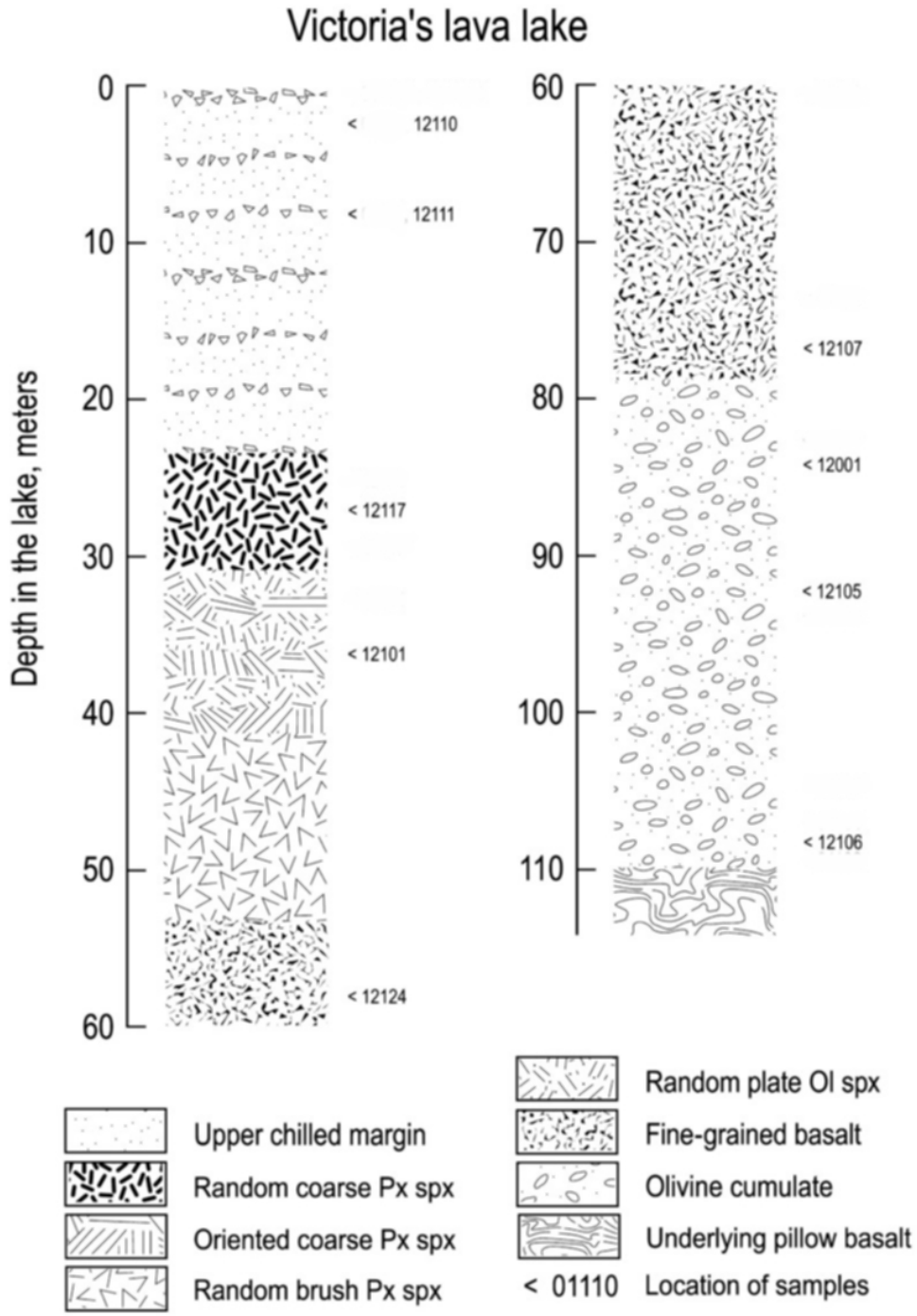

Fig. S4.1 Schematic integrated section of Victoria's lava lake in the Vetreny Belt with location of the samples investigated in this study (Puchtel et al., 2016b).

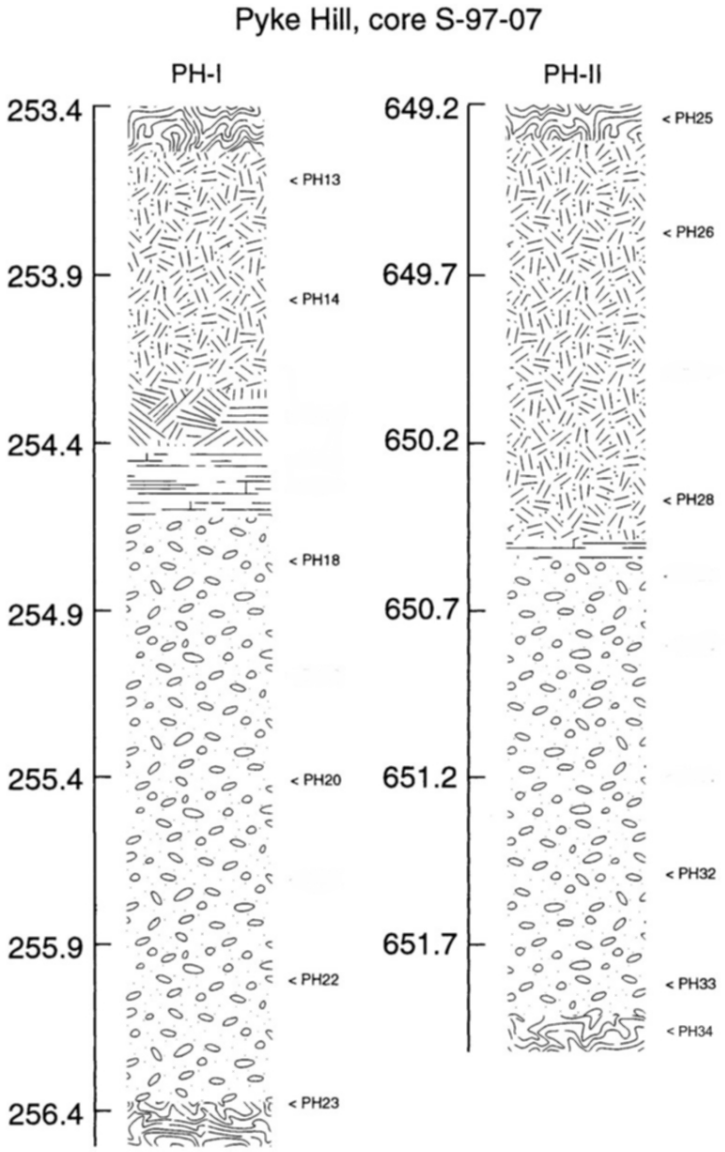

Fig. S4.2 Profiles of the Pyke Hill lava flows in the Abitibi Greenstone Belt modified from previous studies (Puchtel et al., 2004; Puchtel et al., 2009b) and the location of the samples used in this study is indicated. The legends refer to Fig. S4.1.

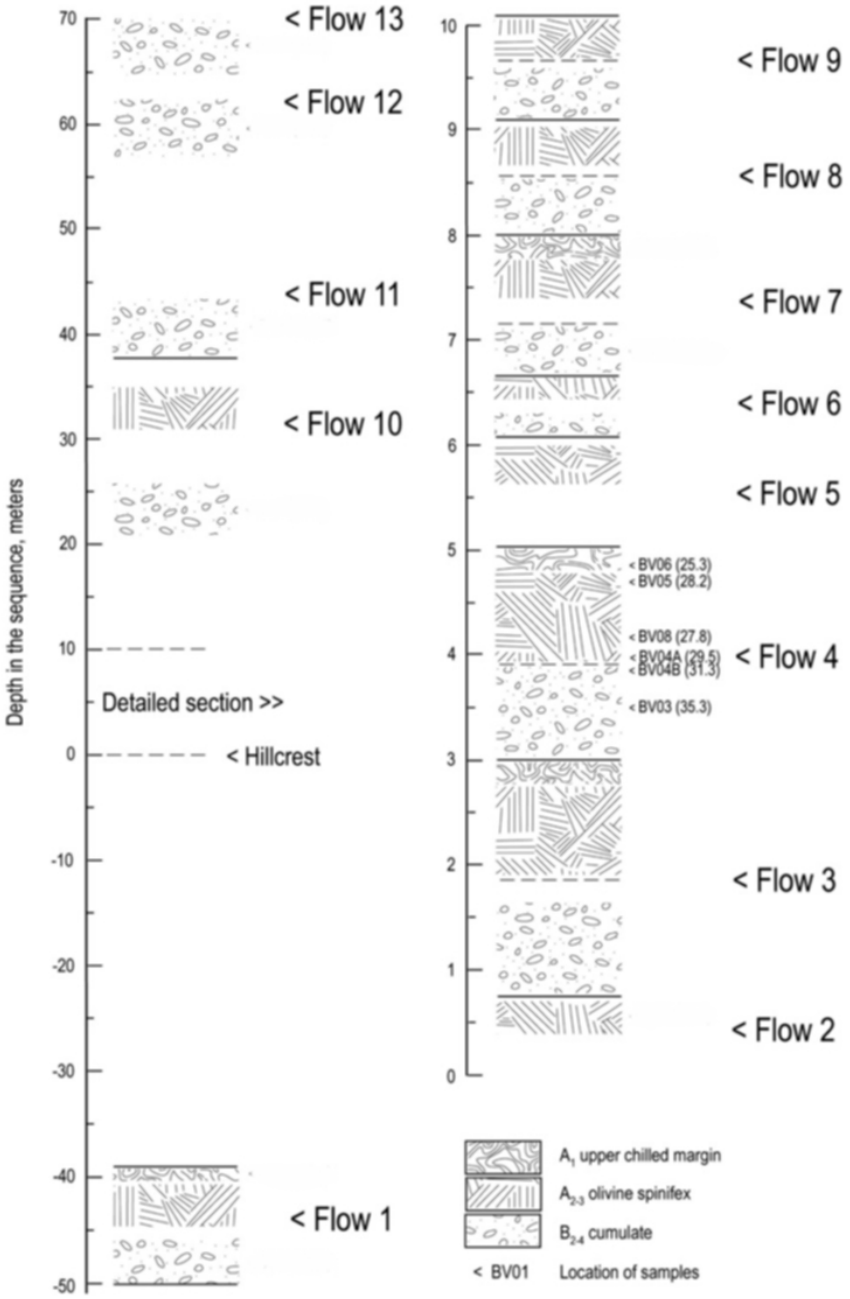

Fig. S4.3 Schematic cross-section of the Komati Formation in the Barberton Greenstone Belt modified from the previous study (Puchtel et al., 2013). The Flow 4, studied in the present work, is the only continuous fully differentiated lava flow in the Komati Formation. Numbers in brackets denote MgO contents in the samples re-calculated on an anhydrous basis.

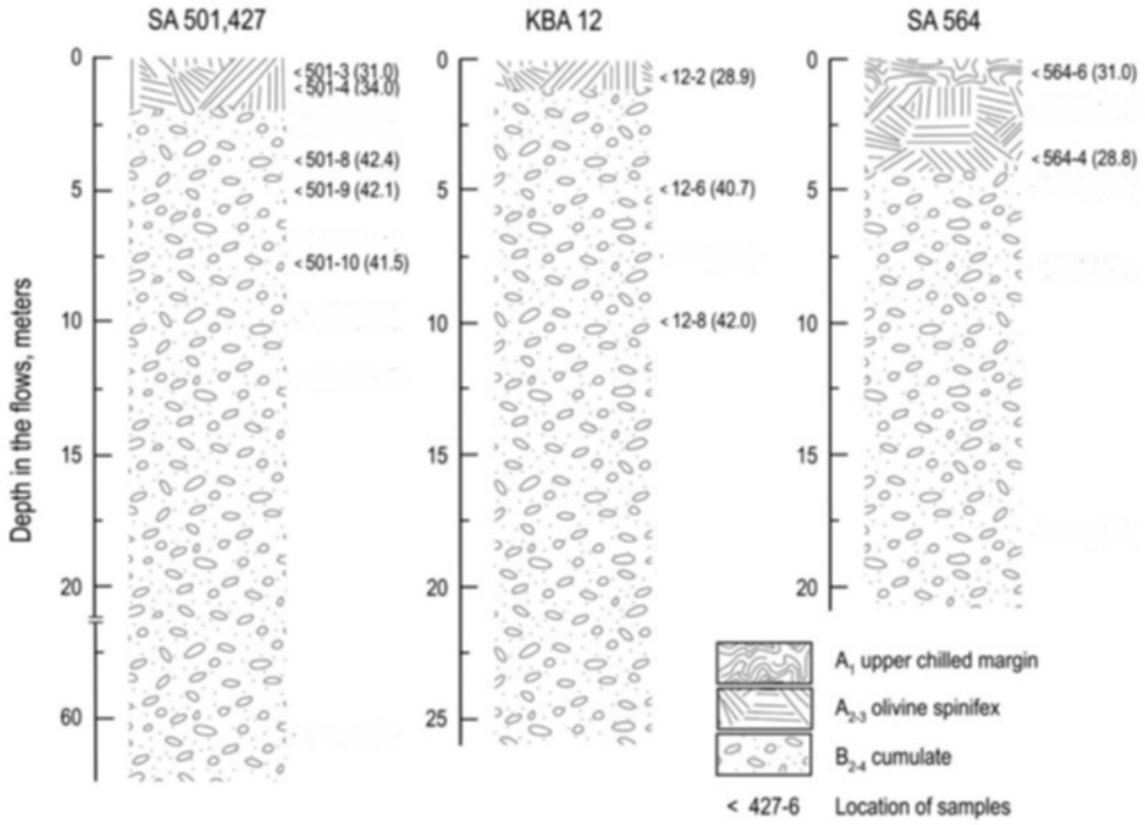

Fig. S4.4 Schematic cross-sections of lava flows SA501, KBA12 and SA564 in the Pioneer type locality of the Weltevreden Formation in the Barberton Greenstone Belt modified from the previous study (Puchtel et al., 2013).

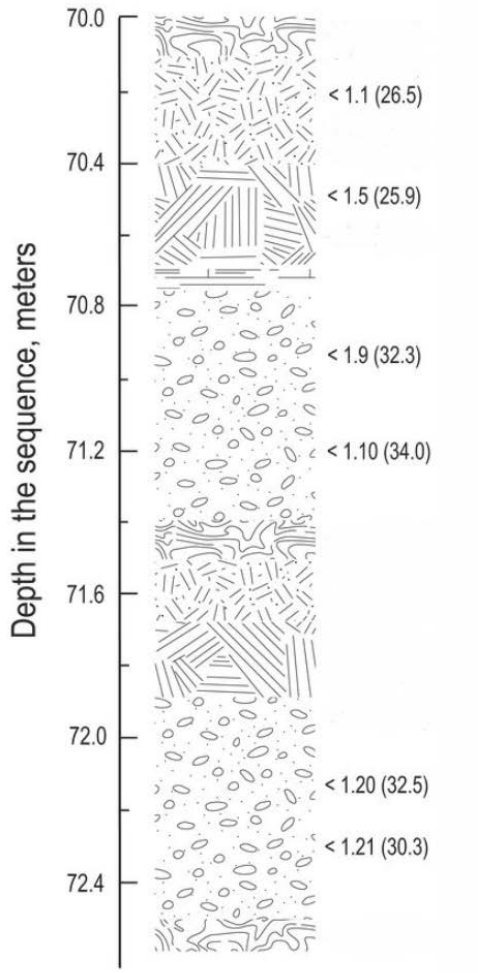

Fig. S4.5 Schematic section of the Carl's flow in the Schapenburg Greenstone Remnant modified from the recent work (Puchtel et al., 2016a). Sample numbers, sample location and the MgO contents of the studied samples are also indicated.

4.8.2 Variation diagrams of chalcophile elements

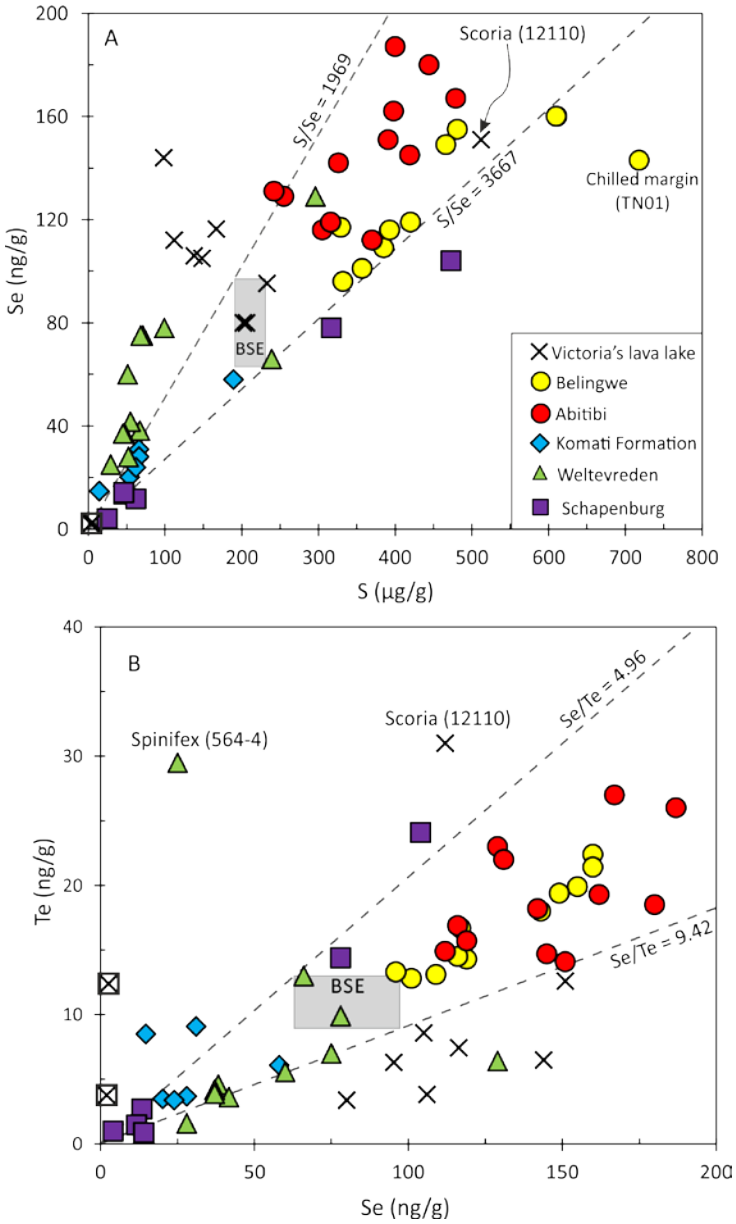

Fig. S4.6 Variation diagrams of S, Se and Te in the Archean komatiites and komatiitic basalts studied in the present work. The BSE values of S, Se and Te was reported previously (Wang and Becker, 2013). Abundances of S, Se and Te in the majority of pre-2.9 Ga komatiites (Komati, Weltevreden and Schapenburg) are lower than those in the post-2.9 Ga komatiites. Distinguished from the other samples the rocks of Victoria's lava lake have slightly lower Te abundances, though Se abundances are comparable.

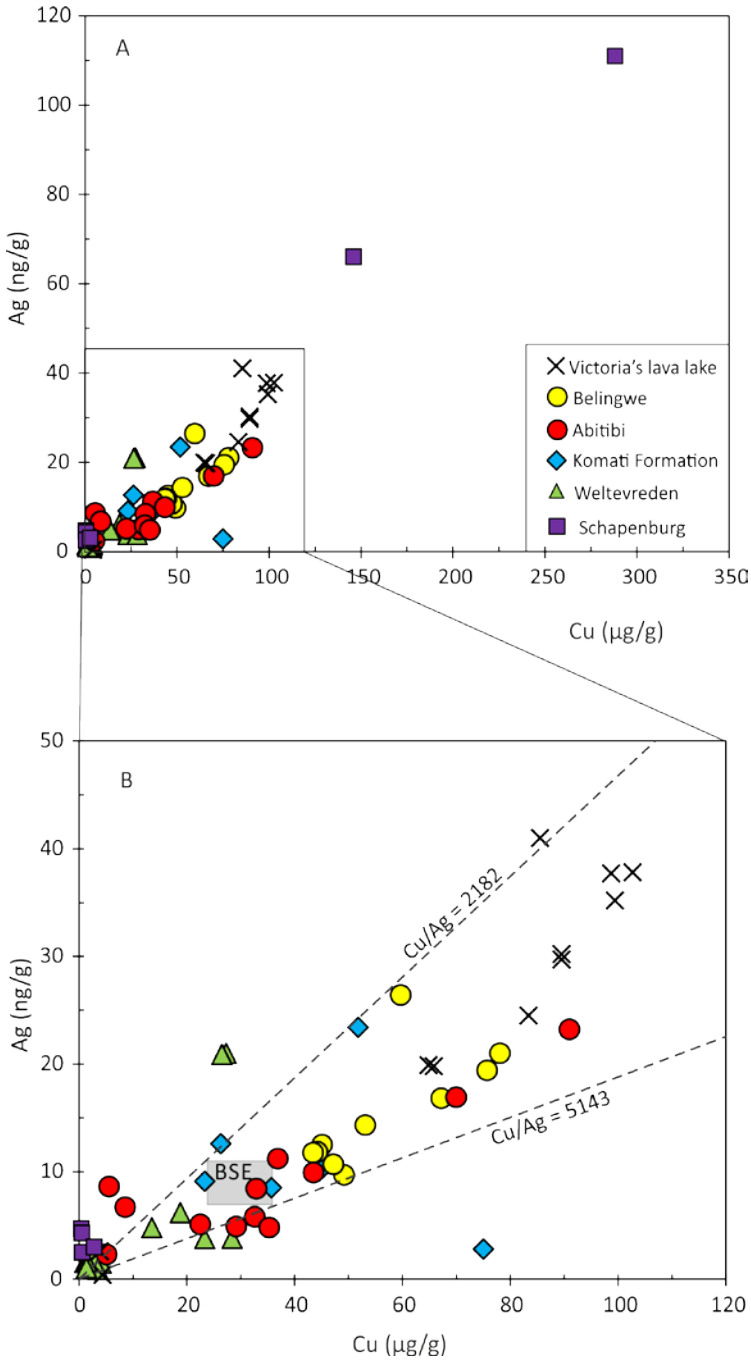

Fig. S4.7 Variation diagrams of Cu and Ag in the Archean komatiites and komatiitic basalts studied in the present work. The BSE values of Cu and Ag was reported previously (Wang and Becker, 2015a). Two samples from the Schapenburg komatiites are characterized by significant enrichments of Cu and Ag compared to the other samples in the present study.

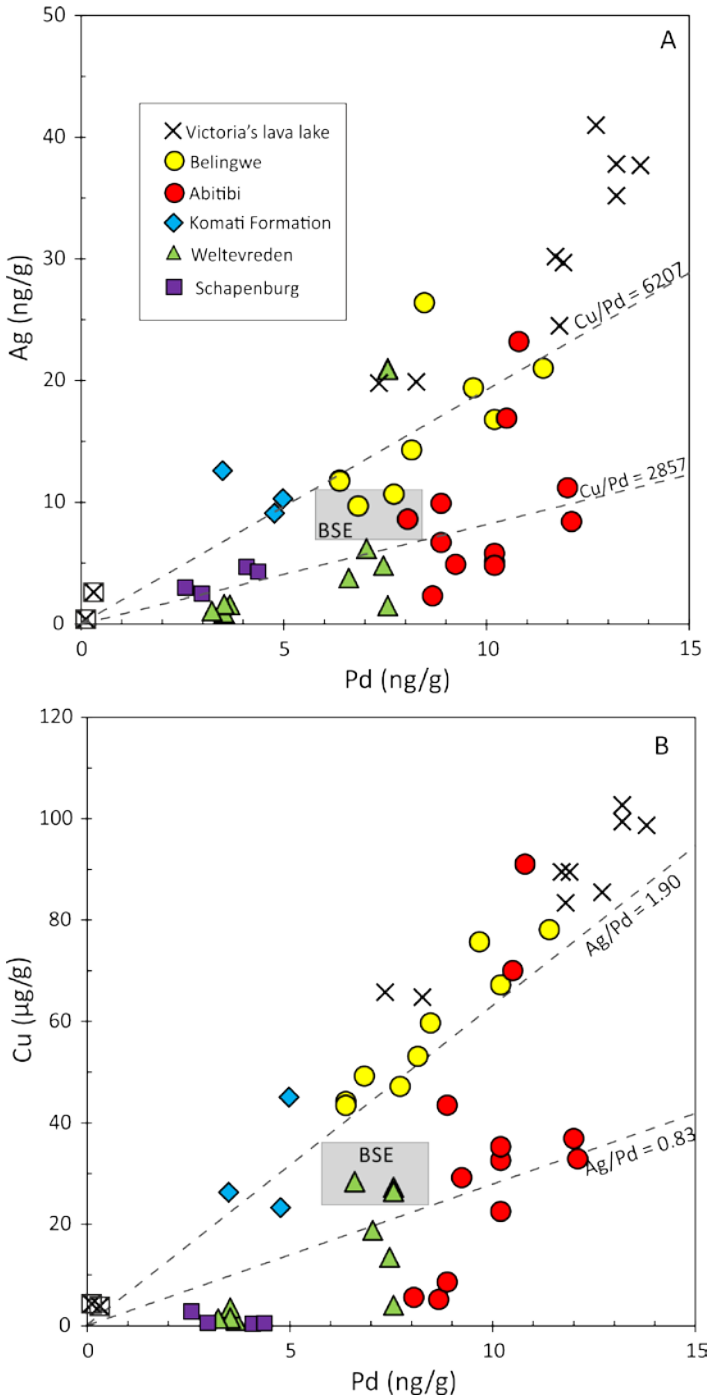

Fig. S4.8 Variation diagrams of Cu, Ag and Pd in the Archean komatiites and komatiitic basalts studied in the present work. Data on Pd in the same aliquots of samples were published previously (Connolly et al., 2011; Puchtel et al., 2016a; Puchtel and Humayun, 2001; Puchtel et al., 2004; Puchtel et al., 2007; Puchtel et al., 2016b; Puchtel et al., 2009a; Puchtel et al., 2009b; Puchtel et al., 2014). The BSE values of Cu and Ag were reported previously (Wang and Becker, 2015a). The BSE value of Pd was adopted from (Becker et al., 2006). Two samples from the Schapenburg komatiites significantly enriched in Cu and Ag were excluded here.

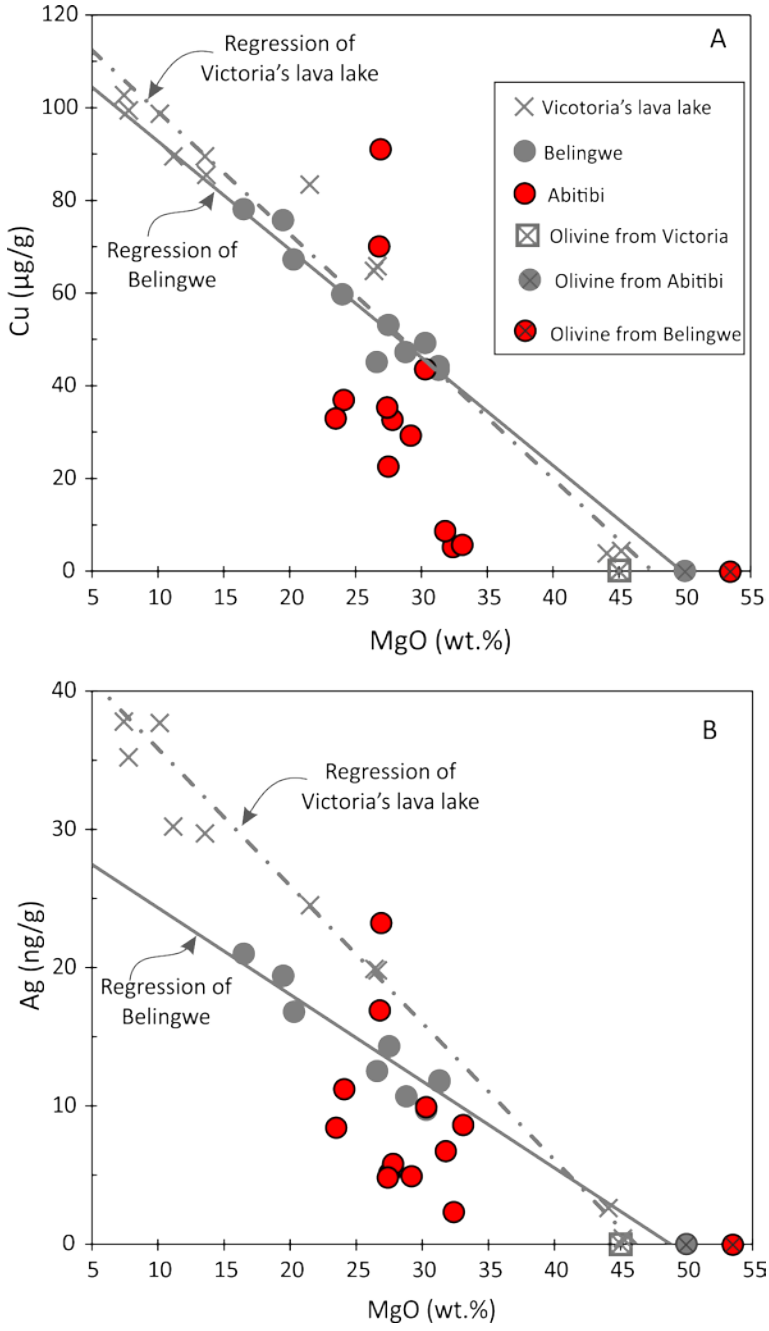

Fig. S4.9 Variation diagrams of Cu and Ag with MgO contents in the Archean komatiites and komatiitic basalts studied in the present work. In contrast to samples from Victoria's lava lake and Belingwe in which the variations of Cu and Ag with MgO are dominated by olivine control line, the relationship of Cu and Ag abundances with MgO contents in the Abitibi komatiites likely dose not pass through the composition of olivine separates. This is an indication for the mobilization of Cu and Ag in the Abitibi rocks.

4.8.3 Rayleigh-type degassing model

The equation designed for Rayleigh-type magmatic degassing was based on the equation 1.5.15 in (Albarède, 1996). The incremental processes related to changes in element ratios are fundamentally controlled by the distillation equation in the equation 1.5.3 in (Albarède, 1996), from which the equation used in this work was derived and modified.

$$d\ln\left(\frac{C_{refractory}}{C_{volatile}}\right)_{melt} = \left(D_{volatile}^{refractory} - 1\right) \times \left(\frac{D_{volatile}}{D_{volatile} - 1}\right) \times d\ln C_{melt}^{volatile} \quad \text{(Equation S4.1)}$$

Where *C* refers to element abundance, and *refractory* and *volatile* refers to refractory and volatile elements, respectively. *D* is the gas-magma partition coefficient, and $D_{volatile}^{refractory}$ is the ratio of gas-magma partition coefficient of refractory and volatile elements. The subscript *melt* refers to the remaining magma after volatile losses.

Because refractory elements have very low D, so Equation S4.1 can be modified to that is used in this work:

$$\left(\frac{C_{refractory}}{C_{volatile}}\right)_{melt} \approx \left(\frac{C_{refractory}}{C_{volatile}}\right)_0 \times \left(\frac{C_{melt}^{volatile}}{C_0^{volatile}}\right)^{\left(D_{volatile}^{refractory} - 1\right)} \quad \text{(Equation S4.2)}$$

Where the subscript *0* refers to the initial magma without volatile losses and magmatic differentiation.

The starting element ratios used in the model are set to the BSE ratios of these elements, which is because of that the primary magma should be undersaturated in sulfide and there hence chalcophile element ratios should not be fractionated from their mantle sources which in this stage are assumed to have a composition comparable to the BSE. The $D_{volatile}^{refractory}$ is fixed to 0.005 in this study, whereas higher $D_{volatile}^{refractory}$, such as 0.5, would result to much flatter curves and $D_{volatile}^{refractory}$ values lower than 0.005 make little differences in the modeling results.

Chapter 5

Abundances of In, Cd, Tl, Mo, Sm and Ba in komatiites and komatiitic basalts: implication for komatiite petrogenesis and mantle evolution

5.1 Abstract

As a product of high-degrees of partial melting, Archean komatiites can be used to constrain the chemical composition of Archean mantle and potentially the bulk silicate Earth (BSE). In this contribution, we analyzed the abundances of In, Cd, Tl, Mo, Sm and Ba in 45 Archean komatiites and komatiitic basalts (including two olivine separates) of distinct petrogenesis and ages by using isotope dilution ICP-MS technique. Indium abundances of the studied samples display a negative linear correlation with MgO contents which follows the olivine control line. Such correlations of Mo and Cd with MgO contents are only obtained in samples from the 2.4 Ga Victoria's lava lake in the Vetreny Belt. Thallium and Ba abundances are significantly mobilized and no simple correlation with MgO contents can be observed. The effect of magmatic volatile degassing on these elements likely are negligible. The high Cd/Yb and low In/Yb in samples from the Komati Formation (0.06 ± 0.01 and 0.027 ± 0.004, 1SD, respectively) relative to those from the Weltevreden Formation (0.034 ± 0.005 and 0.035 ± 0.001, respectively) seem to indicate the retention of garnet in the mantle source of Al-depleted Barberton-type komatiites. While In/Yb ratios of the Schapenburg Greenstone Remnant are comparable to that of the Weltevreden Formation, which probably implies the abundant garnet in the mantle source of Schapenburg komatiites. Estimates for In and Cd abundances in the mantle source of Archean komatiites are consistent with those calculated from mantle peridotites. The depletion of In, Cd and Zn in the BSE relative to CI chondrites are deviated from the depletion trend of volatile lithophile elements. The enrichment of In relative to Cd in the BSE requires nonchondritic components as the building materials for Earth.

5.2 Introduction

Constraining the abundances of siderophile and cosmochemically volatile elements in the bulk silicate Earth (BSE) is of importance for understanding the history of terrestrial accretion and differentiation. In cosmochemistry, elements with half condensation temperatures lower than 1328 K (the half condensation temperature of Fe) under the solar nebula condition are classified as volatile elements (Lodders, 2003). In geochemistry, elements are categorized as siderophile, chalcophile, lithophile and atomphile, based on their partition coefficients among Fe alloy, troilite, silicate or gas during partial melting and magmatic differentiation (Goldschmidt, 1937). Abundances of volatile elements in the BSE are all variably depleted relative to CI chondrites, and the lithophile volatile elements broadly define a volatility depletion trend (Palme and O'Neill, 2014). Depletions of chalcophile volatile elements in the BSE relative to CI chondrites are complicated in that they are partitioned into the Earth's core during terrestrial accretion. Volatile chalcophile elements S, Se and Te in the terrestrial mantle were first scavenged into the core and then enriched by a late chondritic addition after the cessation of core formation (Wang and Becker, 2013). The moderately chalcophile Cu in the BSE seems to be governed by high temperature-pressure core formation in which certain amounts of light elements are involved, such as S and C (Righter, 2011). Recent interpretation concerning Cu isotope composition of the BSE suggested that the deviation of Cu isotopic composition in the BSE from enstatite chondrites were caused by a large-scale sulfide matt during the late stage of core formation (Savage et al., 2015). However, if Cu isotopes were fractionanted during the core formation, they should also show fractionation between non-metasomatic mantle peridotites and non-metasomatic mid-ocean ridge basalts (MORB; Liu et al., 2015; Savage et al., 2015). Such fractionations were not observed in these studies.

The composition of some elements in the BSE is also controversial. Mantle peridotites, komatiites and basalts are conventially used to determine the major and trace element composition of the BSE (McDonough and Sun, 1995; Morgan, 1986), but recently these methods were challenged (Le Roux et al., 2007; Murton et al., 2013; Rubin et al., 2009). Chondritic ratios of S, Se and Te in mantle peridotite were not thought to be a primitive signature, but related to refertilization processes (König et al., 2014). Sulfide-saturated igneous rocks such as MORB cannot be used to estimate the chalcophile element composition of the respective mantle source because of sulfide segregation during magma transport (Lissner et al., 2014; Rehkämper et al., 1999). Komatiites may yield information on large-scale composition complementing data on mantle peridotites and MORB. Komatiites are

spinifex-textured ultramafic rocks with MgO contents greater than 18 wt.% which formed via high-degree of partial melting (30-50%; Arndt, 1977; Arndt et al., 2008). At such high-degrees of partial melting, incompatible chalcophile elements should not be fractionated as deduced from the imcompatible Pt and Pd in komatiites (*e.g.* Puchtel et al., 2004). Even after assimilation of S-poor crustal rocks, komatiite magma may remain sulfide-undersaturated (Keays, 1995). Therefore komatiites are a potential tool to determine incompatible chalcophile element composition of Archean mantle sources.

Indium, Cd and Tl are classified as volatile chalcophile elements during solar nebular condensation, but they are also partially (Tl) and mostly lithophile (In and Cd) during terrestrial magmatism (Heinrichs et al., 1980; Hertogen et al., 1980; Kiseeva and Wood, 2013; Patten et al., 2013; Xiao et al., 2004). Abundances of In and Cd in the BSE were mainly obtained from mantle peridotite and MORB (Palme and O'Neill, 2014; Wang et al., 2016; Witt-Eickschen et al., 2009; Yi et al., 2000; Yi et al., 1995), whereas estimates for Tl in the BSE were poorly constrained based on data from igneous rocks (Lyubetskaya and Korenaga, 2007; Nielsen et al., 2014; Palme and O'Neill, 2014). The geochemical behavior of In, Cd and Tl during high-degrees of partial melting are little documented, and thus data on komatiites may put additional constraints on their BSE budgets. Indium and Cd were shown to mainly partition into clinopyroxene in mantle rocks (Witt-Eickschen et al., 2009), while thallium is mostly chalcophile during the formation of MORB (Hertogen et al., 1980; Nielsen et al., 2014). With the exception of a few laboratory experiments (Adam and Green, 2006; van Westrenen et al., 1999), the role of garnet was rarely considered in the partitioning of In and Cd in natural magmatic rocks. Garnet may play an important role in the petrogenesis of komatiites (Arndt et al., 2008), and therefore komatiites can be used to constrain the partitioning behavior of In and Cd into garnet.

In this study we analyzed 52 well-characterized Archean komatiites and komatiitic basalts from various occurrences and employed the isotope dilution ICP-MS technique to obtain the abundances of In, Cd, Tl, Mo, Sm and Ba in these samples. Based on the element-MgO plots and BSE-normalized diagrams, these data are used to discuss the effects of late-stage alteration, crustal contamination, magmatic degassing and mantle processes. By comparing variations of the element ratios in different types of komatiites, additional constraints on the petrogenesis of komatiites are obtained. Abundances of these elements in the mantle sources of Archean komatiites are calculated on the basis of element-MgO variation diagrams and/or canonical ratios.

5.3 Sample characterization and sample preparation

Komatiites and komatiitic basalts investigated in this study have been used to determine abundances of highly siderophile elements (HSE; Puchtel and Humayun, 2001; Puchtel et al., 2004; Puchtel et al., 2009a; Puchtel et al., 2009b; Puchtel et al., 2014) and chalcophile elements (S, Se, Te, Cu and Ag; Chapter 3 and Chapter 4) in the investigated samples were discussed in Chapter 3 and Chapter 4. Compared to the well-preserved 2.7 Ga komatiites of the Belingwe Greenstone Belt, the primary mineralogy was not preserved in the komatiites investigated in this study which include the 3.5 Ga Komati Formation and 3.3 Ga Weltevreden Formation from the Barberton Greenstone Belt, the 3.5 Ga Carl's flow of the Schapenburg Greenstone Remnant and the 2.7 Ga Pyke Hill flows of Abitibi Greenstone Belt, and the 2.4 Ga komatiitic basalts from Victoria's lava lake of the Vetreny Belt. Primary minerals in these samples were variably altered and were replaced by secondary phases during serpentinization (Anhaeusser, 1980; Lécuyer et al., 1994). With the exception of samples from Victoria's lava lake which underwent minor assimilation of older crustal materials (Puchtel et al., 1997), other komatiites investigated here so far have not yielded no evidence for significant crustal assimilation by the magma. The geologic background and petrologic information of the investigated samples were given in the literature cited above.

5.4 Analytical Techniques and data quality

5.4.1 Analytical techniques

Abundances of In, Cd, Tl, Mo, Sm and Ba in komatiites and komatiitic basalts were obtained by isotope dilution ICP-MS on the same digestion aliquot using HF-HNO_3 digestion in PFA beakers enclosed in pressure bombs. The details of the chemical separation were given by (Wang et al., 2015), and a brief description is given here.

Around 0.5 g sample powder spiked with ^{113}In, ^{110}Cd, ^{203}Tl, ^{97}Mo, ^{149}Sm, and ^{137}Ba was mixed with 4 ml HF and 1 ml HNO_3 into a 15 ml PFA beakers. The beakers were subsequently sealed with Teflon tape and transferred into Teflon liners. The Teflon liners were loaded into pressure bombs manufactured by Parr Instrument Company®. The digestion process took three days at 190℃. After digestion solutions were converted into chloride form, half of which were loaded on pre-cleaned columns filled with 3 ml of anion resin. The *Ba-Sm* fraction was first collected in 4 ml 4.5 mol l^{-1} HCl, and then the *In-Mo* fraction was collected

in 8 ml 0.4 mol l^{-1} HCl, and, at last, the *Cd-Tl* fraction was collected in 28 ml 0.7 mol l^{-1} HNO_3 + 1 ml / 100 ml H_2O_2 and evaporated. After dissolution in HNO_3, intensities of ^{110,111,112,114}Cd and ^{203,205}Tl were determined by Aridus-ICP-MS. The *Ba-Sm* fraction was converted to 3 ml 0.28 mol l^{-1} HNO_3 and intensities of ^{135,136,137,138}Ba and ^{147,149,152,154}Sm were measured by ICP-MS equipped with single pass Scott spray chamber. After the removal of iron in the In-Mo fraction by adding ascorbic acid, In and Mo were purified and collected into 4.5 ml 0.4 mol l^{-1} HCl. The purified In-Mo fraction was converted into 4 ml 0.28 mol l^{-1} HNO_3. Intensities of ^{113,115}In and ^{95,97,98}Mo were determined by Aridus-ICP-MS.

5.4.2 Data quality

The total procedural blanks and abundances of In, Cd, Mo, Tl, Sm and Ba in geological reference materials were given in Table 3.1 in Chapter 3. As shown in section 3.4.2 in Chapter 3 abundances of these elements were well reproduced, and Sm and Ba data are in the range of the certificated values.

5.5 Results

Abundances of In, Cd, Tl, Mo, Sm and Ba in Archean komatiites and komatiitic basalts are given in Table 5.1. Element abundances differ among localities and vary significantly in a single differentiated lava flow. Data on Belingwe komatiites are discussed in detail in Chapter 3 and shown for comparison in diagrams.

Indium abundance varies significantly among komatiites from different localities, and in a single differentiated lava flow it decreases from spinifex subzones to chilled margins and cumulate subzones, accompanied by increasing MgO contents (Fig. 5.1A). For instance, in Victoria's lava lake abundances of In decrease from 46.8-51.5 ng/g of the komatiitic basalts and the pyroxene spinifex subzone to 41-42 ng/g of the flow top breccia and the chilled margin and 26.1-32.4 ng/g of the olivine cumulate subzone. Such distributions can also be found in samples from the Abitibi Greenstone Belt, Komati Formation, Schapenburg Greenstone Remnant and Weltevreden Formation. Abundances of In in komatiites from various occurrances display an uniform correlation with MgO contents (Fig. 5.1A), though samples from the Weltevreden Formation show diviation from the trend defined by other samples.

Though Sm abundances in the present samples display negative correlations with MgO contents (Fig. 5.1B), no uniform trend exist as in the case of In abundances. Abundances of Sm in samples from Victoria's lava lake are the highest, whereas Sm abundances in samples from the Weltevreden Formation are the lowest. As shown in Fig 5.1B, Sm abundances in Al-depleted Barberton-type komatiites (Komati Formation and Schapenburg Greenstone Remnant) are higher than Al-undepleted Munro-type komatiites (Abitibi and Belingwe) at comparable MgO contents. Abundances of Sm obtained by in this study are in agreement with the previous studies (Puchtel et al., 2013; Puchtel et al., 2009b).

As shown in Fig 5.2, the variations of Cd and Mo abundances in samples from Victoria's lava lake are in a similar fashion as that of In, displaying a negative correlation with increasing MgO contents. However, such variations are not observed in samples from the others komatiite suites (Fig. 5.3). For instance, the variation of abundances of Cd in the Weltevreden Formation does not follow any trend, 7.7-19.9 ng/g Cd in cumulate subzone, 44.8-75 ng/g Cd in spinifex subzone and 59.3 ng/g in chilled margin 564-6. Such chaotic variations of Cd abundances also exist in samples from the Komati Formation and Schapenburg Greenstone Remnant. In the case of Mo abundances, in samples from the Abitibi Greenstone Belt abundances of Mo vary from 24 ng/g to 61 ng/g, which do not correspond to the changes of lithological units. Such chaotic variations of Mo abundances are also found in samples from the Komati Formation, Schapenburg Greenstone Remnant and Weltevreden Formation. Mo abundances in some of the present samples were reported in previous studies. We note that with the exception of PH33, 501-3 and 12-2, abundances of Mo obtained in this study are slightly lower than the values in previous report (Greber et al., 2015).

In the present samples abundances of Tl and Ba vary significantly (Fig 5.4) and do not display simple relations with MgO contents. For instance, the Tl abundance of the flow top breccia from Victoria's lava lake is 57.8 ng/g, which is much higher than 14.4 ng/g of the chilled margin. Abundances of Tl in the olivine cumulate subzone from Victoria's lava lake vary from 26.0 ng/g to 48.1 ng/g, whereas abundances of Tl vary from 18.0-24.4 ng/g in the pyroxene spinifex subzone to 28.8-63.1 ng/g in the komatiitic basalts. The Ba abundance of the top flow breccia of Victoria's lava lake is 226 µg/g which is much higher than 74.0 µg/g of the chilled margin. Abundances of Ba in the olivine cumulate subzone of PH-I flow from the Abitibi Greenstone Belt are higher than those in the spinifex subzone, 10.2-23.2 µg/g and 4.02-7.9 µg/g, respectively. Chaotic variations of abundances of Ba and Tl exist in all the

present samples. Furthermore, Ba and Tl are enriched or depleted in the BSE-normalized diagrams (Fig. 5.5) relative to their neighboring elements.

Table 5.1 Bulk rock abundances of In, Cd, Tl, Mo, Sm and Ba in Archean komatiites and komatiitic basalts*

Locality	Sample number	Lithology	In (ng/g)	2σ	Cd (ng/g)	2σ	Tl (ng/g)	2σ	Mo (ng/g)	2σ	Sm (ng/g)	2σ	Ba (µg/g)	2σ	Ce (µg/g)#	$(Ce/Sm)_N$	$(Ba/Sm)_N$
Victoria's lava lake, 2,4 Ga Vetreny belt, Baltic Shield	12110	flow top breccia	41.0	0.4	84	1	57.8	0.9	209	3	2140	25	226	3	17.0	2.6	6.7
	12111	upper chilled margin	42.0	0.5	75	1	14.4	0.3	141	2	2086	24	74.0	0.9	15.5	2.4	2.2
	12117	pyroxene spinifex	45.4	0.5	79	1	18.0	0.4	212	3	2635	31	99	1	15.7	1.9	2.4
	12101	pyroxene spinifex	48.6	0.2	82	1	24.4	0.4	183	2	2560	33	172	2	16.7	2.1	4.3
	12124	fine-grained basalt	51.5	0.2	90	1	63.1	0.9	241	3	3397	42	185	1	18.7	1.8	3.5
	12107	fine-grained basalt	46.8	0.2	75	1	28.8	0.5	192	3	3308	41	153	2	18.7	1.8	2.9
	12001	olivine cumulate	26.2	0.1	49.4	0.6	26.3	0.4	107	2	1169	14	83	1	9.83	2.7	4.5
	12105	olivine cumulate	26.1	0.1	49.6	0.6	26.0	0.4	106	2	1130	13	81	1	9.57	2.7	4.5
	12106	olivine cumulate	32.4	0.1	57.8	1	48.1	0.7	125	2	1789	21	97	1	10.9	2.0	3.4
	12001 Ol	olivine	7.7	0.1	-	-	-	-	1.0	0.9	35.6	0.6	0.91	0.01	0.10	0.9	1.6
	12105 Ol	olivine	5.93	0.08	-	-	-	-	1.6	0.9	51.7	0.8	1.46	0.03	0.11	0.7	1.8
Pyke Hill flows, 2,7 Ga Kidd-Munro Assemblage, Abitibi greenstone belt, Canada	***PH-I***																
	PH13	olivine spinifex	33.2	0.6	39.9	0.6	21.1	0.4	32	1	794	10	4.02	0.05	2.14	0.9	0.3
	PH14	olivine spinifex	32.7	0.5	33.4	0.5	15.7	0.3	38	1	792	10	7.9	0.1	2.16	0.9	0.6
	PH18	olivine cumulate	24.5	0.3	34.9	0.6	11.0	2.0	39	1	484	6	19.1	0.2	1.59	1.1	2.5
	PH20	olivine cumulate	21.1	0.2	26.2	0.4	20.5	0.3	33	1	457	6	10.2	0.1	1.44	1.0	1.4
	PH22	olivine cumulate	25.0	0.2	25.1	0.4	38.1	0.6	40	1	522	7	23.2	0.3	1.65	1.0	2.8
	PH23	chilled margin	27.4	0.2	42.4	0.7	29.4	0.5	24	1	603	9	6.90	0.08	1.98	1.1	0.7
	PH-II																
	PH25	upper chilled margin	27.6	0.4	34.7	0.7	16.7	0.3	26	1	566	7	5.31	0.06	1.91	1.1	0.6
	PH26	olivine spinifex	25.8	0.1	39.7	0.5	10.1	0.2	32	1	670	8	2.22	0.03	1.44	0.7	0.2
	PH28	olivine spinifex	26.2	0.1	37.8	0.5	20.1	0.3	27	1	642	8	5.34	0.07	1.44	0.7	0.5
	PH32	olivine cumulate	19.4	0.1	20.8	0.3	11.4	0.2	61	1	461	5	5.15	0.07	1.09	0.8	0.7
	PH33	olivine cumulate	21.3	0.1	24.9	0.3	10.4	0.2	52	1	510	6	4.14	0.05	1.19	0.8	0.5
	PH34	lower chilled margin	27.7	0.1	35.1	0.4	11.2	0.2	47	1	624	7	3.43	0.04	1.43	0.7	0.3
3,3 Ga Weltevreden Formation, Barberton greenstone belt, South Africa	***SA 501***																
	501-3	olivine spinifex	13.3	0.1	49.6	0.5	12	0.4	14	1	281	3	3.35	0.04	0.939	1.1	0.8
	501-4	olivine spinifex	12.8	0.1	44.8	1	5.9	0.12	12.2	0.9	270	3	7.54	0.09	0.948	1.1	1.8
	501-8	olivine cumulate	7.84	0.1	19.9	0.2	5.0	0.12	14	1	143	2	1.69	0.02	0.516	1.2	0.7
	501-9	olivine cumulate	8.11	0.1	8.9	0.1	3.28	0.1	10.5	0.9	148	2	0.94	0.02	0.495	1.1	0.4
	501-10	olivine cumulate	7.81	0.1	8.16	0.1	3.9	0.2	-	-	136	3	0.96	0.03	0.528	1.3	0.4
	duplicate		7.73	0.1	9.8	0.1	3.66	0.1	19	1	139	2	0.6	0.1			0.3
	KBA 12																
	12-2	olivine spinifex	14.8	0.1	75	1	6.4	0.1	17	1	316	6	7.3	0.1	1.02	1.0	1.5
	dupliacte		15.1	0.1	73.9	0.9	6.4	0.1	20	1	295	4	9.0	0.1			1.9
	12-6	olivine cumulate	8.22	0.1	12.1	0.1	4.21	0.1	8.3	0.9	154	2	0.55	0.01	0.518	1.1	0.2
	12-8	olivine cumulate	7.74	0.1	7.7	0.1	1.42	0.1	11.3	0.9	130	2	0.42	0.02	0.556	1.4	0.2

Locality	Sample number*	Lithology	In (ng/g)	2σ	Cd (ng/g)	2σ	Tl (ng/g)	2σ	Mo (ng/g)	2σ	Sm (ng/g)	2σ	Ba (µg/g)	2σ	Ce(µg/g)[#]	$(Ce/Sm)_N$	$(Ba/Sm)_N$
3,3 Ga Weltevreden Formation	***SA 564***																
	564-6	chilled margin	14.9	0.1	59.3	0.7	9.1	0.1	7.1	0.9	295	4	7.59	0.05	0.929	1.0	1.6
	564-4	olivine spinifex	15.7	0.1			27.2	1	8.8	0.9	332	4	6.27	0.09	0.853	0.8	1.2
Flow 4, 3,48 Ga Komati Formation, Barberton greenstone belt, South Africa	BV06	chilled margin	28.8	0.4	69	1	13.4	0.2	67	1	1397	17	11.2	0.1	6.07	1.4	0.5
	BV05	olivine spinifex	20.6	0.2	45.5	0.8	4.0	0.1	26	1	844	11	6.60	0.04	5.52	2.1	0.5
	BV08	olivine spinifex	21.0	0.3	22.4	0.2	5.2	0.1	24	1	994	12	5.88	0.04	5.62	1.8	0.4
	BV04A	olivine spinifex	22.5	0.2	65	1	12.4	0.2	8.4	0.9	970	13	5.13	0.03	4.55	1.5	0.3
	BV04B	olivine cumulate	20.4	0.2	66	2	24.8	0.5	14	1	1155	15	6.52	0.06			0.4
	BV03	olivine cumulate	16.9	0.1	32.4	0.6	1.88	0.7	21	1	686	9	2.20	0.02	3.42	1.6	0.2
Carl's flow, 3,5 Schapenburg greenstone remnant, South Africa	SCH1,1	olivine spinifex	23.8	0.1	69	1	23.1	0.7	45	1	984	2	2.14	0.03	4.59	1.5	0.1
	SCH1,5	olivine spinifex	25.1	0.1	94	1	14.0	0.2	57	1	1082	13	1.53	0.02	4.94	1.5	0.1
	SCH1,9	olivine spinifex	16.6	0.1	36.1	0.5	0.9	0.1	14	1	737	9	0.65	0.01	3.42	1.5	0.1
	SCH1,10	olivine cumulate	14.8	0.1	27.5	0.3	2.5	0.1	14	1	607	7	0.50	0.01	2.70	1.4	0.1
	SCH1,20	olivine cumulate	17.9	0.1	33.3	0.5	1.37	0.05	16	1	696	8	0.75	0.01	3.32	1.5	0.1
	SCH1,21	olivine cumulate	19.3	0.1	41.9	0.6	0.8	0.1	16	1	836	10	2.42	0.03	3.91	1.5	0.2

*Samples are arranged according to the depth in drill cores. [#] Abundances of Ce from (Puchtel et al., 2013; Puchtel et al., 1997; Puchtel et al., 1996; Puchtel et al., 2007; Puchtel et al., 2009b).

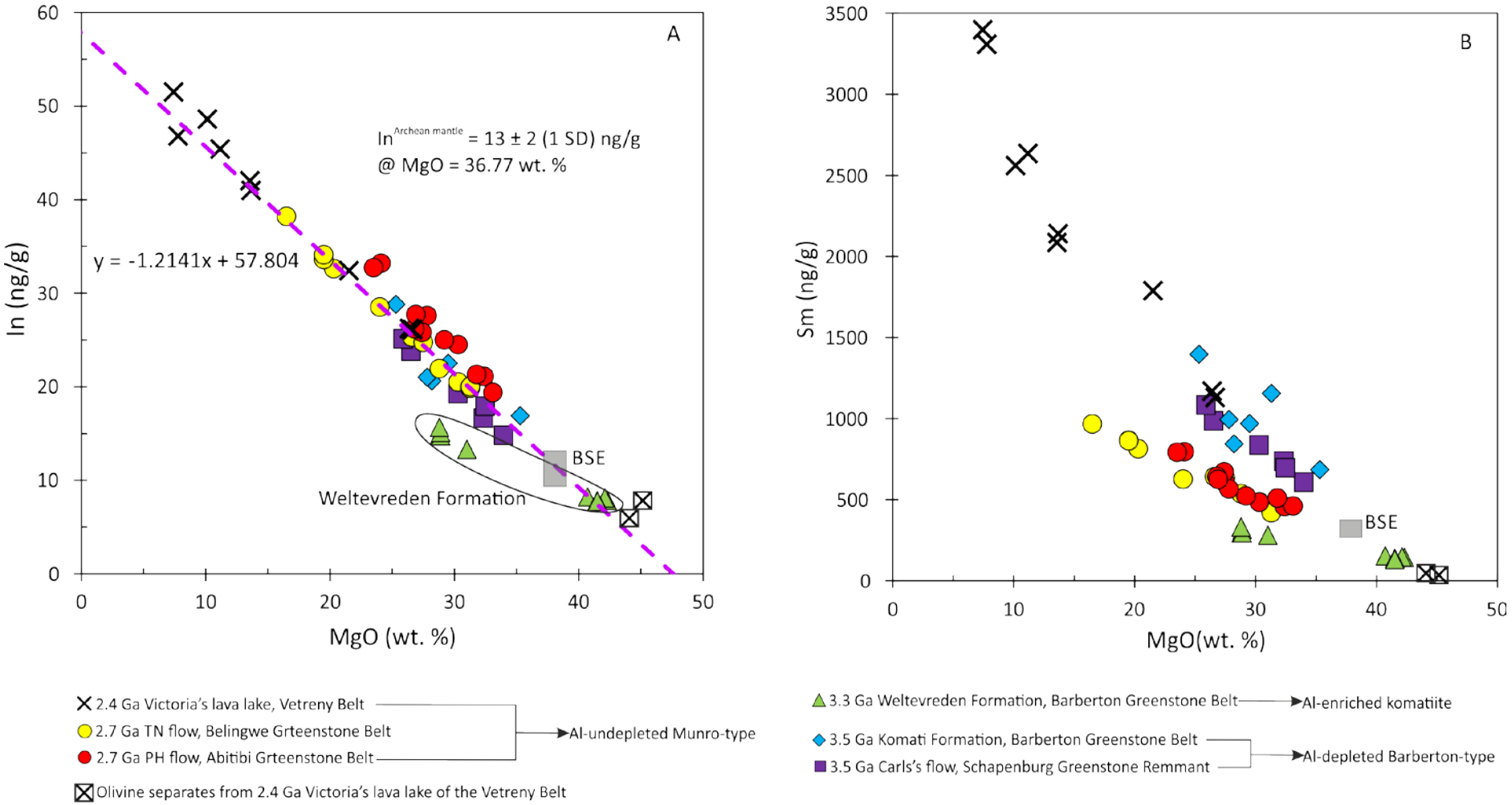
A
$In^{Archean\ mantle}$ = 13 ± 2 (1 SD) ng/g
@ MgO = 36.77 wt. %
y = -1.2141x + 57.804
BSE
Weltevreden Formation
In (ng/g)
MgO (wt. %)
B
Sm (ng/g)
MgO(wt. %)
2.4 Ga Victoria's lava lake, Vetreny Belt
2.7 Ga TN flow, Belingwe Grteenstone Belt
2.7 Ga PH flow, Abitibi Grteenstone Belt
Al-undepleted Munro-type
Olivine separates from 2.4 Ga Victoria's lava lake of the Vetreny Belt
3.3 Ga Weltevreden Formation, Barberton Greenstone Belt
Al-enriched komatiite
3.5 Ga Komati Formation, Barberton Greenstone Belt
3.5 Ga Carls's flow, Schapenburg Greenstone Remmant
Al-depleted Barberton-type

Fig. 5.1 Variations of abundances of In and Sm against MgO contents in Archean komatiites and komatiitic basalts. Abundance of In and Sm in the BSE are adopted from Wang et al. (2016) and Palme and O'Neill (2014), respectively. Abundances of indium in the investigated samples are linearly correlated with MgO contents (Fig 5.1A), indicating the immobility of In during the formation of komatiites. The abundance of indium in the Archean mantle obtained by projecting to MgO = 36.77 wt.% (Palme and O'Neill, 2014) is 13 ± 2 ng/g, which is identical to that in the BSE defined by post-Archean mantle peridotites (Wang et al., 2016). Abundances of Sm in the investigated samples are linearly correlated with MgO, indicating the immobility of Sm during the formation of komatiites and secondary alterations. Slopes of Sm-MgO correlations, however, are variable among different types of komatiites. Abundances of Sm in the Komati Formation and Schapenburg Greenstone Remnant are higher than those in the Belingwe Greenstone Belt and Abitibi Greenstone Belt, indicating the enrichment of light rare earth elements in the mantle sources of the Komati Formation and Schapenburg Greenstone Remnant. Abundances of Sm in the Weltevreden Formation are much lower the other samples in this study.

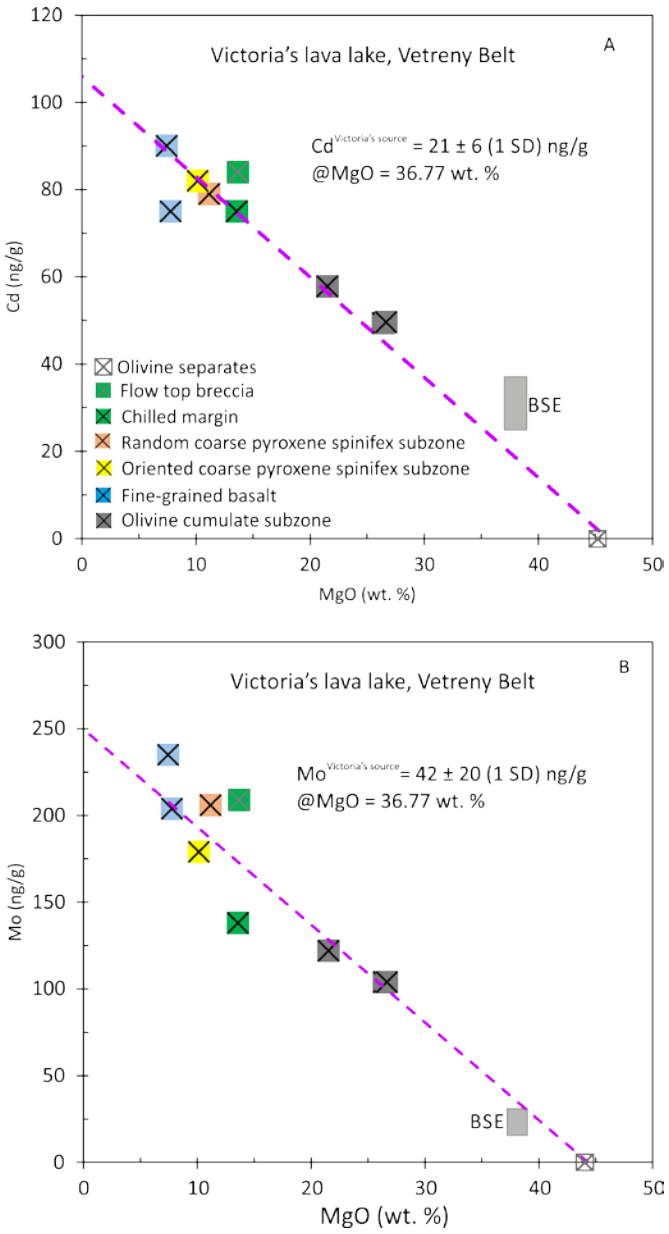

Fig. 5.2 Variations of abundances of Cd and Mo with MgO contents in Victoria's lava lake. A different legend (grey color) is used in this figure to show that abundances of Cd in olivine separates were not determined in the present study. The abundances of Cd and Mo in the BSE are adopted from Wang et al. (2016) and Greber et al. (2015), respectively. The intersections of Cd-MgO and Mo-MgO correlations with the MgO-axis is at the MgO contents (~ 45 wt.%) of cores of two olivine separates of the olivine cumulate subzone. The relative distribution of Mo and Cd in the subzones suggest that magmatic characteristics of Mo and Cd in Victoria's lava lake are well-preserved. Abundances of Mo and Cd in the melt part (spinifex subzones and basalts) are higher than in the primary magma represented by flow top breccia and chilled margin. The cumulate subzone is characterized by low Mo and Cd abundances compared to the other subzones.

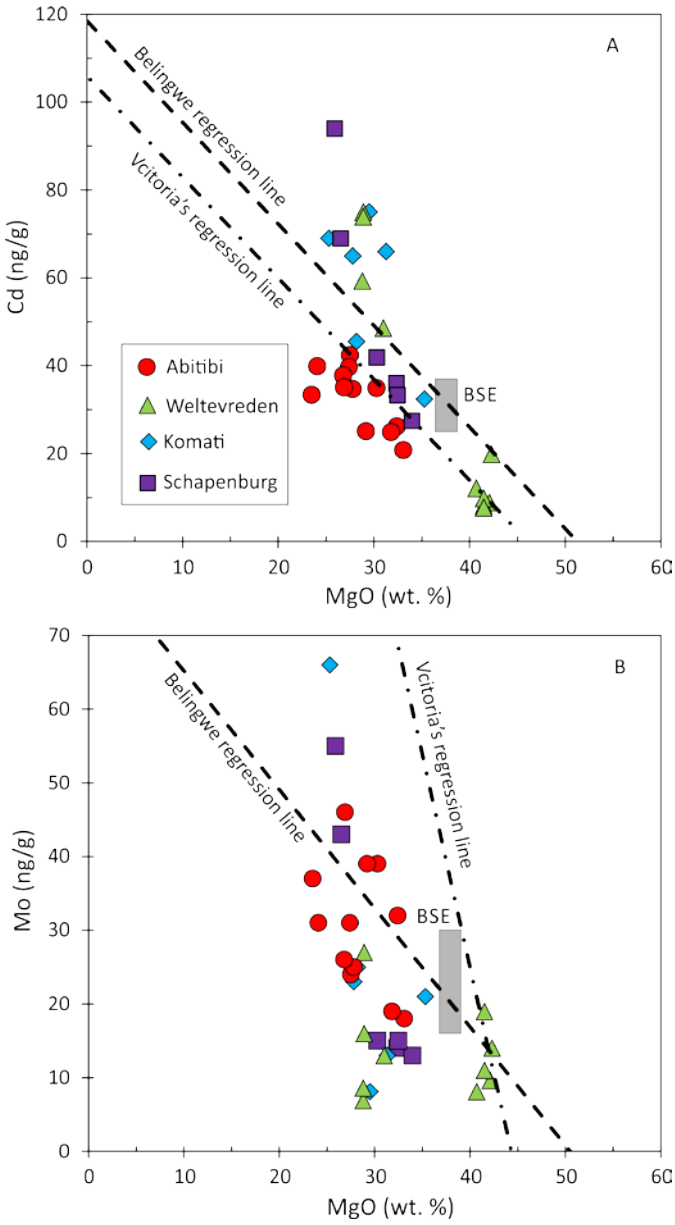

Fig. 5.3 Variations of abundances of Cd and Mo MgO contents in komatiites from Abitibi, Komati Formation, Weltevreden Formation and Schapenburg in comparison with regression lines defined by samples from Belingwe and Victoria's lava lake. The abundances of Cd and Mo in the BSE are adopted from Wang et al. (2016) and Greber et al. (2015), respectively.

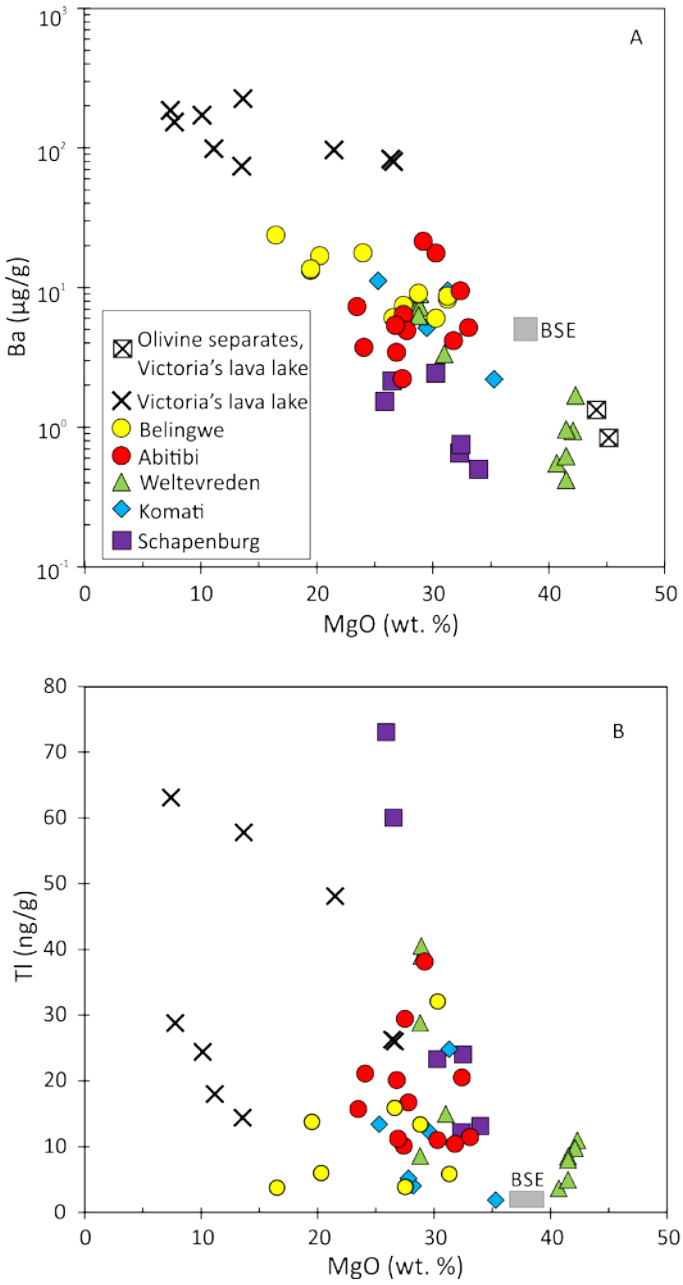

Fig. 5.4 Variations of Ba and Tl abundances with MgO contents in Archean komatiites and komatiitic basalts. The abundances of Ba and Tl in the BSE are from Palme and O'Neill (2014). No simple correlations between Cd and Tl abundances with MgO contents can be obtained from these komatiites.

5.6 Discussion

5.6.1 Preservation of magmatic element abundances

Element-MgO variation diagrams combined with olivine control line was used to evaluate the element mobility in komatiites during low-temperature alteration (*e.g.* Puchtel et al., 2009a; Robin-Popieul et al., 2012). Another approach is based on the notion that the chilled margin represents the undifferentiated komatiite magma which then differentiates into the spinifex subzone and cumulate subzone. Therefore abundances of incompatible elements should decrease from spinifex subzone to chilled margin and cumulate subzone. Both approaches are considered in this study.

Variations of In, Cd, Mo, Sm and Tl abundances against MgO contents of komatiites and komatiitic basalts are displayed in Fig. 5.1-5.6. As can be seen from Fig. 5.1A, with the exception of samples of the Weltevreden Formation, abundances of In are linearly correlated with MgO. The linear correlation of In-MgO indicates the In was immobile in the investigated samples. No simple correlations of Cd-MgO of the Abitibi Greenstone Belt, Komati Formation, Weltevreden Formation and Schapenburg Greenstone Remnant can be observed and the trends they define deviate from the respective olivine control lines (Fig. 5.3A). Abundances of Cd in these regions may have been re-disturbed among different lithologic units of a single lava flow. Besides the Belingwe komatiites in Chapter 3, the linear correlation of Cd-MgO following an olivine control line only occurs for the samples of Victoria's lava lake (Fig. 5.2A), illustrating the good preservation of magmatic characteristics of Cd in these samples.

Igneous signatures of Mo abundances in Archean komatiites were considered to have been preserved (Greber et al., 2015). In this study we evaluate the mobility of Mo by using the element abundances-lithology approach mentioned above. As shown in Fig. 5.2B and 5.3B, only the abundances of Mo in samples from Victoria's lava lake are distributed along the olivine control line, reflecting lithologic control during differentiation and lava emplacement. Abundances of Mo in samples from the Abitibi Greenstone Belt, Weltevreden Formation, Komati Formation and Schapenburg Greenstone Remnant are all redisturbed to various degrees, as indicated by the scatter of data in comparison to samples from Belingwe and Victoria's lava lake. For example, the Mo abundance in the chilled margin, BV06, is much higher than those of the rest samples of the Komati Formation. Considering the high Ba

abundance of BV06 relative to the other samples of the Komati Formation, the abundance of Mo in the chilled margin was probably enriched during secondary alteration. The coupling of Ba and Mo enrichments can also be found in the top flow breccia at Victoria's lava lake. The Mo-MgO variation of the Schapenburg komatiites likely intersect at lower MgO than the average MgO content (~52 wt.%) of cores of olivine separates in cumulate subzone (Fig. 5.3B), indicating the loss of Mo during late-stage alteration. The case of the Weltevreden Formation is complicated because samples were collected from three different lava flows. Although the variations of Mo abundances of different lava flows occur, abundances of Mo in the Weltevreden Formation are not correlated with MgO contents (Fig.5.3B), which reflects the extensive alteration of these samples.

Abundances of Tl in the investigated samples are not correlated with MgO (Fig. 5.4B). Abundances of Tl which is chalcophile in the formation of MORB (Nielsen et al., 2014) display no simple relations with S or Se either. We conclude that because of extensive alteration, the investigated samples did not retain magmatic signatures of Tl that is a fluid-mobile element.

In contrast to the In-MgO correlation (Fig. 5.1A), the negative correlations of Sm with MgO in the investigated samples are characterized by variable slopes (Fig. 5.1B), which are probably inherited from their mantle sources. The scattered variation of Ba and MgO of the investigated samples indicates the mobilization of Ba during secondary alteration, which were also shown by variable depletions of Ba in the BSE-normalized diagrams (Fig. 5.5). As can be seen in Table 5.1 and Fig. 5.8, $(Ce/Sm)_N$ and $(Ba/Sm)_N$ of Victoria's lava lake vary from 1.8 to 2.7 and 2.9 to 6.7, respectively, which are higher than those of others. This may be resulted from the assimilation of crustal materials as revealed by the work on Sm-Nd and Lu-Hf systematics (Puchtel et al., 1997; Puchtel et al., 2016b). The crustal contamination of Victoria's lava lake will be explored further in 5.6.4.2.

5.6.2 Effect of magmatic degassing

Previous studies showed that Cd and In may, like S and Se, be volatile in igneous processes (Greenland and Aruscavage, 1986; Moune et al., 2006; Norman et al., 2004; Rubin, 1997; Symonds et al., 1987; Yi et al., 2000), so the effect of magmatic degassing on these elements has to be considered. Volatility-controlled losses of S are not evident in sulfide-undersaturated komatiites (Chapter 3 and Chapter 4), but abundances of S, Se and Te in

samples from Victoria's lava lake are affected by magmatic degassing to various degrees (Chapter 4). As indicated in the BSE-normalized diagram (Fig. 5.5A), abundances of In and Cd and in Victoria's lava lake are depleted relative to Sm, whereas in the Belingwe Greenstone Belt such depletions are absent (Fig. 5.5B; Chapter 3). Previous studies proposed that Cd may be slightly more volatile than In during the petrogenesis of ocean island basalts (OIB; Norman et al., 2004; Yi et al., 2000), and this may explain the relative depletion of Cd compared to In in the Victoria's lava lake (Fig.5.5A). We note that the In abundances of samples from Victoria's lava lake display a linear correlation with MgO as the other komatiites, which evidences the minimal loss of In in the investigated samples. Even if magmatic degassing occurred to Cd in samples from Victoria's lava lake, the amount was negligible compared to those of S and Se (Chapter 4), because Cd in Victoria's lava lake still display linear correlation with MgO contents and this correlation approximately follows the olivine control line. The depletion of Cd relative to In of the Abitibi Greenstone Belt (Fig. 5.5C) may not be related to magmatic degassing, especially in comparison with Victoria's lava lake which showed strong degassing on S, Se and Te but insignificant volatile losses on Cd and In. Abundances of Cd in pre-2.9 Ga komatiites were not significantly depleted relative to In (Fig. 5.5D-F), so chaotic variations of Cd-MgO in samples from the Weltevreden Formation, Komati Formation and Schapenburg Greenstone Remnant likely are not caused by igneous degassing but reflect late-stage alteration.

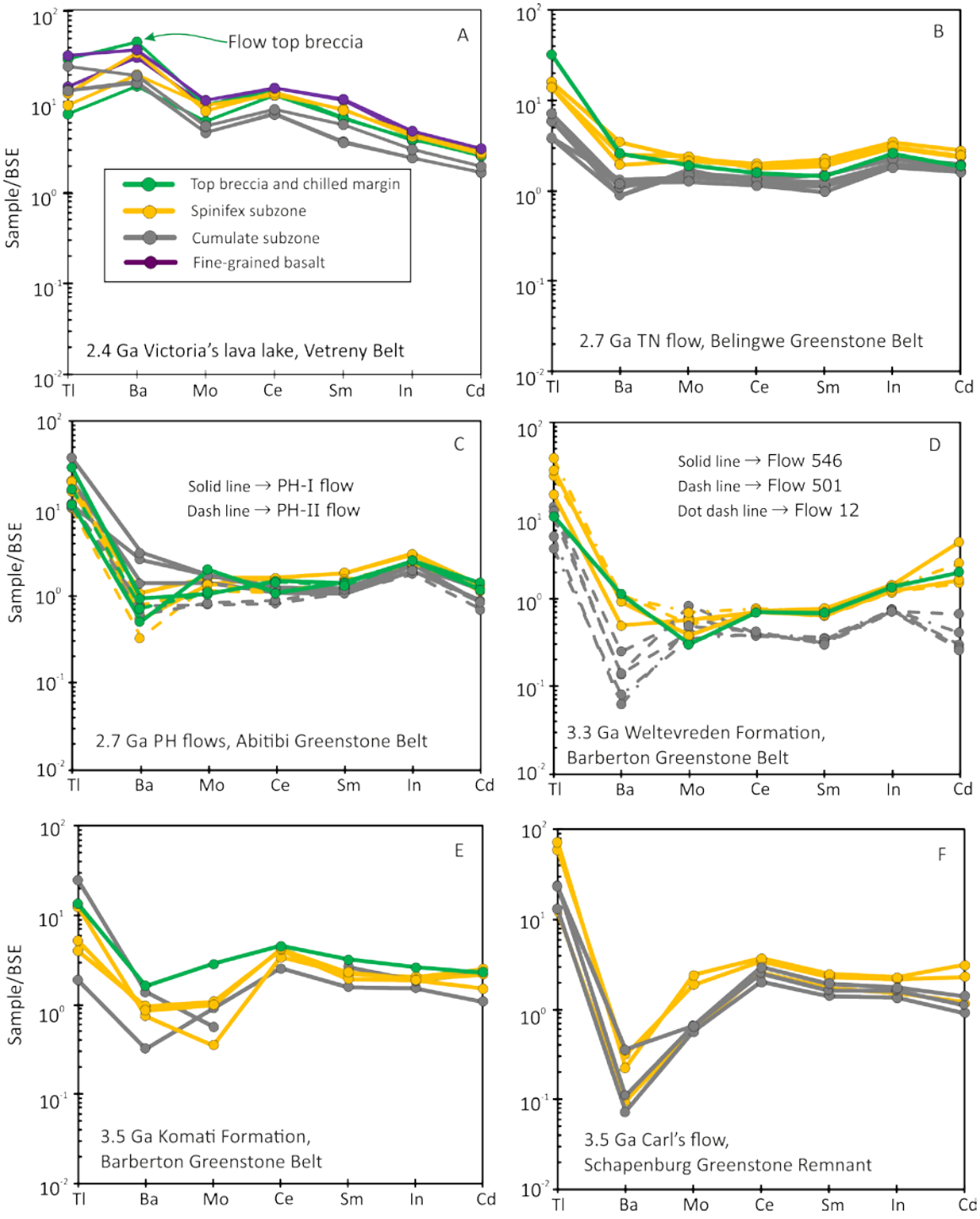
A
Flow top breccia
Top breccia and chilled margin
Spinifex subzone
Cumulate subzone
Fine-grained basalt
2.4 Ga Victoria's lava lake, Vetreny Belt
B
2.7 Ga TN flow, Belingwe Greenstone Belt
C
Solid line → PH-I flow
Dash line → PH-II flow
2.7 Ga PH flows, Abitibi Greenstone Belt
D
Solid line → Flow 546
Dash line → Flow 501
Dot dash line → Flow 12
3.3 Ga Weltevreden Formation,
Barberton Greenstone Belt
E
3.5 Ga Komati Formation,
Barberton Greenstone Belt
F
3.5 Ga Carl's flow,
Schapenburg Greenstone Remnant
Sample/BSE
Tl
Ba
Mo
Ce
Sm
In
Cd

Fig. 5.5 Abundances of the elements of interest in Archean komatiites and komatiitic basalts normalized to those of the BSE. Abundances of In and Cd in the BSE are adopted from Wang et al. (2016), abundances of Sm, Ba and Tl in the BSE are adopted from Palme and O'Neill (2014), and the Mo abundance in the BSE is adopted from Greber et al. (2015). Abundances of these elements in the Belingwe Greenstone Belt are given in the Chapter 3. Since the investigated samples were collected from individual single differentiated lava flows, depletions or enrichments of a specific element relative to its neighboring elements should be uniform in the samples from the same lava flow. Therefore variations of depletions or enrichments of an element indicate that magmatic signatures may not have been preserved. These elements display negative relations with MgO contents (Fig. 5.1-5.4), indicating that they are incompatible during partial melting and lava differentiation. Therefore, higher element abundances in cumulate subzones than in spinifex subzones and chilled margins of an individual lava flow indicate modification of element abundances during secondary alteration. Apparent enrichments of Tl relative to the other elements in the investigated lava flows indicate the influence of secondary processes. Variations of depletions or enrichments of Ba, Mo and Cd in samples from the Abitibi Greenstone Belt (Fig. 5.5C), Weltevreden Formation (Fig. 5.5D), Komati Formation (Fig. 5.5E) and Schapenburg Greenstone Remnant (Fig. 5.5F) suggest that these elements may have been mobilized or redistributed by late-stage alteration. Magmatic characteristics of Sm, In and Ce in the studied lava flows are relatively well-preserved.

5.6.3 Element fractionation during lava differentiation and partial melting

As mentioned in 5.2, Cd, In, Mo, Sm and Ce can be used to constrain the petrogenesis of komatiites because these elements partition in different mantle phases. Therefore fractionations of these elements may have an indication on the mantle source composition. But before this we need to distinguish element fractionations caused by partial melting from those by lava differentiation. Studies of MORB and OIB have shown that the element ratios In (Cd) /Yb, Mo/Ce (Sm) and Tl/Ce in these basalts are approximately invariable with element abundances (Heinrichs et al., 1980; Hertogen et al., 1980; Jenner and O'Neill, 2012; Nielsen et al., 2014; O'Neill and Jenner, 2012; Yi et al., 2000; Yi et al., 1998). Therefore, variations of these element ratios indicate other processes than partial melting which directly reflects the mantle composition.

Although abundances of In are broadly correlated with Cd abundances in the investigated samples, Cd/In ratios of samples from different regions are distinct (Fig. 5.6). The average Cd/In ratio in Victoria's lava lake is 2.3 ± 0.2, which is close to 1.8 ± 0.2 of the Belingwe Greenstone Belt (Chapter 3). Cd/In ratios of Victoria's lava lake and the Belingwe Greenstone Belt are comparable to 1.7 ± 0.4 of MORB and OIB (Jenner and O'Neill, 2012; Yi et al., 2000). The Cd/In ratios in samples from the Komati Formation and Carl's flow from the Schapenburg Greenstone Remnant vary slightly (probably because of late-stage alteration), but they are comparable to those of the Belingwe Greenstone Belt and Victoria's lava lake. The approximately invariable Cd/In ratios in these rocks likely indicate the limited magmatic fractionation of the two elements at high-degree partial melting. Therefore, the variable Cd/In ratios in the Weltevreden Formation require other explanations. Studies on mantle peridotites and basalts have shown that $D^{solid\text{-}melt}$ of Cd may be slightly higher than In (Wang et al., 2016; Witt-Eickschen et al., 2009; Yi et al., 2000), which may fractionate Cd/In in spinifex subzones and cumulate subzones. The Cd/In ratios in the more magnesia cumulate subzones (MgO > 40 wt.%) of the Weltevreden Formation are higher than those in the less magnesia spinifex subzones and chilled margin (MgO = 28-30 wt.%). The Cd/In ratios in the spinifex subzones of the Weltevreden Formation vary from 1.0 to 2.5, whereas in the cumulate subzone the Cd/In ratios range from 3.5 to 8.4. But this hypothesis is not supported by the Rayleigh-type fractional crystallization modeling presented in the Fig. S5.1 in 5.8 Appendix. The model used the abundances of Cd and In in the chilled margin which may represent the

composition of undifferentiated primary magma and the deduced relative partition coefficients of Cd and In from the peridotites (Wang et al., 2016). The partition coefficients of Cd and In obtained from experiments (Adam and Green, 2006) were not used because these data shown the greater incompatibility of Cd than In, which is in contradiction with the observations from natural samples. The alternative is that the variable Cd/In ratios in the Weltevreden Formation are caused by late-stage alteration. As shown in Fig. 5.5D the BSE-normalized Cd patterns display more variations than In, Sm and Ce, evidencing the modification of Cd. Therefore we conclude that fractionated Cd/In ratios in the Weltevreden Formation has limited magmatic significance.

The average Mo/Ce ratio of komatiites and komatiitic basalts in Victoria's lava lake is 0.011 ± 0.003 (1 SD), which is lower than MORB (Mo/Ce = 0.032 ± 0.009) (Kamenetsky and Eggins, 2012; Sims et al., 1990). Based on the limited data, the upper continental crust appears to have a mean value of Mo/Ce = 0.018 ± 0.012 (Rudnick and Gao, 2014; Sims et al., 1990). Therefore in the current precision of Mo/Ce data in terrestrial reservoirs and lack of knowledge on Mo mobility in oceanic basalts, the present work cannot explain the low Mo/Ce in Victoria's lava lake.

5.6.4 The role of garnet and crustal material in the petrogenesis of Archean komatiite

5.6.4.1 The role of garnet in the formation of komatiites

The different types of komatiites primarily reflect the role of garnet compared to other silicates during high-degrees of partial melting. As shown by partitioning experiments (Adam and Green, 2006), the $D^{cpx\text{-}melt}$ values of In, Cd and Yb are 1.02-3.33, 0.53-0.71 and 0.025-0.047, respectively; the $D^{grt\text{-}melt}$ values of In, Cd and Yb are 10.3-87, 0.8-1 and 5-6.25, respectively. Therefore Barberton-type komatiites are expected to have higher Cd/Yb and lower In/Yb ratios than BSE if garnet was retained in the mantle source (Arndt et al., 2008). In contrast, Munro-type and Al-enriched komatiites should be characterized by lower Cd/Yb and higher In/Yb ratios. This is because garnet involves in the formation of Munro-type and Al-enriched komatiites (Arndt et al., 2008).

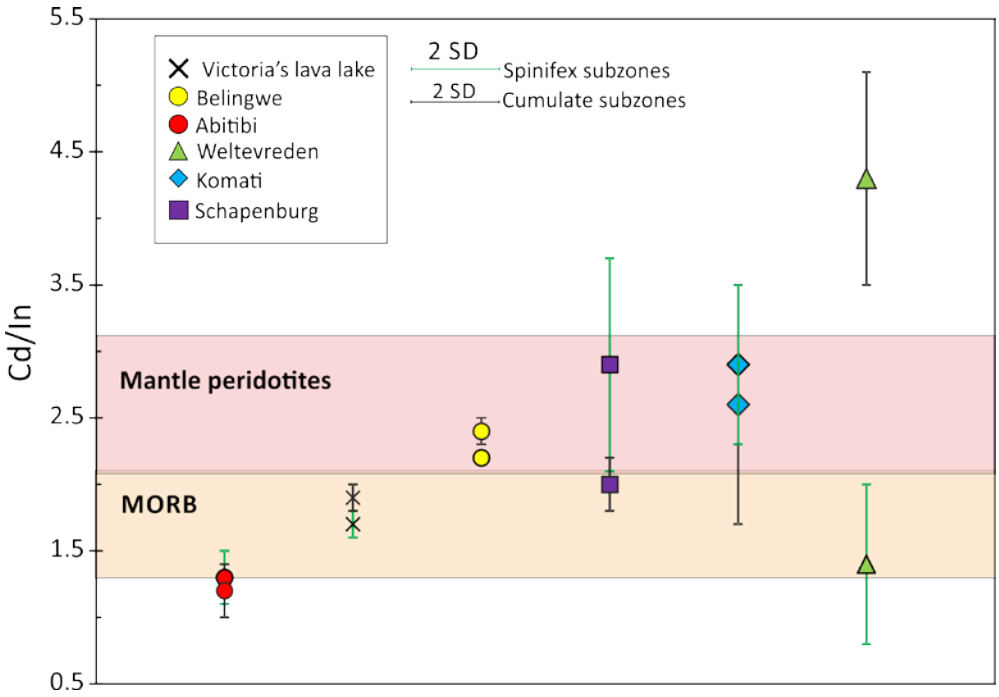

Fig. 5.6 Cd/In ratios of Archean komatiites and komatiitic basalts. Data of mantle peridotites are after Wang et al. (2016). Abundance of In and Cd in MORB are after Jenner and O'Neill (2012) and Yi et al. (2000). Data of In and Cd in the Belingwe Greenstone Belt were presented in the Chapter 3. Ratios of Cd and indium in post-2.9 Ga komatiites differ from each other, whereas Cd/In ratios of pre-2.9 Ga komatiites vary significantly, even in a single differentiated lava flow. Variations of Cd/In ratios of pre-2.9 Ga komatiites were resulted from variable Cd abundances of the investigated samples. Low Cd/In ratios of the Abitibi Greenstone Belt reflect the selective removal of Cd by secondary processes. Cd/In ratios of the Victoria's lava lake represented by komatiitic basalts are comparable to those in MORB. Though the average Cd/In ratio of the cumulate subzone is slightly higher than that of the spinifex subzone of the Belingwe Greenstone Belt, Cd/In ratios of Belingwe komatiites are in the range defined by post-Archean mantle peridotites.

Barberton-type komatiites from the Komati Formation are indeed characterized by a higher Cd/Yb (0.06 ± 0.01, 1 SD) and lower In/Yb (0.027 ± 0.004) than those of Al-enriched komatiites from the Weltevreden Formation (Cd/Yb = 0.034 ± 0.005 and In/Yb = 0.035 ± 0.001). This supports the previous suggestion of substantial garnet involvement in the formation of Al-enriched komatiites (Arndt et al., 2008). The In/Yb (0.033 ± 0.002) of Barberton-type komatiites from the Schapenburg Greenstone Remnant marginally overlaps with that of the Weltevreden Formation, probably indicating the involvement of garnet in the formation of Schapenburg komatiites. Munro-type rocks of the Abitibi Greenstone Belt and Victoria's lava lake have identical In/Yb within in uncertainties (0.031 ± 0.001 and 0.032 ± 0.002, respectively), but distinct Cd/Yb (0.038 ± 0.006 and 0.055 ± 0.002, respectively). The depletion of Cd in the Abitibi Greenstone Belt likely indicate the selective loss caused by seafloor alteration.

As displayed in Fig. 5.7, the mean In/Yb (0.032 ± 0.003) of Archean komatiites investigated in this study covers the gap of In/Yb in MORB (0.026 ± 0.003) and OIB (0.041 ± 0.007; Hertogen et al., 1980; Jenner and O'Neill, 2012; Yi et al., 2000). The discrepancy of In/Yb between MORB and OIB was thought to be caused by partitioning of In into trace sulfides in the OIB sources (Yi et al., 2000). A recent study suggested that sulfide and clinopyroxene enter the melt in constant proportions over a wide range of degrees of partial melting (Nielsen et al., 2014), indicating that sulfide should not fractionated In/Yb in low-degrees partial melting. We note the In/Yb in OIB is comparable to that in the Weltevreden Formation. Therefore, the high In/Yb ratio in OIB may be because of garnet in the mantle source of OIB. We conclude that the role of garnet in the petrogenesis of komatiites can be recognized by using Cd/Yb and In/Yb ratios. Compared to the BSE values, low Cd/Yb and high In/Yb likely indicate the contribution of garnet.

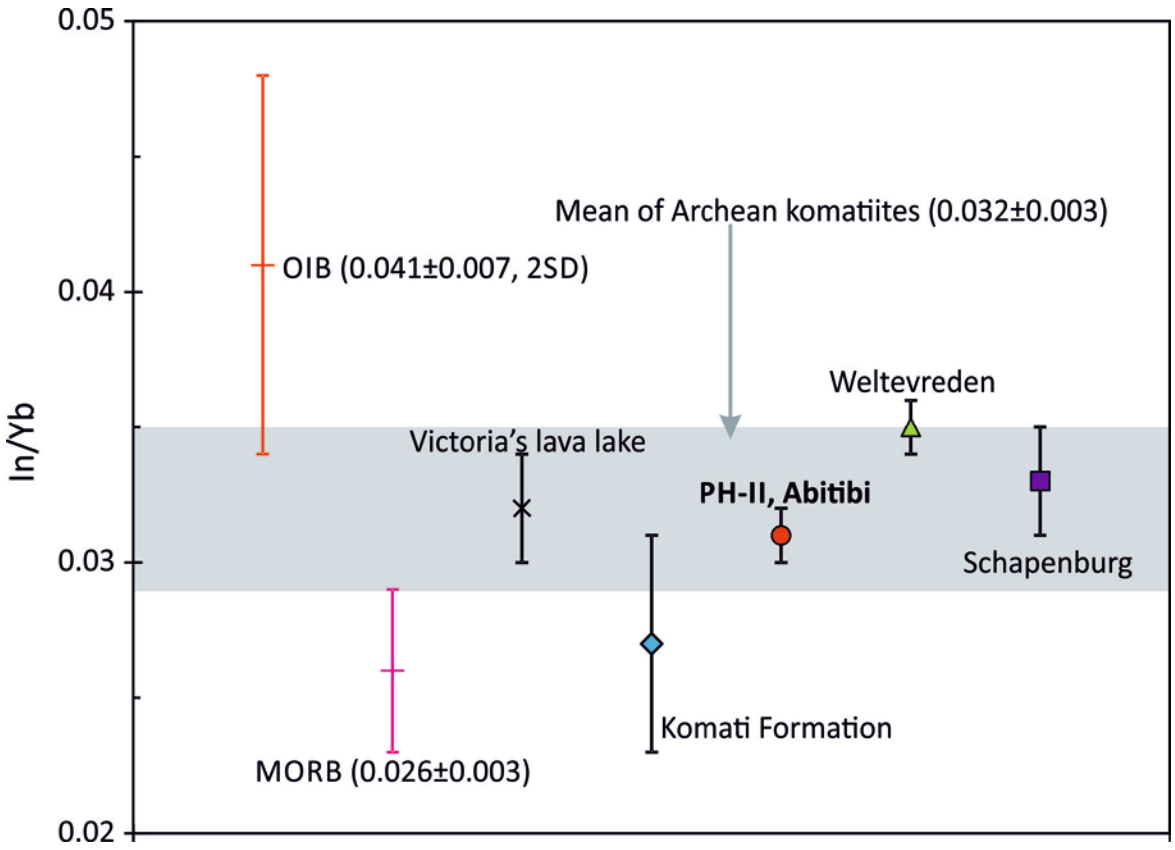

Fig. 5.7 In/Yb ratios of Archean komatiites and komatiitic basalts. In/Yb ratios in MORB and OIB are calculated from previous work (Yi et al., 2000). In/Yb ratios of komatiites and komatiitic basalts presented in this study are comparable. The In/Yb in the BSE was represented by that in MORB (Yi et al., 2000). This diagram shows that the mean In/Yb of Archean komatiites is between that of MORB and OIB.

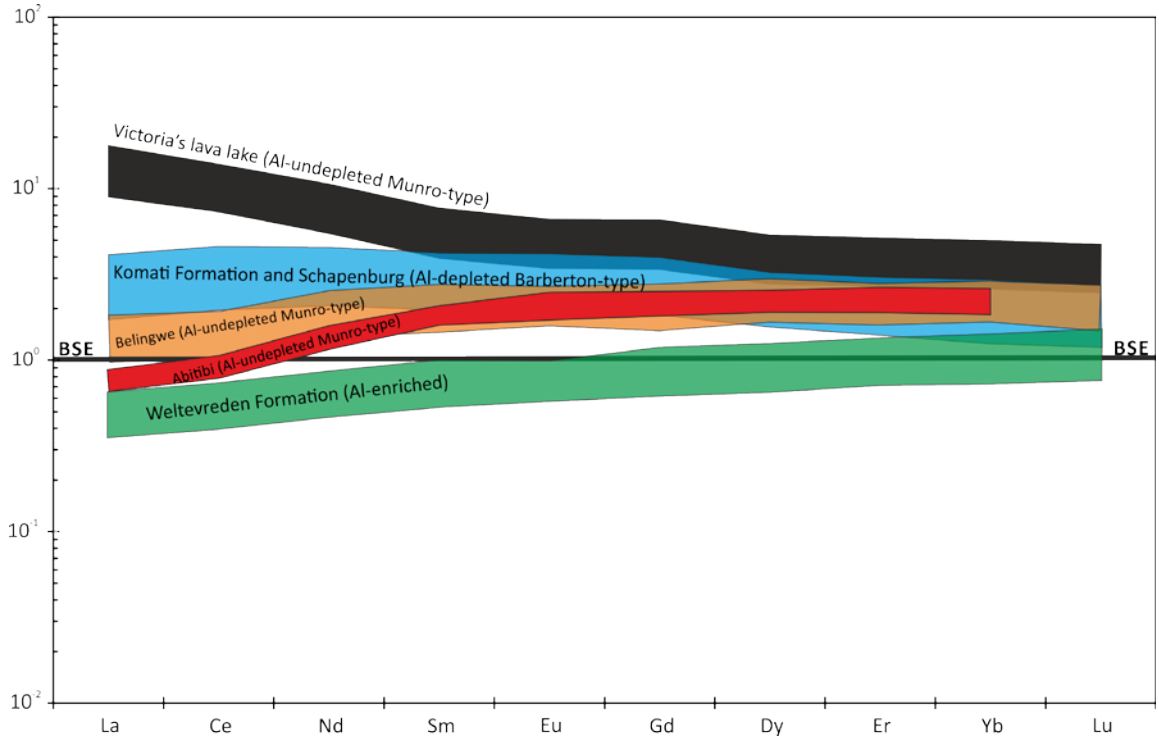

Fig. 5.8 BSE-normalized diagram of rare earth elements in the studied komatiites and komatiitic basalts. The BSE values of REE are from Palme and O'Neill (2014). REE data were obtained on the same sample used in the present study (Puchtel et al., 2016a; Puchtel et al., 2013; Puchtel et al., 1997; Puchtel et al., 2016b; Puchtel et al., 2009b). REE data on the Belingwe Greenstone Belt are also partly from Shimizu et al. (2005). The abundances of light rare earth elements (LREE) in Al-depleted Barberton-type komatiites (Komati Formation and Schapenburg) are higher than those in Al-undepleted Munro-type (Belingwe and Abitibi) and Al-enriched komatiites (Weltevreden Formation).

5.6.4.2 Crustal signature in the Archean komatiites

Another issue related to the petrogenesis of Archean komatiites is the extent of enrichment of incompatible elements in their mantle sources. The BSE-normalized diagram of rare earth elements (Fig.5.8) shows that the abundances of LREE in the Al-depleted Barberton-type komatiites from the Komati Formation and Carl's flow from the Schapenburg Greenstone Remnant are slightly higher than the Al-undepleted Munro-type komatiites from the Belingwe Greenstone Belt and Abitibi Greenstone Belt and the Al-enriched komatiites from the Weltevreden Formation. The enrichment of LREE in the Barberton-type komatiites are also shown in the MgO-Sm diagram (Fig. 5.1B) in which the Sm abundances are higher. Such enrichments indicate that the mantle source of Barberton-type komatiites has higher LREE abundances than the mantle sources of Munro-type and Al-enriched komatiites. This is the first type of enrichment which is named as external enrichment. The second type of enrichment is the internal enrichment. As given in Table 5.1 $(Ce/Sm)_N$ of samples from Victoria's lava lake, Komati Formation and Carl's flow from Schapenburg Greenstone Remnant vary from 1.4 to 2.7, whereas $(Ce/Sm)_N$ of the Belingwe Greenstone Belt and Abitibi Greenstone Belt vary from 0.7 to 1.2. Retention of garnet in the mantle source may lead to the internal enrichment in Barberton-type komatiites, considering that Sm more readily partitions into garnet. However, the batch melting model (details in Fig. S5.2 in 5.8 Appendix) shows that $(Ce/Sm)_N$ decreases from ~1.4 at 10% partial melting to ~1 at 45% partial melting, indicating that komatiites formed by high-degrees (30-50%) should have $(Ce/Sm)_N$ ratios smaller than 1.4. As in the case of Victoria's lava lake, two-end member mixing and assimilation-fractionation-crystallization will result into high $(Ce/Sm)_N$ and high $(Ba/Sm)_N$. Therefore, these processes unlikely are responsible for the high $(Ce/Sm)_N$ and low $(Ba/Sm)_N$ in the Komati Formation and Schapenburg Greenstone Remnant, which require other explanations.

The two types of enrichments may be caused by delamination of residuum of mafic crust after variable degrees of partial melting and the BSE. As shown by abundant studies, Archean metatonalite–trondhjemite–granodiorite were reworked products of older mafic crust (*e.g.* Nagel et al., 2012). Modeling of delamination model has shown that the residuum of

reworked Archean mafic crust could be recycled into the mantle because of gravitational instabilities. With increasing degrees of partial melting of mafic crust, the residuum of mafic crust may have become denser than the underlying mantle. Denser hydrated or anhydrous crustal residues should drip down into the mantle. Fig. 5.9 shows the chemical consequences of such a process for the composition of Archean mantle and, potentially, mantle sources of komatiites. The pink lines in Fig. 5.9 indicate chemical variations of the residue of mafic crust caused by variable degrees of melting. The addition of residual mafic crust (*i.e.* garnet pyroxenite or garnet amphibolite) would impact the chemical composition of the mantle reservoir and hence the melts. The range between the pink line and the BSE are possible mixtures of delaminated mafic crust and the BSE. Samarium and Ce are used in this model because they are not significantly sensitive to residual garnet, as shown in Fig. S5.2 that at high partial melting degrees the fractionation between Ce and Sm is limited. Barium is more incompatible than Ce and Sm and thus it indicates the involvement of crustal components. Furthermore, barium is a fluid-mobile element which can be used to constrain the fluid-involved processes, including dehydration or fluid influx.

Fig. 5.9 shows that $(Ce/Sm)_N$ of the Komati Formation and Schapenburg Greenstone Remnant are in the range of such mixture. $(Ce/Sm)_N$ of the Komati Formation are more variable than those of Schapenburg komatiites, which could indicate the variable degrees of partial melting of the reworked mafic crust delaminated into the mantle source of Komati Formation. The depletion of $(Ba/Sm)_N$ in the Komati Formation and Schapenburg Greenstone Remnant relative to the BSE seems to indicate mobilization of Ba at low-temperature late-stage alteration or dehydration of delaminated mafic crust. The variation of $(Ba/Sm)_N$ of the Abitibi Greenstone Belt and Weltevreden Formation is larger than those of $(Ce/Sm)_N$, 0.2-2.5 of $(Ba/Sm)_N$ and 0.7-1.7 of $(Ce/Sm)_N$, which may suggest Ba mobilization during late-stage alteration. $(Ba/Sm)_N$ of the Belingwe Greenstone Belt vary in a limited range of 0.6-1.8 and $(Ce/Sm)_N$ are rather constant (0.9-1.2). The two high $(Ba/Sm)_N$ values of the Belingwe Greenstone Belt were yielded by the chilled margin TN1 and surface sample ZV14, indicating secondary enrichment of Ba. $(Ba/Sm)_N$ values of the other two surface samples (ZV10 and ZV77) are lower than 1, suggesting selective removal of Ba. $(Ce/Sm)_N$ ratios in samples from the Belingwe Greenstone Belt, Abitibi Greenstone Belt and Weltevreden Formation may imply minimal influences of mafic crustal delamination which may have affected the mantle source composition of samples from the Komati Formation and Schapenburg Greenstone Remnant. Fig. 5. 9 confirms the results of previous studies that the enrichment of highly

incompatible elements in samples from Victoria's lava lake resulted from the minor involvement of upper continental crustal materials. In contrast to the Komati Formation and Schapenburg Greenstone Remnant, both Ba and Ce are enriched compared to Sm in the Victoria's lava lake.

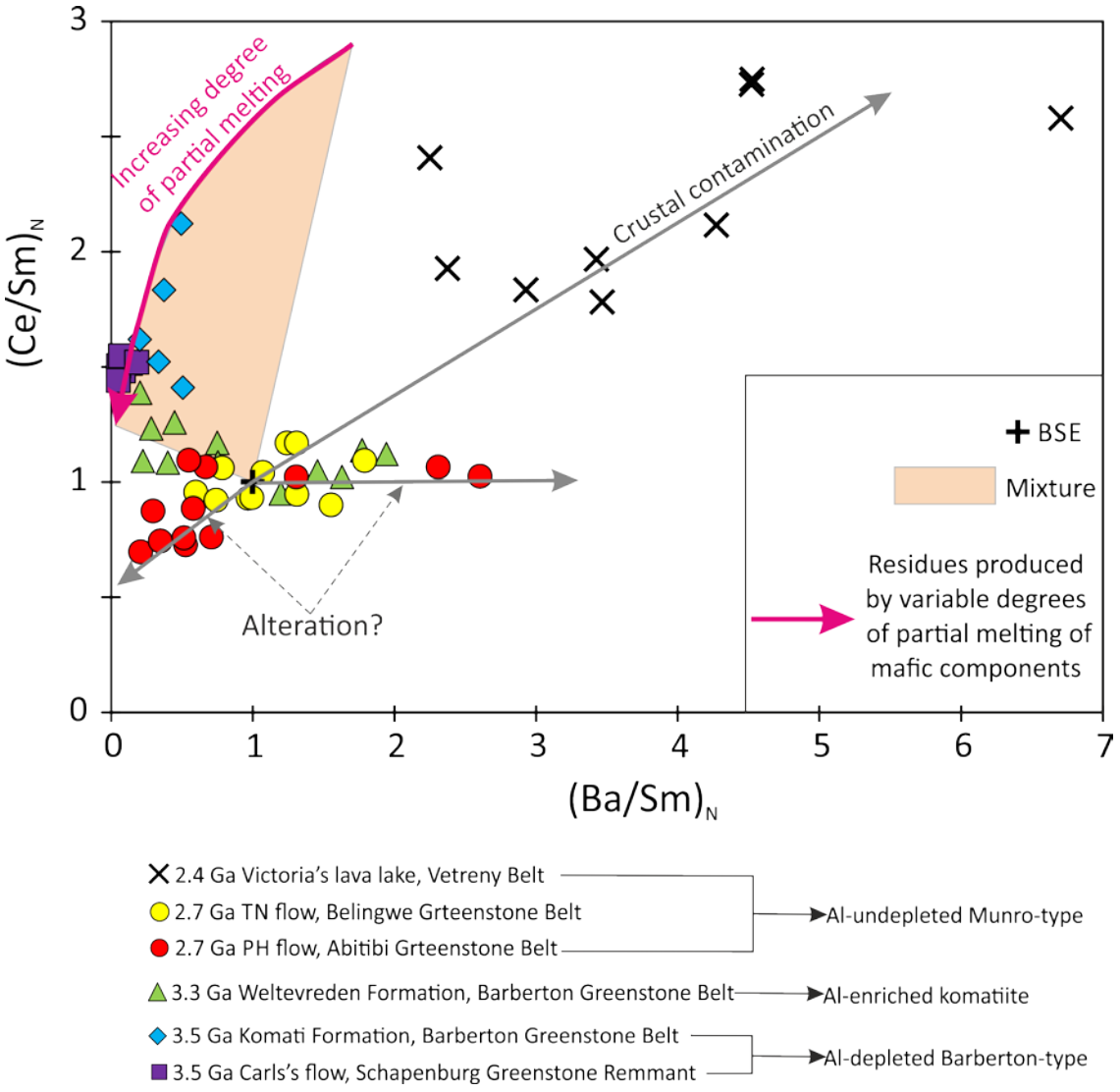
Increasing degree of partial melting
Crustal contamination
Alteration?
BSE
Mixture
Residues produced by variable degrees of partial melting of mafic components
(Ce/Sm)N
(Ba/Sm)N
0
1
2
3
4
5
6
7
2.4 Ga Victoria's lava lake, Vetreny Belt
2.7 Ga TN flow, Belingwe Grteenstone Belt
2.7 Ga PH flow, Abitibi Grteenstone Belt
Al-undepleted Munro-type
3.3 Ga Weltevreden Formation, Barberton Greenstone Belt
Al-enriched komatiite
3.5 Ga Komati Formation, Barberton Greenstone Belt
3.5 Ga Carls's flow, Schapenburg Greenstone Remmant
Al-depleted Barberton-type

Fig. 5.9 Variations of $(Ba/Sm)_N$ with $(Ce/Sm)_N$ in Archean komatiites and komatiitic basalts. Subscripted N means that ratios of the investigated samples are normalized to those of the BSE (Palme and O'Neill, 2014). Variations of $(Ba/Sm)_N$ ratios of samples from Belingwe, Abitibi and Weltevreden are remarkably more variable than $(Ce/Sm)_N$ ratios, indicating the mobility of Ba during late-stage alteration. Komatiitic basalts from Victoria's lava lake are characterized by high $(Ba/Sm)_N$ and $(Ce/Sm)_N$ ratios, which are consistent with the involvement of undehydrated continental crustal materials (Puchtel et al., 1997). $(Ce/Sm)_N$ ratios of Al-depleted komatiites from the Komati Formation and Schapenburg Greenstone Remnant are higher than the other komatiites, but $(Ba/Sm)_N$ of Al-depleted komatiites are lower. The model of participation of reworked mafic components in the formation of Al-depleted komatiites from the Komati Formation and Schapenburg Greenstone Remnant was modified from the model for the generation of TTG from mafic crust (Nagel et al., 2012). Abundances of Ce, Sm and Ba in the primary mafic crustal materials without being reworked were assumed to be 7.5 µg/g, 2.6 µg/g and 3.9 µg/g, which are similar to the composition of MORB (Gale et al., 2013). Partition coefficients used in this model are adopted from the experimental data (Bédard, 2006). We note that abundances of Ce, Sm and Ba in the primary mafic crustal materials play a role in shaping the pink curve of the addition of reworked crustal materials into the mantle source. The pink curve represents the residues of mafic crust after variable degrees (0-15%) of melt extraction.

5.6.5 Abundances of In, Cd, Mo and Tl in the Archean mantle and in the BSE

The mean values of In/Yb ratio in Archean komatiites indicates that the Archean mantle has 15 ± 2 ng/g (1 SD) of In (calculated from Yb = 477 ± 48 ng/g; Palme and O'Neill, 2014). This estimate is identical within uncertainties with that 13 ± 2 ng/g In calculated from the MgO-In variation diagram by project to MgO = 36.77 wt.% in the BSE (Fig. 5.1; Palme and O'Neill, 2014). The In abundance in the Archean mantle is in the range of the BSE values (12-18 ng/g) constrained by post-Archean mantle-derived rocks including mantle peridotites (Wang et al., 2016; Witt-Eickschen et al., 2009) and MORB and OIB (Yi et al., 1995).

As recognized (Jagoutz et al., 1979) and confirmed in 5.6.1, abundances of Cd in samples from the Komati Formation, Weltevreden Formation, Abitibi Greenstone Belt and Schapenburg Greenstone Remnant may have be subject to late-stage alteration. Therefore, only the abundance of Cd in the mantle source of Victoria's lava kale are calculated from the Cd-MgO plot (Fig. 5.2A) which yields Cd = 29 ± 6 ng/g. This value, together with the Cd abundance of the mantle source of Belingwe komatiites (Cd = 32 ± 2 ng/g; Chapter 3) indicate that the Cd abundance Cd in the Archean mantle is indistinguishable from that of the BSE value constrained by post-Archean mantle peridotites (Wang et al., 2016; Witt-Eickschen et al., 2009).

The abundance of Mo (42 ± 20 ng/g) in the mantle source of Victoria's lava lake is calculated from the MgO-Mo variation (Fig. 5.2B) by assuming that the MgO content (36.77 wt.%) in the mantle source is same to that of the BSE (Palme and O'Neill, 2014). As shown in Chapter 3, the Mo abundance in the Belingwe mantle source is 20 ±3 ng/g. Therefore, the Archean mantle may have 20-40 ng/g Mo, which is roughly comparable to the constraint on the Mo abundance in the BSE based on Mo/Ce ratios in MORB (Sims et al., 1990).

Because of the alteration effects, the abundance of Tl in the Archean mantle cannot be constrained by the komatiites investigated in this study.

5.6.6 Controls on the abundances of In, Cd and Mo in the BSE

As a moderately siderophile refractory element, Mo abundance of the BSE is mainly controlled by core-mantle differentiation (Wade and Wood, 2005). Compared to the results of metal-silicate partitioning experiments performed under 1.5 GPa (Wade et al., 2012; Wood et al., 2014), the budget of Mo in the BSE is 5 times lower than the value expected from these

experiments. Core-mantle partition coefficients of Mo obtained in the presence of S and C revealed that Mo is approximately 3-5 times more siderophile if the terrestrial core contains ~2% S and 0.7% carbon (Wade et al., 2012; Wood et al., 2014). The observed Mo/W in the BSE can be reproduced by metal-silicate partitioning experiments, but these experiments did not reproduce the budgets of Mo and W in the BSE.

Abundances of the volatile elements In, Zn and Cd in the BSE cannot be simply explained by the effects of pressure, temperature or light elements in metals involved core formation or late accretion (Wang et al., 2016; Wood et al., 2014). For instance, Zn is 5-10 times more lithophile than In at a large range of core formation conditions (Kiseeva and Wood, 2015; Wang et al., 2016; Wood et al., 2014), requiring that in the BSE In should be more depleted relative to Zn, which is not observed. The suggestion that the half solar nebular condensation temperature of In may be close to that of Zn, which would mean that In might be less volatile than what the current data suggests, did not find supports in many studies (Keays et al., 1971; Larimer, 1967; Larimer and Anders, 1967; Lipschutz and Woolum, 1988; Wang et al., 2016; Witt-Eickschen et al., 2009; Xiao and Lipschutz, 1992). The depletion of Cd relative to In in the BSE was assumed to be caused by preferential volatilization of early-formed crusts of planetsimals (Witt-Eickschen et al., 2009), but no direct evidence exists to support such a scenario. Alternatively, the fractionation of In, Zn and Cd in the BSE may reflect accretion of volatile-bearing materials with somewhat different volatile element patterns and behaviors than chondrites (Wang et al., 2016).

5.7 Summary

In this study we report In, Cd, Tl, Mo, Sm and Ba abundances of 43 Archean komatiites and komatiitic basalts and 2 olivine separates from Victoria's lava lake in Vetreny Belt by applying isotope dilution ICP-MS technique.

The mobility of incompatible elements in komatiites caused by low-temperature alteration and degassing processes was studied. The method is based on the assumption that the chilled margins of komatiite lava flows represent the undifferentiated primary magma, which differentiates into a somehow more evolved melt zone near the top (the spinifex subzone) and a lower cumulate subzone. The abundances of incompatible elements should decrease from the spinifex subzone to the chilled margin and to the cumulate subzone. Any alteration after the emplacement of komatiite magmas would disturb this order if a specific element was mobile. We conclude that In and Sm are immobile in all the investigated samples.

Other elements were variably mobilized. Abundances of Cd and Mo in samples from Victoria's lava lake are correlated with MgO contents along the olivine control lines, and the distribution of Cd and Mo in different differentiated subzones follow the expected order.

Fractionations among these elements in the komatiite magmas are dictated by olivine and pyroxene (In and Cd) in addition to garnet (In and REE) during partial melting which formed the Barberton-type komatiites. Cd/In ratios in Munro-type rocks from Victoria's lava lake and Belingwe Greenstone Belt are comparable to that in oceanic basalts within uncertainties, indicating that In and Cd are not fractionated in during the formation of Munro-type komatiites. Mo/Ce ratios in the Victoria's lava lake are slightly lower than those in the Belingwe Greenstone Belt, which is further lower than that of MORB.

5.8 Appendix

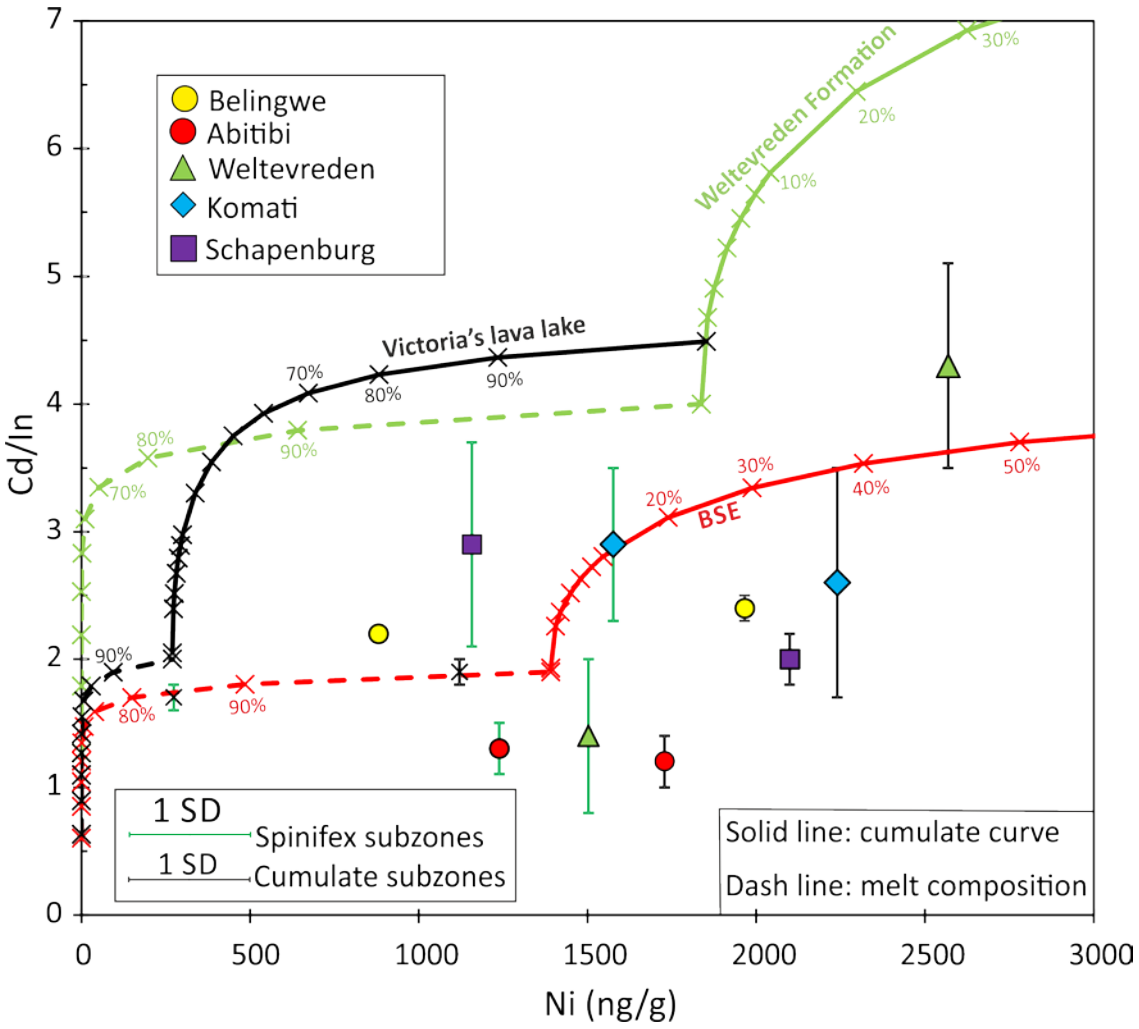

Fig. S5.1 Variations of Cd/In with Ni abundances during fractional crystallization of olivine. Relative partition coefficients of Cd and In are from Wang et al. (2016). The partition coefficient of Ni is from Mysen (1979). The ticks with numbers indicate the fraction of olivine crystallized. Solid lines indicate variations of Cd/In with Ni abundances in olivine cumulates. Dash lines indicate Cd/In variations with Ni abundances in residual melts (spinifex subzones). The starting composition of black curve, light green curve and red curve are the chilled margin composition of Victoria's lava lake and Weltevreden Formation and the BSE values, respectively. The diagram shows that the fractionation of Cd/In in spinifex subzones and cumulate subzones from the Weltevreden Formation (light green triangle) is not caused by the fractional crystallization of olivine.

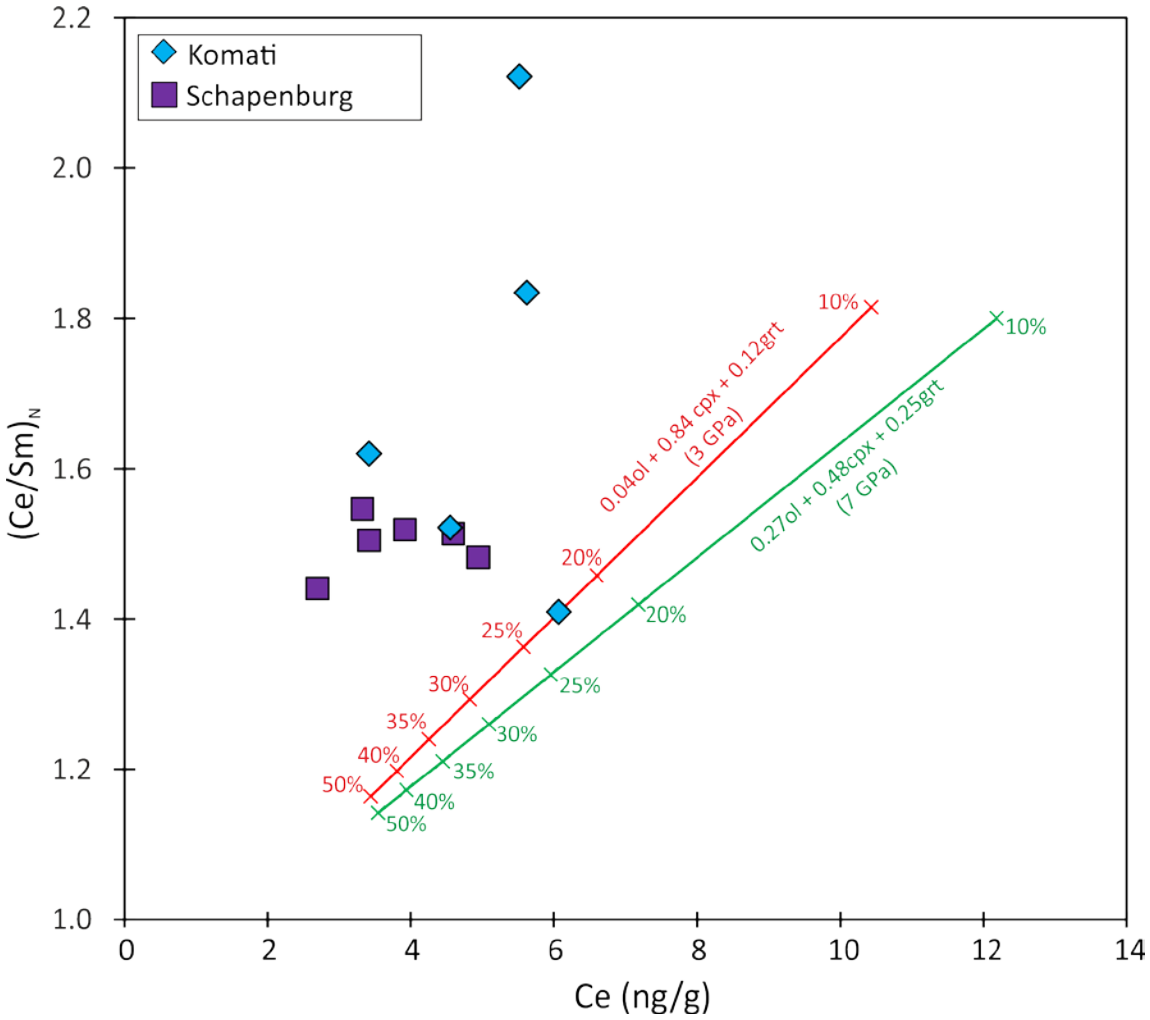

Fig. S5.2 Variations of $(Ce/Sm)_N$ with Ce abundances during batch melts derived from garnet lherzolite-like mantle source. Partition coefficients of Ce and Sm are from Bédard (2006). The ticks with numbers indicate degrees of partial melting. The red line indicates variations of $(Ce/Sm)_N$ with Ce abundances in partial melts from a garnet lherzolite-like source at 3 GPa in the mantle. The green line indicates variations of $(Ce/Sm)_N$ with Ce abundances in partial melts from a garnet lherzolite-like source at 7 GPa in the mantle. The modal composition of garnet lherzolites is from Walter (2014). The starting composition are the BSE values (Palme and O'Neill, 2014). The diagram shows that partial melts produced by >30% degrees are characterized by $(Ce/Sm)_N < 1.3$, indicating that $(Ce/Sm)_N > 1.3$ in samples from the Komati Formation and Schapenburg Greenstone Remnant are unlikely resulted from partial melting of a garnet lherzolite-like source.

Chapter 6

Conclusions and outlook

6.1 Conclusions

The main contribution of this dissertation is to constrain the abundances of highly siderophile (HSE) and strongly chalcophile element abundances in terrestrial Archean rocks, including continental crustal rocks and mantle-derived komatiites. The comprehensive results of Acasta gneisses and Archean komatiites demonstrate that chondritic materials delivered by late veneer had been homogenized in the terrestrial mantle by at least prior to 4.2 Ga.

6.1.1 Archean continental crustal rocks

Abundances of HSE, S, Se and Te in the Acasta Gneiss Complex (AGC) from northwestern Canada are roughly comparable to those in their modern equivalents and do not show evidence for the late heavy bombardment in Acasta area. The majority of Re-Os isotopic systematics were disturbed in the investigated samples by late-stage alteration, but the T_{MA} Re-Os model age of 4.3 ± 0.2 Ga in metadioritic layer AMS 031A is in agreement with the Sm-Nd errorchron age within uncertainty. This implies that the metadioritic layer crystallized from a magma which was extracted from the mantle source at ~4.0 Ga, and the chemical heterogeneities observed in the modern mantle must have already existed prior to 4.0 Ga. The Acasta samples are not derived from a pre-late veneer mantle reservoir with positive ^{182}W anomalies.

6.1.2 Archean mantle-derived rocks

6.1.2.1 Chalcophile element systematics

Chalcophile volatile element abundances of 54 well-characterized Archean komatiites and komatiitic basalts from different localities showed that ratios of S, Se and Te in komatiites from the 2.7 Ga TN flow of the Belingwe Greenstone Belt, the 2.7 Ga PH flows of the Abitibi Greenstone Belt and the 3.5 Ga Komati Formation in the Barberton Greenstone Belt are near-chondritic and indistinguishable from those of mantle peridotites. This supports that post-Archean mantle peridotites can be used to define the chalcophile element composition of the BSE. The near-chondritic ratios of S, Se and Te in the 3.5 Ga Komati Formation indicate that the mantle source of the Komati Formation must have obtained the chondritic materials delivered by late veneer.

Non-chondritic Cu/Ag (2084-5077) ratios in the 2.4 Ga Vetreny komatiites and komatiitic basalts, the 2.7 Ga Belingwe komatiites and the 3.5 Ga Komati komatiites are within the range of the BSE (Cu/Ag = 3500 ± 1200, 2SD) defined by post-Archean mantle peridotites. Together with Cu and Ag data of MORB, we can conclude that Cu and Ag in mantle-derived rocks are not significantly fractionated, which is consistent with sulfide-silicate and metal-silicate partition coefficients obtained under various pressure, temperature and oxygen fugacity conditions.

6.1.2.2 Lithophile element systematics

The mobility of incompatible elements (Cd, In, Mo, Sm and Ba) in komatiites was investigated by a new method that is the sequence of element abundances in chilled margins, spinifex subzones and cumulate subzones. The chilled margin represents the undifferentiated primary magma which differentiates into a somehow more evolved melt zone near the top (the spinifex subzone) and a lower cumulate subzone. The abundances of incompatible elements should decrease from spinifex subzones to chilled margins and cumulate subzones. Any alteration after the emplacement of komatiites will disturb this sequence if a specific element is mobilized. In such a way we conclude that except In and Sm were immobile in all the investigated samples, Cd and Mo were immobile in the Victoria's lava lake and TN flow from the Belingwe. Abundances of Tl and Ba were modified by late-stage alteration in all the investigated samples.

The abundances of these elements in the Archean mantle source are comparable to the BSE. The high BSE In abundance cannot be easily explained by current metal-silicate and sulfide-silicate partitioning experiments. The fractionation of In, Zn and Cd in the BSE may reflect accretion of volatile-bearing materials with somewhat different volatile element patterns and behaviors than chondrites.

6.2 Outlook

In coming studies efforts can be devoted to understand the mechanism decoupling the HSE systematics and ^{182}W isotopic systematics, and the petrogenesis of Archean komatiites.

The decoupling of ^{182}W isotopic systematics and HSE systematics is of great importance to understand the terrestrial core-mantle differentiation and late meteoritic accretion. Positive ^{182}W anomalies in terrestrial samples are used as evidence for isolated pre-late veneer mantle

reservoirs which should be HSE-deficit. However, this is not always the case as shown by this dissertation. Either abundances of HSE in the terrestrial mantle are not relevant to late meteoritic additions after core formation, which is unlikely. Or the isolated pre-late veneer mantle reservoirs with positive ^{182}W anomalies do not receive the portion of W delivered by late accretion. Nucleosynthetic anomalies of HSE, such as Os, Ru and Pd, in Archean rocks with positive ^{182}W anomalies should be different from rocks with no ^{182}W anomalies, especially post-Archean mantle peridotites. This may provide explanation the decoupling of ^{182}W isotopic systematics and HSE systematics. Another approach might be to study W isotopes in different components of rocks characterized by ^{182}W anomalies as shown in a recent work by Liu et al., 2016.

Archean komatiites were thought to be high-degrees partial melts of deep mantle which transported to the surface through mantle plumes. This was the basic assumption used to explain the secular increase of Pt and Pd abundances in mantle sources of Archean komatiites, which might reflect the progressive mixing of late veneer in the mantle before 2.9 Ga (Maier et al., 2009). However, more studies on Archean rocks, especially the Chapter 2, showed that HSE abundances of ~4.0 Ga rocks are not depleted relative to post-Archean samples. Then how to explain the secular increase of Pt and Pd abundances of Archean komatiite sources? If this is not relevant to the mixing of late veneer in the mantle, could it be related to the petrogenesis of komatiites? The Sm-Nd and Lu-Hf compositions of Barberton komatiites showed positive $\varepsilon Hf(T)$ and negative $\varepsilon Nd(T)$ which were thought to reflect cherts in the source of Barberton komatiites (Blichert-Toft et al., 2015). How were deep-sea sediments, if there are, transported into deep mantle? By modern-like subduction? Or by delamination of thick mafic crust?

Chapter 7

References

Abramov, O., Kring, D.A. and Mojzsis, S.J. (2013) The impact environment of the Hadean Earth. *Chemie der Erde - Geochemistry* **73**, 227-248.

Abramov, O. and Mojzsis, S.J. (2009) Microbial habitability of the Hadean Earth during the late heavy bombardment. *Nature* **459**, 419-422.

Ackermn, L., Haluzova, E. and Pasava, J. (2015) Platinum-group element and osmiumsulfur isotopic compositions of Ni-Cu-(PGE) ores from Rožany, Bohemian Massif, *Goldschmidt* **2015**, Prague, Czech Republic.

Adam, J. and Green, T. (2006) Trace element partitioning between mica- and amphibole-bearing garnet lherzolite and hydrous basanitic melt: 1. Experimental results and the investigation of controls on partitioning behaviour. *Contributions to Mineralogy and Petrology* **152**, 1-17.

Agnor, C.B., Canup, R.M. and Levison, H.F. (1999) On the character and consequences of large Impacts in the late stage of terrestrial planet formation. *Icarus* **142**, 219-237.

Albarède, F. (1996) Introduction to geochemical modeling. Cambridge University Press, Cambridge, UK.

Amelin, Y., Krot, A.N., Hutcheon, I.D. and Ulyanov, A.A. (2002) Lead Isotopic Ages of Chondrules and Calcium-Aluminum-Rich Inclusions. *Science* **297**, 1678-1683.

Anhaeusser, C.R. (1980) A geological investigation of the Archaean granite-greenstone terrane south of the Boesmanskop syenite pluton, Barberton Mountain Land, South African Geodynamics Project Paper. University of the Wiwatersrand, Johannesburg, South Africa.

Arevalo Jr, R. and McDonough, W.F. (2010) Chemical variations and regional diversity observed in MORB. *Chemical Geology* **271**, 70-85.

Arndt, N. (1977) The separation of magmas from partially molten peridotite, Carnegie Institue of Washington Yearbook, pp. 424-428.

Arndt, N., Lesher, C.M. and Barnes, S.J. (2008) Komatiite. Cambridge University Press, New York.

Arndt, N.T., Nisbet, E.G. and Cameron, W.G. (1988) Geochemistry of extremely fresh komatiites from the Belingwe belt, Zimbabwe. *Chemical Geology* **70**, 140.

Asafov, E.V., Sobolev, A.S., Gurenko, A.A., , N.T.A. and , V.G.B. (2015) Elevated H_2O and Cl contents in komatiite melts from Abitibi and Belingwe, *Goldschmidt* **2015**, Prague, Czech Republic.

Baker, M.B. and Stolper, E.M. (1994) Determining the composition of high-pressure mantle melts using diamond aggregates. *Geochimica et Cosmochimica Acta* **58**, 2811-2827.

Barnes, S.-J., Pagé, P., Prichard, H.M., Zientek, M.L. and Fisher, P.C. (2016) Chalcophile and platinum-group element distribution in the Ultramafic series of the Stillwater Complex, MT, USA—implications for processes enriching chromite layers in Os, Ir, Ru, and Rh. *Mineralium Deposita* **51**, 25-47.

Barnes, S.-J., Savard, D., Bédard, L.P. and Maier, W.D. (2009) Selenium and sulfur concentrations in the Bushveld Complex of South Africa and implications for formation of the platinum-group element deposits. *Mineralium Deposita* **44**, 647-663.

Becker, H. and Dale, C.W. (2016) Re–Pt–Os isotopic and highly siderophile element behavior in oceanic and continental mantle tectonites. *Reviews in Mineralogy and Geochemistry* **81**, 369-440.

Becker, H., Horan, M.F., Walker, R.J., Gao, S., Lorand, J.P. and Rudnick, R.L. (2006) Highly siderophile element composition of the Earth's primitive upper mantle: Constraints from new data on peridotite massifs and xenoliths. *Geochimica et Cosmochimica Acta* **70**, 4528-4550.

Bédard, J.H. (2006) A catalytic delamination-driven model for coupled genesis of Archaean crust and sub-continental lithospheric mantle. *Geochimica et Cosmochimica Acta* **70**, 1188-1214.

Bekker, A., Barley, M.E., Fiorentini, M.L., Rouxel, O.J., Rumble, D. and Beresford, S.W. (2009) Atmospheric Sulfur in Archean Komatiite-Hosted Nickel Deposits. *Science* **326**, 1086-1089.

Birck, J.L., Barman, M.R. and Capmas, F. (1997) Re-Os isotopic measurements at the femtomole level in Natural Samples. *Geostandards Newsletter* **21**, 19-27.

Bleeker, W. (2003) The late Archean record: a puzzle in ca. 35 pieces. *Lithos* **71**, 99-134.

Blichert-Toft, J., Arndt, N.T. and Gruau, G. (2004) Hf isotopic measurements on Barberton komatiites: effects of incomplete sample dissolution and importance for primary and secondary magmatic signatures. *Chemical Geology* **207**, 261-275.

Blichert-Toft, J., Arndt, N.T., Wilson, A. and Coetzee, G. (2015) Hf and Nd isotope systematics of early Archean komatiites from surface sampling and ICDP drilling in the Barberton Greenstone Belt, South Africa. *American Mineralogist* **100**, 2396-2411.

Borisov, A. and Palme, H. (1995) The solubility of iridium in silicate melts: New data from experiments with Ir10Pt90 alloys. *Geochimica et Cosmochimica Acta* **59**, 481-485.

Bottke, W.F., Walker, R.J., Day, J.M.D., Nesvorny, D. and Elkins-Tanton, L. (2010) Stochastic Late Accretion to Earth, the Moon, and Mars. *Science* **330**, 1527-1530.

Boujibar, A., Andrault, D., Bouhifd, M.A., Bolfan-Casanova, N., Devidal, J.-L. and Trcera, N. (2014) Metal–silicate partitioning of sulphur, new experimental and thermodynamic constraints on planetary accretion. *Earth and Planetary Science Letters* **391**, 42-54.

Bouvier, A. and Wadhwa, M. (2010) The age of the Solar System redefined by the oldest Pb-Pb age of a meteoritic inclusion. *Nature Geosci* **3**, 637-641.

Bowring, S.A. and Housh, T. (1995) The earth's early evolution. *Science* **269**, 1535-1540.

Bowring, S.A., King, J.E., Housh, T.B., Isachsen, C.E. and Podosek, F.A. (1989a) Neodymium and lead isotope evidence for enriched early Archaean crust in North America. *Nature* **340**, 222-225.

Bowring, S.A. and Williams, I.S. (1999) Priscoan (4.00–4.03 Ga) orthogneisses from northwestern Canada. *Contributions to Mineralogy and Petrology* **134**, 3-16.

Bowring, S.A., Williams, I.S. and Compston, W. (1989b) 3.96 Ga gneisses from the Slave province, Northwest Territories, Canada. *Geology* **17**, 971-975.

Brenan, J.M. (2015) Se–Te fractionation by sulfide–silicate melt partitioning: Implications for the composition of mantle-derived magmas and their melting residues. *Earth and Planetary Science Letters* **422**, 45-57.

Brenan, J.M. and Andrews, D. (2001) High-temperature stability oflaurite and Ru-Os-Ir alloy and their role in PGE fractionation in mafic magmas. *The Canadian Mineralogist* **39**, 1747-1748.

Brenan, J.M., Bennett, N.R. and Zajacz, Z. (2016a) Experimental Results on Fractionation of the Highly Siderophile Elements (HSE) at Variable Pressures and Temperatures during Planetary and Magmatic Differentiation in: Harvey, J., Day, J.M.D. (Eds.), Reviews in Mineralogy and Geochemistry: Highly Siderophile and Strongly Chalcophile Elements in High-Temperature Geochemistry and Cosmochemistry. Mineralogical Society of America, Chantilly, Virginia, U.S.A.

Brenan, J.M., Bennett, N.R. and Zajacz, Z. (2016b) Experimental results on fractionation of the highly siderophile elements (HSE) at variable pressures and temperatures during planetary and magmatic differentiation. *Reviews in Mineralogy and Geochemistry* **81**, 1-87.

Brenan, J.M. and McDonough, W.F. (2009) Core formation and metal-silicate fractionation of osmium and iridium from gold. *Nature Geosci* **2**, 798-801.

Brenan, J.M., McDonough, W.F. and Ash, R. (2005) An experimental study of the solubility and partitioning of iridium, osmium and gold between olivine and silicate melt. *Earth and Planetary Science Letters* **237**, 855-872.

Brenan, J.M., McDonough, W.F. and Dalpé, C. (2003) Experimental constraints on the partitioning of rhenium and some platinum-group elements between olivine and silicate melt. *Earth and Planetary Science Letters* **212**, 135-150.

Cameron, E.M. and Hattori, K. (1987) Archean gold mineralization and oxidized hydrothermal fluids. *Economic Geology* **82**, 1177-1191.

Campbell, I.H., Griffiths, R.W. and Hill, R.I. (1989) Melting in an Archean mantle plume: Heads it's basalts, tails it's komatiites. *Nature* **339**, 697.

Canup, R.M. (2012) Forming a Moon with an Earth-like composition via a Giant Impact. *Science* **338**, 1052-1055.

Canup, R.M. and Asphaug, E. (2001) Origin of the Moon in a giant impact near the end of the Earth's formation. *Nature* **412**, 708-712.

Caro, G. (2011) Early silicate Earth differentiation. Annual Review of Earth and Planetary *Sciences* **39**, 31-58.

Chambers, J.E. (2014) 2.4-Planet Formation, in: Turekian, H.D.H.K. (Ed.), Treatise on Geochemistry (Second Edition). Elsevier, Oxford, pp. 55-72.

Chauvel, C., Dupré, B. and Arndt, N.T. (1993) Pb and Nd isotopic correlation in Belingwe komatiites and basalts, in: M. J. Bickle, E., Nisbet, G. (Eds.), The Geology of the Belingwe Greenstone Belt, Zimbabwe. A study of the evolution of Archaean continental crust. A.A. Balkema, Rotterdam/Brookfield, pp. 167–174.

Chou, C.-L. (1978) Fractionation of siderophile elements in the Earth's upper mantle, The 9th Lunar and Planetary science conference, Houston, USA, pp. 219-230.

Chou, C.-L., Shaw, D.M. and Crocket, J.H. (1983) Siderophile trace elements in the Earth's oceanic crust and upper mantle. *Journal of Geophysical Research: Solid Earth* **88**, A507-A518.

Cohen, B.A., Swindle, T.D. and Kring, D.A. (2005) Geochemistry and ^{40}Ar-^{39}Ar geochronology of impact-melt clasts in feldspathic lunar meteorites: Implications for lunar bombardment history. *Meteoritics & Planetary Science* **40**, 755-777.

Connolly, B.D., Puchtel, I.S., Walker, R.J., Arevalo, R., Piccoli, P.M., Byerly, G., Robin-Popieul, C. and Arndt, N. (2011) Highly siderophile element systematics of the 3.3 Ga Weltevreden komatiites, South Africa: Implications for early Earth history. *Earth and Planetary Science Letters* **311**, 253-263.

Creaser, R.A., Papanastassiou, D.A. and Wasserburg, G.J. (1991) Negative thermal ion mass spectrometry of osmium, rhenium and iridium. *Geochimica et Cosmochimica Acta* **55**, 397-401.

Ćuk, M. and Stewart, S.T. (2012) Making the Moon from a fast-spinning Earth: A Giant Impact followed by resonant despinning. *Science* **338**, 1047-1052.

Dale, C.W., Burton, K.W., Pearson, D.G., Gannoun, A., Alard, O., Argles, T.W. and Parkinson, I.J. (2009) Highly siderophile element behaviour accompanying subduction of oceanic crust: Whole rock and mineral-scale insights from a high-pressure terrain. *Geochimica et Cosmochimica Acta* **73**, 1394-1416.

Dale, C.W., Gannoun, A., Burton, K.W., Argles, T.W. and Parkinson, I.J. (2007) Rhenium–osmium isotope and elemental behaviour during subduction of oceanic crust and the implications for mantle recycling. *Earth and Planetary Science Letters* **253**, 211-225.

Dale, C.W., Luguet, A., Macpherson, C.G., Pearson, D.G. and Hickey-Vargas, R. (2008) Extreme platinum-group element fractionation and variable Os isotope compositions in Philippine Sea Plate basalts: Tracing mantle source heterogeneity. *Chemical Geology* **248**, 213-238.

Dale, C.W., Macpherson, C.G., Pearson, D.G., Hammond, S.J. and Arculus, R.J. (2012) Inter-element fractionation of highly siderophile elements in the Tonga Arc due to flux melting of a depleted source. *Geochimica et Cosmochimica Acta* **89**, 202-225.

Danyushevky, L.V., Gee, M.A.M., Nisbet, E.G. and Cheadle, M.J. (2002) Olivine-hosted melt inclusions in Belingwe komatiites: Implications for cooling history, parental magma composition and its H_2O content. *Goldschmidt* **2002**, Davos, Switzerland.

Dauphas, N., Poitrasson, F., Burkhardt, C., Kobayashi, H. and Kurosawa, K. (2015) Planetary and meteoritic Mg/Si and variations inherited from solar nebula chemistry. *Earth and Planetary Science Letters* **427**, 236-248.

de Moor, J.M., Fischer, T.P., Sharp, Z.D., King, P.L., Wilke, M., Botcharnikov, R.E., Cottrell, E., Zelenski, M., Marty, B., Klimm, K., Rivard, C., Ayalew, D., Ramirez, C. and Kelley, K.A. (2013) Sulfur degassing at Erta Ale (Ethiopia) and Masaya (Nicaragua) volcanoes: Implications for degassing processes and oxygen fugacities of basaltic systems. *Geochemistry, Geophysics, Geosystems* **14**, 4076-4108.

Ertel, W., O'Neill, H.S.C., Sylvester, P.J. and Dingwell, D.B. (1999) Solubilities of Pt and Rh in a haplobasaltic silicate melt at 1300°C. *Geochimica et Cosmochimica Acta* **63**, 2439-2449.

Falloon, T.J. and Green, D.H. (1988) Anhydrous Partial Melting of Peridotite from 8 to 35 kb and the Petrogenesis of MORB. *Journal of Petrology* **Special Volume**, 379-414.

Fan, J. (1995) Geochemistry and petrogenesis of unaltered and altered vocanic sequences in the Southern Abitibi Greenstone Belt, Department of Geological Sciences. University of Saskatchewan, Saskatoon, Canada, p. 381.

FauerA, F., Arndt, N. and Libourel, G. (2006) Formation of Spinifex Texture in Komatiites: an Experimental Study. *Journal of Petrology* **47**, 1591-1610.

Fehr, M.A., Rehkämper, M. and Halliday, A.N. (2004) Application of MC-ICPMS to the precise determination of tellurium isotope compositions in chondrites, iron meteorites and sulfides. *International Journal of Mass Spectrometry* **232**, 83-94.

Fernandes, V.A., Fritz, J., Weiss, B.P., Garrick-Bethell, I. and Shuster, D.L. (2013) The bombardment history of the Moon as recorded by ^{40}Ar-^{39}Ar chronology. *Meteoritics & Planetary Science* **48**, 241-269.

Fiorentini, M., Beresford, S., Barley, M., Duuring, P., Bekker, A., Rosengren, N., Cas, R. and Hronsky, J. (2012a) District to Camp Controls on the Genesis of Komatiite-Hosted Nickel Sulfide Deposits, Agnew-Wiluna Greenstone Belt, Western Australia: Insights from the Multiple Sulfur Isotopes. *Economic Geology* **107**, 781-796.

Fiorentini, M.L., Bekker, A., Rouxel, O., Wing, B.A., Maier, W. and Rumble, D. (2012b) Multiple Sulfur and Iron Isotope Composition of Magmatic Ni-Cu-(PGE) Sulfide Mineralization from Eastern Botswana. *Economic Geology* **107**, 105-116.

Fiorentini, M.L., Beresford, S.W., Stone, W.E. and Deloule, E. (2012c) Evidence of water degassing during emplacement and crystallization of 2.7 Ga komatiites from the Agnew-Wiluna greenstone belt, Western Australia. *Contributions to Mineralogy and Petrology* **164**, 143-155.

Fischer-Gödde, M. and Becker, H. (2012) Osmium isotope and highly siderophile element constraints on ages and nature of meteoritic components in ancient lunar impact rocks. *Geochimica et Cosmochimica Acta* **77**, 135-156.

Fischer-Gödde, M., Becker, H. and Wombacher, F. (2011) Rhodium, gold and other highly siderophile elements in orogenic peridotites and peridotite xenoliths. *Chemical Geology* **280**, 365-383.

Fitoussi, C. and Bourdon, B. (2012) Silicon Isotope Evidence Against an Enstatite Chondrite Earth. *Science* **335**, 1477-1480.

Fleet, M.E. and Pan, Y. (1994) Fractional crystallization of anhydrous sulfide liquid in the system Fe-Ni-Cu-S, with application to magmatic sulfide deposits. *Geochimica et Cosmochimica Acta* **58**, 3369-3377.

Fonseca, R.O.C., Mallmann, G., O'Neill, H.S.C., Campbell, I.H. and Laurenz, V. (2011) Solubility of Os and Ir in sulfide melt: Implications for Re/Os fractionation during mantle melting. *Earth and Planetary Science Letters* **311**, 339-350.

Neukum, G. and Ivanov, B.A. (1994) Cratering size distributions and impactprobabilities on Earth from lunar, terrestrial planet, and asteroid cratering data, in: Gehrels, T. (Ed.), Hazards Due to Comet and Asteroids. University of Arizona Press, Tucson, pp. 359-416.

Gale, A., Dalton, C.A., Langmuir, C.H., Su, Y. and Schilling, J.-G. (2013) The mean composition of ocean ridge basalts. *Geochemistry, Geophysics, Geosystems* **14**, 489-518.

Giuliani, A., Fiorentini, M.L., Martin, L.A.J., Farquhar, J., Phillips, D., Griffin, W.L. and LaFlamme, C. (2016) Sulfur isotope composition of metasomatised mantle xenoliths from the Bultfontein kimberlite (Kimberley, South Africa): Contribution from subducted sediments and the effect of sulfide alteration on S isotope systematics. *Earth and Planetary Science Letters* **445**, 114-124.

Gleißner, P., Drüppel, K. and Becker, H. (2012) Osmium isotopes and highly siderophile element fractionation in the massif-type anorthosites of the Mesoproterozoic Kunene Intrusive Complex, NW Namibia. *Chemical Geology* **302-303**, 33-47.

Goldschmidt, V.M. (1937) The principles of distribution of chemical elements in minerals and rocks. The seventh Hugo Muller Lecture, delivered before the Chemical Society on March 17th, 1937. *Journal of the Chemical Society* (**Resumed**), 655-673.

Gomes, R., Levison, H.F., Tsiganis, K. and Morbidelli, A. (2005) Origin of the cataclysmic Late Heavy Bombardment period of the terrestrial planets. *Natur*e **435**, 466-469.

Greber, N.D., Puchtel, I.S., Nägler, T.F. and Mezger, K. (2015) Komatiites constrain molybdenum isotope composition of the Earth's mantle. *Earth and Planetary Science Letters* **421**, 129-138.

Greenland, L.P. and Aruscavage, P. (1986) Volcanic emission of Se, Te, and As from Kilauea volcano, Hawaii. *Journal of Volcanology and Geothermal Research* **27**, 195-201.

Guitreau, M., Blichert-Toft, J., Mojzsis, S.J., Roth, A.S.G., Bourdon, B., Cates, N.L. and Bleeker, W. (2014) Lu–Hf isotope systematics of the Hadean–Eoarchean Acasta Gneiss Complex (Northwest Territories, Canada). *Geochimica et Cosmochimica Acta* **135**, 251-269.

Handler, M.R., Bennett, V.C. and Dreibus, G. (1999) Evidence from correlated Ir/Os and Cu/S for late-stage Os mobility in peridotite xenoliths: Implications for Re-Os systematics. **Geology 27**, 75-78.

Hartmann, W.K. (1975) Lunar "cataclysm": A misconception? *Icarus* **24**, 181-187.

Hartmann, W.K., Quantin, C. and Mangold, N. (2007) Possible long-term decline in impact rates: 2. Lunar impact-melt data regarding impact history. *Icarus* **186**, 11-23.

Harvey, J. and Day, J.M.D. (2016) Introduction to highly siderophile nd stongly chalcophile elements in high temperature geochemistry and cosmochemistry. *Reviews in Mineralogy and Geochemistry* **81**, iii-xiv.

Haughton, D.R., Roeder, P.L. and Skinner, B.J. (1974) Solubility of Sulfur in Mafic Magmas. *Economic Geology* **69**, 451-467.

Heinrichs, H., Schulz-Dobrick, B. and Wedepohl, K.H. (1980) Terrestrial geochemistry of Cd, Bi, Tl, Pb, Zn and Rb. *Geochimica et Cosmochimica Acta* **44**, 1519-1533.

Hémond, C., Hofmann, A.W., Vlastélic, I. and Nauret, F. (2006) Origin of MORB enrichment and relative trace element compatibilities along the Mid-Atlantic Ridge between 10° and 24°N. *Geochemistry, Geophysics, Geosystems* **7**, doi:10.1029/2006GC001317.

Hertogen, J., Janssens, M.J. and Palme, H. (1980) Trace elements in ocean ridge basalt glasses: implications for fractionations during mantle evolution and petrogenesis. *Geochimica et Cosmochimica Acta* **44**, 2125-2143.

Hildebrand, R.S., Hoffman, P.F. and Bowring, S.A. (2010) The Calderian orogeny in Wopmay orogen (1.9 Ga), northwestern Canadian Shield. *Geological Society of America Bulletin* **122**, 794-814.

Hirschmann, M.M., Ghiorso, M.S., Wasylenki, L.E., Asimow, P.D. and Stolper, E.M. (1998) Calculation of Peridotite Partial Melting from Thermodynamic Models of Minerals and Melts. I. Review of Methods and Comparison with Experiments. *Journal of Petrology* **39**, 1091-1115.

Holzheid, A., Sylvester, P., O'Neill, H.S.C., Rubie, D.C. and Palme, H. (2000) Evidence for a late chondritic veneer in the Earth's mantle from high-pressure partitioning of palladium and platinum. *Nature* **406**, 396-399.

IAG (2015a) Harzburgit Kraubath (MUH-1). IAGeo Limited, Nottingham, UK, p. 1.

IAG (2015b) Komatiite Ontario (OKUM). IAGeo Limited, Nottingham, UK, p. 1.

Iizuka, T., Horie, K., Komiya, T., Maruyama, S., Hirata, T. and Hidaka, H. (2006a) Reworking of Hadean continental crust in the Acasta Gneiss Complex of NW Canada: Evidence from zircon U–Pb and Lu–Hf isotopes. *Geochimica et Cosmochimica Acta* **70**, A369.

Iizuka, T., Horie, K., Komiya, T., Maruyama, S., Hirata, T., Hidaka, H. and Windley, B.F. (2006b) 4.2 Ga zircon xenocryst in an Acasta gneiss from northwestern Canada: Evidence for early continental crust. *Geology* **34**, 245-248.

Iizuka, T., Komiya, T., Johnson, S.P., Kon, Y., Maruyama, S. and Hirata, T. (2009) Reworking of Hadean crust in the Acasta gneisses, northwestern Canada: Evidence from in-situ Lu–Hf isotope analysis of zircon. *Chemical Geology* **259**, 230-239.

Iizuka, T., Komiya, T. and Maruyama, S. (2007a) Chapter 3.1 The Early Archean Acasta Gneiss Complex: Geological, Geochronological and Isotopic Studies and Implications for Early Crustal Evolution, in: Martin J. van Kranendonk, R.H.S., Vickie, C.B. (Eds.), Developments in Precambrian Geology. Elsevier, pp. 127-147.

Iizuka, T., Komiya, T., Ueno, Y., Katayama, I., Uehara, Y., Maruyama, S., Hirata, T., Johnson, S.P. and Dunkley, D.J. (2007b) Geology and zircon geochronology of the Acasta Gneiss Complex, northwestern Canada: New constraints on its tectonothermal history. *Precambrian Research* **153**, 179-208.

Jacobson, S.A., Morbidelli, A., Raymond, S.N., O'Brien, D.P., Walsh, K.J. and Rubie, D.C. (2014) Highly siderophile elements in Earth's mantle as a clock for the Moon-forming impact. *Nature* **508**, 84-87.

Jagoutz, E., Palme, H., Baddenhausen, H., Blum, K., Cendales, M. and Dreibus, G. (1979) The abundances of major, minor and trace elements in the Earth's mantle as derived from primitive ultramafic nodules, Lunar and Planetary Science Conference, 10th. Pergamon Press, Houston, Tex., pp. 2031-2050.

Jeffrey, N.C., Robert, C.H., Julie, M.P. and Anthony, R.D. (2001) Size-selective Concentration of Chondrules and Other Small Particles in Protoplanetary Nebula Turbulence. *The Astrophysical Journal* **546**, 496.

Jenner, F.E. and O'Neill, H.S.C. (2012) Analysis of 60 elements in 616 ocean floor basaltic glasses. *Geochemistry, Geophysics, Geosystems* **13**, doi:10.1029/2011GC004009.

Jugo, P.J. (2009) Sulfur content at sulfide saturation in oxidized magmas. Geology 37, 415-418.

Kamenetsky, V.S. and Eggins, S.M. (2012) Systematics of metals, metalloids, and volatiles in MORB melts: Effects of partial melting, crystal fractionation and degassing (a case study of Macquarie Island glasses). *Chemical Geology* **302-303**, 76-86.

Kareem, K. (2005) Komatiites of the Weltevreden Formation, Barberton Greenstone Belt, South Africa: Implications for the chemistry and temperature of the Archean mantle, Department of Geology and Geophysics. Louisiana State University, Baton Rouge, p. 233.

Keays, R.R. (1995) The role of komatiitic and picritic magmatism and S-saturation in the formation of ore deposits. *Lithos* **34**, 1-18.

Keays, R.R., Ganapathy, R. and Anders, E. (1971) Chemical fractionations in meteorites—IV abundances of fourteen trace elements in L-chondrites; implications for cosmothermometry. *Geochimica et Cosmochimica Acta* **35**, 337-363.

Kent, A.J.R., Hauri, E., Woodhead, J. and Hergt, J.M. (2009) Volatile contents of Belingwe komatiites; mantle volatile contents and the effects of degassing. *Geochimica et Cosmochimica Acta* **73**, A640.

Kiseeva, E.S. and Wood, B.J. (2013) A simple model for chalcophile element partitioning between sulphide and silicate liquids with geochemical applications. *Earth and Planetary Science Letters* **383**, 68-81.

Kiseeva, E.S. and Wood, B.J. (2015) The effects of composition and temperature on chalcophile and lithophile element partitioning into magmatic sulphides. *Earth and Planetary Science Letters* **424**, 280-294.

Kleine, T., Munker, C., Mezger, K. and Palme, H. (2002) Rapid accretion and early core formation on asteroids and the terrestrial planets from Hf-W chronometry. *Nature* **418**, 952-955.

Kokubo, E. and Ida, S. (1998) Oligarchic Growth of Protoplanets. *Icarus* **131**, 171-178.

Kokubo, E. and Ida, S. (2000) Formation of Protoplanets from Planetesimals in the Solar Nebula. *Icarus* **143**, 15-27.

König, S., Lissner, M., Lorand, J.-P., Bragagni, A. and Luguet, A. (2015a) Mineralogical control of selenium, tellurium and highly siderophile elements in the Earth's mantle: Evidence from mineral separates of ultra-depleted mantle residues. *Chemical Geology* **396**, 16-24.

König, S., Lorand, J.-P., Luguet, A. and Graham Pearson, D. (2014) A non-primitive origin of near-chondritic S-Se-Te ratios in mantle peridotites; implications for the Earth's late accretionary history. *Earth and Planetary Science Letters* **385**, 110-121.

König, S., Luguet, A., Lorand, J.-P., Lissner, M. and Graham Pearson, D. (2015b) Reply to the comment on "A non-primitive origin of near-chondritic S-Se-Te ratios in mantle peridotites: Implications for the Earth's late accretionary history" by König S. et al. [Earth Planet. Sci. Lett. 385 (2014) 110–121]. *Earth and Planetary Science Letters* 417, 167-169.

König, S., Luguet, A., Lorand, J.-P., Wombacher, F. and Lissner, M. (2012) Selenium and tellurium systematics of the Earth's mantle from high precision analyses of ultra-depleted orogenic peridotites. *Geochimica et Cosmochimica Acta* **86**, 354-366.

Kruijer, T.S., Kleine, T., Fischer-Godde, M. and Sprung, P. (2015) Lunar tungsten isotopic evidence for the late veneer. *Nature* **520**, 534-537.

Labidi, J., Cartigny, P. and Moreira, M. (2013) Non-chondritic sulphur isotope composition of the terrestrial mantle. *Nature* **501**, 208-211.

Larimer, J.W. (1967) Chemical fractionations in meteorites-I. Condensation of the elements. *Geochimica et Cosmochimica Acta* **31**, 1215-1238.

Larimer, J.W. and Anders, E. (1967) Chemical fractionations in meteorites-II. Abundance patterns and their interpretation. *Geochimica et Cosmochimica Acta* **31**, 1239-1270.

Lassiter, J.C. (2002) Evidence for Re loss during magma degassing: Implications for Re concentration variations in OIB and MORB, American Geophysical Union, San Francisco, USA.

Le Roux, V., Bodinier, J.L., Tommasi, A., Alard, O., Dautria, J.M., Vauchez, A. and Riches, A.J.V. (2007) The Lherz spinel lherzolite: Refertilized rather than pristine mantle. *Earth and Planetary Science Letters* **259**, 599-612.

Lécuyer, C., gruau, G., Anhaeusser, C.R. and Fourcade, S. (1994) The origin of fluids and the effects of metamorphism on the primary chemical compositions of Barberton komatiites: New evidence from geochemical (REE) and isotopic (Nd, O, H, ^{39}Ar-^{40}Ar) data. *Geochimica et Cosmochimica Acta* **58**, 969-984.

Lee, C.-T.A., Luffi, P., Chin, E.J., Bouchet, R., Dasgupta, R., Morton, D.M., Le Roux, V., Yin, Q.-z. and Jin, D. (2012) Copper Systematics in Arc Magmas and Implications for Crust-Mantle Differentiation. *Science* **336**, 64-68.

Lee, D.-C. and Halliday, A.N. (1995) Hafnium-tungsten chronometry and the timing of terrestrial core formation. *Nature* **378**, 771-774.

Lee, D.-C., Halliday, A.N., Snyder, G.A. and Taylor, L.A. (1997) Age and Origin of the Moon. *Science* **278**, 1098-1103.

Lehtonen, M. (2005) Rare earth element characteristics of pyrope garnets from the Kaavi-Kuopio kimberlites-implications for mantle metasomatism. *Bulletin of the Geological Society of Finland* **77**, 31-47.

Li, C. and Ripley, E.M. (2005) Empirical equations to predict the sulfur content of mafic magmas at sulfide saturation and applications to magmatic sulfide deposits. *Mineralium Deposita* **40**, 218-230.

Li, J. and Agee, C.B. (1996) Geochemistry of mantle-core differentiation at high pressure. *Nature* **381**, 686-689.

Li, Y. (2014) Chalcophile element partitioning between sulfide phases and hydrous mantle melt: Applications to mantle melting and the formation of ore deposits. *Journal of Asian Earth Sciences* **94**, 77-93.

Li, Y. and Audétat, A. (2012) Partitioning of V, Mn, Co, Ni, Cu, Zn, As, Mo, Ag, Sn, Sb, W, Au, Pb, and Bi between sulfide phases and hydrous basanite melt at upper mantle conditions. *Earth and Planetary Science Letters* **355-356**, 327-340.

Lipschutz, M.E. and Woolum, D.S. (1988) Highly labile elements, in: Kerridge, J.F., Matthews, M.S. (Eds.), Meteorites and the early solar system. University of Arizona Press, Tucson, AZ, USA, pp. 462-487.

Lissner, M., König, S., Luguet, A., le Roux, P.J., Schuth, S., Heuser, A. and le Roex, A.P. (2014) Selenium and tellurium systematics in MORBs from the southern Mid-Atlantic Ridge (47-50°S). *Geochimica et Cosmochimica Acta* **144**, 379-402.

Liu, J., Touboul, M., Ishikawa, A., Walker, R.J. and Graham Pearson, D. (2016) Widespread tungsten isotope anomalies and W mobility in crustal and mantle rocks of the Eoarchean Saglek Block, northern Labrador, Canada: Implications for early Earth processes and W recycling. *Earth and Planetary Science Letters* **448**, 13-23.

Liu, S.-A., Huang, J., Liu, J., Wörner, G., Yang, W., Tang, Y.-J., Chen, Y., Tang, L., Zheng, J. and Li, S. (2015) Copper isotopic composition of the silicate Earth. *Earth and Planetary Science Letters* **427**, 95-103.

Liu, X., Xiong, X., Audétat, A., Li, Y., Song, M., Li, L., Sun, W. and Ding, X. (2014) Partitioning of copper between olivine, orthopyroxene, clinopyroxene, spinel, garnet and silicate melts at upper mantle conditions. *Geochimica et Cosmochimica Acta* **125**, 1-22.

Liu, Y. and Brenan, J. (2015) Partitioning of platinum-group elements (PGE) and chalcogens (Se, Te, As, Sb, Bi) between monosulfide-solid solution (MSS), intermediate solid solution (ISS) and sulfide liquid at controlled fO_2-fS_2 conditions. *Geochimica et Cosmochimica Acta* **159**, 139-161.

Locmelis, M., Pearson, N.J., Barnes, S.J. and Fiorentini, M.L. (2011) Ruthenium in komatiitic chromite. *Geochimica et Cosmochimica Acta* **75**, 3645-3661.

Lodders, K. (2003) Solar system sbundances and sondensation semperatures of the elements. *The Astrophysical Journal* **591**, 1220-1247.

Lorand, J.-P. and Alard, O. (2010) Determination of selenium and tellurium concentrations in Pyrenean peridotites (Ariege, France): New insight into S/Se/Te systematics of the upper in mantle samples. *Chemical Geology* **278**, 120-130.

Lorand, J.-P., Alard, O. and Luguet, A. (2010) Platinum-group element micronuggets and refertilization process in Lherz orogenic peridotite (northeastern Pyrenees, France). *Earth and Planetary Science Letters* **289**, 298-310.

Lyubetskaya, T. and Korenaga, J. (2007) Chemical composition of Earth's primitive mantle and its variance: 1. Method and results. *Journal of Geophysical Research: Solid Earth* **112**, B03211.

Maier, W.D., Barnes, S.J., Campbell, I.H., Fiorentini, M.L., Peltonen, P., Barnes, S.-J. and Smithies, R.H. (2009) Progressive mixing of meteoritic veneer into the early Earth's deep mantle. *Nature* **460**, 620-623.

Mallmann, G. and O'Neill, H.S.C. (2007) The effect of oxygen fugacity on the partitioning of Re between crystals and silicate melt during mantle melting. *Geochimica et Cosmochimica Acta* **71**, 2837-2857.

Maltese, A., Sprung, P., Scherer, E.E., Mezger, K. and Bleeker, W. (2015) Multiple-system geochronology on Acasta layered gneisses, *Goldschmidt* **2015**, Prague, Czeck Republic.

Mann, U., Frost, D.J., Rubie, D.C., Becker, H. and Audétat, A. (2012) Partitioning of Ru, Rh, Pd, Re, Ir and Pt between liquid metal and silicate at high pressures and high temperatures - Implications for the origin of highly siderophile element concentrations in the Earth's mantle. *Geochimica et Cosmochimica Acta* **84**, 593-613.

Marchi, S., Bottke, W.F., Elkins-Tanton, L.T., Bierhaus, M., Wuennemann, K., Morbidelli, A. and Kring, D.A. (2014) Widespread mixing and burial of Earth/'s Hadean crust by asteroid impacts. *Nature* **511**, 578-582.

Marowsky, G. and Wedepohl, K.H. (1971) General trends in the behavior of Cd, Hg, Tl and Bi in some major rock forming processes. *Geochimica et Cosmochimica Acta* **35**, 1255-1267.

Mathez, E.A. (1976) Sulfur solubility and magmatic sulfides in submarine basalt glass. *Journal of Geophysical Research* **81**, 4269-4276.

Mavrogenes, J.A. and O'Neill, H.S.C. (1999) The relative effects of pressure, temperature and oxygen fugacity on the solubility of sulfide in mafic magmas. *Geochimica et Cosmochimica Acta* **63**, 1173-1180.

McDonough, W.F. and Sun, S.s. (1995) The composition of the Earth. *Chemical Geology* **120**, 223-253.

Meisel, T., Walker, R.J. and Morgan, J.W. (1996) The osmium isotopic composition of the Earth's primitive upper mantle. *Nature* **383**, 517-520.

Mojzsis, S.J., Arrhenius, G., McKeegan, K.D., Harrison, T.M., Nutman, A.P. and Friend, C.R.L. (1996) Evidence for life on Earth before 3.800 million years ago. *Nature* **384**, 55-59.

Mojzsis, S.J., Cates, N.L., Caro, G., Trail, D., Abramov, O., Guitreau, M., Blichert-Toft, J., Hopkins, M.D. and Bleeker, W. (2014) Component geochronology in the polyphase ca. 3920 Ma Acasta Gneiss. *Geochimica et Cosmochimica Acta* **133**, 68-96.

Moorbath, S., Whitehouse, M.J. and Kamber, B.S. (1997) Extreme Nd-isotope heterogeneity in the early Archaean-fact or fiction? Case histories from northern Canada and West Greenland. *Chemical Geology* **135**, 213-231.

Morbidelli, A., Marchi, S., Bottke, W.F. and Kring, D.A. (2012) A sawtooth-like timeline for the first billion years of lunar bombardment. *Earth and Planetary Science Letters* **355-356**, 144-151.

Morbidelli, A. and Wood, B. (2014) Late Accretion and the Late Veneer, in: Badro, J., Walter, M. (Eds.), The Early Earth. eprint arXiv:1411.4563.

Morgan, J.W. (1986) Ultramafic xenoliths: Clues to Earth's late accretionary history. *Journal of Geophysical Research: Solid Earth* **91**, 12375-12387.

Moune, S., Gauthier, P.-J., Gislason, S.R. and Sigmarsson, O. (2006) Trace element degassing and enrichment in the eruptive plume of the 2000 eruption of Hekla volcano, Iceland. *Geochimica et Cosmochimica Acta* **70**, 461-479.

Mungall, J.E., Andrews, D.R.A., Cabri, L.J., Sylvester, P.J. and Tubrett, M. (2005) Partitioning of Cu, Ni, Au, and platinum-group elements between monosulfide solid solution and sulfide melt under controlled oxygen and sulfur fugacities. *Geochimica et Cosmochimica Acta* **69**, 4349-4360.

Mungall, J.E. and Brenan, J.M. (2014a) Partitioning of platinum-group elements and Au between sulfide liquid and basalt and the origins of mantle-crust fractionation of the chalcophile elements. *Geochimica et Cosmochimica Acta* **125**, 265-289.

Murton, B.J., Smith, H. and Fitton, G. (2013) Does MORB reflect upper mantle diversity? *Fall Meeting* **2013**, American Geophysical Union.

Mysen, B.O. (1979) Nickel partitioning between olivine and silicate melt; Henry's law revisited. *American Mineralogist* **64**, 1107-1114.

Nagel, T.J., Hoffmann, J.E. and Münker, C. (2012) Generation of Eoarchean tonalite-trondhjemite-granodiorite series from thickened mafic arc crust. *Geology* **40**, 375-378.

Newsom, H.E. and Palme, H. (1984) The depletion of siderophile elements in the Earth's mantle: new evidence from molybdenum and tungsten. *Earth and Planetary Science Letters* **69**, 354-364.

Newsom, H.E., White, W.M., Jochum, K.P. and Hofmann, A.W. (1986) Siderophile and chalcophile element abundances in oceanic basalts, Pb isotope evolution and growth of the Earth's core. *Earth and Planetary Science Letters* **80**, 299-313.

Nielsen, S.G., Shimizu, N., Lee, C.-T.A. and Behn, M.D. (2014) Chalcophile behavior of thallium during MORB melting and implications for the sulfur content of the mantle. *Geochemistry, Geophysics, Geosystems* **15**, 4905-4919.

Nisbet, E.G., Arndt, N.T., Bickle, M.J., Cameron, W.E., Chauvel, C., Cheadle, M., Hegner, E., Kyser, T.K., Martin, A., Renner, R. and Roedder, E. (1987) Uniquely fresh 2.7 Ga komatiites from the Belingwe greenstone belt, Zimbabwe. *Geology* **15**, 1147-1150.

Nisbet, E.G., Cheadle, M.J., Arndt, N.T. and Bickle, M.J. (1993) Constraining the potential temperature of the Archaean mantle: A review of the evidence from komatiites. *Lithos* **30**, 291-307.

Norman, M.D., Garcia, M.O. and Bennett, V.C. (2004) Rhenium and chalcophile elements in basaltic glasses from Ko'olau and Moloka'i volcanoes: Magmatic outgassing and composition of the Hawaiian plume. *Geochimica et Cosmochimica Acta* **68**, 3761-3777.

O'Neill, S.C.H. and Jenner, F.E. (2012) The global pattern of trace-element distributions in ocean floor basalts. *Nature* **491**, 698-704.

O'Neill, H.S.C. and Mavrogens, J.A. (2002) The Sulfide Capacity and the Sulfur Content at Sulfide Saturation of Silicate Melts at 1400°C and 1 bar. *Journal of Petrology* **43**, 1049-1087.

Pagé, P., Barnes, S.-J., Bédard, J.H. and Zientek, M.L. (2012) In situ determination of Os, Ir, and Ru in chromites formed from komatiite, tholeiite and boninite magmas: Implications for chromite control of Os, Ir and Ru during partial melting and crystal fractionation. *Chemical Geology* **302-303**, 3-15.

Palme, H., Lodders, K. and Jones, A. (2014) 2.2-Solar System Abundances of the Elements, in: Turekian, H.D.H.K. (Ed.), Treatise on Geochemistry (Second Edition). Elsevier, Oxford, pp. 15-36.

Palme, H. and O'Neill, H.S.C. (2007) 2.01-Cosmochemical Estimates of Mantle Composition, in: Turekian, H.D.H.K. (Ed.), *Treatise on Geochemistry*. Pergamon, Oxford, pp. 1-38.

Palme, H. and O'Neill, H.S.C. (2014) 3.1-Cosmochemical Estimates of Mantle Composition, in: Turekian, H.D.H.K. (Ed.), *Treatise on Geochemistry* (Second Edition). Elsevier, Oxford, pp. 1-39.

Park, J.-W., Hu, Z., Gao, S., Campbell, I.H. and Gong, H. (2012) Platinum group element abundances in the upper continental crust revisited-New constraints from analyses of Chinese loess. *Geochimica et Cosmochimica Acta* **93**, 63-76.

Patten, C., Barnes, S.-J., Mathez, E.A. and Jenner, F.E. (2013) Partition coefficients of chalcophile elements between sulfide and silicate melts and the early crystallization history of sulfide liquid: LA-ICP-MS analysis of MORB sulfide droplets. *Chemical Geology* **358**, 170-188.

Peach, C.L., Mathez, E.A. and Keays, R.R. (1990) Sulfide melt-silicate melt distribution coefficients for noble metals and other chalcophile elements as deduced from MORB: Implications for partial melting. *Geochimica et Cosmochimica Acta* **54**, 3379-3389.

Peucker-Ehrenbrink, B., Bach, W., Hart, S.R., Blusztajn, J.S. and Abbruzzese, T. (2003) Rhenium-osmium isotope systematics and platinum group element concentrations in oceanic crust from DSDP/ODP Sites 504 and 417/418. *Geochemistry, Geophysics, Geosystems* **4**, 8911.

Peucker-Ehrenbrink, B., Hanghoj, K., Atwood, T. and Kelemen, P.B. (2012) Rhenium-osmium isotope systematics and platinum group element concentrations in oceanic crust. *Geology* **40**, 199-204.

Philip, J.C., Zoë, M.L., Tim, E., Michael, J.W. and Sarah, T.S. (2015) Compositional evolution during rocky protoplanet accretion. *The Astrophysical Journal* **813**, arXiv:1509.07504v1.

Pinarelli, L., Boriani, A. and Del Moro, A. (1988) Rb-Sr Geochronology of Lower Permian plutonism in Massiccio dei Laghi, Southern Alps (NW Italy). *Rendiconti della Societa Italiana di Mineralogia e Petrologia* **43**, 411-428.

Plessen, H.-G. and Erzinger, J. (1998) Determination of the Platinum-Group Elements and Gold in Twenty Rock Reference Materials by Inductively Coupled Plasma-Mass Spectrometry (ICP-MS) after Pre-Concentration by Nickel Sulfide Fire Assay. *Geostandards Newsletter* **22**, 187-194.

Prouteau, G. and Scaillet, B. (2013) Experimental constraints on sulphur behaviour in subduction zones: Implications for TTG and adakite production and the global sulphur cycle since the Archean. *Journal of Petrology* **54**, 183-213.

Puchtel, I.S., Blichert-Toft, J., Touboul, M., Horan, M.F. and Walker, R.J. (2016a) The coupled ^{182}W-^{142}Nd record of early terrestrial mantle differentiation. *Geochemistry, Geophysics, Geosystems* **17**, doi:10.1002/2016GC006324.

Puchtel, I.S., Blichert-Toft, J., Touboul, M., Walker, R.J., Byerly, G.R., Nisbet, E.G. and Anhaeusser, C.R. (2013) Insights into early Earth from Barberton komatiites: Evidence from lithophile isotope and trace element systematics. *Geochimica et Cosmochimica Acta* **108**, 63-90.

Puchtel, I.S., Brandon, A.D., Humayun, M. and Walker, R.J. (2005) Evidence for the early differentiation of the core from Pt-Re-Os isotope systematics of 2.8-Ga komatiites. *Earth and Planetary Science Letters* **237**, 118-134.

Puchtel, I.S., Haase, K.M., Hofmann, A.W., Chauvel, C., Kulikov, V.S., Garbe-Schönberg, C.D. and Nemchin, A.A. (1997) Petrology and geochemistry of crustally contaminated komatiitic basalts from the Vetreny Belt, southeastern Baltic Shield: Evidence for an early Proterozoic mantle plume beneath rifted Archean continental lithosphere. *Geochimica et Cosmochimica Acta* **61**, 1205-1222.

Puchtel, I.S., Hofmann, A.W., Mezger, K., Shchipansky, A.A., Kulikov, V.S. and Kulikova, V.V. (1996) Petrology of a 2.41 Ga remarkably fresh komatiitic basalt lava lake in Lion Hills, central Vetreny Belt, Baltic Shield. *Contributions to Mineralogy and Petrology* **124**, 273-290.

Puchtel, I.S. and Humayun, M. (2001) Platinum group element fractionation in a komatiitic basalt lava lake. *Geochimica et Cosmochimica Acta* **65**, 2979-2993.

Puchtel, I.S., Humayun, M., Campbell, A.J., Sproule, R.A. and Lesher, C.M. (2004) Platinum group element geochemistry of komatiites from the Alexo and Pyke Hill areas, Ontario, Canada. *Geochimica et Cosmochimica Acta* **68,** 1361-1383.

Puchtel, I.S., Humayun, M. and Walker, R.J. (2007) Os-Pb-Nd isotope and highly siderophile and lithophile trace element systematics of komatiitic rocks from the Volotsk suite, SE Baltic Shield. *Precambrian Research* **158**, 119-137.

Puchtel, I.S., Touboul, M., Blichert-Toft, J., Walker, R.J., Brandon, A.D., Nicklas, R.W., Kulikov, V.S. and Samsonov, A.V. (2016b) Lithophile and siderophile element systematics of Earth's mantle at the Archean-Proterozoic boundary: Evidence from 2.4 Ga komatiites. *Geochimica et Cosmochimica Acta* **180**, 227-255.

Puchtel, I.S., Walker, R.J., Anhaeusser, C.R. and Gruau, G. (2009a) Re-Os isotope systematics and HSE abundances of the 3.5 Ga Schapenburg komatiites, South Africa: Hydrous melting or prolonged survival of primordial heterogeneities in the mantle? *Chemical Geology* **262**, 355-369.

Puchtel, I.S., Walker, R.J., Brandon, A.D. and Nisbet, E.G. (2009b) Pt-Re-Os and Sm-Nd isotope and HSE and REE systematics of the 2.7Ga Belingwe and Abitibi komatiites. *Geochimica et Cosmochimica Acta* **73**, 6367-6389.

Puchtel, I.S., Walker, R.J., Touboul, M., Nisbet, E.G. and Byerly, G.R. (2014) Insights into early Earth from the Pt-Re-Os isotope and highly siderophile element abundance systematics of Barberton komatiites. *Geochimica et Cosmochimica Acta* **125**, 394-413.

Rehkämper, M., Halliday, A.N., Fitton, J.G., Lee, D.C., Wieneke, M. and Arndt, N.T. (1999) Ir, Ru, Pt, and Pd in basalts and komatiites: new constraints for the geochemical behavior of the platinum-group elements in the mantle. *Geochimica et Cosmochimica Acta* **63**, 3915-3934.

Reimink, J.R., Chacko, T., Stern, R.A. and Heaman, L.M. (2014) Earth's earliest evolved crust generated in an Iceland-like setting. *Nature Geosci* **7**, 529-533.

Renner, R., Nisbet, E.G., Cheadle, M.J., Arndt, N.T., Bickle, M.J. and Cameron, W.E. (1994) Komatiite Flows from the Reliance Formation, Belingwe Belt, Zimbabwe: I. Petrography and Mineralogy. *Journal of Petrology* **35**, 361-400.

Ridley, J., Mikucki, E.J. and Groves, D.I. (1996) Archean lode-gold deposits: fluid flow and chemical evolution in vertically extensive hydrothermal systems. *Ore Geology Reviews* **10**, 279-293.

Righter, K. (2011) Prediction of metal–silicate partition coefficients for siderophile elements: An update and assessment of PT conditions for metal-silicate equilibrium during accretion of the Earth. *Earth and Planetary Science Letters* **304**, 158-167.

Righter, K., Humayun, M. and Danielson, L. (2008) Partitioning of palladium at high pressures and temperatures during core formation. *Nature Geosci* **1**, 321-323.

Rizo, H., Walker, R.J., Carlson, R.W., Touboul, M., Horan, M.F., Puchtel, I.S., Boyet, M. and Rosing, M.T. (2016) Early Earth differentiation investigated through 142Nd, 182W, and highly siderophile element abundances in samples from Isua, Greenland. *Geochimica et Cosmochimica Acta* **175**, 319-336.

Robin-Popieul, C.C.M., Arndt, N.T., Chauvel, C., Byerly, G.R., Sobolev, A.V. and Wilson, A. (2012) A New Model for Barberton Komatiites: Deep Critical Melting with High Melt Retention. *Journal of Petrology*, doi:10.1093/petrology/egs042

Rose-Weston, L., Brenan, J.M., Fei, Y., Secco, R.A. and Frost, D.J. (2009) Effect of pressure, temperature, and oxygen fugacity on the metal-silicate partitioning of Te, Se, and S: Implications for earth differentiation. *Geochimica et Cosmochimica Acta* **73**, 4598-4615.

Roth, A.S.G., Bourdon, B., Mojzsis, S.J., Rudge, J.F., Guitreau, M. and Blichert-Toft, J. (2014) Combined^{147,146}Sm-^{143,142}Nd constraints on the longevity and residence time of early terrestrial crust. *Geochemistry, Geophysics, Geosystems* **15**, 2329-2345.

Rubin, K. (1997) Degassing of metals and metalloids from erupting seamount and mid-ocean ridge volcanoes: Observations and predictions. *Geochimica et Cosmochimica Acta* **61**, 3525-3542.

Rubin, K.H., Sinton, J.M., Maclennan, J. and Hellebrand, E. (2009) Magmatic filtering of mantle compositions at mid-ocean-ridge volcanoes. *Nature Geosci* **2**, 321-328.

Rudnick, R.L. and Gao, S. (2014) 4.1 - Composition of the Continental Crust, in: Turekian, H.D.H.K. (Ed.), Treatise on Geochemistry (Second Edition). Elsevier, Oxford, pp. 1-51.

Ryder, G. (1990) Lunar samples, lunar accretion and the early bombardment of the Moon. *Eos, Transactions American Geophysical Union* **71**, 313-323.

Sano, Y., Terada, K., Hidaka, H., Yokoyama, K. and Nutman, A.P. (1999) Palaeoproterozoic thermal events recorded in the ~4.0 Ga Acasta gneiss, Canada: evidence from SHRIMP U-Pb dating of apatite and zircon. *Geochimica et Cosmochimica Acta* **63**, 899-905.

Sassani, D.C. and Shock, E.L. (1990) Speciation and solubility of palladium in aqueous magmatic-hydrothermal solutions. *Geology* **18**, 925-928.

Savage, P.S., Moynier, F., Chen, H., Shofner, G., Siebert, J., Badro, J. and Puchtel, I.S. (2015) Copper isotope evidence for large-scale sulphide fractionation during Earth's differentiation. *Geochemical Perspectives Letters* **1**, 53-64.

Scherer, E.E., Sprung, P., Bleeker, W. and Mezger, K. (2010) The Acasta Gneisses revisited: Evidence for an early depleted mantle, American Geophysical Union, *Fall Meeting* **2010**, abstract V44B-01, San Francisco, CA.

Schoenberg, R., Kamber, B.S., Collerson, K.D. and Moorbath, S. (2002) Tungsten isotope evidence from 3.8-Gyr metamorphosed sediments for early meteorite bombardment of the Earth. *Nature* **418**, 403-405.

Schönbächler, M., Carlson, R.W., Horan, M.F., Mock, T.D. and Hauri, E.H. (2010) Heterogeneous Accretion and the Moderately Volatile Element Budget of Earth. *Science* **328**, 884-887.

Seal, R.R. (2006) Sulfur isotope geochemistry of sulfide minerals. *Reviews in Mineralogy and Geochemistry* **61**, 633-677.

Seo, J.H., Guillong, M. and Heinrich, C.A. (2012) Separation of molybdenum and copper in porphyry deposits: The roles of sulfur, redox, and pH in ore mineral deposition at Bingham Canyon. *Economic Geology* **107**, 333-356.

Sharp, M., Gerasimenko, I., Loudin, L.C., Liu, J., James, O.B., Puchtel, I.S. and Walker, R.J. (2014) Characterization of the dominant impactor signature for Apollo 17 impact melt rocks. *Geochimica et Cosmochimica Acta* **131**, 62-80.

Shimizu, K., Nakamura, E. and Maruyama, S. (2005) The geochemistry of ultramafic to mafic volcanics from the Belingwe Greenstone Belt, Zimbabwe: magmatism in an Archean continental large igneous province. *Journal of Petrology* **46**, 2367-2394.

Shore, M. and Fowler, A.D. (1999) The origin of spinifex texture in komatiites. *Nature* **397**, 691-694.

Simon, A.C. and Pettke, T. (2009) Platinum solubility and partitioning in a felsic melt–vapor–brine assemblage. *Geochimica et Cosmochimica Acta* **73**, 438-454.

Sims, K.W.W. and DePaolo, D.J. (1997) Inferences about mantle magma sources from incompatible element concentration ratios in oceanic basalts. *Geochimica et Cosmochimica Acta* **61**, 765-784.

Sims, K.W.W., Newsom, H.E. and Gladney, E.S. (1990) Chemical fractionation during formation of the Earth's core and continental crust: clues from As, Sb, W and Mo., in: Newsom, H.E., Jones, J.H. (Eds.), Origin of the Earth. Oxford University Press, Oxford, UK, pp. 291–317.

Sobolev, A.V., Asafov, E.V., Gurenko, A.A., Arndt, N.T., Batanova, V.G., Portnyagin, M.V., Garbe-Schönberg, D. and Krasheninnikov, S.P. (2016) Komatiites reveal a hydrous Archaean deep-mantle reservoir. *Nature* **531**, 628-632.

Sprung, P. (2010) A perspective on the ^{176}Lu-^{176}Hf system, its integrity in extra-terrestrial and terrestrial matter, and its application to Hadean to early Archean samples from the Acasta Gneiss Complex, Canada, Institut for Mineralogy. Westfälische Wilhelms-Universität Münster, Münster, Germany.

Stefánsson, A., Keller, N.S., Robin, J.G. and Ono, S. (2015) Multiple sulfur isotope systematics of Icelandic geothermal fluids and the source and reactions of sulfur in volcanic geothermal systems at divergent plate boundaries. *Geochimica et Cosmochimica Acta* **165**, 307-323.

Stefánsson, A. and Seward, T.M. (2003) Experimental determination of the stability and stoichiometry of sulphide complexes of silver(I) in hydrothermal solutions to 400°C. *Geochimica et Cosmochimica Acta* **67**, 1395-1413.

Stern, R.A. and Bleeker, W. (1998) Age of the world's oldest rocks refined using Canada's SHRIMP: The Acasta Gneiss Complex, Northwest Territories, Canada. *Geoscience Canad*a **25 (1)**, 27-31.

Shorttle, O. (2015) Geochemical variability in MORB controlled by concurrent mixing and crystallisation. *Earth and Planetary Science Letters* **424**, 1-14.

Sun, W., Bennett, V.C., Eggins, S.M., Kamenetsky, V.S. and Arculus, R.J. (2003) Enhanced mantle-to-crust rhenium transfer in undegassed arc magmas. *Nature* **422**, 294-297.

Symonds, R.B., Rose Jr, W.I., Reed, M.H., Lichte, F.E. and Finnegan, D.L. (1987) Volatilization, transport and sublimation of metallic and non-metallic elements in high temperature gases at Merapi Volcano, Indonesia. *Geochimica et Cosmochimica Acta* **51**, 2083-2101.

Szilas, K., Kelemen, P.B. and Rosing, M.T. (2015) The petrogenesis of ultramafic rocks in the 3.7 Ga Isua supracrustal belt, southern West Greenland: Geochemical evidence for two distinct magmatic cumulate trends. *Gondwana Research* **28**, 565-580.

Tang, Y.-J., Zhang, H.-F., Ying, J.-F. and Su, B.-X. (2013) Widespread refertilization of cratonic and circum-cratonic lithospheric mantle. *Earth-Science Reviews* **118**, 45-68.

Tera, F., Papanastassiou, D.A. and Wasserburg, G.J. (1974) Isotopic evidence for a terminal lunar cataclysm. *Earth and Planetary Science Letters* **22**, 1-21.

Testi, L., Birnstiel, T., Ricci, L., Andrews, S., Blum, J., Carpenter, J., Dominik, C., Isella, A., Natta, A., Williams, J. and Wilner, D. (2014) Dust Evolution in Protoplanetary Disks,

in: Beuther, H., Klessen, R., Dullemond, C., Henning, T. (Eds.), Protostars and Planets VI. University of Arizona Press Tucson, AZ, USA.

Torsten, P., Jürgen, B. and Thomas, H. (2000) Analogous experiments on the stickiness of micron-sized preplanetary dust. *The Astrophysical Journal* **533**, 454.

Touboul, M., Liu, J., O'Neil, J., Puchtel, I.S. and Walker, R.J. (2014) New insights into the Hadean mantle revealed by ^{182}W and highly siderophile element abundances of supracrustal rocks from the Nuvvuagittuq Greenstone Belt, Quebec, Canada. *Chemical Geology* **383**, 63-75.

Touboul, M., Puchtel, I.S. and Walker, R.J. (2012) ^{182}W evidence for long-term preservation of early mantle differentiation products. *Science* **335**, 1065-1069.

Touboul, M., Puchtel, I.S. and Walker, R.J. (2015) Tungsten isotopic evidence for disproportional late accretion to the Earth and Moon. *Nature* **520**, 530-533.

van Westrenen, W., Blundy, J. and Wood, B. (1999) Crystal-chemical controls on trace element partitioning between garnet and anhydrous silicate melt. *American Mineralogist* **84**, 838-847.

Viljoen, M.J. and Viljoen, R.P. (1969a) The geology and geochemistry of the Lower Ultramafic Unit of the Onverwacht Group and a proposed new class of igneous rocks. *Geological Society of South Africa* **Special Publication 2**, 55-86.

Viljoen, R.P. and Viljoen, M.J. (1969b) The geological and geochemical significance of the upper formations of the Onverwacht Group. *Geological Society of South Africa* **Special Publication 2**, 113-152.

Vockenhuber, C., Oberli, F., Bichler, M., Ahmad, I., Quitté, G., Meier, M., Halliday, A.N., Lee, D.C., Kutschera, W., Steier, P., Gehrke, R.J. and Helmer, R.G. (2004) New half-life measurement of ^{182}Hf: Improved chronometer for the Early Solar System. *Physical Review Letters* **93**, 172501.

Völkening, J., Walczyk, T. and G. Heumann, K. (1991) Osmium isotope ratio determinations by negative thermal ionization mass spectrometry. *International Journal of Mass Spectrometry and Ion Processes* **105**, 147-159.

Vollstaedt, H., Mezger, K. and Leya, I. (2015) Tracing the origin and evolution of volatile elements in the Inner Solar System by selenium isotopes, *Goldschmidt* **2015**, Prague, Czech Republic.

Wade, J. and Wood, B.J. (2005) Core formation and the oxidation state of the Earth. *Earth and Planetary Science Letters* **236**, 78-95.

Wade, J., Wood, B.J. and Tuff, J. (2012) Metal–silicate partitioning of Mo and W at high pressures and temperatures: Evidence for late accretion of sulphur to the Earth. *Geochimica et Cosmochimica Acta* **85**, 58-74.

Walker, R.J., Horan, M.F., Shearer, C.K. and Papike, J.J. (2004) Low abundances of highly siderophile elements in the lunar mantle: evidence for prolonged late accretion. *Earth and Planetary Science Letters* **224**, 399-413.

Walker, R.J. and Nisbet, E. (2002) ^{187}Os isotopic constraints on Archean mantle dynamics. *Geochimica et Cosmochimica Acta* **66**, 3317-3325.

Wallace, P. and Carmichael, I.S.E. (1992) Sulfur in basaltic magmas. *Geochimica et Cosmochimica Acta* **56**, 1863-1874.

Walter, M.J. (2014) 3.10-Melt extraction and compositional variability in mantle lithosphere A2 - Holland, Heinrich D, in: Turekian, K.K. (Ed.), *Treatise on Geochemistry* (Second Edition). Elsevier, Oxford, pp. 393-419.

Wang, Z. and Becker, H. (2013) Ratios of S, Se and Te in the silicate Earth require a volatile-rich late veneer. *Nature* **499**, 328-331.

Wang, Z. and Becker, H. (2014) Abundances of Sulfur, Selenium, Tellurium, Rhenium and Platinum-Group Elements in Eighteen Reference Materials by Isotope Dilution Sector-Field ICP-MS and Negative TIMS. *Geostandards and Geoanalytical Research* **38**, 189-209.

Wang, Z. and Becker, H. (2015a) Abundances of Ag and Cu in mantle peridotites and the implications for the behavior of chalcophile elements in the mantle. *Geochimica et Cosmochimica Acta* **160**, 209-226.

Wang, Z. and Becker, H. (2015b) Comment on “A non-primitive origin of near-chondritic S-Se-Te ratios in mantle peridotites: Implications for the Earth's late accretionary history” by König S. et al. [Earth Planet. Sci. Lett. 385 (2014) 110–121]. *Earth and Planetary Science Letters* **417**, 164-166.

Wang, Z., Becker, H. and Gawronski, T. (2013) Partial re-equilibration of highly siderophile elements and the chalcogens in the mantle: A case study on the Baldissero and Balmuccia peridotite massifs (Ivrea Zone, Italian Alps). *Geochimica et Cosmochimica Acta* **108**, 21-44.

Wang, Z., Becker, H. and Wombacher, F. (2015) Mass Fractions of S, Cu, Se, Mo, Ag, Cd, In, Te, Ba, Sm, W, Tl and Bi in Geological Reference Materials and Selected Carbonaceous Chondrites Determined by Isotope Dilution ICP-MS. *Geostandards and Geoanalytical Research* **39**, 185-208.

Wang, Z., Laurenz, V., Petitgirard, S. and Becker, H. (2016) Earth's moderately volatile element composition may not be chondritic: Evidence from In, Cd and Zn. *Earth and Planetary Science Letters* **435**, 136-146.

Wedepohl, K.H. (1995) The composition of the continental crust. *Geochimica et Cosmochimica Acta* **59**, 1217-1232.

Willbold, M., Elliott, T. and Moorbath, S. (2011) The tungsten isotopic composition of the Earth/'s mantle before the terminal bombardment. *Nature* **477**, 195-198.

Willbold, M., Mojzsis, S.J., Chen, H.W. and Elliott, T. (2015) Tungsten isotope composition of the Acasta Gneiss Complex. *Earth and Planetary Science Letters* **419**, 168-177.

Witt-Eickschen, G., Palme, H., O’Neill, H.S.C. and Allen, C.M. (2009) The geochemistry of the volatile trace elements As, Cd, Ga, In and Sn in the Earth’s mantle: New evidence from in situ analyses of mantle xenoliths. *Geochimica et Cosmochimica Acta* **73**, 1755-1778.

Wood, B.J., Kiseeva, E.S. and Mirolo, F.J. (2014) Accretion and core formation: The effects of sulfur on metal–silicate partition coefficients. *Geochimica et Cosmochimica Acta* **145**, 248-267.

Wood, B.J., Walter, M.J. and Wade, J. (2006) Accretion of the Earth and segregation of its core. *Nature* **441**, 825-833.

Woodhead, J., Kent, A.J., Hergt, J., Bolhar, R. and Rowe, M.C. (2005) Volatile contents of komatiite magmas and the Archaean mantle: Insights from melt inclusions in komatiites, American Geophysical Union, Fall Meeting.

Workman, R.K. and Hart, S.R. (2005) Major and trace element composition of the depleted MORB mantle (DMM). *Earth and Planetary Science Letters* **231**, 53-72.

Xiao, T., Guha, J. and Boyle, D. (2004) High thallium content in rocks associated with Au-As-Hg-Tl and coal mineralization and its adverse environmental potential in SW Guizhou, China. *Geochemistry: Exploration, Environment, Analysis* **4**, 243-252.

Xiao, X. and Lipschutz, M.E. (1992) Labile trace elements in carbonaceous chondrites: A survey. *Journal of Geophysical Research: Planets* **97**, 10199-10211.

Yang, J., Siebert, C., Barling, J., Savage, P., Liang, Y.-H. and Halliday, A.N. (2015) Absence of molybdenum isotope fractionation during magmatic differentiation at Hekla volcano, Iceland. *Geochimica et Cosmochimica Acta* **162**, 126-136.

Yardley, B.W.D. and Cleverley, J.S. (2013) The role of metamorphic fluids in the formation of ore deposits. Geological Society, London, Special Publications 393.

Yi, W., Halliday, A.N., Alt, J.C., Lee, D.-C., Rehkämper, M., Garcia, M.O., Langmuir, C.H. and Su, Y. (2000) Cadmium, indium, tin, tellurium, and sulfur in oceanic basalts: Implications for chalcophile element fractionation in the Earth. *Journal of Geophysical Research: Solid Earth* **105**, 18927-18948.

Yi, W., Halliday, A.N., Lee, D.-C. and Christensen, J.N. (1995) Indium and tin in basalts, sulfides, and the mantle. *Geochimica et Cosmochimica Acta* **59**, 5081-5090.

Yi, W., Halliday, A.N., Lee, D.-C. and Rehkämper, M. (1998) Precise Determination of Cadmium, Indium and Tellurium Using Multiple Collector ICP-MS. *Geostandards Newsletter* **22**, 173-179.

Yu, M.-Q., Liu, G.-Q. and Jin, Q. (1983) Determination of trace arsenic, antimony, selenium and tellurium in various oxidation states in water by hydride generation and atomic-absorption spectrophotometry after enrichment and separation with thiol cotton. *Talanta* **30**, 265-270.

Zhou, M.-F. (1994) PGE distribution in 2.7-Ga layered komatiite flows from the Belingwe greenstone belt, Zimbabwe. *Chemical Geology* **118**, 155-172.

CV is removed for the safety of personal data.

Acknowledgements

O tempora! I came to Harry Becker's group as an idiot of geochemistry and what I can only hope after four years' training is that I am not much a *ignoramus*. I would probably have been like a fledgling just out of nest trying to learn how to survive in the jungle. At that time many troubles I must have made for many people around. I appreciate in heart the tolerance, generosity and unaccountable helps you offered me.

Prof. Dr. Harry Becker must have been in great patience with me. For not a short time after I started my work here, I had not been in the required qualification which would make me work by my own without making simple mistakes. The first poster I made cost much energy for Harry to correct *verbatim*. He has devoted greatly to make me know what science is and how to do it. There is no courtesy if I say without his patience, responsibility and kindness that I could not have improved so much both in science and in the view of life. Certainly I has benefited a lot from his critical thinking as reading scientific outputs and from his wisdom as designing and organizing research projects. I have a lot to learn from him for the rest of my career life.

Great appreciation must go to Prof. Dr. Gerhard Franz in TU Berlin for being the second reviewer of my thesis and in my PhD committee. I am indebted to him because he had to read a work presented in no good English and needed-to-be-improved science.

I am very thankful to Dr. Peter Sprung (Uni-Köln) and Prof. Dr. Erik Scherer (Uni-Münster) who shared the precious Acasta samples with me and provided generously any information I was in need of. No small amount of thanks must go to Dr. Igor Puchtel (University of Maryland) who shared his unparalleled collection of komatiites. This thesis is built on their field work and researches.

Much gratitude has to be given to Dr. Konard Hammerschmidt, Ms. Monika Feth, Mr. Christian Meyer, Mr. Timo Gawronski and Dr. Yogita Kadlag who have taught me how to work in the laboratory and how to use the instruments. Dr. Hammerschmidt gave me the safety instructions and showed me how to use the TIMS. Ms. Feth maintained the clean lab in good state that guaranteed my lab work to run smoothly. Christian showed the first time how to weigh in spikes and samples into HPAS tubes and how to operate the HPAS. Timo and

Yogita helped me greatly in adjusting the ICP-MS, chemical separation and all the small details one has to know if one wants to work in geochemistry. I owe a lot to them.

I am very thankful to Dr. Zaicong Wang, Dr. Elis Hoffmann, Dr. Uwe Wiechert and Dr. Philipp Gleißner. It is their contributions to the group that I can enjoy an excellent scientific atmosphere. I benefited much from the small chats with them. It is precisely these daily chats and discussions that opened my mind to some scientific issues I did not know. They shared their knowledge generously and I have nothing that would compensate. Zaicong, especially in the komatiite project, gave me numerous instructions, helps and guidance which in no small part ensured the completion of my PhD work. Shared enthusiasm in understanding the petrogenesis of komatiites brought many fruitful thoughts from Elis to me. These thoughts we plan to make it public. We, Uwe and me, are neighbors for almost three years. He was in B204 and I was in B204a. His good taste and smart comments in science made me know that many works can be done better. Philipp provided a lot of help in maintaining the ICP-MS. I remember that there was a time that I broke into his office almost every day because the ICP-MS did not run as I expected. It is a great pleasure to have discussions with you.

Mr. Marc Weynell and Dr. Simon Hohl as my friends gave me a lot of hints on living in Berlin. Without their effort of integrating me in this great city, my life here must be boring out of imagination. It was because the invitation from Ms. Elfrun Lehmann and Harry to their house that I had the chance to know what to eat at Christmas. Elfrun also helped me a lot to get the scholarship which enabled me to finish my PhD.

Special acknowledgements go to Ms. Kathrin Schneider and Dr. Elis Hoffmann who generously translated the summary into German. It is a task that seems easy but not so. However, any disconformities between the English summary and its German version must be caused by my inability of clarity in drafting the English summary. Also regarding to the summary, Prof. Dr. Harry Becker suggested me have a Chinese version which may add an exotic flavor to the dissertation.

I really would like to make a list including all the people I need to express my thanks. All the members in the geochemistry group contributed to form a delightful and wonderful environment. Helps from Ms. Michaele Schreiber (secretary) and Mr. Michael Golinski (IT technician) are gratefully acknowledged. All the Dr.-to-bes, Kathrin Schneider, Dennis Vanderliek, Oliver Jäger, Franziska Schubring, Tim Roth and so on, I am thankful for your helps and I am sure that better science will come from your efforts.

Financial funding agencies, CSC (China Scholarship Council), DAAD (German Academic Exchange Service), DFG (German Research Foundation) and FUB (Freie Universität Berlin) are gratefully acknowledged for granting me scholarships and covering my conference costs. Many thanks go to Ms. Stefanie Kirsch in the Center for International Cooperation (CIC, FUB). She organized nearly everything which made my first several weeks in Berlin very pleasant.

In the end I thank my parents, my sister and my brother. Though they do not understand what I was doing, it is them who trust me unlimitedly. It is also from them that I draw my courage and strength to continue on this long way. They are partly the reason that I believe that I am in a good world.

I would like to conclude with a poem-Hälfte des Lebens-of Friedrich Hölderlin. I translated from its English version and in comparison with its German version.

向湖委下的土，

满载黄梨与野玫瑰。

顽皮的天鹅，

交饮如爱，

将头浸入，

清静圣洁的水中。

但当冬日来临，

鲜花，阳光，

大地的阴影，

我将于何处寻？

高墙耸立，

冰冷静寂。

风标嘎嘎，

转在风里。

Chunhui Li (李春辉)

Berlin, 28 June, 2016

博士記

二零一一年秋返蓉，師曰：“何不負笈歐美？”囑予細謀之。遂備考參選。越明年五月，教育部張榜，余附驥尾。

時年九月，余由京至德意志國都柏林，晴黃滿地，音容行止皆異。臘月，隨師貝克由自由大學赴明斯特商太古代事，於此始入科研。

初，未蒙小子也，諸事皆昧。梅耶君始授，在聰、尤格塔、提慕諸君輒便即教，經年方立。初，甚不易也。當此時，偶有錯動，則憂恍疊至，晝夜疲馳，如喪家之犬，不知何以，不知何之。

二零一四年夏，赴美利堅參會，群賢畢至，少長鹹集，談吐星月，指揮今古。余鄙陋甚，回德始發奮也。

二零一四年，太古代事畢。然彼不足以成文，師貝克遂籌科馬提岩事，幸成。余之科馬提岩事，順也，實賴在聰君不吝談授。越明年五月，科馬提岩亦畢，師貝克曰：“可作文。”今文始成。

科研如解牛，道術兩參，因熟而佳。然欲獲博士銜，須體力心力俱佳，不驕不餒，不急不棄，方可缓圖也。

四載攸然，諸事將畢，余作文以結之。

維年七月八日，柏林。